

**Robust design of integrated upstream and
recovery operations for antibody manufacture
using scale-down mimics and predictive modelling**



Martina Sebastian

The dissertation is submitted for the degree of
Doctor of Engineering (EngD) in Biochemical Engineering

August 2022

I, Martina Sebastian confirm that the work presented in this thesis is my own. Where information has been derived from other sources, I confirm that this has been indicated in the thesis.

I would like to dedicate this thesis to my mum who has always been my inspiration,
my husband for always being there and my children for their love and patience.

Abstract

Disk-stack centrifugation followed by depth filtration is the cornerstone in the clarification of mammalian cell cultures used for biopharmaceutical manufacture. The drive for higher cell culture productivities has led to cell culture harvests with increased solids concentration and cell debris that can be difficult to clarify with the existing recovery platforms. Due to the limitations in the available scale-down models for the upstream-recovery sequence, these challenges are often first faced upon scale-up leading to facility fit issues and an increase in the costs of manufacture. The aim of this thesis is to address this challenge through building a novel integrated framework for the upstream-recovery sequence. The framework leverages scale-down mimics with modelling techniques using multivariate data analysis (MVDA) and bioprocess economics for a holistic view of the upstream and recovery operations.

To map the upstream-recovery design space, an integrated small scale platform was set up comprising a high throughput microbioreactor system, a centrifugation mimic based on a capillary shear device (CSD) and cholesterol concentration as a filterability predictor. The thesis focused on using this novel set up with Design of Experiments (DoE) and MVDA to derive cause-and effect correlations for upstream (e.g. product titre) and recovery (e.g. solids concentration and filterability) metrics as a function of operating conditions. The results revealed trade-offs between increasing titre, the solids load onto the centrifuge and the centrate's filterability. The work also identified the impact of cell culture viability and centrifugation shear on intact antibody monomer content.

The predictive models and cholesterol-based correlation for filterability were integrated into a bioprocess economics model, which was built to determine the cost of goods (COG) for the recovery operation. This enabled a better prediction of the impact of shear on facility fit, throughput and COG [under uncertainty]. Windows of Operation for the integrated upstream-recovery sequence were generated to determine the sweet spot in terms of cell culture operating conditions (harvest day, seeding density) and recovery shear levels that meet multiple conflicting output targets, namely titre, product loss, filter area, COG and throughput.

A major challenge in using high throughput experimentation such as the framework proposed in this thesis is the associated burden of high volume of analytics. To address this challenge, novel rapid approaches were developed that accurately predicted solids concentration and cell damage using the particle size distribution (PSD) data from a routinely used automated cell counter. By leveraging existing PSD data, this has the potential to reduce analytical resource and time.

The work in this thesis showed the benefits of using a holistic approach to the optimisation of the upstream-recovery sequence of operations. The developed framework can be used to design more efficient processes earlier in the development cycle accelerating development timelines and reducing costs.

Impact Statement

The thesis established a novel framework for the holistic view of upstream- recovery sequence through developing tools that enable predictions of the process performance earlier in the development cycle. This framework offers a number of benefits for the bioprocess development. For instance, it enables selection of the optimal cell culture and recovery strategies early in the development by accounting for the interactions between upstream culture characteristics and performance of the recovery operations. This way the proposed framework can identify early on the combinations of upstream parameters and the centrifugation operation that are likely to have a detrimental impact on critical quality attributes such as purity in terms of antibody reduction and host cell proteins (HCP). Moreover, this enables developers to devise strategies to mitigate against adverse impact on the product through changes in the manufacturing approach – for instance, changing the harvest day or the seeding density. The novel economics model with integrated experimentally derived predictive correlations and stochastic inputs facilitates an informed decision-making process. The possibility for early process and economics assessment enables accelerated development timelines and achieving a more cost-efficient process, facilitating the more rapid access of patients to cheaper medicines. The thesis also provides novel methods for LDH and solids concentration assessment that replace traditional time- and resource-consuming techniques. This enables gaining more knowledge about the process. Furthermore, the novel techniques use

PSD data that is routinely collected during cell counting, which means that this approach enables the analysis of historical data, for which these measurements are available. Finally, apart from industry this thesis can impact future academic research. The established tools can be used to investigate the impact of upstream and recovery on other downstream parameters and link to more product quality attributes and performance metrics.

The work described in this thesis has been endorsed by industry experts who took part in sponsoring this research and who highlight its impact below.

R&D resource & time savings helping to accelerate process development:

“The application of the integrated upstream-recovery framework developed in the collaboration provided tools to better understand the process sequence and anticipate potential facility fit issues in early R&D rather than at later process development stages. Through better process understanding at small R&D scale, the framework helps mitigate against potential product losses and avoid the need for process optimisation at pilot scale. This has already led to a reduction in resources and time required for optimising the upstream-recovery sequence that is traditionally carried out at pilot scale requiring >50L but now can be performed at bench scale process using millilitre quantities. AstraZeneca views this time and resource saving as critical as it helps accelerate the process development and avoids wasting precious resource – for instance, a single 500L pilot scale run to test various centrifugation conditions can cost of up to 130K in labour and direct costs (considering the costs of upstream, primary and secondary recovery).”

Richard Turner, Executive Director, AstraZeneca

Leveraging PSD data for improved process understanding:

“The tool for particle size distribution (PSD) data analysis enabled predictions of cell culture solids concentration and cell lysis whilst avoiding the need for additional sampling and laborious analytics that often discourage collecting such measurements. The time for measurement was reduced from ~6 hours using the traditional approach to a few minutes leveraging the PSD data analysis using the proposed model when working with the high throughput ambr15 microbioreactor system with 48 vessels. Having these measurements at small scale will help anticipate difficult to clarify harvests at earlier development stages and opens up the possibility of enhancing cell line selection to consider solids concentration and cell lysis as metrics. The additional process knowledge will also help facility fit predictions to mitigate the risk of exceeding the capacity of installed clarification systems.”

Matthew Cheeks, Senior Director, Biopharmaceutical Development, AstraZeneca

Acknowledgements

I would like to take this opportunity to express my gratitude to my UCL academic supervisors – Prof Suzanne Farid, Prof Nigel Titchener-Hooker and Dr. Stephen Goldrick – as well as my industrial supervisors – Richard Turner, Matthew Cheeks, David Gruber, Alison Mason and Aled Charles. Their support and guidance have played a great role in helping me complete the EngD project.

I would also like to thank a number of AstraZeneca staff that have been indispensable in my work. First of all, I would like acknowledge the great support I received from the upstream team on training me on the equipment and helping me troubleshoot. Equally important was the support and patience I was given by the downstream team, in particular David Gruber and Aled Charles, when working on the centrifugation and depth filtration scale-down mimics. Last but not least, I would like to thank the analytics team for their support with Protein A and HCP assays.

Nomenclature

| | |
|--------------|--|
| ADC | Antibody drug-conjugates |
| AIC | Akaike information criterion |
| AMBR | Advanced Microscale Bioreactor |
| ANOVA | Analysis of variance |
| BIC | Bayesian information criterion |
| CCD | Centre composite design |
| CCF | Cell culture fluid |
| CFD | Computational fluid dynamics |
| CHO | Chinese hamster ovary |
| COG | Cost of goods |
| CPP | Critical process parameter |
| CQA | Critical quality attribute |
| CS | Culture station |
| CSD | Capillary shear device |
| DO | Dissolved oxygen |
| DoE | Design of experiment |
| EBA | Expanded bed adsorption chromatography |

Nomenclature

| | |
|--------------|--|
| EMOA | Evolutionary multiobjective algorithm |
| FMEA | Failure mode and effects analysis |
| HCP | Host cell proteins |
| HPLC | High performance liquid chromatography |
| HT | High throughput |
| IVC | Integral viable cell count |
| LDH | Lactate dehydrogenase |
| MADM | Multiple attribute decision-making |
| MILP | Mixed-integer linear programming model |
| MNB | Miniature bioreactor |
| MVC | Maximum viable cell count |
| MVDA | Multivariate data analysis |
| OFAT | One factor at a time |
| PAT | Process analytics technologies |
| PBS | Phosphate buffered saline |
| PCA | Principal component analysis |
| PLS | Partial least squares |
| PRESS | Predictive residual sum of squares |
| PSD | Particle size distribution |
| QbD | Quality by design |
| QbT | Quality by testing |

Nomenclature

| | |
|-------------|-------------------------------|
| RDS | Rotating disc shear device |
| SDM | Scale Down Model |
| TEPC | Total equipment purchase cost |
| TFF | Tangential flow filtration |
| USD | Ultra scale-down |
| VCC | Viable cell count |

Table of Contents

| | |
|---|-----------|
| Abstract | 4 |
| Impact Statement | 6 |
| Acknowledgements | 9 |
| Nomenclature | 10 |
| Table of Contents..... | 13 |
| Table of Tables..... | 18 |
| Table of Figures | 22 |
| Chapter 1 | 36 |
| 1 Introduction | 36 |
| 1.1 Industry overview..... | 37 |
| 1.1.1 Antibodies: market overview..... | 37 |
| 1.1.2 Platform manufacturing process for CHO cell derived therapies | 40 |
| 1.2 Current recovery operations | 43 |
| 1.2.1 Recovery sequence selection..... | 43 |
| 1.2.2 Disc-stack centrifugation..... | 47 |
| 1.2.3 Depth filtration | 49 |
| 1.3 Upstream optimisation and the impact on recovery step | 54 |
| 1.3.1 Approaches to upstream optimisation | 54 |
| 1.3.2 Impact of upstream parameters on recovery performance | 58 |

Table of Contents

| | | |
|------------------|---|------------|
| 1.4 | Scale-down models for upstream and recovery | 60 |
| 1.4.1 | Upstream scale-down technologies | 61 |
| 1.4.2 | Scaling down the recovery operation | 63 |
| 1.5 | Multivariate data analysis (MVDA) techniques in bioprocess modelling ... | 67 |
| 1.6 | Decisional tools for bioprocess optimisation | 69 |
| 1.7 | Aims and organisation of thesis | 72 |
| Chapter 2 | | 74 |
| 2 | Materials and Methods | 74 |
| 2.1 | Wet lab experimental protocols..... | 74 |
| 2.1.1 | Reagents | 74 |
| 2.1.2 | Bench scale and scale-down process steps..... | 74 |
| 2.1.3 | Analytical methods | 78 |
| 2.2 | Theoretical considerations | 84 |
| 2.2.1 | Disc stack centrifugation..... | 85 |
| 2.2.2 | Filtration fouling models..... | 91 |
| 2.3 | Statistical methods..... | 93 |
| 2.3.1 | DoE considerations | 93 |
| 2.3.2 | Definitions..... | 95 |
| 2.3.3 | Standard least square models..... | 98 |
| 2.3.4 | PLS model development | 99 |
| 2.4 | Key software and programming languages | 101 |
| 2.4.1 | Statistical analysis | 101 |
| 2.4.2 | Data pre-treatment and bioprocess modelling | 101 |
| Chapter 3 | | 103 |
| 3 | Linking cell culture parameters to upstream and recovery metrics.... | 103 |
| 3.1 | Introduction | 103 |

Table of Contents

| | | |
|------------------|--|------------|
| 3.2 | Experimental approach | 106 |
| 3.2.1 | Ambr experiments | 106 |
| 3.2.2 | Stepwise regression and model selection | 107 |
| 3.2.3 | Robustness analysis..... | 108 |
| 3.3 | Results and discussion | 108 |
| 3.3.1 | Growth Culture Kinetics | 108 |
| 3.3.2 | Predictive models for the upstream and recovery metrics | 112 |
| 3.3.3 | Building a window of operation for ambr1 constrained by titre and [solids] | 114 |
| 3.3.4 | Investigating the impact of seeding density on the window of operation for ambr2 | 119 |
| 3.4 | Conclusions | 124 |
| Chapter 4 | | 126 |
| 4 | Derivation of predictive correlations for the upstream-centrifugation-depth filtration sequence | 126 |
| 4.1 | Introduction | 126 |
| 4.2 | Methodology | 129 |
| 4.2.1 | Summary of cell culture conditions for the pilot scale characterisation studies..... | 129 |
| 4.2.2 | Experimental setup for spiking studies using a Null cell line..... | 130 |
| 4.2.3 | Experimental setup for studying the impact of centrifugation and depth filtration on antibody reduction..... | 131 |
| 4.2.4 | Ambr3 and ambr4 DoE studies..... | 132 |
| 4.2.5 | Antibody size analysis | 134 |
| 4.3 | Results and discussion | 135 |
| 4.3.1 | Centrifuge characterisation for low viability cell cultures using [cholesterol]..... | 136 |
| 4.3.2 | Using [cholesterol] to predict filter capacity (L/m ²)..... | 138 |

Table of Contents

| | | |
|------------------|---|------------|
| 4.3.3 | The impact of the recovery operation on monomer content and HCPs | 140 |
| 4.3.4 | The impact of depth filtration, centrifugation shear and hold on antibody reduction | 144 |
| 4.3.5 | Linking the ambr to the centrifugation mimic | 147 |
| 4.4 | Conclusions | 156 |
| Chapter 5 | | 157 |
| 5 | Building a decisional tool for the recovery operation of mammalian cell processes | 157 |
| 5.1 | Introduction | 157 |
| 5.2 | Methodology | 160 |
| 5.2.1 | Model description | 160 |
| 5.2.2 | Upstream and recovery unit operations sizing | 163 |
| 5.2.3 | Recovery model assumptions | 173 |
| 5.2.4 | COG calculations..... | 177 |
| 5.2.5 | Case studies assumptions..... | 180 |
| 5.3 | Results and Discussion | 184 |
| 5.3.1 | COG _{REC} comparison for different scenarios | 184 |
| 5.3.2 | The impact of upstream conditions on COG _{REC} | 189 |
| 5.3.3 | The impact of process variability on facility fit..... | 197 |
| 5.4 | Conclusions | 205 |
| Chapter 6 | | 206 |
| 6 | Enhanced harvest performance predictability through advanced multivariate data analysis of mammalian cell culture particle size distribution | 206 |
| 6.1 | Introduction | 206 |
| 6.2 | Methodology | 210 |

Table of Contents

| | |
|---|------------|
| 6.2.1 Case study set up..... | 210 |
| 6.2.2 Particle size analysis | 212 |
| 6.3 Results and discussion | 213 |
| 6.3.1 Relationship between LDH release and cell culture viability..... | 213 |
| 6.3.2 Investigating the relationship between Vi-Cell XR PSD data and cells viability..... | 218 |
| 6.3.3 Leveraging PSD data to predict LDH release using PLS techniques .. | 221 |
| 6.3.4 Levering PSD data to predict [solids] using PLS techniques | 223 |
| 6.3.5 Volume and time savings | 226 |
| 6.4 Conclusions | 227 |
| Chapter 7 | 228 |
| 7 Conclusions and future work..... | 228 |
| 7.1 Introduction..... | 228 |
| 7.2 Key conclusions..... | 228 |
| 7.3 Limitations of the work | 231 |
| 7.4 Future work..... | 231 |
| References..... | 235 |
| Appendix | 273 |
| Chapter 3 Appendix..... | 273 |
| Chapter 4 Appendix..... | 276 |
| Characterising the pilot-scale centrifuge using established approaches | 276 |
| Chapter 5 Appendix..... | 284 |
| Chapter 6 Appendix..... | 287 |

Table of Tables

| | |
|--|-----|
| Table 1.1 Examples from literatures showing the impact of bioreactor physico-chemical conditions on the upstream performance..... | 57 |
| Table 2.1 The sigma factor calculation for different small scale centrifuges..... | 90 |
| Table 2.2 Equations describing the four main blocking mechanisms adapted from (Bolton et al., 2006) | 92 |
| Table 3.1 Experimental setup for DoE studies in ambr1 and ambr2 | 107 |
| Table 4.1 Description of the cell culture material used for the centrifuge characterisation studies | 129 |
| Table 4.2 Summary of experimental conditions in ambr 3 and 4..... | 133 |
| Table 4.3 Summary of results from bench-scale filter sizing experiments using X0HC secondary depth filter (23cm ²) at constant pressure. The filter capacity was calculated using V_{max} | 139 |
| Table 4.4 Summary of key results for titre, [solids] and OD550 for various harvest days and seeding densities for A) ambr3 and B) ambr4 | 154 |
| Table 5.1 Summary of the database of common centrifuges and their key characteristics used in the decisional tool..... | 165 |
| Table 5.2 Key equations for the centrifugation design and operation..... | 166 |

Table 5.3 Summary of depth filtration equipment and consumables used in the model.....169

Table 5.4 Model assumptions for the recovery operation174

Table 5.5 Filtration capsules and filtration cartridges costs175

Table 5.6 Other consumables used with filter holders and capsules175

Table 5.7 Summary of the costs for the filter holders and domes.....176

Table 5.8 Costs of depth filtration and centrifugation kids176

Table 5.9 Other key costs for the process (Reagents and Labour cost assumptions)177

Table 5.10 Parameters used for estimating the Lang factor for the recovery process (adapted from Novais et al. (2001) and Pollock, (2014)).....178

Table 5.11 Process economics main equations*179

Table 5.12 Overall process assumptions used for assessing the COG of the recovery operation for different titre and demand scenarios in **Section 5.3.1**181

Table 5.13 Key assumptions used to investigate the impact of pH, seeding density and temperature shift on the recovery process economics in **Section 5.3.2**181

Table 5.14 Key assumptions used in **Section 5.3.2.2** to investigate the impact of bioreactor seeding density, harvest day and centrifugation on recovery process economics.....182

Table 5.15 Case studies 4 and 5 on facility fit assessment. A) Overall setup for the cases studies; B) Scenarios used for building a window of operation in case study 4 (**Section 5.3.3.1**) C) Monte Carlos simulation in case study 5 (**Section 5.3.3.2**) 183

Table 6.1 Summary of experimental data used to build the PLS models for LDH release and [solids].....211

Table 3.1-A Example of prediction models for titre (ambr1) generated using stepwise regression. The selection rule is based on maximising R^2 k-fold. The stepwise regression was performed in Jmp. The models in terms of actual factors as well as the R^2 predicted for the models were generated in Design-Expert, all other statistics were computed in Jmp.....273

Table 4.1-A Filter capacity studies to support pilot scale centrifuge 1 characterisation279

Table 5.1-A Examples of process duration (hours) for different filter capacities and fluxes286

Table 6.1-A Jmp report on PLS models generation with different number of factors (latent variables) using the NIPALS algorithm and k-fold cross validation with k-fold = 7. The models are generated using all PSD data for the viable cells.....287

Table 6.2-A Jmp report on PLS models generation with different number of factors (latent variables) using the NIPALS algorithm and k-fold cross validation with k-fold = 7. This is a pruned model using only PSD data (predictors) with VIP score higher

than 0.8. The box highlighted in purple shows the final PLS model that was chosen based on min Pres and max Prob>van der Voet T^2288

Table 6.3-A Assumptions used in the calculation of volumes and time required for LDH and PCV ([solids]) measurements using the traditional wet-lab approach and the novel PLS-based method.....290

Table of Figures

Figure 1.1 Key stages, constraints and metrics in the drug development cycle, adapted from Farid (2012) 39

Figure 1.2 Typical mAb manufacturing platform (Kelley et al., 2009; Shukla et al., 2007; Curling, 2009) 42

Figure 1.3 Schematic representation of the particles’ journey through the depth filter (Shukla and Kandula, 2009) 50

Figure 1.4 Depth filter flow path for top and bottom outlet configuration (Collins et al., 2009)..... 53

Figure 1.5 Schematic representation of the ambr[®] 15 Bioreactor (**Nienow et al., 2013**)..... 63

Figure 2.1 Forces acting upon a particle suspended during centrifugation, adapted from Tebbe et al., (1996) 86

Figure 3.1 Fed-batch cell culture kinetics for ambr1 (box with light grey border - - -) and ambr2 (box with blue border - - -). A),D),G),J) and M) conditions at low pH target of 6.8; B), E), H), K) and N) describes conditions at mid pH of 7 and C), F), I), L) and O) is for high pH conditions of 7.2. For ambr1 temperature shift was applied on day 4 from 35.5°C to 33.0°C for A), B) and C) and constant temperature of 35.5°C

for D), E), F). For ambr2 constant temperature of 35.5⁰C was applied M), N),O) and temperature shift on day 4 from 35.5⁰C to 34.5⁰C - J),K),L) and temperature shift to 33.5⁰C -) G), H) and I). The symbols represent different seeds: ● low seed below 0.6 x 10⁶ cells/mL; ▼ mid seed between 0.6 and 0.9 x 10⁶ cells/mL and ◆ high seed above 0.9 x 10⁶ cells/mL.....111

Figure 3.2 Predictive equations in terms of coded factors for ambr1 (■ –) and ambr2 (■ –) for: A) Titre (g/L) with adj. R² = 0.79 (ambr1), pred. R² = 0.74 (ambr1), k-fold R² = 0.70 (ambr1) and adj. R² = 0.83 (ambr2), pred. R² = 0.74 (ambr2), k-fold R² = 0.76 (ambr2); B) [Solids] (%v/v) with adj. R² = 0.74 (ambr1), pred. R² = 0.64 (ambr1), k-fold R² = 0.68 (ambr1) and adj. R² = 0.67 (ambr2), pred. R² = 0.63 (ambr2), k-fold R² = 0.65 (ambr2); C) Harvest turbidity (NTUs) with adj. R² = 0.88, pred. R² = 0.86, k-fold R² = 0.86 for ambr2; D) Cell specific glucose consumption (ng/cell/day) with adj. R² = 0.84 (ambr1), pred. R² = 0.79 (ambr1), k-fold R² k-fold = 0.90 (ambr1) and adj. R² = 0.89 (ambr2), pred. R² = 0.86 (ambr2); E) Osmolality (mOsm/kg) with adj. R² = 0.89, pred. R² = 0.85 (ambr2); F) d10 (µm) with adj. R² = 0.88, pred. R² = 0.86 for ambr2. (ambr2). S.density = Seeding density; Harv.day = Harvest day113

Figure 3.3 Contour plots showing the impact of seeding density and pH on A) [solids] for conditions with a temperature shift; B) [solids] for conditions without a temperature shift; C) titre for harvest day 14 for conditions with a temperature shift; D) titre for harvest day 14 for conditions without a temperature shift; E) titre on day 16 for conditions with a temperature shift; E) titre on day 16 for conditions without a

Table of Figures

temperature shift. The temperature shift was carried out on day 4 from 35.5°C to 33.0°C..... 115

Figure 3.4 Window of operation (greyed out area) for ambr1 constrained by maximum [solids] of 9%v/v and minimum titre of 6g/L. The arrows point in the direction of desirability – increasing titre or decreasing [solids]. The red dot indicates the set operating parameters for the process so that it is within the window of operation..... 116

Figure 3.5 Probability distributions for ambr1, harvest day 14 for A) [solids] and B) titre at target seeding density of 0.65×10^6 cells/mL; C) [solids] and D) titre at target seeding density of 0.75×10^6 cells/mL; E) [solids] and F) titre for target seeding density of 0.85×10^6 cells/mL. The results were generated using 5000 simulation runs with seeding density inputted as triangular distribution ($\pm 0.15 \times 10^6$ cells/mL from target seeding density). 118

Figure 3.6 Heatmaps for ambr2 showing the impact of varying temperature and pH at low seeding density conditions on A) titre (g/L), D) [solids] (%v/v) and G) turbidity (NTUs); at mid seeding density on B) titre (g/), E) [solids] (% v/v) and H) turbidity (NTUs) and high seeding density for C) titre(g/L), F) [solids] (% v/v) and I) turbidity (NTUs). The seeding densities for the experiment are provided in **Table 3.1**..... 121

Figure 3.7 Windows of operation constrained by a-turbidity < 3000 NTU, b- [solids] < 9 % v/v, c- titre > 4g/L for A); C) and E), and by d- $d_{10} > 8.5 \mu\text{m}$, e- osmolality < 400 mOsm/kg and f- $q_{\text{gluc.}} > 0.2$ & < 0.32 gluc.(ng)/cell/day for B); D) and F). The

windows were built for ambr2 at harvest day 14 and different seeding density conditions - A) and B) low seeding density (0.6×10^6 cells/mL); C) and D) mid seeding density (0.9×10^6 to 1.2×10^6 cells/mL) and E) and F) high seeding density (more than 1.2×10^6 cells/mL). 123

Figure 4.1 Experimental setup used for GS-CHO Null spiking studies, investigating the impact of upstream conditions (cell cultures harvested at different time points) and centrifugation shear (using a CSD centrifugation mimic) on the levels of HCP and mAb reduction..... 130

Figure 4.2 Experimental setup for studying the impact of centrifugation shear (using a CSD centrifugation mimic), secondary depth filtration (using a bench-scale setup at constant flow) and filtrate hold on antibody reduction measured via capillary electrophoresis (CE analysis) using a BioAnalyzer..... 131

Figure 4.3 Workflow for analysis of the size data from the LabChip GXII. The data is first visualised for quick analysis. The CSV files from the LabChipGXII are imported in Matlab. The data is analysed for the different size antibodies and fragments generated from reduction at the disulfide bridge and is combined with all additional information available for the samples (e.g. harvest day, shear levels etc.). 134

Figure 4.4 Pilot scale centrifuge characterisation studies using A) comparison in the cholesterol levels between the mimic centrate generated using different CSD flowrates (■) and the pilot scale centrifuge MBPX404 ran at 9000RPM and 120L/h (▬) and B) comparison in the depth filtration (X0HC 23cm²) flux declines between the

Table of Figures

mimic centrate generate at 52.5 mL/min flowrate in the CSD and the pilot scale centrate (generated at 9000RPM and 120L/h)..... 137

Figure 4.5 Cholesterol concentration (mg/L) versus filter capacity (L/m²) for the cell culture and harvest conditions described in **Table 4.3**..... 139

Figure 4.6 Antibody size distribution for IgG1 λ and IgG1 κ after the fully purified mAb was spiked into a non-producer cell line (GS-CHO Null) and subjected to different levels of shear: NS – no shear, LS – low shear (21mL/min in the CSD) and HS- high shear (41mL/min in the CSD). Electropherogram (as outputted from LabChip GXII) for A) IgG 1 κ and B) IgG1 λ showing the different antibody fragments and C) a summary of the total intact antibody calculated as a percentage of the area of intact antibody from the overall area..... 141

Figure 4.7 HCP concentration (ng HCP/g mAb) for IgG1λ and IgG1κ, which were spiked into CS-CHO Null cell culture harvests collected on day 10, 12 or 14 of cell culture. The samples were subjected to different levels of shear (no shear (NS) = 0 mL/min in the CSD (□), low shear (LS) = 21 mL/min in the CSD (■), high shear (HS) = 41 mL/min (■)). 144

Figure 4.8 Gel electrophoresis image showing the levels of intact antibody – band at > 150 kDa – A) for different shear levels (flowrates mL/min) in the capillary shear device, hold (hold time in the cell culture material) and the use of DepF (Depth filtration); B) showing the electropherogram for lane 4 and 9 where antibody reduction was observed..... 146

Figure 4.9 Growth culture kinetics for ambr3 and ambr4 showing viable cell density (cells/mL) for A) ambr3 and B) ambr4 and cell culture viability (%) for C) ambr3 and D) ambr4. A description of the low, mid and high seeding density levels can be found in **Table 4.2**..... 148

Figure 4.10 Levels of intact antibody (%) vs A) cell culture LDH release (%) and B) Centrate LDH release (%) for different levels of shear ((■ – no shear (NS); ■ – low shear (LS) and ■ – high shear (HS)) for ambr4 harvests. 151

Figure 4.11 The predictive equations in terms of coded factors for A) titre (g/L); B) [solids] (% v/v) and C) [cholesterol] (mg/mL) and actual coefficients for all three models summarised in D). The statistics for the model are as follows adj. $R^2 = 0.82$ (titre model), pred. $R^2 = 0.76$ (titre model), k-fold $R^2 = 0.75$ (titre model); adj. $R^2 = 0.77$ ([solids] model), pred. $R^2 = 0.71$ [solids] model, k-fold $R^2 = 0.66$ [solids] model, adj. $R^2 = 0.82$ ([cholesterol] model), pred. $R^2 = 0.75$ ([cholesterol] model, k-fold $R^2 = 0.76$ ([cholesterol] model. The predictors for the equations are H.day – harvest day, S.density – seeding density and shear level (mL/min in CSD)..... 155

Figure 5.1 Structure of the decisional tool used for the recovery operation assessment..... 162

Figure 5.2 A schematic representation of a filter holder that can fit different filters of size X, Y and Z and can accommodate multiple racks (right-hand side)..... 170

Figure 5.3 A schematic representation of stainless steel domes of different diameters. 170

Table of Figures

Figure 5.4 Comparison of the contribution to the overall $\text{COG}_{\text{REC}}/\text{g}$ between centrifugation and the depth filtration operation for different manufacturing scenarios: yearly demand of 100kg, 500kg and 900kg and titre of A) 3 g/L, B) 6g/L and C) 9 g/L. The black bars describe the overall costs of the recovery operation consisting of the primary recovery (centrifugation) and secondary recovery (depth filtration). The white colour describes the direct costs for the centrifugation (Cent) or depth filtration step (DepF) and the dark grey describes the indirect costs for the steps. The pie charts for each titre and demand scenario show the distribution in costs between the centrifugation and depth filtration step. 185

Figure 5.5 Overall breakdown for the $\text{COG}_{\text{REC}}/\text{g}$ for different scenarios for A) low titre of 3g/L and low demand of 100kg/year; B) high titre of 9g/L and low demand of 100 kg/year; C) low titre of 3 g/L and high demand of 900 kg/year and D) high titre 9g/L and high demand of 900 kg/year. For the pie charts the white colour describes the material costs (including consumables and reagents), the black represents the labour costs and grey colour corresponds to the indirect costs. The process economics model was run in design mode using, stainless steel bioreactors, disc-stack centrifuge (Cent) and stainless steel domes for filtration (Dep F). 186

Figure 5.6 Comparison of the COG $\$/\text{g}$ between a depth filtration operation using stainless steel domes vs. filter holders for different manufacturing scenarios (left to right): low titre of 3 g/L and low demand of 100kg/year; high titre of 9g/L and low

demand of 100kg/year; low titre of 3g/L and high demand of 900kg/year and D) high titre of 9g/L and high demand of 900kg/year..... 189

Figure 5.7 Impact of pH and seeding density on A) and D) percentage change in COG from the optimum COG_{REC} (g/\$) = 4.89 marked with a star; B) and E) Bioreactor volume (L) **in blue**, titre in **green** and centrifuge size (L/h) in **purple**; C) and F) the [solids] (% v/v) **in blue** and discharge interval (s) **in purple** - the **yellow** box shows the conditions, where the solids discharge interval violates the 120s limit. The harvest day is set to 14, demand is set to 500 kg/yr, the centrifuge was sized based on flowrate, the filtration area is max 55m² per filter holder and the filter capacity is 300L/m²..... 193

Figure 5.8 Applying an improved approach to centrifugation sizing accounting for the impact of [solids] to investigate the impact of pH and seeding density on A) and D) percentage change in COG from the optimum COG_{REC} (5.2 \$/g); B) and E) Bioreactor volume (L) **in blue**, titre (g/L) in **green** and centrifuge size (L/h) in **purple**; C) and F) the [solids] (% v/v) **in blue** and discharge interval (s) **in purple** - the **yellow** box shows the conditions, where the centrifuge has increased in size to meet the max discharge interval of 120s. A); B) and C) conditions without a temperature shift and D); E) and F) conditions with a temperature shift. The harvest day is set to 14, demand is set to 500 kg/yr, the centrifuged was sized based on flowrate, the filtration area is max 55m² per filter holder and the filter capacity is 300L/m²..... 194

Figure 5.9 The impact of harvest day and seeding density on A) Bioreactor volume (in purple) and titre (in blue); B) [solids] (in blue) and centrifuge flowrate (in purple); the increase in COG_{REC}(%) compared to an optimum (marked with an asterisk(*)) for C) low shear and D) high shear conditions; and filter area (m², in dark blue) and filter capacity (L/m² in blue) for E) low shear and F) high shear. The max filter holder capacity is 33m²..... 196

Figure 5.10 Window of operation in grey for varying seeding densities and harvest days for a scenario A) without the use of predictive correlations for filter capacity, and [solids] using a fixed depth filtration filterability = 300L/m² and [solids] = 5%; G) with predictive correlations. The windows are constrained by B) and H) titre (g/L); C) and D) Throughput (kg/yr); D) and J) COG_{REC} (\$/g), E) and K) depth filtration area (m²) ; F) and L) product loss due to depth filtration capacity. The window in A) is constrained by B);C);D);E) and F) and the window in G) is constrained by H);I);J);K) and L). The process is based on Merck Millipore filter holder with max holder capacity of 33m², Culturefuge 300 with max flowrate of 6,000L/h and solids holding space of 20L and a bioreactor size of 10,000L. The yellow area indicates process constraints. HD is harvest day and SD is seeding density. 199

Figure 5.11 Contour plots for the recovery operation for a process with a high shear, showing the impact of seeding density and harvest day on A) COG_{REC} \$/g; B) Filter requirements (m²); C) Product loss (%) and D) Throughput (kg/year). The process is based on Merck Millipore filter holder with max holder capacity of 33m², Culturefuge

300 with flowrate of 6,000L/h and solids holding space of 20L and a bioreactor size of 10,000L.....201

Figure 5.12 Risk analysis showing the impact of seeding density and harvest day variation for different target harvest days on the probability of failing to meet target metrics - minimum throughput of 550 kg/year (black line —), maximum COG_{REC} of 7 \$/g (red line —), maximum loss due to the centrifugation step of more than 10% (blue dashed line - -), maximum product loss due to the secondary depth filtration of 10% (green dashed line- -) for a process using A) a small centrifuge with 6.7 L solids holding space and B) a large centrifuge with 20 L solids holding space. The orange dashed line (- -) shows the maximum acceptable level of risk for the target throughput and COG_{REC}.....204

Figure 6.1 Workflow for analysing the PSD data outputted from Vi-Cell XR. The raw data is extracted from the Vi-Cell XR in the form of CSV files and an algorithm in Matlab was used to pre-treat and structure the data for further analysis. PLS models were built for the pre-treated data using Jmp.....212

Figure 6.2 Percentage LDH release vs Vi-Cell XR viability measurements for the fresh harvest (no shear) described in **Table 6.1** for four different projects: Project null (GS-CHO Null) in dark grey (■), Project A in light grey (■), Project B in dark blue (■) and Project C in light blue (■). The red line (—) indicates 100% LDH release. All samples above 95% have been adjusted to 100%. The points below 100% LDH and

Table of Figures

60% viability (as outputted from the Vi-Cell) release were used to plot the grey line of best fit (---).215

Figure 6.3 Impact of shear on (A) apparent change in total cell number (TCN) as outputted from the Vi-Cell XR for various mammalian cell culture harvests for three projects and (B) the appearance of cell debris and dead cells clumps for high shear samples compared to no and low shear. Harvests from four different bench scale runs were collected on different days of cell culture: day 8, 10, 12 and 14 and subsequently subjected to low and high shear in the capillary shear device. The apparent total cell number change was calculated as a difference between the total cell number before and after shear.217

Figure 6.4 Particle size data distribution for ambr4 experiments as outputted from the Vi-Cell for 24 bioreactor runs with different target seeding densities and harvest days. The solid line depicts the mean of the PSD, the dotted lines depict the standard deviation for A) Day 5 (n=24), B) Day 8 (n=24), C) Day 10 (n=24). D) Day 12 (n=17) and E) Day 12 for various viability ranges (>85% viability and n=3; 72% to 82% and n=6; 62% to 67% and n=4; 24% to 36%and n=3)220

Figure 6.5 PLS model predicting LDH release using PSD data for the viable cells as outputted from the Vi-Cell. In A) the actual LDH release is shown by the bars, the filled squares depict the predicted LDH release for the dataset used to calibrate the model, while the empty circles show the predicted percentage solids concentration for the external validation (test) dataset. The different colour bars refer to different

projects - project null (■); project A (■); project B (■) and project C (■), $R^2Y = 83\%$ and $R^2X = 96\%$ and the R^2 for the test (external validation dataset) is 90%222

Figure 6.6 PLS model for [solids] with A) actual versus predicted [solids] and B) VIP plot with the predictors used in the model. In A) the actual [solids] are shown by bars, the filled squares depict the predicted solids concentration for the dataset used to calibrate the model, while the empty circles show the predicted percentage solids concentration for the validation dataset. The different colour bars refer to different projects (A – light grey and C – dark grey), $R^2Y = 81\%$ and $R^2X = 86\%$. TCN-total cell number (million cells/mL), VCN – Viable cell number (million cells/mL) , viab. – viability225

Figure 6.7 Comparison in time and volume daily requirement for ambr15 with 48 vessels for A) LDH release measurements using manual sampling and a colorimetric assay vs the novel PLS –based estimation and B) [Solids] measurements using manual sampling vs the novel PLS –based estimation. The assumptions for the calculations can be found in **Appendix (Table 6.3 A)**226

Figure 4.1-A Pilot scale centrifuge shear characterisation through LDH measurements in the pilot scale centrifuge at 120L/min and 7000 rpm and the capillary shear device at various flowrates for cell culture A (**Table 4.1**). The squares (■) indicate that the measurement was for the CSD device and the circle (●) is the LDH measurement for the pilot scale centrifuge – flowrate for that measurement is calculated using linear regression for LDH vs flowrate for the CSD. The colour

Table of Figures

indicates different hold times before measurement – white (hold=121 min), red (hold = 260 min) and blue (hold = 313 min). The total cell number was 17.63×10^6 cells/mL and the viability was 88.7%.....277

Figure 4.2-A Pilot scale versus mimic concentrates' filterability for the experiments described in **Table 4.1-A**.....280

Figure 4.3-A Comparison of pressure increase in A) and B) and the flux decline in C) and D) between large scale (■ LS) and mimic generated using the capillary shear device (● CSD) at the mimic conditions described before. The constant flux is at 100LMH for cell culture A, B), the constant pressure is at 10PSI for C) and 15PSI for D).....281

Figure 4.4-A Pilot scale centrifuge (MPBX404, Alfa Laval, Lund, Sweden) characterisation based on A) LDH release upon shear in the pilot scale centrifuge at 7000RPM (■) and 8000RPM (●) and for the CSD at flowrate between 30 and 45mL/min flowrate B) Comparison in the flux decline between the pilot scale at 8000RPM and mimic cenrtate at 41mL/min. The cell culture material was from a pilot scale run, harvested at day 15 (**Table 4.1**).....283

Figure 5.1-A Ratios between various disc-stack centrifuges design parameters A) bowl volume (L) vs flowrate (L/h); B) stopping time vs bowl volume (L) and C) WFI per discharge vs bowl volume (L).....284

Table of Figures

Figure 5.2-A The impact of centrifugation flowrate and bowl rotation speed on the levels of shear, operation time and clarification efficiency. Centrifuge LAPX404 used for the calculation.....285

Figure 6.1-A Actual vs predicted parity plot for the LDH release vs the PLS model selected in **Table 6.2-A**.....289

Chapter 1

1 Introduction

The rising pressures for developing cheaper mAb therapies highlights the need to drive the cost of manufacture down. In an effort to address this need the industry has pursued to increase upstream productivities often through higher cell densities or extended cell culture duration. However, the higher turbidity and solids content in these feed streams can pose significant challenges for the recovery operations and it is often not clear if the recovery steps can cope with the feed until the process is already at pilot scale. These synergies between upstream and the recovery operations bring the need to establish tools that will enable a holistic view of the upstream-recovery sequence in order to develop a more cost-efficient process overall. To address this challenge this thesis proposes a novel toolbox that builds on existing scale-down mimics, multivariate data analysis (MVDA) techniques and adapts a bioprocess economics model to incorporate experimentally derived predictive correlations to assess the COG and facility fit for different manufacturing scenarios.

The aim of this section is to provide the reader with the context and motivation underpinning the research. The literature review follows an inverted pyramid structure starting from a market overview and narrowing down to more specific and

technical research related topics. Thus **Section 1.1** gives a general overview of the sector highlighting how mAbs have established their presence on the market and the general approach to their manufacturing. The following **Section 1.2** describes the primary and secondary recovery operations. **Section 1.3** reviews studies on upstream optimisation with an emphasis on the impact of upstream parameters on primary recovery. **Section 1.2** and **1.3** give enough context for introducing upstream, centrifugation and depth filtration scale-down models in **Section 1.4**. **Section 1.5** introduces different multivariate data analysis techniques, process metrics and optimisation algorithms. **Section 1.6** gives an overview of different economics models and decisional tools applied in the modelling and optimization of biopharmaceutical manufacturing processes. The last section will focus on the research gap this thesis will aim to fill as well as the proposed experimental approach and objectives.

1.1 Industry overview

1.1.1 Antibodies: market overview

Therapeutic monoclonal antibodies (mAbs) are one of the leading classes of therapeutics accounting for one in five FDA approvals with the 100th mAb approved by the FDA in 2021 and expected revenue of \$300 billion by 2025 (Mullard, 2021; Lu et al., 2020). Mammalian cell lines are used to produce mAbs, with Chinese hamster ovary (CHO) cells established as the most commonly used expression system (Khan, 2013). Over the years these cell lines have been optimised to reach

high cell densities and product titres, from tens of mg/L to 10 g/L (Xu et al., 2020).

With the maturation of the sector, new market and regulatory challenges have emerged. Since some of the products have been on the market for over 20 years their patents have expired. This has enabled the emergence of biosimilars - therapies where the products are near identical to the original biologics; the first biosimilar antibodies were approved in September 2013 – Infliximab (Remsima, Celltrion Healthcare) (Ecker, et al., 2015). Since then 26 biosimilars have been approved by the FDA and 55 by the EMA (Gherghescu and Delgado-Charro, 2021; Royzman and Shah, 2019).

As the biopharma sector has developed and established best practices the regulatory bodies have also gained more understanding about the process, tightened their requirements and consequently introduced the concept of Quality by Design (QbD) approach to bioprocess development. This initiative encourages manufacturers to build the quality of the product in the process design through in-depth understanding of how key process inputs – often called Critical Process Parameters (CPPs) – are linked to important outputs e.g. product quality, safety and efficacy often termed Critical Quality Attributes (CQA) (del Val et al., 2010). Design of Experiments (DoE) is one of the key tools to facilitate the application of QbD (Yu et al., 2014). It is a paradigm shift from the one-factor-at-a-time (OFAT) approach to process optimisation to a systematic approach that implements statistical thinking at the very start of process development. Politis et al. (2017) present a summary of 38

publications showing the use of DoE for the development of pharmaceutical process. The DoE in combination with advanced statistical methods is used to define a design space for the process, which is a combination of the critical process parameters that have been shown to ensure the required product quality. This approach offers greater understanding about the process, which streamlines the introduction of process changes or dealing with deviations since no process re-validation is required as long as the process is operating within the design space. In that sense QbD offers a risk-based approach to process development, where the product quality is built into the process.

| Critical Path | Drug Development Cycle (Preclinical, Phase I-III) | | | | Market |
|---------------------|---|------------------------|----------------------------|--------------|-----------------------|
| Process Development | Process development | → Scale-up development | → Process characterisation | | Post-approval changes |
| Constraints | Time | Capacity | Budget | Regulatory | Skilled labour |
| Metrics | Speed | Ease of scale-up | COG | Facility fit | Robustness |

Figure 1.1 Key stages, constraints and metrics in the drug development cycle, adapted from Farid (2012)

The more stringent regulatory environment together with the rising competition from biosimilars - increasing number of alternative biologics on the market - and the fact that similar therapy targets are being investigated by more than one company increases the pressure to deliver cost-effective solutions for biologics manufacturing

(Farid, 2012; Li et al., 2010). Biosimilars have shorter times for approval - 8 years compared to 12 for original biopharmaceuticals – and lower development costs of 100 to 200M \$ compared to about a 1,000M \$ for original products (Agbogbo et al., 2019). The emergence of biosimilars puts emphasis on the cost of manufacture as the selling price is driven down by the increase in competition (Shukla et al., 2017).

As a result key decisions about portfolio management and metrics such as COG (Cost Of Goods), speed to market and facility utilisation are becoming central to a company's success. Furthermore, the weight of importance of different metrics changes as the product advances through the pipeline. **Figure 1.1** shows that while in the initial stages of process development the speed is very important in order to be able to assess a number of drug candidates, it is the COG and facility fit, which are more important at the late stages of clinical trials. Once the product is launched on the market process robustness is of utmost importance for regulatory compliance.

This complex market environment has pushed towards streamlining process development, which involves implementing similar manufacturing strategy across different products. This industry approach is widely known as platform manufacturing and it is going to be discussed further in the following section.

1.1.2 Platform manufacturing process for CHO cell derived therapies

A typical mAb platform process flowsheet is presented in **Figure 1.2**. The manufacturing process starts with a fed-batch production bioreactor that runs over a period of around two weeks. This part of the process usually uses mammalian cell

culture; in 2015 all but three mAbs were produced in this expression system (Ecker et al., 2015). The cell culture is followed by clarification – typically using disc-stack centrifugation - and depth filtration. At this stage the aim is to remove the cells, cell debris and colloidal material. The clarification is followed by membrane filtration and then followed by Protein A that captures the antibody, while the polishing chromatographic steps – for instance, CEX (Cation Exchange Chromatography) and AEX (Anion Exchange Chromatography) – ensure the removal of HCPs (Host Cell Proteins), DNA and other adventitious species e.g. viruses, high and low molecular aggregate species (Sisodiya et al., 2012).

Economic drivers have led to improvements in different steps. For instance, protein A chromatography is one example, where industry has pushed to reduce costs and as a result fast flow resins have been developed that can withstand multiple cleaning cycles and increase throughput and binding capacity (Curling, 2009; Gagnon, 2012; Joseph et al., 2006). In recent years, to further increase throughput and reduce processing time, membrane chromatography has been developed as an alternative to traditional packed bed chromatography (Boi et al., 2020 and Liu et al., 2016).

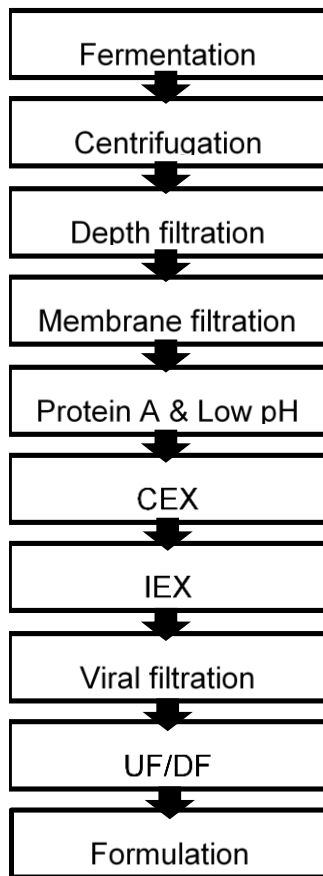


Figure 1.2 Typical mAb manufacturing platform (Kelley et al., 2009; Shukla et al., 2007; Curling, 2009)

The increase in yield in the upstream process and the concomitant increase in cell culture densities have also inevitably put pressure on the purification train – for instance, requiring columns with higher loading capacity - and on the recovery step, which needs to clarify harvests with higher solids content (Gimenez et al., 2015; Gupta et al., 2020 and Singh et al., 2013; lammarino et al., 2007). It is also important to note that the recovery step can also impact on the subsequent capture step. For instance, high shear in the centrifugation step can increase the amount of cellular

debris and lead to filter fouling and release of intracellular species with impact on product quality – e.g. antibody reduction.

This current approach to flowsheet development has two main consequences. On the one hand, any new manufacturing process has to fit the existing manufacturing platform. Second, improvements in individual unit operations may shift the manufacturing bottlenecks. Therefore, in order to efficiently optimise the process, it is important to gain understanding about the interactions between the different steps. The proposed integrated framework for the upstream-recovery operation in this thesis aims to offer a new approach to addressing this issue.

1.2 Current recovery operations

In the previous section the role of the recovery operation was presented in the context of the whole bioprocessing flowsheet. Here the focus will be on the different options for primary and secondary recovery with their relevant advantages and disadvantages. Furthermore, the centrifugation and depth filtration steps are going to be discussed in detail since this sequence of operations is to form the basis for the integrated scaled-down upstream-recovery platform applied in the thesis.

1.2.1 Recovery sequence selection

The main purpose of the recovery step is to deliver a particle-free feed for the chromatography column. This is usually achieved via a two-step process. The first step removes cells and large cell debris – primary recovery – typically centrifugation or depth filtration, while the subsequent step removes smaller particulates and

colloid material – secondary recovery – often depth filtration. This two-step process is usually followed by an absolute membrane filtration operation with a nominal pore size of 0.1 μm , 0.25 μm or 0.45 μm to reduce residual turbidity.

However, there are a number of alternatives for the recovery step and the choice will often depend on a number of factors such as scale of operation and the properties of the harvested broth – cell density and particle size distribution. For instance, centrifugation is often the method of choice for primary recovery for processes above 2000L scale while microfiltration or primary plus secondary depth filtration are often the preferred option for smaller scales (Shukla and Kandula, 2009). Centrifugation can also be preferred due to the relative ease of scale-up, high solids holding capacity and throughput and lower direct costs (Shukla et al., 2007; Gupta et al., 2020). In the following paragraphs a brief summary is given of the advantages and disadvantages of different recovery steps alternative to depth filtration and centrifugation.

Microfiltration in the form of tangential flow filtration (TFF) is a competing technology for clarification but it is very sensitive to the feed properties such as cell density, viability and medium composition; it requires a feed that contains less than 3% solids to achieve desired product stream concentration (Tebbe et al., 1996; Liu et al., 2010). Microfiltration is primarily adopted for perfusion processes (Gupta et al., 2020). It can be operated using cassettes or hollow fibres. The advantage of microfiltration over continuous centrifugation is that the stream is clarified to a degree

where it only requires minimal filtration after that. One of the main disadvantages when operated in batch mode is the need to dilute the product stream to increase the yield (van Reis et al., 1991). Another disadvantage of this method is the creation of a polarised layer (Shukla and Kandula, 2009). This phenomenon is linked to the accumulation and concentration of colloidal suspension (consisting of macromolecules and particles above 1 μm) at the membrane surface (Bacchin et al., 2002). When this occurs the membrane is less permeable to the solute (usually water) due to high osmotic pressure and consequently this leads to the formation of the so called gel layer and fouling of the membrane. The fouling of the membrane has also been linked to the filtration flux. Van Reis and Zydney (2007) showed that there is a critical flux, above which filter fouling occurs. The flux limitation and the lower filter capacities for high-solids feeds mean that extensive filter area and longer processing times are required for difficult to clarify feeds (e.g. high solids and turbidity) and large fermentation volumes (e.g. 10,000L broths). Van Reis and Zydney (2007) report that hollow fibres (174m²) and flat sheet (186m²) have been used for the large-scale clarification of proteins from high solids CHO cell culture with relatively high yield and the possibility to re-use the membrane.

Alternating tangential flow (ATF) systems are often applied for the continuous harvest of biologics linked to perfusion bioreactors (Clincke et al., 2013; Karst et al., 2016; Kelly et al., 2014). The ATF shows lower shear than TFF due to the back and forth liquid flow achieved using a diaphragm pump (Wang et al., 2017). Some of the main challenges with ATF is the filter fouling and product retention in the membrane,

which can lead to significant product losses of more than 43%, depending on the membrane pore size, material and the overall process – for instance cell viability (Su et al., 2021).

The harvested cell culture can be pre-treated to facilitate the clarification step. Common approaches include precipitation and flocculation. Precipitation aims at lowering the solubility, which can be achieved by varying the pH, conductivity or the addition of precipitates, while flocculation causes particles to clusters, which could be via non-ionic interaction of negatively charge cells and cellular debris, for instance (McNerney et al., 2015; Singh et al., 2016). A number of studies have demonstrated that the flocculation can enhance the clarification step through decreasing the turbidity of the feed, increasing the filter solids holding capacity and reducing the overall filter area requirements (Hadpe et al., 2020; Kang et al., 2013; McNerney et al., 2015; Riske et al., 2007; Schmitt et al., 2017)

Another alternative for cell broth clarification is expanded bed adsorption chromatography (EBA). It represents an integrated step for product recovery and capture (Roque et al., 2004). Moreover, it allows feeds with high solids content and it is not prone to clogging and fouling (Russel et al., 2007). However, its use is limited due to issues related to uniform flow distribution within the column.

A more recent innovation in the clarification of mammalian cell cultures is the acoustic wave separator. Hong et al. (2020) highlights that this approach can reduce costs, labour and levels of shear compared to a centrifugation operation. In this type

of separators the particles get trapped by the ultrasonic waves, they coalesce and fall due to gravity. Details about different approaches to acoustic wave separators can be found in various publications (Banerjee et al., 2021; Somasundaram et al., 2018; Wu et al., 2019).

In the following sections centrifugation and depth filtration based recovery steps are to be discussed in detail. To better understand their operation, the main parameters that impact their performance are going to be elucidated.

1.2.2 **Disc-stack centrifugation**

Disc-stack design centrifugation coupled with depth filtration is ubiquitously applied for the solid-liquid separation of mammalian cell culture harvests. The choice of the centrifugation operation is driven by the relative ease-of-scale-up for the step and its ability to cope with a wide range of CHO cell harvests in terms of solids concentration ([solids]) and particle size distribution (PSD) compared to alternative filtration technologies.

The design characteristics of the centrifuge have a direct impact on its performance. One such important design feature is the centrifuge inlet zone where the feed is accelerated to the bowl speed – the centrifugal force can exceed 12 000g (Joseph et al., 2016). It has been demonstrated that this zone can generate high levels of shear; the amount will depend on the inlet configuration and this shear could lyse the shear-sensitive mammalian cells. The cell lysis can increase turbidity levels and challenge the subsequent filtration operation and lead to the release of intracellular

species, which can affect the product quality such as glycosylation pattern and product degradation – antibody reduction at the disulfide bridge (Aucamp et al., 2014; Tebbe et al., 1996; Trexler-Schmidt et al., 2010). To reduce the level of shear, centrifuges have been developed with flooded (hydro-hermetically sealed) inlet, which exerts less shear when the cells are accelerated to the speed of the bowl (Aucamp et al., 2014; Tebbe et al., 1996). Tait et al. (2009) showed that typical energy dissipation rates in the feed zone of an industrial centrifuge with a hermetic feedzone are equal to $0.019 \times 10^6 \text{ Wkg}^{-1}$ and non-hermetic design $0.37 \times 10^6 \text{ Wkg}^{-1}$ respectively.

The mechanism used for solids discharge is another important centrifuge design characteristic. There are two main approaches for solids discharge – continuous solids discharge and intermittent solids charges. In the case of continuous discharge the solids move upwards through channels and are continuously discharged through nozzles (Richardson and Walker, 2018). In the case of intermittent discharge the solids are discharged periodically (e.g. when 50 to 70% of the bowl is full) – either through full or partial discharge, in which case water can be used to push the sediment (Roush and Lu, 2008; Shukla and Kandula, 2009). One of the main challenges with intermittent discharge is the creation of aerosols, which can cause cell damage (Hundley and Königsson, 2020).

Changes in the centrifuge design and process setup upon scale-up can significantly impact on the process performance. For instance, Pohlscheidt Michael et al. (2013)

showed that the bowl speed may need to change to meet clarification requirements and the flowrate may need to be adapted to meet processing times. The same study showed increase in cell damage (expressed as LDH release) due to the use of a drain vessel with a different piping configuration (a different heat exchanger than the small scale process).

The achieved clarification in the centrifuge will affect the subsequent stages. For example, the carry-over of colloidal material in the supernatant of a centrifuge will impose a larger load on the guard filter, which is placed before the chromatography columns or will even impact on the columns themselves (Chan, et al., 2006).

This section showed that there are many factors that impact the centrifugation process - centrifuge's designs (hermetic, non-hermetic, nozzle versus intermittent discharge), centrifuge's operation (different bowl speeds and flowrate), the scale-dependent process setup (using heat exchanger). The complexity of the step highlights the importance of developing scale down-models and gaining understanding about the operation early on in the development cycle.

1.2.3 Depth filtration

Depth filtration can be applied for both primary and secondary recovery. The primary recovery filter has an open pore structure (pore size range of up to 10 μ m) and its purpose is for the removal of cells and cell debris while the secondary filter has tighter structures (between 0.1 to 4 μ m) and retains colloidal material (Liu et al. 2010; O'Brien et al. 2012). One of the main route of product loss occurs through

entrapment in the filter bed (Sampath et al., 2014). The path of the particles and their retention in the filter media is described in **Figure 1.3**.

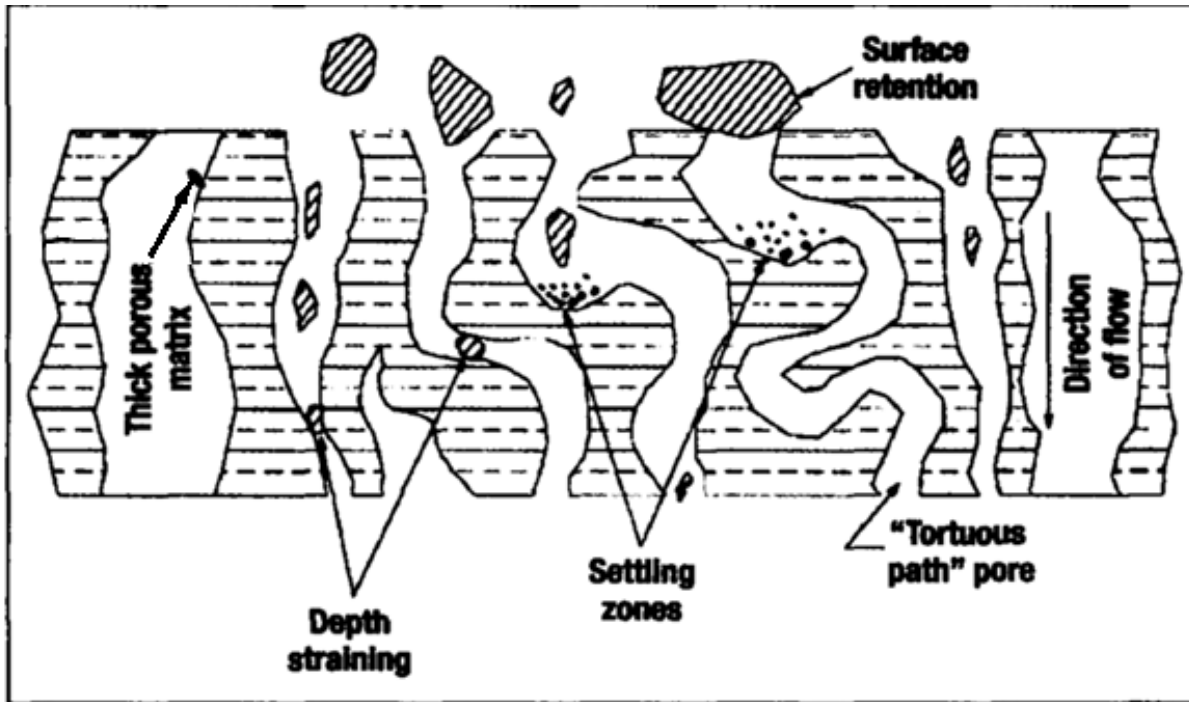


Figure 1.3 Schematic representation of the particles' journey through the depth filter (Shukla and Kandula, 2009)

Depth filters are usually made of cellulose or propylene fibres and the addition of filter aids - such as diatomaceous earth, perlite and activated carbo that can reduce the fouling - and an ionic charged resin binder that confers positive charge to the media and can therefore bind negatively charged impurities (Liu et al., 2010; Nejatishahidein et al., 2020; Wang et al., 2006; van Reis and Zydney, 2007; Shukla and Kandula, 2009; Russel et al. 2007; Yigzaw et al. 2006). Thus depth filtration achieves separation through both adsorption and size exclusion.

As mentioned above, some of the filters contain naturally derived components (e.g. cellulose); it is important to note that the cellulosic filter manufacturing is a wet – laid process that does not lead to the creation of uniformly distributed porous matrix, which is translated into high degree of variability in the filter performance (Yavorsky et al., 2003). However, the synthetic depth filters (e.g. polypropylene and non-woven) offer more consistency and reduce the impurities (Nguyen et al., 2019; Gupta et al., 2020).

The flow in the filter can be described through Darcy's law which correlates the pressure drop to the flow rate

$$Q = \frac{dV}{dt} = \frac{\Delta P A}{\mu R_m} \quad (1.1)$$

where Q is the rate of filtration (m³/s), μ is the dynamic permeate viscosity (N s m⁻²), A is the filter area (m²), R_m is the membrane specific resistance (m⁻¹), ΔP is the pressure drop (Pa) and V is the volume of fluid passing through the filter (m³) for time t (s) (Reynolds et al., 2003; Bolton et al., 2006). **Equation (1.1)** shows that the rate of filtration will depend on the membrane specific resistance as well as on the feed properties such as viscosity. Furthermore, the increase in rate of filtration can be achieved either through increasing pressure or flow rate.

The depth filtration step has four main modes of operation: constant-pressure, constant-rate and variable-pressure or variable-rate filtration (Reynolds et al., 2003). The depth filtration step at scale is usually performed at constant flow until a maximum pressure (P_{max}) is reached and the filter capacity is often given in terms of

litres per filter area (Pegel et al. 2011; Sampath et al. 2014). However, filter capacity can be calculated using constant pressure operation and estimating the value of V_{\max} (maximum volume of filtrate per filtration area, calculated using the pore-constriction model of filter fouling as described in **Section 2.2.2**). At large scale the filtration operation is typically set up as a stack of multiple lenticular discs. This often leads to pressure increases along the liquid path which is hard to predict and model (Collins et al., 2009) (**Figure 1.4**).

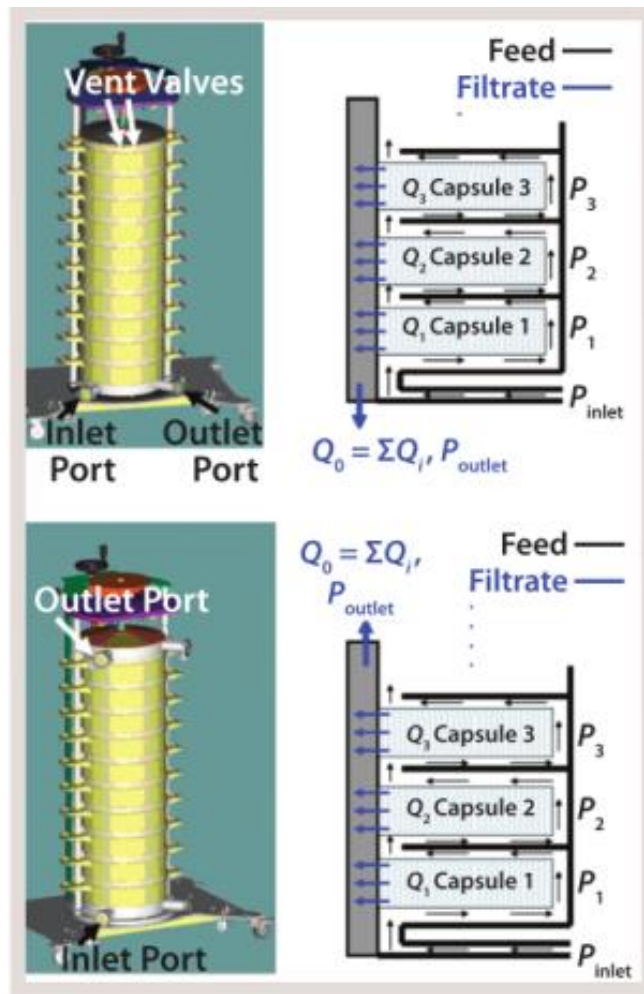


Figure 1.4 Depth filter flow path for top and bottom outlet configuration (Collins et al., 2009)

1.3 Upstream optimisation and the impact on recovery step

In this section the focus is first on studies that investigate the impact of different parameters on upstream performance – mainly in terms of productivity, cell growth and product quality. In the second subsection (**Section 1.3.2**) the review analyses studies that consider the impact of varying upstream parameters and cell culture properties on the recovery performance.

1.3.1 Approaches to upstream optimisation

One of the main objectives of upstream optimisation is to maximise fermentation titres (mAb g/L) while maintaining the desired product quality (Li et al., 2010; Shang et al., 2021; Xu et al., 2018; Zhang, 2009). Therefore, process optimisation initiatives are often seeking to increase cell specific productivity (q_p) or the concentration of viable cells (Meleady et al., 2011; Schellenberg et al., 2022; Yao et al., 2021).

Process intensification and continuous processing offers opportunities for reaching higher productivities and reducing facility footprint and thus driving the COG of manufacture down (Chen et al., 2018). Recent studies have reported productivities reaching 100 pg/cell/day and cell densities of 200×10^6 cells/mL for perfusion processes (De Jesus and Wurm, 2011; Zhang et al., 2015) and more than 5 to 10 g/L for a fed-batch process (Handlogten et al., 2018; Kelley et al., 2018; Shukla et al., 2017).

Other common approaches for increasing cell culture productivity are through media and feeds optimisation, cell line engineering and changes in the physiochemical (e.g.

pH and temperature) and operating conditions (feeds initiation). There are also some alternative novel approaches such as the one proposed by He et al. (2022), where the titres were increased through the introduction of re-cloning strategy for late lead clone screening from an established research or working cell bank.

The current section focuses on providing an overview of studies linking bioreactor physicochemical conditions to upstream performance. **Table 1.1** summarises reported results from various studies investigating the impact of pH, temperature, osmolality and feeding strategy on the cell culture performance. From this analysis it is apparent that these parameters have an impact on productivity, cell viability, cell growth, metabolism and impurity levels.

An observed cell culture response may be the result of an underlying relationship between operating parameters e.g. lowering temperature increases the oxygen solubility (Darja et al., 2016). There are other of studies reporting similar relationships, where the change in one parameter inadvertently alters other parameters, which in turn impact the process. For instance, according to Trummer et al. (2006) increased temperature and pH leads to higher glucose consumption and lactate production, which is detrimental to both cells and product. Another parameter, which is often studied considering its link to other parameters is pCO₂. Elevated pCO₂ is suspected to alter the pH within the cell even if the pH in the bioreactor is controlled, which leads to changes in the cell metabolism (Kimura and Miller, 1996). Furthermore, bioreactors are often controlled through the addition of

sodium bicarbonate, which means that an increase in $p\text{CO}_2$ is associated with higher osmolality levels (Zanghi et al., 1999). According to Zhu et al. (2005) when there is both elevated $p\text{CO}_2$ and osmolality the negative effect on the cells is much larger in terms of cell growth and viability than when each is present individually.

There are also cases where changing one parameter changes the impact of another parameter on the process, which means that there is an interaction between the parameters. For instance, Yoon et al. (2005) observes that the impact of pH (6.85-7.80) increases with decreasing temperature (37.0°C to 32.5°C). According to the same study no lag phase is observed at 37°C and the maximum cell growth is more tightly correlated with the pH. Furthermore, the study shows that although cell titre and viability might increase, the product quality may be negatively affected by higher pH (7.2) and lower temperature (33°C) due to the formation of aggregates. Han et al. (2009) investigated the interaction between temperature and osmolality. It was demonstrated that the combined effect of low temperature (32°C) and high osmolality (470 mOsm/kg) leads to significant decrease in product degradation.

These parameters interactions highlight the need for holistic view of the process based on the investigation of the impact of individual parameters as well as interactions between parameters for enhanced understanding about the design space in line with the QbD approach.

Table 1.1 Examples from literatures showing the impact of bioreactor physico-chemical conditions on the upstream performance.

| Parameter | Metabolism | Cell growth | Cellular Impurities | Cell viability | Product quality | Volumetric productivity | Brief description of parameter change | Source |
|------------------|------------|-------------|---------------------|----------------|-----------------|---------------------------------------|---|--------------------------------|
| Temperature | | | | ↑ | | ↑ | Temperature shift day 3 from 37°C to 33°C | (Rameez et al., 2014) |
| | x | | ↑ | ↑ | | ↑ | Temperature shift day 6 to 32° leads to prolonged stationary phase | (Tait et al., 2013) |
| | x | ↓ | | ↑ | | ↑ | Temperature shift at 60h to 33°C | (Bollati-Fogolin et al., 2005) |
| | ↓* | | | ↓ | | ↑ | Temperature shift to 34°C and 31°C | (Rezaei et al., 2013) |
| | x | ↑ | ↓ | ↑ | | ↑ | Cell culture temperature below 37°C (between 30°C and 35°C) | (Furukawa and Ohsuye, 1998) |
| | ↓* | ↓ | ↑ | | | | Cell culture temperature of 33°C | (Hwang et al., 2011) |
| | ↓* | ↓ | | ↑ | | ↑ | Cell culture temperature of 32.5°C | (Yoon et al., 2005) |
| | X | ↓ | | | X | X | Lowering temperature to 30°C and 32°C Increasing temperature to 39°C | (Trummer et al., 2006) |
| pH | ↑ | ↑ | | | | pH of 7.00 to 7.20 | | |
| | | x | | | | ↑ Lowering pH to 6.80 | | |
| | | | | | | ↓ Increase in pH from 6.85 to 7.00 | (Rameez et al., 2014) | |
| | x | | | ↑ | | ↑ pH increase to 7.00 – 7.20 | (Yoon et al., 2005) | |
| pCO ₂ | | ↓ | | | | | Increase in pCO ₂ from 50mmHg to 150mmHg | (Zhu et al., 2005) |
| | | | | | ↓ | | Increase in pCO ₂ | (Zanghi et al., 1999) |
| | | ↓ | | | | | Increase in pCO ₂ | (Kimura and Miller, 1996) |
| Feeding strategy | | ↑ | | | | ↑ | Intermittent feeding vs bolus feeding | (Rameez et al., 2014) |
| | | ↑ | | ↑ | | ↑ | Feeding strategy based on glucose consumption rate | (Toussaint et al., 2016) |
| Osmolality | x | ↓ | | ↓ | | ↑ | Increase in osmolality from 310mOsm/kg to 450mOsm ³ | (Zhu et al., 2005) |
| | | ↓ | | | ↑ | ↑ | Biphasic increase in osmolality to 470 mOsm/kg | (Han et al., 2009) |

↑= increase
↓= decrease
X = impact

* Glucose consumption and lactate production

1.3.2 Impact of upstream parameters on recovery performance

Being the first step in the production process upstream has the potential to impact all subsequent downstream operations. Currently, there is a limited number of studies linking upstream parameters to the recovery performance and in particular primary recovery through centrifugation and secondary recovery through depth filtration. This section will provide a review of literature linking upstream parameters to recovery.

One such study investigating the impact of cell culture conditions on disc-stack centrifugation was conducted by Iammarino et al. (2007). It showed that the performance of the centrifuge was negatively impacted by lower viabilities and higher cell densities. Furthermore, the cell density had greater impact with decreasing cell viability. According to the same study this impact extends to the secondary depth filtration step where the same trends were observed.

It is important to note that cell density and viability are an output from the cell culture operation and hence they cannot be directly controlled. Therefore, there is a need to first understand what leads to the difficult to clarify cell culture harvests and then establish the direct relationship between the upstream parameters and recovery operation.

Tait et al. (2013) investigates the impact of upstream mild hypothermic conditions on downstream operations. The study reveals that lowering cell culture temperature leads to prolonged cell viability and less sensitivity to shear stress. The morphological cell analysis showed that the cells were mostly in G1/S phase and consequently larger in size than the cells in G2 (cultured at 37°C). However, the

study demonstrated that it is the cell culture hypothermic conditions and not the size that drives the higher cell viability and recovery. One hypothesis is that changes in the cell membrane occur as a result of cold induced signalling pathways, a phenomenon known as homeoviscous adaptation. According to this theory cells, including mammalian cells, have pathways that lead to cell membrane rigidization at low temperatures (Los and Murata, 2004). Another finding was that there were a lot fewer cells at late apoptotic stages at low temperature (32^oC) than at high temperature (37^oC) and late apoptotic cells although still viable are more susceptible to shear stress (Tait et al., 2013). According to Chan et al., (2006) the sensitivity of the cells is proportional to the mean bursting membrane tension, which tends to increase during the rapid growth phase resulting in cells which are more resilient to disruption. Furthermore, the study investigates short term temperature reduction prior to harvest and demonstrates that it significantly improves recovery for low viability cultures.

Cell culture age has also been investigated for its impact on primary recovery. According to Lau et al., (2013) the number of non-viable cells increases as the culture ages and that poses higher requirements for the centrifugation and depth filtration step.

Another parameter that may be linked to primary recovery performance is osmolality. The impact of osmolality on CHO cells was investigated by Sarkadi et al. (1984). The study demonstrated that hyperosmotic conditions lead to cells shrinkage which may consequently impact primary recovery performance.

There are a limited number of studies that aim at optimising both upstream and harvesting and elucidating the impact of upstream parameters on primary recovery (King et al., 2007; Salte et al., 2007). Optimising the upstream operation disregarding the impact of cell culture properties on the recovery performance may lead to broths that are difficult to harvest and clarify e.g. high cell density, low viability, late apoptotic stage etc. The current study aims at filling this gap through investigating the impact of cell culture parameters and their interactions with primary (disc-stack centrifugation) and secondary (depth filtration) recovery.

Scale-down and high throughput technologies in upstream, centrifugation and depth filtration are required to enable the investigation of the impact of upstream conditions on the cell culture and recovery performance. The following section provides an overview of the different approaches and technologies applied in the field for scaling down the unit operations.

1.4 Scale-down models for upstream and recovery

The development of industrial scale processes is costly and time-consuming and typically occurs at a stage where the speed of process development is key to getting the product through validation to market (Rameez et al. 2014; Chan et al. 2006). Therefore, the scale-down models are important first because they enable rapid and cost-effective assessment of the new drug candidate's compatibility with the platform process as well its financial feasibility. Second, it informs the large scale manufacturing process development, providing insight into how potential changes can impact the process at a later stage (Tait, et al., 2009).

1.4.1 Upstream scale-down technologies

Early upstream process development employs small scale systems that allow screening different clones and physicochemical conditions. Different systems offer different advantages in terms of number of experiments that can be performed in parallel, process monitoring and control and scalability. There are broadly two main approaches – using shaken or stirred tank systems, which are going to be discussed in more details below.

1.4.1.1 Shaken scale-down models

Initial screening in almost 90% of experimental trials used to be traditionally carried out in 50-500mL flasks (Nienow et al., 2013). Although they offer high throughput capability there are still challenges associated with the pH, DO and agitation control (Moses & Manahan 2012; Rameez et al. 2014). The use of multiwell plates is also applied to inform process design. Furthermore, various relationships have been established for this format, for calculating the power number, flow conditions: “In phase” and “Out of phase”, gas liquids mass transfer coefficients (kLa) and critical shaking frequency (N_{crit}) (Büchs et al. 2000; Doig et al. 2005; Hermann et al. 2003; Micheletti et al. 2006). More recently there have been reports of the use of 96 well-plates (96w) with automated liquid handler allowing up to 384 clones to be screened (Wang et al., 2018).

1.4.1.2 Advanced Microscale Bioreactors (ambr™)

In recent years small scale bioreactor systems have established as industry standard for screening studies during clone selection and optimisation and more recently as scale-down models for the GMP process (Sandner et al., 2018). The most commonly

employed bioreactor is the automated single-use stirred microscale bioreactor such as - ambr® (Sartorius Stedim, Germany). The ambr system is offered in two different scales ambr15 (**Figure 1.5**) with a working volume of 15mL and ambr250 with a working volume of 250mL. The bioreactors are equipped with a Rushton or marine impeller depending on their application: microbial culture or mammalian cells respectively. The number of vessels that can be run simultaneously is fixed for the ambr15 and it is 24 for the system with 2 culture stations (CS) and 48 when there are 4 CS available. One limitation of the ambr system is that all vessels in a culture station have to be subjected to the same agitation and temperature (Rameez, et al., 2014).

There are a number of studies characterising the ambr15 system and demonstrating its capability to reproduce results from 3L, 15L and 200L bioreactor when comparing the impact of changing pH, temperature and DO for the different scales on growth profiles and titre (Hsu et al., 2012; Janakiraman et al., 2015; Moses & Manahan 2012; Nienow et al. 2013). Most recently the platform has even been applied to mimic a perfusion cell culture using cell settling (Jin et al., 2021; Sewell et al., 2019).

Some of the disadvantages that have been highlighted in literature are the higher specific productivity observed, the fact that it only does bolus additions and consequently cannot be used for feed optimisation. Furthermore, the temperature control in the bioreactor depends on the ambient temperature, higher P/V (W/m^3) values are observed when scaling up at constant tip speed (for the ambr15 system which operates a transient rather than turbulent flow regime) and the bioreactor is

characterised by poor mixing at the air-liquid interface (Nienow et al. 2013; Moses & Manahan 2012; Rameez et al. 2014).

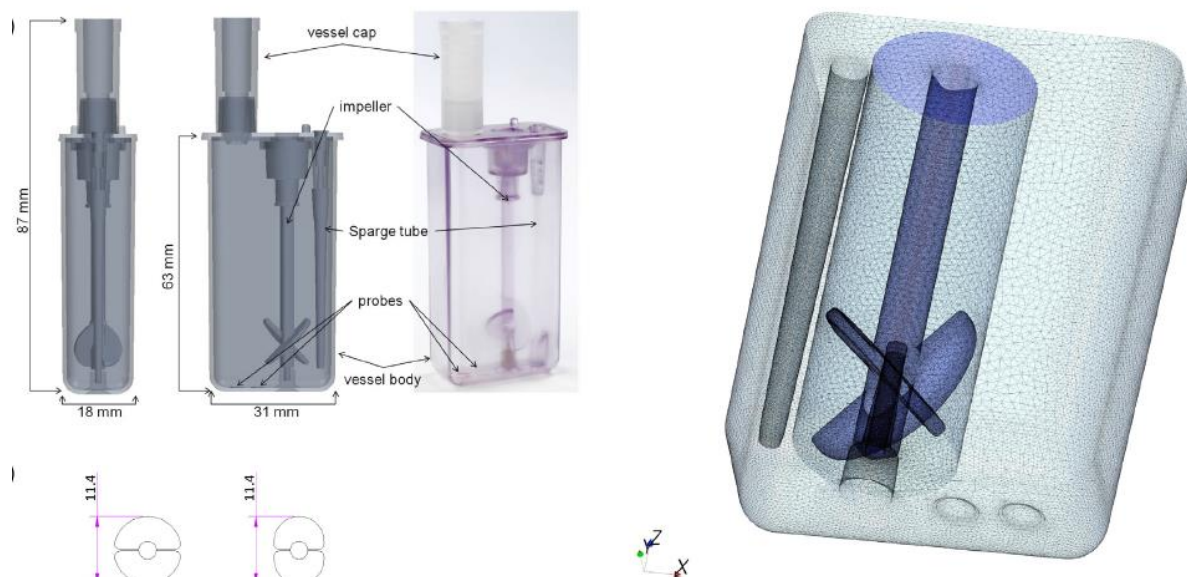


Figure 1.5 Schematic representation of the ambr® 15 Bioreactor (Nienow et al., 2013)

Since the ambr is a good mimic of the large scale operation and it is able to simulate various physico-chemical conditions, it is going to be implemented in this study for generating cell culture broths with different properties.

1.4.2 Scaling down the recovery operation

This section provides an overview of different strategies that have been employed for scaling down the centrifugation and filtration operation with emphasis on the type and scale of devices that were used and their relevant throughput.

1.4.2.1 USD Centrifugation

Mimicking large and pilot plant centrifugation operation at small scale is associated with a number of challenges. First the, feedzone of an industrial centrifuge is linked to high levels of shear stress and second, there is a characteristic flow pattern

between the discs, which disturbs the sedimentation process. The main approach to ultra-scale-down (USD) centrifugation is therefore, the decoupling of the shear stress experienced at the centrifuge inlet and the clarification achieved at different bowl speeds and flow rates. The damaging shear forces are typically mimicked by a rotating shear device (RDS) or capillary shear device (CSD), while the clarification is carried out using benchtop, multiwell plate or swinging bucket batch centrifugation (Boychyn et al., 2004; Lau et al., 2013; Maybury et al., 2000; Tait et al., 2009; Westoby et al., 2011).

A major factor that impacts the particle size distribution is the shear stress at the inlet of the centrifuge. Levy et al. (1999) developed a rotating disc shear device (RDS) that mimics the shear stress experienced during downstream processing. The focus of the study was the impact of shear on super-coiled plasmid DNA during plasmid-based gene therapies manufacturing. The shear rate (s^{-1}) was calculated as a function of Reynolds number and the rotational speed, and the value only corresponded to the shear at the tip of the impeller. Following on that work Boychyn et al. (2001) used computational fluid dynamics (CFD) to characterize the shear stress at the inlet of an industrial multi-chamber centrifuge. Later Boychyn et al. (2004) applied CFD to evaluate the shear in a disc-stack centrifuge configuration. In both studies conditions in the RDS were identified that generated the same energy dissipation rates (W/kg) as in a large scale centrifuge. The RDS device has later been successfully used in a number of studies for evaluating centrifugation performance (Aucamp et al., 2014; Hutchinson et al., 2006; Tait et al., 2009; Tustian et al., 2007)

Westoby et al. (2011) proposed an alternative to the RDS - a CSD. Furthermore, a correlation was developed that links turbidity and angular velocity for the pilot scale centrifuge and turbidity and energy dissipation rate for the CSD. One of the main advantages of the CSD is that it eliminates the need for a CFD since the energy dissipation rate can be calculated directly using the device simple dimensions. Joseph et al. (2016) also applied different levels of shear (energy dissipation rates of 1.2 to 10.7×10^5 W/kg) using the CSD to mimic the shear experienced by CHO cells at the inlet of an industrial disc-stack centrifuge. Furthermore, the study compared the shear between the RDS and CSD based on equivalent lactate dehydrogenase release (LDH) between the two devices. Finally, the study showed that it is possible to use the CSD device to generate centrate comparable to the centrate from a large scale centrifuge based on its filterability and turbidity. RDS and CSD have also been used to investigate the shear endured during downstream processing: disc-stack centrifuge discharge, passage through pumps and valves (Aucamp et al., 2014; Chan et al., 2006; Levy et al., 1999).

In the current work a CSD is to be applied due to its ease-of-use and relative small amounts of material required (10mL) compared to the 20mL for the RDS.

1.4.2.2 **USD filtration: modelling and scale-down**

Filtration is usually scaled down linearly based on feed volume per filter area. Small scale experiments are typically performed using batch laboratory tests on the same filter geometry – for instance, for depth filtration using small scale filter housing from PALL® – minimum area of 12cm² (Kang et al., 2013) or Millipore® 23cm² mini pod system (Riske et al. 2007; Sampath et al. 2014; Yavorsky et al. 2003; Yigzaw et al.

2006). The experiments can be performed applying constant flow or constant pressure. The constant pressure is typically achieved through air compression or vacuum while the constant flow can be performed via an ÄKTAexplorer (Cytiva, Marlborough, US) system, for instance. Performing the experiments at constant flow requires more material than the constant pressure, therefore, the latter is often the method of choice for depth filtration bench scale studies. However, predicting the constant flow filtration performance using constant pressure experiments can be challenging. To address this challenge, Goldrick, Joseph, et al. (2017) proposed an approach that correlates the coefficient of the models describing the fouling mechanism (e.g. Cake-Adsorption) in the constant pressure filtration to the filter capacity at constant flow. There is only a small body of literature dealing with USD filtration. For instance, Reynolds et al. (2003) showed the use of an USD continuous filtration device to model flux rate and cake formation. Chandler and Zydney, (2004) used small scale, down to 96-well plate with 0.3cm^2 area for filtration. Jackson et al. (2006) and Kong et al. (2010) took a different approach using multiwell filter design with 0.3cm^2 and 0.28cm^2 filtration area per well respectively and integrated it with an automated liquid handler Tecan™ and TesVac™ vacuum system to simulate constant pressure. Lau et al. (2013) used a similar setup to investigate the impact of primary depth filtration on product quality and contaminants removal for a CHO cells based process for the production of a fusion protein. Noyes et al. (2015) also developed a USD device for depth filtration for constant flux experiments, successfully mimicking the lab scale operation. However the device was custom-made requiring for the depth filter media to be sealed in polypropylene washer using

epoxy. The novel filter design enabled the rapid evaluation of various filters with feeds with different characteristics.

This brief review shows that there are a number of scale-down models for the filtration operation. However most of those models were applied for primary depth filtration, used membrane filtration or used constant flux filtration which requires larger feed volume. The focus of this work will be to size the secondary depth filtration process using minimum amount of material and effort so that it is compatible with the small scale parallel bioreactor system.

1.5 Multivariate data analysis (MVDA) techniques in bioprocess modelling

Due to the inherent complexity of the bioprocess development, statistical tools are required to aid the decision making process as the drug advances through the pipeline. In this section different methodologies for building predictive models are presented.

MVDA has gained popularity in industry due to its ability to deal with challenging multidimensional data, experimental error and noise (Rathore et al., 2007). Multiple linear regression (MLR) and analysis of variance (ANOVA) are commonly applied MVDA technique used to build predictive models for the process in order to define the design space and window of operation in line with the QbD approach. There are many examples where DoE and MVDA are applied to bioprocess optimisation with the goal of identifying an optimum (Delahaye et al., 2015; Herzer et al., 2015; Looby et al., 2011).

MLR analysis with DoE has been applied to study the impact of upstream conditions on key critical quality attributes and process performance (Goldrick *et al.*, 2017 and Moses and Manahan, 2012). For larger and more complex datasets, the original multidimensional data can be reduced to fewer dimensions through “projections” (Sarah M. Mercier *et al.*, 2013). Principal component analysis (PCA) and partial least squares (PLS) techniques use the projections (latent variables) to identify patterns within the data and to build a predictive model based on the variance between the predictors and observations (Rajalahti and Kvalheim, 2011). An example of using such large data sets for upstream process development is the study carried out by Suarez-Zuluaga *et al.* (2019). In their work PCA and PLS techniques were used to analyse all historic raw data generated from 26 bioreactor runs. The study proposed a workflow that enables the identification and analysis of the most critical parameters affecting the bioreactor performance. Mercier *et al.* (2013) apply similar techniques to early raw data from bioprocess development, for this purpose the raw data was pre-treated - smoothed and where necessary normalised, so that it did not disturb the models. The PCA revealed the sensitivity of the process to bioreactor scale. These studies demonstrate the potential of leveraging readily available large datasets through the use of advanced statistical techniques to gain valuable insights into processes without the need for costly and lengthy experimentation.

Some of the statistical models described in this section will be applied in the thesis to develop predictive correlations for the upstream-recovery operation. The derived correlations for the process will be incorporated into bigger bioprocess models, where the predictions will be linked to mass balance equations, stochastic inputs

and optimisation algorithms. The next section will provide an overview of bioprocess decisional tools applying similar approaches.

1.6 Decisional tools for bioprocess optimisation

As shown earlier in **Section 1.1** different metrics increase in relative importance as the drug advances through the development cycle. In the initial stage the focus will be on speed since it is important to assess drug candidates in a time-efficient manner. If it progresses further then material will have to be supplied for clinical trials, which means that the focus is shifted to the ease of scale up in order to manufacture enough quantity. Naturally as the scale increases with the advancement of the drug candidate so does the volume required for clinical trials and finally commercial supply. That implies that the cost of manufacturing will also increase and play a more important role in the overall business case. There are a number of studies that have investigated the COG for different scales, process steps and stages of process development – the next few paragraphs summarise some of the key publications on the topic.

Decisional tools have been applied to address various questions in biopharmaceutical bioprocessing. For instance, they have been applied to investigate the benefits of batch vs continuous manufacture for different scenarios. Pollock et al. (2013) analysed the cost drivers for a continuous process using spin filter or ATF technologies and compared them against a fed-batch process counterpart. Furthermore, the study looked into the economic, environmental and operational feasibility of the different manufacturing approaches. Mahal et al. (2021)

extends the comparison of continuous vs traditional manufacture to the process development and clinical trials manufacturing costs.

There are a number of studies that focus on the economics assessment and optimisation of the downstream operations. Allmendinger et al. (2014) used an evolutionary multiobjective algorithm (EMOA) to optimise the downstream steps for various performance metrics and manufacturing scenarios while Liu et al. (2013) applied a different approach to the optimisation of the chromatography operations using mixed-integer linear programming model (MILP).

Similarly, bioprocess decisional tools have also been applied to other modalities and applications such as the evaluation of cell-free synthesis process for antibody drug conjugates (ADC) manufacture (Stamatis and Farid, 2021) or in the field of advanced therapies for the economics assessment of lentiviral vector manufacture (Comisel et al., 2021) and cell therapies (Pereira Chilima et al., 2020). Some of these publications focus on the inherent biologic variability and manufacturing uncertainty. For, instance Stonier et al. (2012) highlights the challenges of facility fit when different projects need to fit into the same platform, which could lead to mismatches between equipment sizes and oversizing or under-sizing a step. The study uses Monte Carlo stochastic simulations to assess the risk to facility fit.

There are limited number of studies that focus on an economics appraisal of the recovery operation (Felo et al., 2013; Popova et al., 2016). In both studies the conditions in the upstream were not directly linked to the recovery operation, which will be one of the goals of this thesis.

There are a number of computer-aided tools that can be used for biopharmaceutical economics appraisal such as BioSolve™ process economics simulation tool (BioPharm services, Bucks, UK), Aspen Batch Plus™ (Aspen Technology, Inc., MA, US) and Intelligen SuperPro (Intelligen Inc., NJ, USA) (Torres-Acosta et al., 2015; Broly et al., 2010; Shanklin et al., 2001). These tools are able to perform energy and mass balances, equipment sizing as well as some cost estimates and analysis (Biosolve and SuperPro). A main drawback of such tools is that they cannot model dynamic time-dependent operations, which is the case of bioprocessing. A dynamic model is more appropriate, when there is the need to allocate resources based on availability. Farid et al. (2007) present such prototype computer-aided decisional tool SimBiopharma that allows the integration of process, business and risk reducing objectives into a single framework. Furthermore, Stonier et al. (2012) applies the tool developed by Farid et al. (2005) to evaluate manufacturing strategies under uncertainties such as fluctuating product demands and titre. Many of the other studies described earlier in this section also used dedicated, non-commercially available tools (Mahal et al., 2021; Comisel et al., 2021; Allmendinger et al., 2014; Pereira Chilima et al., 2020; Stamatis and Farid, 2021)

As it can be inferred from this brief overview, a successful bioprocess decisional tool may have to meet a number of criteria such as accounting for the uncertainty of the process, incorporating its dynamic nature and being able to explore a large decisional space.

1.7 Aims and organisation of thesis

The literature review highlighted efforts in using scale-down technologies to model upstream and recovery operations. Furthermore, it described examples where advanced statistical techniques and analysis have been used to better understand bioprocessing. However, there is a knowledge gap in the understanding of the impact of upstream parameters on primary and secondary recovery operation, which is due to the lack of holistic approach to bioprocess optimisation. Therefore, the overall aim of this thesis is to close this gap through the creation of a systematic approach to mapping the design space for upstream and recovery through leveraging scale-down models and MVDA techniques. The goal is to link upstream, centrifugation and depth filtration operations in one overarching model capable of revealing process trade-offs, economics, robustness and risk, thus enabling a more informed decision making process. Below is presented an overview of each chapter and how it has contributed to achieving the goals of the thesis.

Chapter 2 gives an overview of the materials and methods used in the thesis. It also provides the theoretical considerations underpinning the centrifugation scale-down and depth filtrations models. The chapter describes the different statistical models that were applied and the software that was used to facilitate the data organization and pre-treatment, statistical and other analysis and bioprocess modelling.

Chapter 3 applied a DoE study in the ambr to map the design space for the upstream and recovery metrics. Cause-and-effect correlations were derived linking the upstream conditions (temperature, seeding density, harvest day and pH) to titre, [solids] and turbidity.

Chapter 4 extended the analysis to the centrifugation operation and the impact of the centrifugation shear on process performance. A CSD was used to characterize the shear in a pilot scale centrifuges. The shear in the centrifugation operation and the conditions in the upstream were linked to the levels of mAb monomer content and HCPs. A cholesterol-based correlation for filterability was established, which was implemented in a DoE study using the ambr linked to the CSD to map the design space for upstream and recovery.

Chapter 5 was focused on building an economics model for the upstream-recovery sequence, which incorporated the predictive correlations derived in **Chapter 3** and **4**. Windows of operation were built constrained by economics and process performance metrics. The impact of the process uncertainty on the performance was assessed through applying stochasticity to uncertain inputs –such as seeding density.

Chapter 6 presents the use of advanced MVDA techniques to predict [solids] and levels of cell lysis leveraging PSD data from routinely used cell counter (Vi-Cell XR™). The goal was to enable to analysis of these metrics at small scale through time and resource savings for the measurement.

Chapter 7 provides a summary of the main conclusions from the thesis and indicates possible directions for future work.

Chapter 2

2 Materials and Methods

This chapter provides the general materials and methods applied in this thesis. It also provides the theoretical considerations for the recovery operation. Each results chapter expands on the developed experimental approach and setup used to generate the results pertaining to that chapter.

2.1 Wet lab experimental protocols

2.1.1 Reagents

All reagents used for the mammalian cell culture processes were sterilised: for the antifoam (10% v/v semethicone) through an autoclave sterilisation cycle; glucose (50% v/v), media and feeds through sterile-grade filters and in some instances the sterile ready-made solutions were obtained, for instance polyphosphate buffered solution (PBS) (Gibco®, Thermo Fisher Scientific, MA, US). The media and feeds preparation recipes are proprietary to AstraZeneca.

2.1.2 Bench scale and scale-down process steps

2.1.2.1 Cell culture processes

The cell culture runs were performed in automated microbioreactor systems - the ambr15® (Sartorius Stedim, Germany) – or in bench scale (7L) bioreactor systems. The ambr is a high throughput (HT) automated system of 24 or 48 single miniature

bioreactors (MNB) at 11 to 16mL working volume. The system consists of two or four culture stations (CS), with 12 bioreactors each. Temperature and stirring are controlled for the entire culture station, while DO and pH have individual control loops for each MNB. This is achieved through integrated optical sensors for pH and DO on the bottom of each bioreactor. The whole system is placed inside a biosafety cabinet. All additions to the bioreactors are performed aseptically via a liquid handling arm. All pipette boxes are replaced manually and all deep well plates with reagents and feeds are monitored daily to ensure there is enough for routine operation.

All bioreactors were inoculated post a 24-hour media hold. The seed used for inoculation was expanded for 14 days, with passages every three to four days. To achieve the target seeding density the inoculum was diluted to twice the desired bioreactor concentration, based on 50% v/v inoculum and 50% v/v media in the MNB. Off-line pH measurements were taken on day 1, 3, 7, 10 and 14 to account for potential pH drift.

The bench-scale experiments were performed in 7-L glass bioreactors (Chemglass, Vineland, NJ) with approximately 5-L working volume, controlled by DASGIP® (Eppendorf, DASGIP, Germany) or ez-Control® (Applikon Biotechnology B.V., The Netherlands) controllers.

The pH was controlled via base additions (Sodium Carbonate, Na_2CO_3) and CO_2 flowrate via a proportional integral controller (PID). A DO set point of 50% was targeted for both scales (MNB and bench-scale), which was achieved by altering the O_2 flow rate through a PID controller.

The bioreactors were fed daily with glucose, triggering addition when glucose drops below 5 g/L (up to day 5) and trigger of 7g/L (after day 5). The mammalian cell culture was fed every two days from day two with AstraZeneca proprietary feeds – feed A and B. Feeds for all scales were through bolus additions. The feeding strategy and glucose supplementation were comparable between the scales. Between 3 to 5 samples were taken for titre over the last 7 days of cell culture. The sampling protocol for the different experiments are provided in **Section 3.2.1** for ambr1 and ambr2, and **Section 4.2.2** for ambr3 and ambr4.

2.1.2.2 Centrifugation shear mimic

The capillary shear device (CSD) utilised in this study consists of a 10 cm long Upchurch Scientific® stainless steel capillary (VWR.co.uk order # 554-3222) attached to a chromatography skid – ÄKTAEplorer™ or ÄKTA™ Pure (Cytiva, MA, US), which delivers the constant flow through the capillary. The capillary features a very small inner OD of 0.01” (0.0254 cm). Further details about the CSD are discussed by Westoby et al. (2011) and Joseph et al. (2017, 2016).

2.1.2.3 Swing out –bucket centrifuge

To generate the mimic centrates the samples were centrifuged in Soval™ Legend™ XTR (ThermoFisher Scientific, MA, US). The duration of the centrifugation cycle was calculated using the Q/Σ theory. The sigma value was calculated as follows:

$$\Sigma_{lab} = \frac{\omega^3(3-2x-2y)V}{\ln\left(\frac{2r_2}{r_2+r_1}\right)6g}, \quad (2.1)$$

where inner and outer radii of the suspension are defined as r_2 and r_1 (m)- these

have been measured for various sample volumes; x and y (s) are the centrifugation's acceleration and deceleration times, which have been derived experimentally, courtesy of ThermoScientific™ (part of ThermoFisher Scientific, MA, US); ω is the rotational speed (rounds per second) and g is the acceleration due to gravity (m/s^2).

2.1.2.4 Depth filtration setup

The bench scale depth filtration studies were carried out at constant pressure and constant flow. The depth filter that was used in both cases was a single use capsule (pod format) with 23 cm^2 filtration area - Millistack X0HC (Merck Millipore, MA, USA). The filters were first wetted with water for 20min and then flushed with air for the removal of residual water (Goldrick et al., 2016).

2.1.2.5 High throughput protein A purification

The protein purification used $200\mu\text{L}$ Protein A columns - PreDicator RoboColumn™ MabSelect SuRe (Cytiva, Marlborough, US) resin. The capture step was carried out on the Freedom, EVO™ system (Tecan Group Ltd, Männedorf, Switzerland) using a dedicated programming script for the columns' sanitisation, equilibration, loading, elution and wash 1 and wash 2 steps. The columns were first sanitized with 0.5M NaOH and then equilibrated with 50 mM Tris (pH 7.4) 100mM acetic acid. After column loading, the product was eluted at pH 3.6 using 25mM Sodium Acetate (approximately $1\text{ mL} = 5$ column volumes). The columns were washed with 50mM Tris 0.5M NaOH. All samples were neutralised post protein A and filtered to remove any precipitates.

2.1.3 Analytical methods

2.1.3.1 Cell counts

Viable cell number (VCN) and total cell number (TCN) were measured in the Vi-Cell™ XR (Beckam Coulter, High Wycombe, UK) for all cell cultures. Dilution (1 in 5) was applied after day 5 (at approximately more than 10^6 cells/mL). The Vi-cell is an image-based automated cell counter that uses the trypan blue exclusion method to measure viability, where only non-viable cells are permeable to the dye. The cell counter provides information about the amount of live (non-stained) and dead (stained) cells and their particle size distribution.

2.1.3.2 Off-line pH measurements

The off-line pH measurements for pH sensor calibration and offset adjustment were performed using the ABL90 FLEX Analyzer (Radiometer, UK) or Nova FLEX (Nova Biomedical, USA). For accurate measurements the sample containers were capped to avoid CO₂ escape. The ABL90 FLEX Analyzer was used with the ambr system while the Nova FLEX was mostly used with the bench scale systems due to the larger volume required for the sample for the latter instrument.

2.1.3.3 Cell culture nutrients and metabolites

The glucose concentration measurement was used to determine the glucose feed additions. All samples were spun at 3000g for 5 min before being measured on an automated analyzer YSI 2900 (YSI Incorporated, OH, US). The instrument's operation is based on an enzyme coupled reaction. When the sample reacts with the enzyme it is oxidised, which leads to the formation of hydrogen peroxide (H₂O₂). The

hydrogen peroxide is in turn oxidised by a platinum anode and the generated electron flow is proportional to the glucose concentration. As an alternative instrument - Nova FLEX (Nova Biomedical, MA, USA) was also used. Similarly to the YSI 2900, this analyzer uses a substrate and an enzyme to generate a product that can be measured.

2.1.3.4 **Solids concentration determination**

The solids concentration was determined using packed cell volume (PCV) tubes (TPP®, Techno Plastic Products AG, Switzerland). The bottom of the tubes has a capillary, which is graduated to accurately measure the volume of solids in the sample. The tube was filled with 40µL of cell culture material (in triplicates) and the samples were then spun at 2500g for one minute in a swing-out bucket centrifuge – Thermo Scientific Sorvall Legend ®T Plus (ThermoFisher Scientific, MA, US) – so that the solids settle in the capillary. The amount of solids in the capillary is used to calculate the [solids] % v/v. This protocol has been widely adopted within AstraZeneca to measure PCV for the centrifugation operation. However, it is important to note that different speeds, duration and volumes may impact the sedimentation of the solids and consequently the PCV of the sample. A larger volume of 100µL sample was also tested to investigate the impact on the measurement but no impact was seen. To ensure consistency the same methodology described above (40µL volume, centrifuged at 2500g for 1 minute) was applied across all samples. More details about the PCV protocol can be found in Stettler *et al.* (2006).

2.1.3.5 Lactate dehydrogenase (LDH) release evaluation

The LDH Cytotoxicity Assay Kit II (ab65393, Abcam, Cambridge, United Kingdom) was used to quantify the amount of LDH release. It measures LDH via an enzymatic coupling reaction, in which LDH oxidises lactate to generate NADH and then NADH reacts with the reaction buffer WST to form a yellow colour. The sample for the assay have to be diluted down to 0.5×10^6 cells/mL, which is a achieved via a two-step dilution; first to 5×10^6 cells/mL followed by a 10 times dilution. A low and a high control are prepared for each sample. In order to prepare the low/negative control, the sample is spun down and the supernatant is collected. The high control is prepared separately using $100 \mu\text{L}$ of the sample containing the cells and $10 \mu\text{L}$ of lysing buffer, which is incubated for 30min. The sheared sample is prepared in the same way as the negative control; it is spun down, $100 \mu\text{L}$ of the supernatant is aliquoted into an Eppendorf tube, and the volume is adjusted to $110 \mu\text{L}$ with PBS. $10 \mu\text{L}$ samples plus $100 \mu\text{L}$ of the reaction buffer are plated in 96-well plate in triplicates and two blank samples with media are also included to measure the background of the sample. The absorbance is then measured every 10 min at two wavelengths 420nm and 650nm using the Optima plate reader (BMG Labtech Ltd, Aylesbury, UK). The background at 650 nm is subtracted for each sample and the percentage LDH release for each samples is calculated as follows:

$$R^{LDH} = \frac{(ABS_{450}^{sample} - ABS_{650}^{sample}) - (ABS_{450}^{blank} - ABS_{650}^{blank})}{(ABS_{450}^{sample_{lysed}} - ABS_{650}^{sample_{lysed}}) - (ABS_{450}^{blank} - ABS_{650}^{blank})} \quad (2.2)$$

where R^{LDH} is the percentage of LDH release, ABS_{450}^{sample} is the sample's absorbance at 450nm, $ABS_{450}^{sample_{lysed}}$ is the absorbance at 450nm of the lysed sample and ABS_{450}^{blank}

is the absorbance of the blank sample (media) at 450nm. The background is measured at 650nm: ABS_{650}^{sample} for the sample, ABS_{650}^{lysed} for the lysed sample and ABS_{650}^{blank} for the blank.

2.1.3.6 Cholesterol concentration

The cholesterol concentration of various samples was measured using the EnzyChrom™ AF Cholesterol Assay Kit E2CH-100 from Bioassay Systems (Hayward, CA, US). The measurement can be done using a colorimetric or fluorometric procedure. Based on previous work conducted by Senczuk *et al.*, (2016), it was decided to use the fluorometric method. The assay uses a reagent that achieves cholesterol ester hydrolysis, oxidation and colour reaction in one step as described in the assay protocol. The intensity of the fluorescence is correlated to the cholesterol concentration. A standard curve was generated for 0 to 2mg/dL. The cholesterol concentration was calculated as follows:

$$[\text{cholesterol}] = \frac{F^{Sample} - F^{Blank}}{Slope^{Std\ curve}} \quad (2.3)$$

Where F is the fluorescence at $\lambda_{ex} = 530nm$ and $\lambda_{em} = 585nm$ for the sample (F^{Sample}), the blank media (F^{Blank}) and $Slope^{Std\ curve}$ is the slope of the standard curve.

2.1.3.7 Turbidity measurements

Turbidity was measured in terms of nephelometric turbidity units (NTU) using Orion™ (ThermoFisher Scientific, MA, US) based on light scattering. For all measurements, the liquid was checked for bubbles and solids settling.

2.1.3.8 Particle Size Distribution (PSD) analysis in the Mastersizer

The Mastersizer2000™ (Malvern, Worcestershire, UK) was used to measure percentage volume based PSD. Between five and three measurements were taken for each sample and the results were averaged. An output used from this analysis is the d10, which indicates the 10th percentile of a cumulative distribution or that 10% of all particles by volume are below this size.

The refractive index for the particles is assumed to be 1.59, which is a typical value for CHO cells and the refractive index of the dispersant (PBS or water) is 1.33 (Caputo et al., 2021; Zheng et al., 2023). For each measurement the weighted residual, which represents the lack of fit between the model and the PSD was no more than 1%. Higher values indicate poor fit due to problems with the measurement, for instance, bad adsorption values (adsorptive value = 1).

2.1.3.9 **Titre determination**

The titre was measured via a Protein A high pressure liquid chromatography (HPLC). Various sample volumes were loaded onto the column and then the product was eluted using low pH (pH = 2). The elution peak was determined at UV of 280nm. The obtained peak was integrated and the antibody concentration was measured using a reference curve (Antemie, 2016) .

2.1.3.10 **HCP analysis**

The HCP determination was performed using the Gyrolab™ xP workstation (Gyros, Uppsala, Sweden). It is a high throughput automated analysis that uses CDs (Compact Discs) with microcapillary channels. The analysis is based on a proprietary

to the industrial partner (AstraZeneca) in-house process with lower limit of quantification of 20ng/mL and upper limit of 80,000ng/mL.

2.1.3.11 **Antibody reduction analysis**

2.1.3.11.1 **LabChip GXII**

Protein A purified samples (protocol described in **Section 2.1.2.5**) were diluted to 1 mg/mL in 1X PBS and capped with N-Ethylmaleimide (NEM) to prevent further disulfide bond reduction during denaturation. The samples were then heated in a thermocycler at 100°C for 5 min while the protein ladder was heated on a heating block at 100°C for 5 min. Following that, the samples, and the ladder were diluted with ultra-pure water and loaded on a 96-well plate. The LabChip GXII (Perkin Elmer, Waltham, MA, US) was loaded with the relevant gel dye, destain solution, low protein expression marker. The chip, ladder and buffer were then loaded onto the LabChip GXII analyzer (Perkin Elmer, Waltham, MA, US). The instrument uses laser-induced fluorescence to detect and quantify the intact antibody monomers and fragments. The LabChip GXII software generates detailed electropherogram and gel-like images. In addition a comma separated (CSV) file is generated containing the information used to generate the electropherogram. The data from the CSV files was extracted using a Matlab (MathWorks®) program that was built here for plotting and antibody size quantification.

2.1.3.11.2 **Bioanalyzer**

The 2100 Bioanalyzer (Agilent, Santa Clara, CA, US) uses the same principle as the LabChip GXII instrument for measuring the amount of intact monomer and antibody fragments of different sizes, however, it provides lower throughput. The samples (at

max 4g/L concentration) were capped with NEM as described before. Reduced samples were generated using dithiothreitol (DTT). The reduced and non-reduced samples were mixed with protein sample buffer (Agilent Technologies, 2006) (5µm of samples + 5µm of buffer) and heated at 80°C on a heating block. Following that, the samples were centrifuged for 30s at 13,000 rpm to stop the reaction and cool the samples. The samples, the ladder, the gel dye and the destain buffer were added to the chip for analysis by the BioAnalyser. Similarly to the LabChip GXII a gel-like image is generated and a CSV file with the raw data.

2.1.3.12 Calculations

2.1.3.12.1 Integral viable cell count

The viable cell count was used to calculate the integral viable cell count (IVC):

$$IVC = \sum_{i=2}^n \frac{(VCN_i + VCN_{i-1})}{2} (t_i - t_{i-1}), \quad (2.4)$$

where VCN_i is the viable cell number at time t_i and VCN_{i-1} is the viable cell number at time t_{i-1} .

2.1.3.12.2 Cell culture productivity q_p

The cell specific productivity (q_p , pg/cell//day) is calculated as follows:

$$q_p = \frac{titre_{harvest}}{IVC_{harvest}} \quad (2.5)$$

where the $titre_{harvest}$ is the titre at harvest and $IVC_{harvest}$ is the internal viable cell count.

2.2 Theoretical considerations

2.2.1 Disc stack centrifugation

Understanding the principles of the disc-stack centrifugation is key for identifying the cell culture properties that may impact on the process performance. The solids-liquid separation in the disc-stack centrifuge is driven by centrifugal forces. Each particle moves at a laminar flow in the gap between the discs. Once it hits the upper disc the liquid flow no longer impacts on it and it slides down to the solids holding space. **Figure 2.1** shows the forces exerted on the particle. On one hand there is the settling centrifugal velocity based on the Stoke's law equation for particles suspended in fluid:

$$v_g = \frac{d_p^2(\rho_p - \rho_i)g}{18\mu}, \quad (2.6)$$

where v_g is particle centrifugal velocity (m/s), d_p represents particle diameter (m), $(\rho_p - \rho_i)$ is the density difference between the particles and liquid (kg/m^3) and μ is the viscosity (pa s). This equation is subject to a number of assumptions: laminar flow, spherical particles and non-hindered settling (Mannweiler and Hoare, 1992; Ambler, 1959). **Equation (2.6)** highlights the impact of the viscosity and particle size on the centrifugation separation. The rheological properties of the feed will be impacted by the apparent viscosity of the solids, which has been linked to [solids], solids particle settling velocity and angle of response of solids (Iordan et al., 2008; Quemada, 1998; Häggmark and Königsson, 2018).

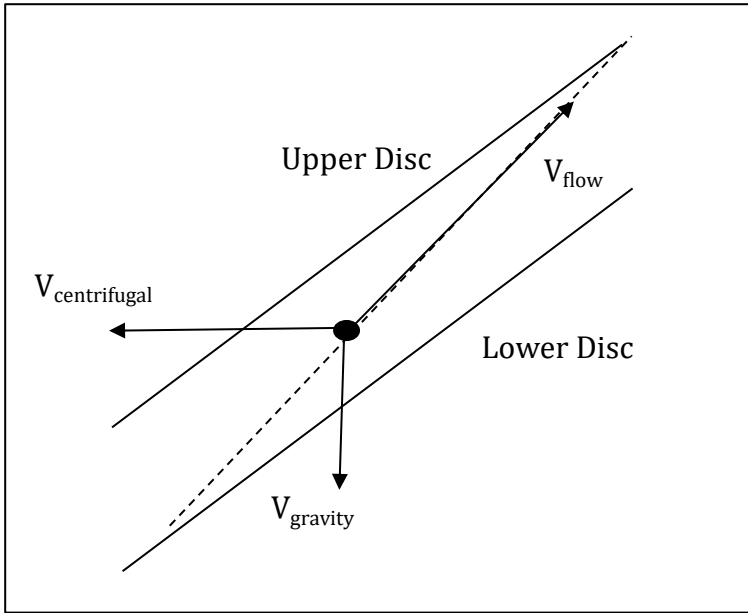


Figure 2.1 Forces acting upon a particle suspended during centrifugation, adapted from Tebbe et al., (1996)

The centrifugal field is another force exerted on the particle, given by:

$$v_c(r) = \frac{v_g \omega^2 r}{g}, \quad (2.7)$$

where $v_c(r)$ is the particle terminal settling velocity (m/s) in a centrifugal field where ω (s^{-1}) is the angular velocity and r is the settling radius (m) (Mannweiler and Hoare, 1992; Ambler, 1959).

Ambler (1959) combines these two equations – **Equation (2.6)** and **Equation (2.7)** - and adds a term for the residence time of the particles in the liquid to find the distance travelled by the particle in a bowl:

$$x = v_s t = \frac{\omega^2 r * d_p^2 (\rho_p - \rho_i) g}{g * 18\mu} * \frac{V}{Q}, \quad (2.8)$$

where the t is time (h), V is volume of the liquid in the bowl (L) and Q is the volumetric flowrate (L/h). The equation assumes that v_s (the velocity with which the particle approaches the bowl's wall) is constant since the layer of thickness, s , on the centrifuge wall is relatively small compared to the radius of rotation (Ambler, 1959). For an ideal system $x = s/2$, where half of the particles of diameter d will sediment. The equation can also be expressed in terms of flowrate as:

$$Q = 2v_g \Sigma$$

where v_g is described in **Equation (2.6)**.

Σ represents the centrifuge size or the equivalent settling area for theoretical settling tank:

$$\Sigma = \frac{V \omega^2 r_e}{g s_e} \quad (2.9)$$

where V is the volume of the bowl, ω is the rotational speed and r_e and s_e are the effective radius and settling distance for the centrifuge (Ambler, 1959).

The disc-stack's centrifuge configuration with multiple discs increases their settling area and hence separation capacity. The equivalent clarification area (m^2) of a disc-stack centrifuge is calculated as follows (Doran, 2013):

$$\Sigma = \frac{2\pi \omega^2 (N - 1)}{3g \tan \theta} (r_2^3 - r_1^3) \quad (2.10)$$

Where ω is the angular velocity (s^{-1}), N is the number of discs, θ is the angle of the slope of the discs, r_1 and r_2 are the inner and outer diameter respectively of the discs (m), g is the acceleration due to gravity.

Equation (2.8) implies that there is a critical particle diameter, above which all particles are removed (Chatel et al., 2014). It depends on the flowrate, settling area and the solids volume fraction. Clarkson et al. (1993) proposes two equations for defining the critical particle diameter (d_c). The first one describes the case when the amount of solids is relatively small and the fluid is not very viscous e.g. 4% yeast suspension **Equation (2.11)** and for high solids content (**Equation (2.12)**):

$$d_c = \sqrt{\left(\frac{18Q\mu}{\Delta\rho\Sigma g}\right)} \quad (2.11)$$

$$d_c = \sqrt{\left(\frac{18Q\mu}{\Delta\rho\Sigma(1-C_v)\sigma g}\right)}, \quad (2.12)$$

where σ accounts for the particles' sphericity (4.6 for spherical particles), C_v is the concentration of solids in the suspension (% v/v), $\Delta\rho$ is the density difference between the solids and the liquid phase (kg/m^3) and g is the acceleration due to gravity (m/s^2).

The critical particle diameter is important since it can be used to predict clarification from particle size distribution data. A study by Chatel et al. (2014) uses the critical particle diameter to predict clarification performance as a function of particle size distribution data.

$$(\%) \text{ Clarification prediction} = \sum_{N=0}^{\infty} V(d_i) \times (1 - T(d_i)) \quad (2.13)$$

$$T(d_i) = (d/d_c)^2 \text{ for } d < d_c,$$

$$T(d_i) = 1 \text{ for } d > d_c$$

where $V(d_i)$ is the percentage volume of particles of diameter i (m). The grade efficiency curve ($T(d_i)$) accounts for the fact that the particles are evenly distributed over the surface of the disc which, means that some particles are closer to the outlet and will be separated despite being below the d_c (Mannweiler and Hoare, 1992)

The scale-down of an industrial scale centrifuge is usually carried out on the basis of constant Q/Σ :

$$\frac{Q}{\Sigma} = \frac{V}{tc\Sigma} \quad (2.14)$$

In **Equation (2.14)** Σ is the settling area (m^2), Q is the volumetric throughput (m^3/h) in a disc stack (or other continuous centrifuge), V is the sample volume in the bench-top centrifuge, c is a correction factor and t is time (h). The correction factor – c – accounts for the bulk liquid flow between the discs that disturbs the sedimentation process – it is typically between 0.27-0.73 (Aucamp et al., 2014; Boychyn et al., 2004; Joseph et al., 2016). **Equation ((2.14)** represents the ratio of equivalent flow rate to equivalent settling area; the log probability of this this ratio is typically in linear correlation with the separation efficiency, which is measured as the percentage solids removed:

$$\% \text{ Clarification} = \frac{NTU_{\text{feed}} - NTU_{\text{centrate}}}{NTU_{\text{feed}} - NTU_{\text{well clarified}}}, \quad (2.15)$$

where nephelometric units (NTU) is a measurement for turbidity. NTU_{feed} is the turbidity of the feed, NTU_{centrate} is the turbidity of the centrate and $NTU_{\text{well clarified}}$ is a well clarified sample. The clarification can also be calculated in terms of optical density (OD) instead of NTU.

Table 2.1 The sigma factor calculation for different small scale centrifuges

| Type of centrifuge | Sigma factor* | Equation # | Source |
|----------------------------------|--|------------|------------------------|
| Benchtop centrifuge | $\Sigma_{lab} = \frac{V_{lab}\omega}{2g \ln\left(\frac{2r_2}{r_2+r_1}\right)}$ | (2.16) | (Ambler, 1959) |
| Swinging bucket batch centrifuge | $\Sigma_{lab} = \frac{\omega^3(3-2x-2y)V}{\ln\left(\frac{2r_2}{r_2+r_1}\right)6g}$ | (2.17) | (Maybury et al., 2000) |
| Multiwell plate centrifuge | Same as Equation (2.17) above but $r_1 = \sqrt{(p + (q - L)\cos\theta + a\sin\theta)^2 + b^2}$ $r_1 = \sqrt{(p + q\cos\theta + a\sin\theta)^2 + b^2}$ | (2.18) | (Tait et al., 2009) |

*V is the volume of centrifuge vessel e.g. Eppendorf tube (m³), x and y are the fractional times of acceleration and deceleration (%), r₁ is the distance from the centre of rotation to the top of the liquid and r₂ is to the bottom of the liquid respectively, g is acceleration due to gravity (m/s²), ω is angular velocity (s⁻¹), p is the length of the horizontal arm of the rotor (m), q is the length from the swing out arm to the base of the centre of the plate (m), and θ is the angular deviation of the plate from 90° during centrifugation and L is the average height of the suspension in the well

Since the feed zone centrifugation shear can lead to increase in turbidity, non-shear sensitive material (polyvinyl acetate) can be used in order to accurately estimate the correction factor in **Equation (2.14)** (Tait et al., 2009). The Σ has been calculated for various benchtop centrifuges (summarised in **Table 2.1**) enabling the generation of mimic centrates for the large scale disc-stack centrifuge operation using benchtop systems.

The equations in in **Table 2.1** show some specific parameters to consider for the bench top centrifugation. For instance, **Equation (2.17)** shows that the acceleration and deceleration time of the swing bucket centrifuge impact on the equivalent settling area Σ (Maybury et al., 2000). **Equation (2.18)** shows that the position of the well on the microplate impacts on the Σ value for that well (Tait et al., 2009).

2.2.2 Filtration fouling models

There are two main mechanisms of filtration fouling – pore blockage (deposition of particles on the filter surface) or pore constriction (deposition of particles in the pores of the filter) (Affandy et al. 2013; Bolton et al. 2006; Sampath et al. 2014; Roush and Lu, 2008; Van Den Berg & Smolders 1990). Based on these mechanism, there are four models that are applied predominantly: Standard blocking, Intermediate blocking, Cake filtration, Complete blocking and combinations between different models, which Bolton et al. (2006) found to describe the observed filter fouling (**Table 2.2**).

Table 2.2 Equations describing the four main blocking mechanisms adapted from (Bolton et al., 2006)

| Model | Equation* | Model constants |
|-----------------------|---|----------------------------------|
| Standard blocking | $V = J_0 t \left(1 + \frac{k_s V_0}{A_0} t \right)^{-1}$ | $k_s \text{ (m}^{-1}\text{)}$ |
| Intermediate blocking | $V = \frac{1}{k_i} (\ln(1 + k_i J_0 t))$ | $k_i \text{ (m}^{-3}\text{)}$ |
| Complete blocking | $V = \frac{J_0}{k_b} [1 - \exp(-k_b t)]$ | $k_b \text{ (s}^{-1}\text{)}$ |
| Cake filtration | $V = \frac{1}{J_0 k_c} (\sqrt{1 + (2k_c V_0^2 t)} - 1)$ | $k_c \text{ (s.m.}^{-2}\text{)}$ |

* J_0 is the initial flux (LMH), V is filtered volume (L), A is the filter area (m^2) and t is time (h)

The filtration models described in **Table 2.2** are based on Darcy's law (**Equation (1.1)**) and therefore the fouling mechanism will depend on properties of the fluid e.g. viscosity and the foulant e.g. particle size. During cake filtration the particles accumulate on the surface creating a permeable cake, which gradually increases in thickness. For the standard blocking mechanism it is assumed that particles accumulate on the pore's wall gradually constricting its size, therefore this model is also known as the pore constriction model. One of the main assumptions for the model is that the pores have a cylindrical shape (Bolton et al., 2006; Sampath et al., 2014). It is often used when this is the expected mechanism of fouling e.g. secondary depth filtration. Furthermore, in its linearised form it allows easy evaluation of the membrane capacity V_{\max} :

$$\frac{t}{V} = \frac{1}{Q_0} + \frac{1}{V_{max}} t, \quad (2.19)$$

where V is the total volume of collected filtrate (L), Q_0 is the initial flux (LMH) and V_{max} is the maximum volume of filtrate collected before the flux is prohibitively slow.

The complete blocking model describes a process where the particles seal completely the pores and prevent any flow. Finally, for the intermediate blocking model, portion of the particles block the pores while some accumulate on the surface (Bolton et al., 2006; Sampath et al., 2014).

2.3 Statistical methods

2.3.1 DoE considerations

The methodology of building predictive models was briefly mentioned in the context of the QbD paradigm. However, here the analysis will be further extended to highlight the different DoE approaches and considerations for selecting a type of DoE.

In the early stages of process development when little is known about the process the experimental approach is usually limited to small experimental sets or univariate experiments – OFAT. In late development full statistical designs are used for process characterisation (Sarah M Mercier et al., 2013). The use of statistically designed experiments reduces the number of experiments while at the same time it can reveal important information about the natural variability (error) and the impact of different factors.

When choosing the type of DoE it is important to consider, the goal of the study, the factor effects and interactions expected, the desired precision, efficiency of the

design and the expected curvature. The set levels for the factors (the range) will define the experimental region. If the range is too narrow, the observed response may not be enough to build a model i.e. it may not differ significantly from the fluctuation in the response attributed to the intrinsic variability of the bioprocesses. There is an observed trade-off between the efficiency of the design and its precision. The first characteristic refers to the number of experiments required to build a model and precision refers to the standard deviation of the response under identical conditions.

Another factor to consider is the resolution of the design since it will impact the level of confounding. The latter is related to the ability of the model to attribute effects unambiguously to a factor or factor interaction, where the effect is the level of change in the average response. Interactions are also important because often the level of impact of one factor is dependent on the level of another (Mason et al., 2003). For instance, as it was pointed out in **Section 1.3** high pCO₂ and osmolality have a more detrimental impact on cells when elevated together rather than individually.

Finally, the choice of statistical design will primarily depend on the knowledge about the process, and the number of parameters to investigate and resources' availability. When the number of parameters is too large but only a few are expected to have an impact on the process super saturated designs may be applied (SAS Institute Inc., 2009; Li and Lin, 2003). Similarly if there are no constraints in terms of resources and time or only a small number of parameters is to be investigated e.g three, and curvature or factor interactions are expected a three-level full factorial may be applied. As mentioned earlier, one of the problems with reducing the number of runs

is confounding. This is due to the fact that the same computation is used to estimate more than one effects in which cases the confounded effects are called aliases.

Information about the confounding in a design is given by its resolution. For instance, for a fractional factorial design of resolution 3, often termed as R III, main effects are confounded with two factor interactions but they are not confounded with any other main effects. This makes this design ideal for screening for main effects or when interactions are not expected. To evaluate the confounding from the resolution of the design the number of factors or factor interactions is subtracted from the resolution.

When a curvature is observed in the model a response surface design may be appropriate. One design to identify curvature is the Central Composite design (CCD), which usually consists of a two-level full factorial design with centre and axial points. Another alternative to the full factorial design that makes good use of experimental runs is the Box-Behnken design which reduces the number of points but it does not look at the extremes.

2.3.2 Definitions

This section describe the key statistics that have been used throughout the thesis.

2.3.2.1 R-squared adjusted, predicted and k-fold

R-squared indicates how well a model fits the data by determining the percentage variability in the data that can be explained by the model. The value is based on the mean of the dependent variable y (\bar{y}) and the predictor variable x (\bar{x}).

$$\mathbf{R}^2 = \frac{[\sum_{i=1}^n (x_i - \bar{x})(y_i - \bar{y})]^2}{\sum_{i=1}^n (x_i - \bar{x})^2 \sum_{i=1}^n (y_i - \bar{y})^2} \quad (2.20)$$

R-squared adjusted is the R^2 that has been adjusted for the number of terms in the model. The R^2 -adjusted for a model increases only if the new term improves the model more than it could have been simply improved by chance. It takes into account the number of observations (N) and the number of predictor variables (P).

$$\mathbf{R}_{\text{adjusted}}^2 = 1 - \frac{(1 - R^2)(N - 1)}{N - P - 1} \quad (2.21)$$

The R-squared predicted is a measure of the predictive capabilities of the model. Its calculation is based on the total sum of squares for all terms in the model corrected for the mean and predictive residual sum of squares (PRESS) ((Eriksson et al., 2006):

$$\mathbf{R}^2_{\text{predicted}} = 1 - \left(\frac{\text{PRESS}}{\text{totalSS}} \right) \quad (2.22)$$

The predictive residual sum of squares is calculated by fitting the data while omitting one observation so that:

$$\mathbf{PRESS} = \sum_{k=1}^n \sum_{i=1}^{n-1} (Y_{obs_i} - Y_{pred_{i,k}})^2 \quad (2.23)$$

where Y_{obs_i} is the observed value for the i^{th} observation and $Y_{pred_{i,k}}$ is the predicted value for the i^{th} observation and the k^{th} model generated omitting one of the observations and n is the total number of observations.

TotalSS is the total sum of squares including the model and the residuals:

$$\mathbf{TotalSS} = \mathbf{SSE} + \mathbf{SSR} \quad (2.24)$$

where SSE is the error sum of squares for the model and SSR is the regression sum of square error, which are calculated as follows:

$$\mathbf{SSE} = \sum_{i=1}^n (Y_{obs_i} - Y_{model_i})^2 \quad (2.25)$$

$$\mathbf{SSR} = \sum_{i=1}^n (Y_{model_i} - \bar{Y}_{obs})^2 \quad (2.26)$$

where Y_{model_i} is the predicted value by the model for the i^{th} observation and \bar{Y}_{obs} is the mean for the observed values.

The R^2 k-fold is calculated as follows:

$$\mathbf{R^2\ k-fold} = 1 - \frac{\frac{1}{k} \sum_{i=1}^k \mathbf{SSE}_i}{\frac{1}{k} \sum_{i=1}^k \mathbf{SSR}_i} \quad (2.27)$$

where \mathbf{SSE}_i is the error sum of squares in each of the k folds and \mathbf{SSR} (also called the treatment vector) represents a vector of the treatment sum of squares in each of the k folds.

2.3.2.2 Root mean squared of error

Root mean square is a metric that is often used to evaluate linear regression models. It looks at how good is the model at predictions when you compared the actual observed vales to the predicted values.

$$\mathbf{RMSE} = \sqrt{\frac{\sum_{i=1}^n (Y_{obs,i} - Y_{model,i})^2}{n}} \quad (2.28)$$

2.3.2.3 Akaike information criterion (AIC) and Bayesian information criterion (BIC),

Akaike information criterion (AIC) and Bayesian information criterion (BIC), can be used to show if the model is overfitting the data. In both cases the value on its own has little meaning and it is usually considered relative to the rest of the models that have been generated – for instance via stepwise regression. The goal is to minimize AIC and BIC, which are calculated as follows:

$$\text{AIC} = -2 \text{Loglikelihood} + 2k + 2k(k+1)/(n-k-1) \quad (2.29)$$

$$\text{BIC} = -2 \log\text{Likelihood} + k\ln(n), \quad (2.30)$$

where

$$\log\text{Likelihood} = 1/2n(\ln(\text{SSE}/n) + \ln(2\pi)) + 1$$

where n is the number of parameters and k is the number of observations.

2.3.3 Standard least square models

The standard least squares method is a type of regression analysis, which finds the best fit for the data – slope coefficient and intercept – that minimizes the sum of the square errors or residuals (SSE). This statistical technique is used to predict a dependent variable using a set of independent variables:

$$y = \beta_0 + \beta_1 X_1 + \beta_2 X_2 + \dots + \beta_n X_n + \epsilon \quad (2.31)$$

where y is the predicted value, β_0 is the intercept, β_1 to β_n are the regression coefficients for variable X_1 to X_n and ϵ is the error for the model.

2.3.3.1 Model assumptions

In order to fit a least square regression model a number of assumptions have to be satisfied:

- Normality of residuals: a histogram of the residuals is plotted to check for any deviations from normality due to skewness or kurtosis. In addition a Shapiro-Wilk test is performed in JMP® to check for normality of residuals.
- Autocorrelation of residuals: any correlations between adjacent observations may lead to overestimation of the predictor coefficients. Durbin-Watson statistic (calculated in JMP®) can be used to measure autocorrelation with values near 2 indicating lack of autocorrelation.
- Linearity of the model: If the model is not linear that can easily be identified from trends in the plot of residuals vs predicted.

2.3.3.2 Model selection via stepwise regression

A stepwise regression approach were chosen to select the terms in the model. The stepwise approach uses forward addition and backward elimination to generate the optimum model (Goldrick, Joseph, et al., 2017). A k-fold cross validation was performed for the models with different number of terms. The optimum model was selected based on maximising the R^2 k-fold and minimizing the AIC and BIC statistics.

2.3.4 PLS model development

PLS is an advanced MVDA technique that is particularly suited for modelling data with large number of correlated predictor variables. The dimensionality of the data is

reduced through the projection of the data on small number of vectors (latent variables) which are orthogonal by nature and hence non-correlated. For the PLS analysis the X (the predictor matrix) and Y (the response matrix) are centered so that the mean is 0 and scaled to unit variance. PLS does a linear decomposition of X into a matrix of scores (T), loadings (P) and residuals (E) and response matrix Y is decomposed in a similar manner so that:

$$X = TP' + E$$

$$Y = UQ' + F$$

where U is the extracted factors or scores Y; Q is loadings for Y and F is the residuals for Y (Goldrick et al., 2018). The goal for the PLS analysis is to maximise the covariance between the scores. Further details about the model can be found here (Goldrick et al., 2020; Tsanaktsidou et al., 2020; Wold et al., 2002)

The NIPALS algorithm (Wold et al., 1987) was applied to build models with different number of latent variables (scores). K-fold cross validation was performed where the data was split into subsets (k-folds). Through iterative process, each subset was taken out of the analysis to be used as an internal validation data set, while the rest of the data was used as a calibration data set – this was performed for all subsets. The PLS model with the optimum number of factors (latent variables) was selected based on minimum PRESS and prob van der Voet $T^2 > 0.1$ (der Voet T^2 tests shows if a model with different numbers of latent variables is significantly different from the optimum model). Where necessary the model was “pruned” removing variables with variable importance on projection (VIP) less than 0.8 – the VIP score

indicates the importance of each variable and detailed information about its calculation can be found in Wold, Sjöström and Eriksson (2002).

2.4 Key software and programming languages

2.4.1 Statistical analysis

JMP® Pro (SAS Institute Inc., Version 12.0.1 to 15.0.0, NC, US) was used in this thesis to build the DoE applied in **Chapter 4** as well as the statistical analysis in **Chapter 3**, **Chapter 4** and **Chapter 6**. The software offers very detailed reports for various multivariate data analysis techniques used in this thesis. For instance, in **Chapter 3** and **Chapter 4**, Jmp was used to perform stepwise regression and build predictive models, and in **Chapter 6** it was applied to build PLS models using the NIPALS algorithms and cross-validation.

Jmp® was also applied for process robustness analysis. 5000 thousand simulations were performed using triangular distributions for the input parameters: target pH and seeding density in **Chapter 3**.

The cause-and-effect correlations models built in Jmp were also replicated in Design Expert® (Stat-Ease Inc., Version 9 to 11, MN, US). The outputs include a predictive model equation in terms of coded factors, which allows evaluating the contribution of individual terms to the mean of the response and the R^2 -predicted for the model.

2.4.2 Data pre-treatment and bioprocess modelling

2.4.2.1 Python

Python is an object oriented programming language that offers a number of advantages over other programming languages such as being an open source,

offering a rich library of available functions and packages. It is a very efficient language requiring less code than other languages. Python was the programming language used to build the economics model for the recovery operation (an extension of an already existing economics model built in this environment).

2.4.2.2 **Matlab**

Matlab® (The MathWorks, Inc., Version 2015 to 2018b, Natick, MA) was used for the overall organisation and pre-treatment of the data throughout the thesis and in particular for the PLS analysis in **Chapter 6**. For the organization of the data, “structures” were implemented. Each structure represents an experiment with “fields” to store the conditions and the results for the experiment. Programs were also written to pre-treat and analyse the data in the “fields”, where necessary – for instance, calculating % LDH release, [Cholesterol] from a reference curve, antibody reduction from an electropherogram, normalizing and binning the particle size distribution (PSD) data etc.

Chapter 3

3 Linking cell culture parameters to upstream and recovery metrics

3.1 Introduction

The industry's pursuit for increasing cell culture titres (g/L), has resulted in very high cell density cultures, which for CHO fed-batch processes often exceed 40×10^6 cells/mL at harvest. This poses significant challenges for the harvest operation that needs to separate the elevated amount of solids from the harvested fluid. The goal of this chapter is to apply a holistic approach to the optimisation of cell culture conditions considering the need to maximise upstream productivity, while minimising the burden for the subsequent recovery step by reducing the turbidity and solids concentration ([solids]).

The [solids] is an important recovery metric due to its impact on the centrifugation performance: the higher the [solids], the more frequent the discharge intervals for a continuous disc-stack centrifuge, which leads to product loss as product is ejected with each discharge. The separation in the disc-stack centrifuge is driven by centrifugal force and hence the bigger the size of the particle, the easier it is to separate. There is a critical diameter (d_c) for the particle, above which there is a higher probability that the particle will be recovered during the centrifugation

operation (as described by **Equations (2.11) and (2.12)**). Hence, the smaller the particles in the harvest, the higher the probability that they would not be recovered during the centrifugation operation.

The turbidity of the cell culture harvest is another important parameter for the recovery operation, since high turbidity levels are associated with more difficult to clarify harvests. The turbidity levels increase due to the rise in biomass (amount of solids) during cell growth and also due to the increase in cellular debris (smaller particles) towards the end of the process when cell culture viability declines.

Currently, the optimisation of the upstream process in early process development usually disregards the recovery operation. For instance, temperature and pH are only optimised with respect to titre and product CQAs (Brunner et al., 2017; Gronemeyer et al., 2014; Hennicke et al., 2019; Ivarsson et al., 2014; Ivarsson et al., 2015; Kishishita et al., 2015; Sou et al., 2015; Trummer et al., 2006), not considering the impact of these parameters on the recovery operation in terms of [solids] or turbidity. Furthermore, due to their impact on productivity and product CQAs, these parameters are often locked in during the early development stage.

It is important to note that the pH and temperature will also impact on cell metabolism e.g. glucose consumption and osmolality levels, which has the potential to alter product quality. There are a number of studies that have investigated this impact (Chung et al., 2018; deZengotita et al., 2002; Gilbert et al., 2014; Kamachi and Omasa, 2018; Sissolak et al., 2019; Tae Kyung Kim et al., 2000; Trummer et al., 2006; Qin et al., 2019; Yoon et al., 2005; Yuk et al., 2011 and Zhu et al., 2005).

None of the studies mentioned so far considered the impact of pH and temperature in the context of varying seeding densities and harvest day conditions and the impact of these conditions on the recovery operation. To address the lack of understanding about the interactions between upstream and recovery performance, this chapter proposes mapping the design space for the upstream and recovery operation through the application of a DoE approach in the ambr platform. The cell culture pH and temperature, the initial seeding density and the day of harvest were used to predict key upstream metrics and inputs for the recovery operation. The upstream metrics included cell culture productivity, osmolality and glucose consumption and the recovery metrics were [solids], particle size (d10) and turbidity.

The analysis of the ambr runs was first focused on the cell culture growth kinetics and the conditions that resulted in increased maximum viable cell count (MVC) (**Section 3.3.1**). **Section 3.3.2** focuses on the derivation of cause-and-effect correlations that link the upstream conditions to upstream and recovery performance metrics. In **Section 3.3.3** and **3.3.4** these correlations were used to build windows of operation for two separate DoE studies. In the first DoE study (ambr1 in **Section 3.3.3**), a window of operation was presented constrained by [solids] and titre. The robustness of the window was tested through the application of stochasticity to the seeding density as this is a parameter that is hard to control during large scale operation. In the second DoE study (ambr2 in **Section 3.3.4**), the window of operation was constrained by titre, [solids] and turbidity.

The overall goal of this chapter was to derive-cause-and effect correlations to better understand the trade-offs between upstream and recovery metrics. This approach

will enable a more informed decision-making process when defining the upstream parameters for the process. Developing these correlations was essential to be able to build a more predictive process economics model in Chapter 5. This model will provide insights into the impact of upstream and recovery operations on facility fit and economics.

3.2 Experimental approach

3.2.1 Ambr experiments

The results presented in this chapter are from two separate DoE studies in the ambr - ambr1 with 24 bioreactors and ambr2 with 36 bioreactors (3 out of 4 culture stations). Due to operational limitation the two ambrs used two clones of the same cell line. For ambr1, a full factorial design was employed with target harvest day varied at three levels (harvest day 13, 15 and 17) and target seeding density varied at three levels (0.5, 0.7 and 0.9 x10⁶ cells/mL). Since temperature can only be changed per culture station (consisting of 12 bioreactor vessel), it was only possible to vary the temperature at two levels (temperature shift to 33°C on day 4 and a constant temperature of 35.5°C). Therefore, for the DoE design and subsequent analysis the temperature parameter for ambr1 was considered a categorical factor and there were two centre points for the low and high temperature. Based on the statistical analysis of ambr1, it was decided to focus on the same parameters as they showed to have a significant relationship with the models generated in the parameters' tested ranges. Furthermore, for ambr2 it was possible to perform more runs and set three temperature levels. Based on the analysis from ambr1 and the possibility to do more runs in ambr2 it was decided to move to a higher resolution

design, and therefore a central composite design was employed. For ambr2 the seeding density range was widened from ambr1 to see if this would result in a bigger impact on the process – from 0.5, 0.7, 0.9 x10⁶ cells/mL for ambr1 to 0.6, 0.9, 1.2 x10⁶ cells/mL for ambr 2. For ambr1 and ambr2 0.5mL samples for titre were collected on the harvest day for each bioreactor. The harvest titre was critical for the process economics model in Chapter 5 to size recovery operations and assess facility fit.

Table 3.1 Experimental setup for DoE studies in ambr1 and ambr2

| Project | ambr1 | | | | ambr2 | | | | | |
|---|--------------------------|--------|------|--------|--------------------------|---------|------|---------|------|---------|
| | Cell culture A (clone 1) | | | | Cell culture A (clone 2) | | | | | |
| | CS1 | | CS2 | | CS1 | | CS2 | | CS3 | |
| Temperature shift on day 4 | 33 | | 35.5 | | 33.5 | | 34.5 | | 35.5 | |
| Seeding density (x10 ⁶ cells/mL) expected* | 0.40 | (0.5)* | 0.41 | (0.5)* | 0.57 | (0.60)* | 0.61 | (0.60)* | 0.59 | (0.60)* |
| | 0.56 | (0.7)* | 0.67 | (0.7)* | 0.98 | (0.90)* | 0.98 | (0.90)* | 1.12 | (0.90)* |
| | 0.83 | (0.9)* | 0.88 | (0.9)* | 1.25 | (1.20)* | 1.15 | (1.20)* | 1.30 | (1.20)* |
| pH | 6.8 | | | | 6.8 | | | | | |
| | 7.0 | | | | 7.0 | | | | | |
| | 7.2 | | | | 7.2 | | | | | |
| H. day expected* | 12.9 | (13)* | | | | | 13.0 | (13)* | | |
| | 13.8 | (15)* | | | | | 13.9 | (14)* | | |
| | 15.8 | (17)* | | | | | 15.0 | (15)* | | |

* Target set points for the DoE

3.2.2 Stepwise regression and model selection

The results from the DoE studies described in the previous section were analysed using the JMP® software (SAS Institute Inc., Version 12.0.1 to 15.0.0, NC, US) and Design-Expert® software (Stat-Ease Inc., Version 9 to 11, MN, US). First stepwise regression technique (as described in **Section 2.3.3.2**) was applied to the results from the DoE to build 24 models with up to eight predictors as per the example given

in **Appendix (Table 3.1-A)**. Each of the 24 models was also generated using Design-Expert®; this software also computed R^2 predicted for the model. The JMP algorithm was set to maximize for R^2 k-fold and the optimum model was selected based on minimum BIC and AIC and maximum difference between the R^2 pred. and R^2 adj. of 0.2. When the models had very similar statistics, the model with the least number of terms was chosen. Finally, process knowledge was also used to inform the choice of a model if the statistics for the models were similar.

3.2.3 Robustness analysis

Monte Carlo simulations for the seeding density were carried out using Jmp. The stochastic inputs were set as triangular distributions and 5000 runs were performed for each simulation. The outputs from the simulations were presented as distributions.

3.3 Results and discussion

3.3.1 Growth Culture Kinetics

Increasing maximum viable cell number (MVC) and prolonging cell culture viability can lead to higher cell culture productivities. Therefore, in this section the goal was to investigate the impact of the upstream conditions of temperature and pH, the initial bioreactor seeding density and day of harvest on the cell growth profile, the MVC and cell culture viability.

Ambr1 and ambr2 were analysed separately as there were significant differences in growth rate and productivity between the two runs, which can be due to differences in the clones or the generation number of the cells (data not available). Furthermore,

3 to 4 cell count measurements for ambr2 were missing due to a fault in the instrument. Initially, blocking was used to build models for ambr1 and 2 together, however, the analysis did not yield meaningful results (data not shown). Therefore, ambr1 and ambr2 were analysed separately in this section.

Figure 3.1 reveals that temperature and pH have a significant impact on cell growth, while the increase in seeding density could to an extent reduce the impact of suboptimal pH (pH 6.8 and pH 7.2) and temperature (lower temperature) on maximum viable cell count (MVC). For ambr1 for the conditions with a temperature shift (**Figure 3.1a, b and c**), the cell culture achieved lower MVC compared to the cell culture without a temperature shift (**Figure 3.1d, e and f**). **Figure 3.1** shows that the low pH had a detrimental impact on cell growth, leading to a large drop in MVC compared to the optimum achieved at mid pH conditions, irrespective of temperature. For example, the maximum MVC achieved for the low pH was 25×10^6 cells/mL compared to the optimum MVC of 39×10^6 cells/mL at mid pH and the low temperature conditions. The above findings were also seen for ambr2, where the lower pH and temperature led to lower cell growth for the first 7 days of cell culture.

These temperature and pH findings are in line with previous studies that have showed suppressed cell growth for temperature shift conditions from 37°C to 30°C or 33°C (Fox et al., 2005; Kaufmann et al., 1999; Moore et al., 1997 and Bollati-Fogolín et al., 2005) as well for a combination of temperature shift and low pH conditions (Hwang et al., 2011; Oguchi et al., 2006). However, some of these studies reported prolonged cell culture viability for the temperature shift and low pH

conditions, which was not observed here. This could be due to the fact that the temperature shift and low pH conditions were suboptimal for this cell line.

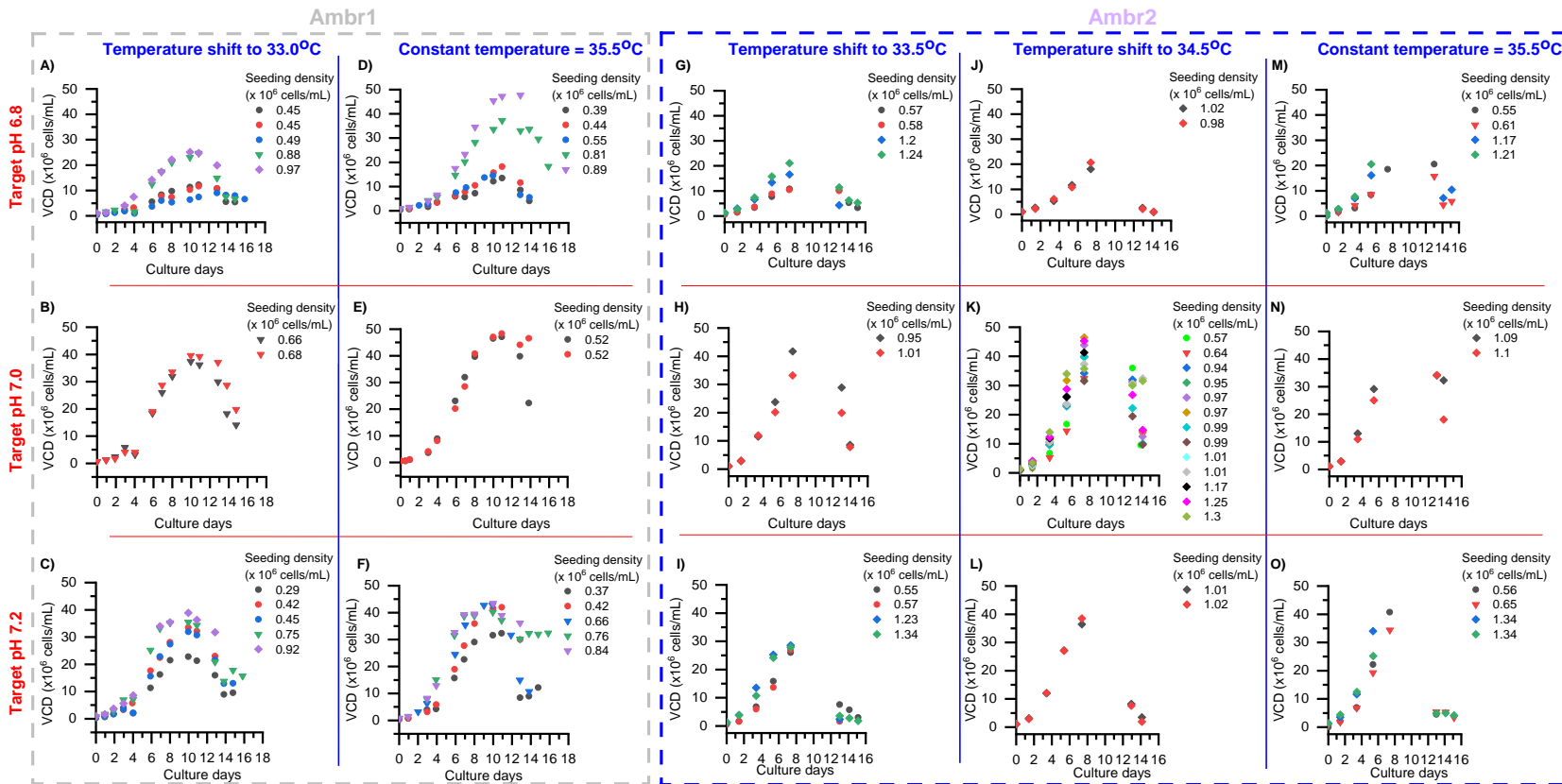


Figure 3.1 Fed-batch cell culture kinetics for ambr1 (box with light grey border - - -) and ambr2 (box with blue border - - -). A),D),G),J) and M) conditions at low pH target of 6.8; B), E), H), K) and N) describes conditions at mid pH of 7 and C), F), I), L) and O) is for high pH conditions of 7.2. For ambr1 temperature shift was applied on day 4 from 35.5°C to 33.0°C for A), B) and C) and constant temperature of 35.5°C for D), E), F). For ambr2 constant temperature of 35.5°C was applied M), N),O) and temperature shift on day 4 from 35.5°C to 34.5°C - J),K),L) and temperature shift to 33.5°C - G), H) and I). The symbols represent different seeds: ● low seed below 0.6×10^6 cells/mL; ▼ mid seed between 0.6 and 0.9×10^6 cells/mL and ◆ high seed above 0.9×10^6 cells/mL

*Due to a faulty instrument there were missing cell counts between day 8 and day 12 for ambr2

3.3.2 Predictive models for the upstream and recovery metrics

As shown in the previous section, the seeding density, pH and temperature impact the overall growth profile and the MVC achieved for the process. This is important since reaching higher titres may be achieved through conditions that increase the cell culture turbidity and [solids], shifting the burden to the subsequent clarification operation.

In this section, temperature, pH, seeding density and harvest day were used to build predictive models (as described in **Section 2.3.3.2**) for titre, [solids], turbidity (data available for ambr2 only), d10 (data available for ambr2 only), osmolality (data available for ambr2 only) and glucose consumption. The equations in terms of coded factors are summarized in **Figure 3.2**.

Figure 3.2 reveals that seeding density, temperature, pH and harvest day impact on all upstream and recovery metrics. In some instances seeding density interacts with temperature or pH (**Figure 3.2 a** and **b**) meaning that the impact of pH or temperature will depend on the seeding density. In the following section the models are to be investigated using contour plots describing the different combinations.

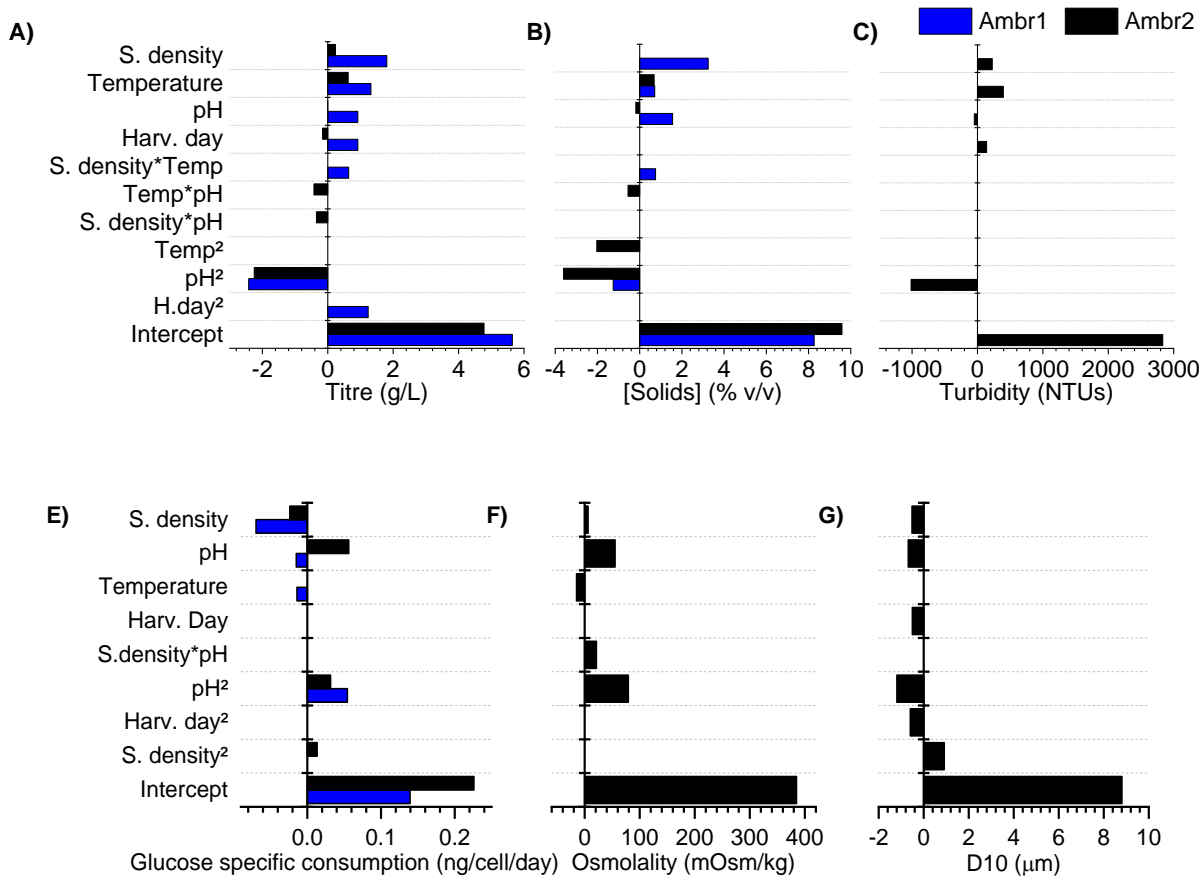


Figure 3.2 Predictive equations in terms of coded factors for ambr1 (■ –) and ambr2 (■ –) for: A) Titre (g/L) with adj. $R^2 = 0.79$ (ambr1), pred. $R^2 = 0.74$ (ambr1), k-fold $R^2 = 0.70$ (ambr1) and adj. $R^2 = 0.83$ (ambr2), pred. $R^2 = 0.74$ (ambr2), k-fold $R^2 = 0.76$ (ambr2); B) [Solids] (%v/v) with adj. $R^2 = 0.74$ (ambr1), pred. $R^2 = 0.64$ (ambr1), k-fold $R^2 = 0.68$ (ambr1) and adj. $R^2 = 0.67$ (ambr2), pred. $R^2 = 0.63$ (ambr2), k-fold $R^2 = 0.65$ (ambr2); C) Harvest turbidity (NTUs) with adj. $R^2 = 0.88$, pred. $R^2 = 0.86$, k-fold $R^2 = 0.86$ for ambr2; D) Cell specific glucose consumption (ng/cell/day) with adj. $R^2 = 0.84$ (ambr1), pred. $R^2 = 0.79$ (ambr1), k-fold R^2 k-fold = 0.90 (ambr1) and adj. $R^2 = 0.89$ (ambr2), pred. $R^2 = 0.86$ (ambr2); E) Osmolality (mOsm/kg) with adj. $R^2 = 0.89$, pred. $R^2 = 0.85$ (ambr2); F) d10 (μm) with adj. $R^2 = 0.88$, pred. $R^2 = 0.86$ for ambr2. (ambr2). S.density = Seeding density; Harv.day = Harvest day

3.3.3 Building a window of operation for ambr1 constrained by titre and [solids]

Following the QbD approach to process development the predictive models derived earlier were used to build feasible operating windows for the ambr1 and ambr2. The goal was to identify trade-offs between upstream and recovery metrics and test the susceptibility of the process to the inherent variability in the seeding density.

3.3.3.1 Effects of pH, temperature and seeding density on titre and [solids] for different harvest days

Contour plots for [solids] and titre were built using the correlations derived in the previous section and plotted using OriginPro (OriginLab®) for ambr1 (**Figure 3.3**). The contours exhibit a curvature profile with maximum [solids] achieved at ~ pH 7.1 and high seeding density condition. There is one interaction term for seeding density with temperature, which explains the different shape of the contour plots (**Figure 3.3 a and b**). For the conditions without a temperature shift, the increase in seeding density led to higher titre than for the conditions with a temperature shift. The highest solids concentration is predicted for the high seeding density conditions at ~ pH 7.1 and no temperature shift.

The contour plot for the titre model has a similar profile, with the highest titre achieved at pH 7 – 7.1. There is again an interaction term observed – temperature*seeding density – so that for the conditions without a temperature shift, seeding density has higher impact on titre than conditions without a temperature shift. The late harvest day led to overall increase in titre, with maximum titre predicted for day 16 at pH between 7 and 7.1 and high seeding density conditions.

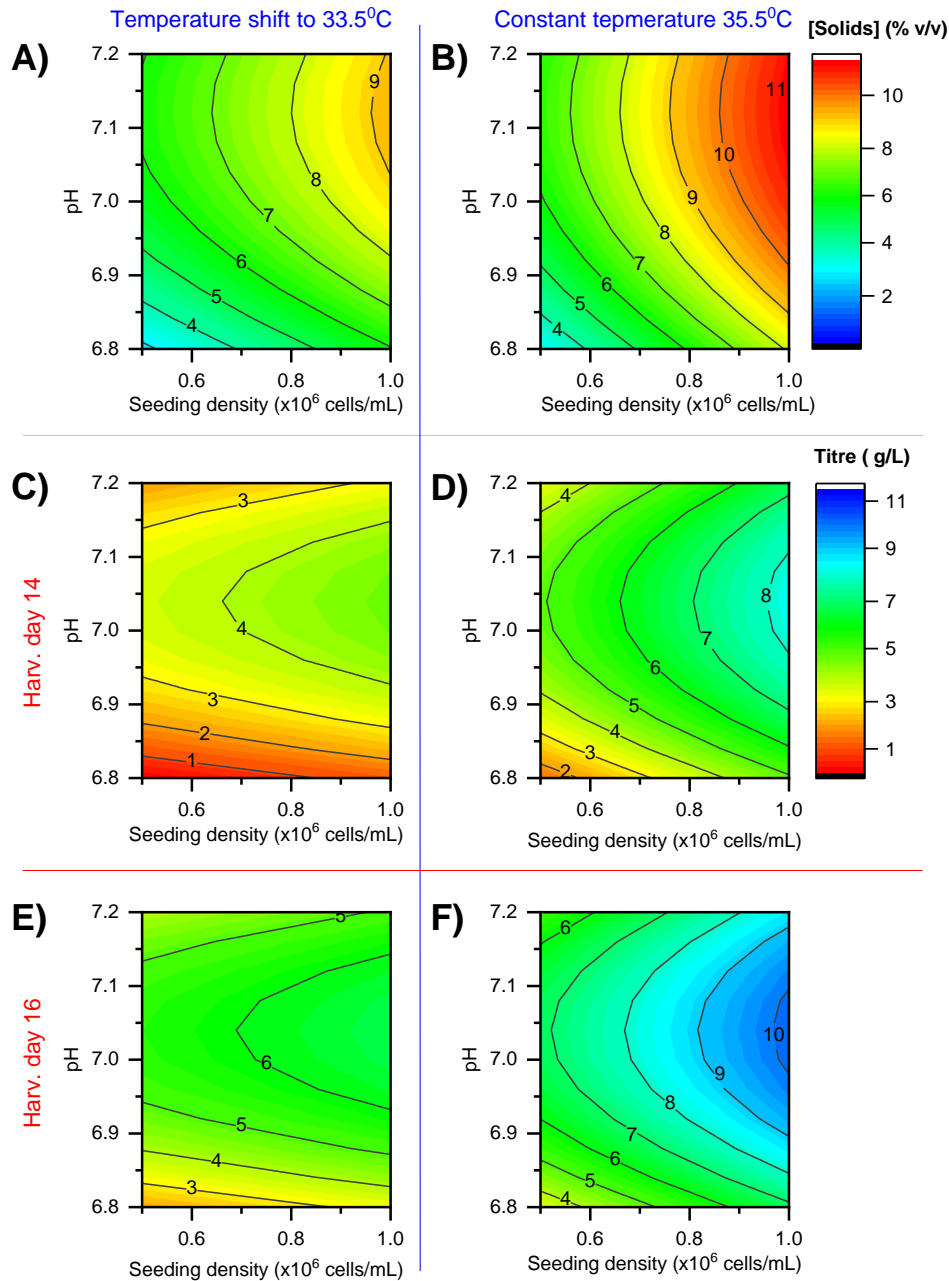


Figure 3.3 Contour plots showing the impact of seeding density and pH on A) [solids] for conditions with a temperature shift; B) [solids] for conditions without a temperature shift; C) titre for harvest day 14 for conditions with a temperature shift; D) titre for harvest day 14 for conditions without a temperature shift; E) titre on day 16 for conditions with a temperature shift; E) titre on day 16 for conditions without a temperature shift. The temperature shift was carried out on day 4 from 35.5°C to 33.0°C

3.3.3.2 Window of operation

Biomanufacturing processes can be constrained by the [solids] due to limitations in the centrifugation solids handling capacity and by minimum titre required to meet yearly demand. However, it may be harder to control these outputs due to variability in the process inputs such as the seeding density. At large scale the seeding density in the bioreactor is not tightly controlled; since the inoculum volume and seed train are fixed, therefore the final seeding density will be highly susceptible to the natural process variability.

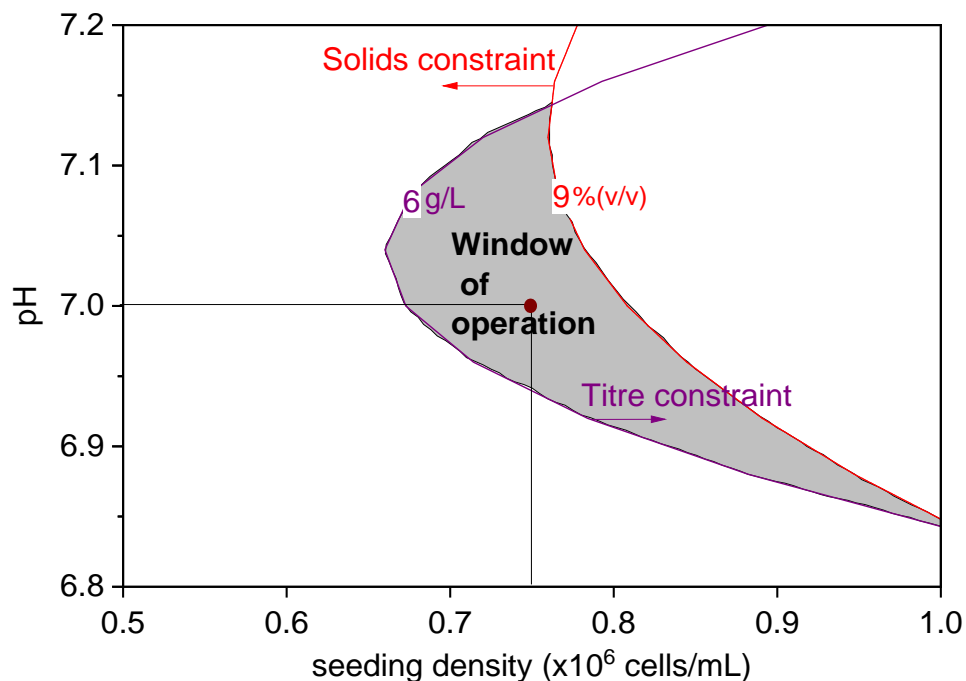


Figure 3.4 Window of operation (greyed out area) for ambr1 constrained by maximum [solids] of 9%v/v and minimum titre of 6g/L. The arrows point in the direction of desirability – increasing titre or decreasing [solids]. The red dot indicates the set operating parameters for the process so that it is within the window of operation.

To demonstrate the impact [solids] and titre constraints can have on the design space, a window of operation was built for a hypothetical process with a [solids] constraint of $< 9\%$ v/v and a minimum titre of 6 g/L (**Figure 3.4**). In order to operate within the process constraints the process parameters were set at pH 7, seeding density of 0.75×10^6 cells/cm² and harvest day 14 (shown as a red dot in **Figure 3.4**). For the seeding density, there is narrow range, for which the process is operating within the window. For a process, where the seeding density can be tightly controlled, a higher seeding density can be chosen to increase the titre.

3.3.3.3 Risk-based approach for selecting target seeding density

To investigate the impact of seed train variability on the process, namely the risk of exceeding [solids] and maximizing titre, probability distributions were applied to the seeding density parameter. In **Figure 3.5** target seeding densities between 0.65×10^6 cells/mL and 0.85×10^6 cells/mL were investigated with a variability of $\pm 0.15 \times 10^6$ cells/mL represented by a triangular distribution. The probabilities of failing to meet the target [solids] or titre are indicated.

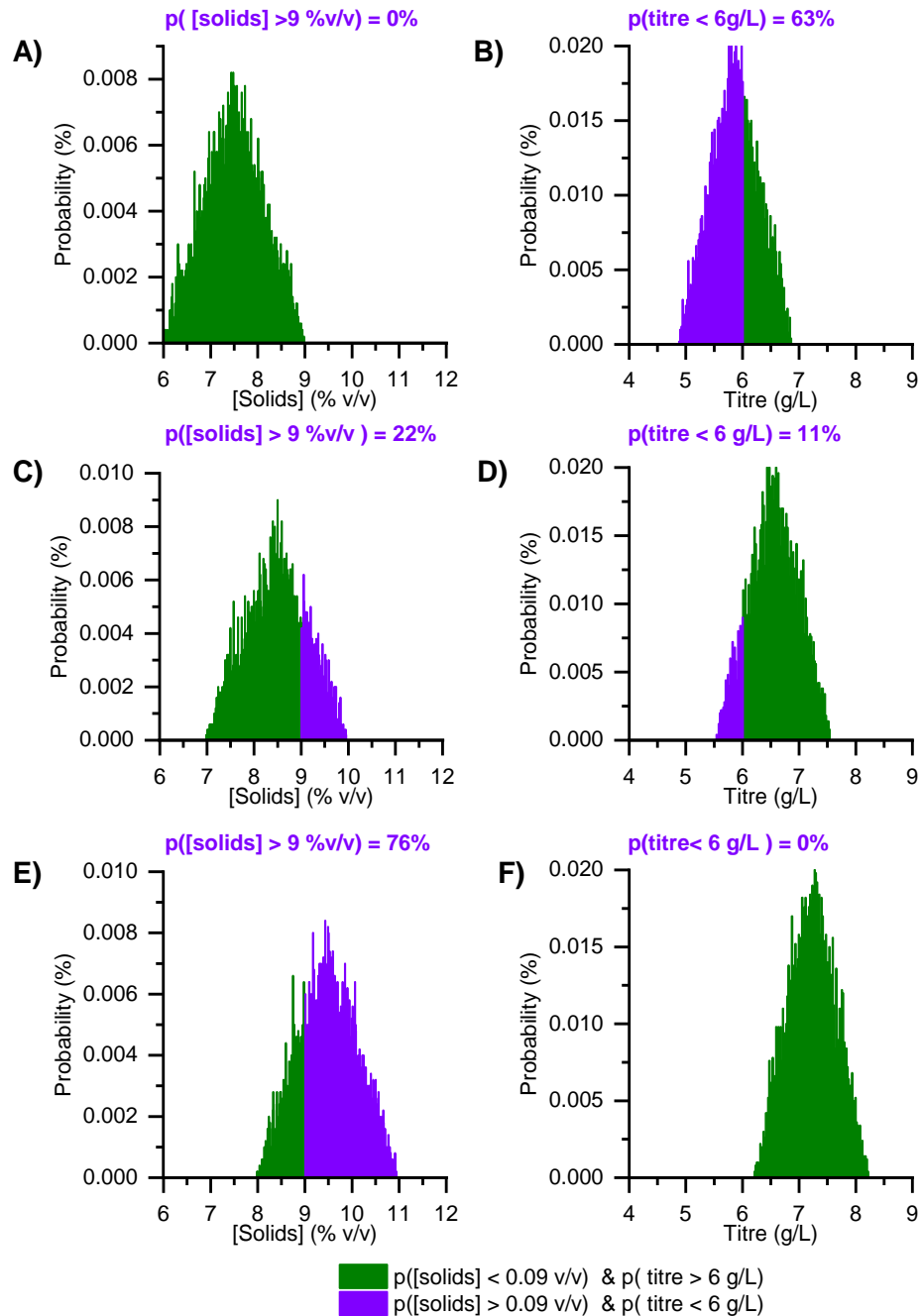


Figure 3.5 Probability distributions for ambr1, harvest day 14 for A) [solids] and B) titre at target seeding density of 0.65×10^6 cells/mL; C) [solids] and D) titre at target seeding density of 0.75×10^6 cells/mL; E) [solids] and F) titre for target seeding density of 0.85×10^6 cells/mL. The results were generated using 5000 simulation runs with seeding density inputted as triangular distribution ($\pm 0.15 \times 10^6$ cells/mL from target seeding density).

Figure 3.5 reveals that lowering the seeding density can be chosen to reduce the risk of exceeding [solids] limitations, while increasing the seeding density reduces the risk of not reaching the target titre. Hence it is not possible to achieve both objectives whilst manipulating the seeding density. For example, at the lower seeding density the likelihood of failing to meet the [solids] criterion is 0 whilst there is a high chance of failing to meet the titre criterion of 63%. In contrast, at the higher seeding density this is reversed with a zero chance of failing to meet titre but a high chance of failing to meet [solids] (76%).

3.3.4 Investigating the impact of seeding density on the window of operation for ambr2

3.3.4.1 Impact of seeding density on titre, [solids] and turbidity for different pH and temperature combinations

As it was shown earlier (**Figure 3.2**) the predictive correlations for ambr2 were different than the ones for ambr1. This could be due to the different clones used, unintended variations in the seed train, and variations in the conditions (e.g. different seeding density ranges and temperatures). In addition, more metrics were evaluated for ambr2 compared to ambr1 such as turbidity.

Similarly to ambr1, a desirable area was set for the process, which can be seen in green (**Figure 3.6**) – high titre, low turbidity and [solids] – and in red are the least desirable areas – low titre and high turbidity. The analysis shows that the optimum for titre and the least desirable value for turbidity are achieved for the same conditions - pH of ~ 7 and no temperature shift. For the [solids] the least optimum conditions (high [solids]) are at mid pH and mid temperature conditions (**Figure**

3.6.d, e and f. Titre and turbidity have similar contour profiles where for every increase above pH of 7 or drop below pH of 7, high temperature is needed to achieve the same level of titre or turbidity. For instance, at pH 7 and temperature shift to 33.5°C the titre levels are comparable to the lower pH ~ 6.85 and high temperature of 35.5°C. **Figure 3.6** also shows that seeding density impacts on the titre or turbidity that could be reached for the process. This can represent a risk for the process where seeding density is poorly controlled resulting in elevated turbidity or lower titre, or can be used as a risk mitigation strategy against low titre.

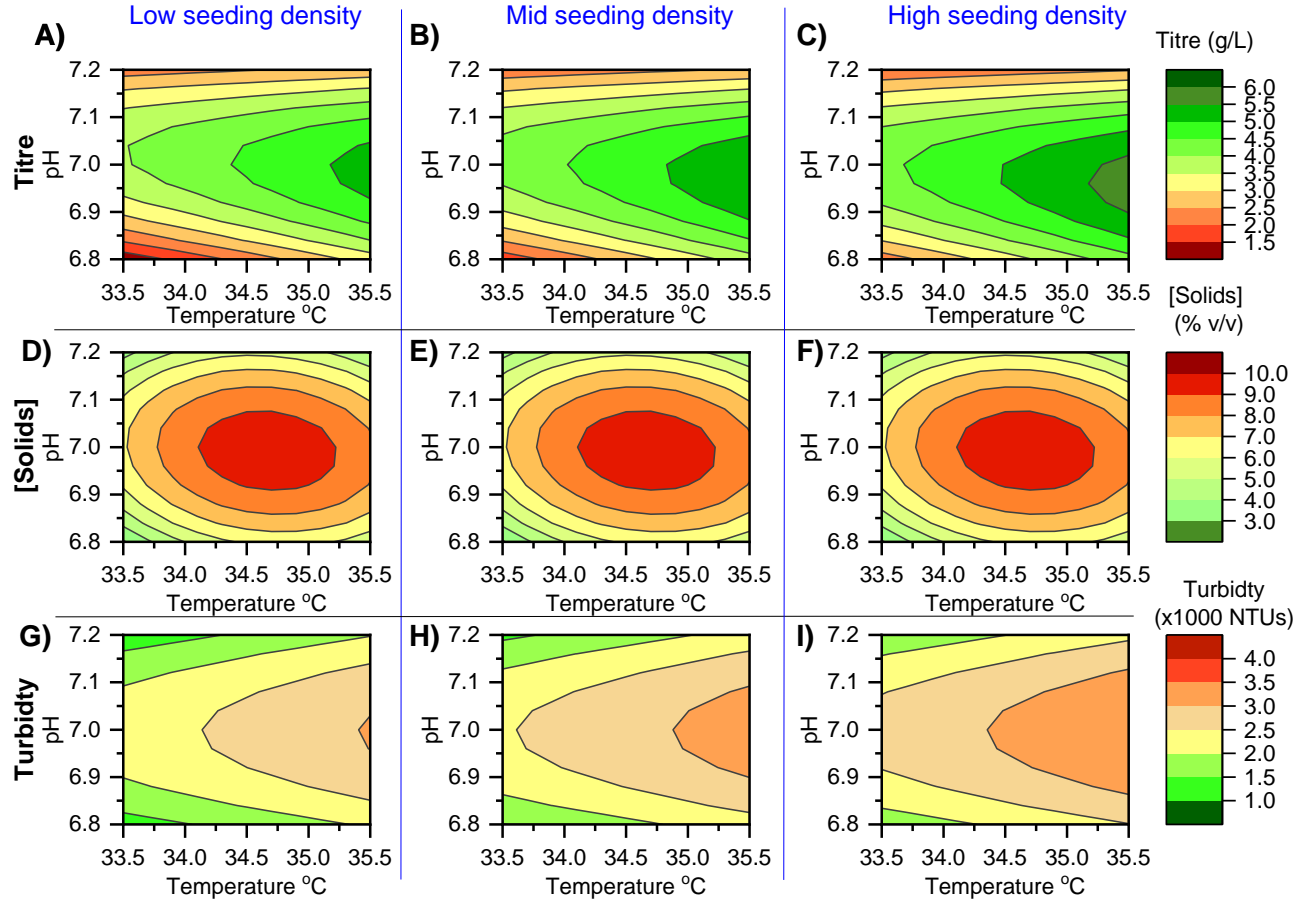


Figure 3.6 Heatmaps for ambr2 showing the impact of varying temperature and pH at low seeding density conditions on A) titre (g/L), D) [solids] (%v/v) and G) turbidity (NTUs); at mid seeding density on B) titre (g), E) [solids] (% v/v) and H) turbidity (NTUs) and high seeding density for C) titre(g/L), F) [solids] (% v/v) and I) turbidity (NTUs). The seeding densities for the experiment are provided in **Table 3.1**.

3.3.4.2 Impact of seeding density on the process window of operation

The contour plots from **Figure 3.6** were overlaid to create feasible windows of operation for three different seeding density levels; the windows were based on a hypothetical process constrained by maximum turbidity of 3000NTUs, maximum [solids] of 9%v/v and minimum titre of 4g/L (**Figure 3.7**). As it was discussed earlier changes in the upstream conditions can indirectly impact on product quality and process performance by inadvertently altering cell culture conditions, for which there may be no strict targets - such as osmolality, cell metabolism and PSD. For instance, changes in pH and increase in lactate due to decreased cell culture viability are linked to changes in osmolality, drop in cell culture viability can also be linked to shift to smaller particle size and changes in pH. Therefore, a second window of operation was built which reflects some of these additional parameters that may impact on the process but where the link to process performance is less clear. The limits for these additional metrics were set to less than 8.5 μ m for d10 (as described in **Section 2.1.3.8**), less than 400 mOsm/kg for osmolality and between 0.2 and 0.32 for glucose consumption. These limits were chosen so that they were close to what was observed for the standard process at pH of 7 and no temperature shift.

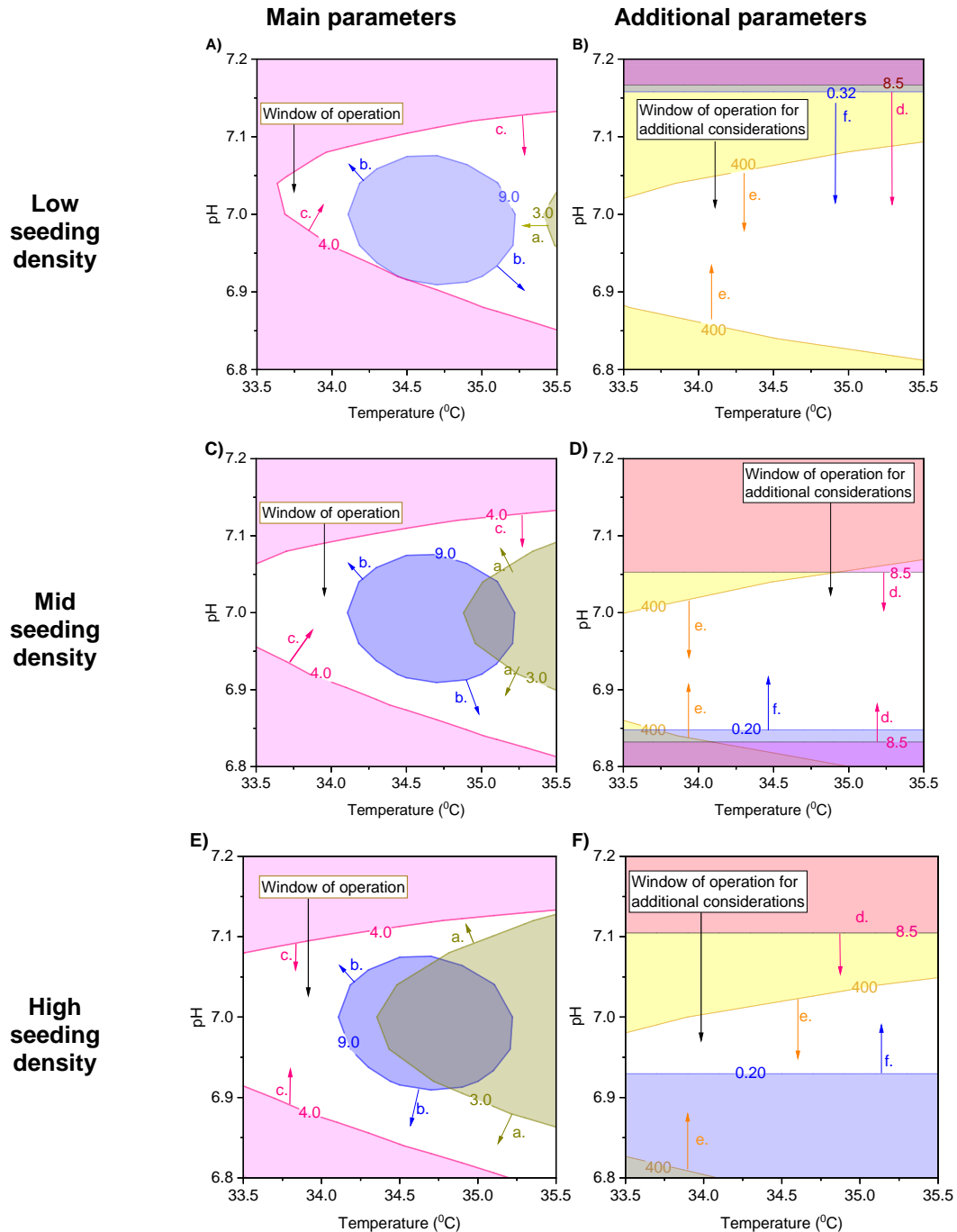


Figure 3.7 Windows of operation constrained by a-turbidity < 3000 NTU, b- [solids] < 9 % v/v, c- titre > 4g/L for A); C) and E), and by d- d₁₀ > 8.5μm, e- osmolality < 400 mOsm/kg and f- q_{gluc.} > 0.2 & < 0.32 gluc.(ng)/cell/day for B); D) and F). The windows were built for ambr2 at harvest day 14 and different seeding density conditions - A) and B) low seeding density (0.6×10^6 cells/mL); C) and D) mid seeding density (0.9×10^6 to 1.2×10^6 cells/mL) and E) and F) high seeding density (more than 1.2×10^6 cells/mL).

Figure 3.7 shows that the seeding density has a significant impact on the two sets of windows of operation – the main and the additional window. For the low seeding density conditions, the main window of operation was mainly constrained by titre and [solids] rather than turbidity (**Figure 3.7a**). However, as the seeding density increased, the turbidity played a greater role in restricting the window of operation. Yet higher seeding densities also led to the window of operation widening at the low temperature conditions (temperature shift to 33.5°C, **Figure 3.7c** and **e**) and enabling a wider pH range (6.9 to 7.1, **Figure 3.7c**).

Although there was a feasible window of operation across all seeding densities, the window of operation for the additional parameters was reduced as the seeding density increased. For the low seeding density, the window of operation is only constrained by the increase in osmolality (**Figure 3.7b**). For mid-seeding density conditions, the window is further constrained by the decrease in d10 and the lower glucose consumption (**Figure 3.7d**). For the high seeding density conditions the window is constrained by glucose consumption and the osmolality levels. These additional considerations can provide a basis for further investigation.

3.4 Conclusions

Disconnect between upstream and recovery process optimisation in early process development can generate difficult to clarify harvests. This chapter bridged this gap through the application of a QbD approach to the upstream development, where both upstream and recovery metrics were considered.

The analysis of the ambr1 and ambr2 growth culture kinetics showed how the seeding density could alter the impact of pH and temperature on MVC. The higher seeding density led to overall higher MVC, moreover, the higher seed could negate the negative impact of suboptimal pH or temperature conditions on MVC.

Predictive models were built for upstream and recovery, which revealed that seeding density, harvest day, temperature and pH also impacted on titre, [solids] and turbidity. The derived causes-and-effect correlations enabled windows of operation to be generated accounting for the linkage between upstream and recovery metrics, showing trade-offs between optimising for upstream (titre) and recovery ([solids] and turbidity). The work presented in this chapter lays the foundations of the development of the upstream recovery framework and allow linking the process to bioprocess economics.

Chapter 4

4 Derivation of predictive correlations for the upstream-centrifugation-depth filtration sequence

4.1 Introduction

The previous chapter revealed important trade-offs between upstream and recovery metrics when optimizing the conditions in the upstream. This chapter extends the investigation to the impact of both the upstream parameters and the centrifugation operation on the process. The impact of centrifugation shear is explored on the centrate's filterability as well as on the product- and process- related impurities, in terms of levels of antibody reduction and host cell proteins. Furthermore, this chapter developed tools that enable a holistic view of the upstream and recovery operation through linking the small scale upstream experimentation in the ambr to the centrifugation mimic.

The impact of the centrifugation step on process performance is often disregarded for early process development - for instance, for bench scale studies the centrifugation step is typically replaced by depth filtration. As a consequence the impact of the centrifugation shear is often not well understood at the early stages of

process development. To overcome this limitation a number of studies have proposed scaling down the centrifugation step through decoupling the centrifugation shearing and clarification (Maybury et al., 2000; Boychyn et al., 2004; Lau et al., 2013; Tait et al., 2009; Westoby et al., 2011). This way the feed material is first sheared to mimic the impact of centrifugation shear on the particle size distribution, and then clarified in a benchtop or swing-bucket centrifuge to mimic the levels of clarification - usually based on centrate's turbidity (NTUs) or optical density (OD_{550nm}).

The level of shear between the different scales is compared indirectly through measuring the release of intracellular components such as LDH due to cell membrane disintegration. However, this approach can be challenging for low viability cell cultures, where cell membranes have lysed, and there may be little to no difference in LDH concentration between the intracellular and extracellular space. To address this challenge, the current study proposed an improved approach to the characterisation of the pilot scale centrifuge based on [cholesterol] to characterize the shear for low viability harvests. Furthermore, this chapter demonstrated that the [cholesterol] can also be used as a correlate for centrate filterability so that filter requirements can be determined with the small centrifugation mimic without the need for scaling down the depth filtration operation.

The centrifugation step may also impact on the levels of product and process related impurities. Common product related impurities result from antibody reduction at the disulfide bond in the antibody hinge region leading to the formation of half antibodies and antibody fragments. Typical process related impurities are host cell proteins

(HCPs); often the whole process needs to reduce to <100ppm HCP (Chon and Zarbis-Papastoitsis, 2011). The centrifugation shear can increase the level of HCPs due to cell disruption and the concomitant release of intracellular components. Some of the released components have been shown to lead to antibody reduction as they are involved in reduction pathways (Handlogten et al., 2017; Kao et al., 2010). Mimicking antibody reduction using scale-down centrifugation models is challenging due to different environmental conditions between the small and the large scale-processes – e.g. more aeration in the small scale due to lower volume to surface ratios in storage vessels post centrifugation shear. The centrifugation mimic presented here was adapted to enable reduction at small scale.

The overall goal of the chapter was to develop tools that can be integrated in the scale-down framework for mimicking the upstream and recovery steps holistically. **Section 4.3.1** described the methodology applied for characterizing the shear level in the existing pilot scale centrifuge, through achieving comparable levels of LDH, [cholesterol] and filterability. In **Section 4.3.2** the filterability of various pilot-scale and mimic concentrates (generated using the centrifugation mimic and pilot scale centrifuge) was correlated to the levels of [cholesterol] so that the latter could be used as a correlate for filter capacity (L/m^2). **Section 4.3.3** investigated the impact of centrifugation shear on the levels of antibody reduction and HCPs. In **Section 4.3.4** the combined impact of centrifugation shear and the depth filtration operation on the levels of antibody reduction (inverse to intact monomer/antibody) was investigated. **Section 4.3.5** implemented a framework based on an ambr linked to a centrifugation mimic. This platform was used to map the design space for upstream-

recovery metrics. Establishing this framework was essential for the decisional tool development and implementation in Chapter 5, which links the upstream conditions to process economics and facility fit.

4.2 Methodology

4.2.1 Summary of cell culture conditions for the pilot scale characterisation studies

Three cell culture runs were used in the characterisation studies (**Table 4.1**). Cell culture A and B were used to characterize the shear and clarification performance of the two different pilot scale centrifuges – Pilot scale 1 (LAPX404, AlfaLaval UK) and Pilot scale 2 (MBPX404, AlfaLaval UK). Cell culture C at low viability – 28% (as outputted from Vi-Cell XR) was used with a novel approach for characterising the centrifugation shear using [cholesterol] to overcome the limitations with LDH. The replacement of the pilot scale centrifuge in the facility led to the need to switch from one centrifuge to another (Pilot scale 1 to Pilot scale 2).

Table 4.1 Description of the cell culture material used for the centrifuge characterisation studies

| Material | Scale | Study | Total cell density (x10 ⁶ cells/mL) | Cell culture viability (%) |
|----------------|-----------------------|---|--|----------------------------|
| Cell culture A | CSD/ Pilot scale 1 | Centrifugation characterisation using LDH | 17 | 89 |
| Cell culture B | CSD/ Pilot scale 2 | Centrifugation characterisation using LDH | 28 | 94 |
| Cell culture C | CSD/ Pilot scale 2 | Centrifugation characterisation using LDH and [cholesterol] | 30 | 28 |

4.2.2 Experimental setup for spiking studies using a Null cell line

A summary of the experimental setup for the spiking studies is presented in **Figure 4.1**. Two bench-scale bioreactors were run for up to 14 days with non-producing GS-CHO Null cell line. Cell culture material was collected on day 10, 12 and 14. The harvested cell culture material was spiked with purified mAbs - either mAb A (IgG1 λ) or mAb B (IgG1 κ) - targeting a concentration of 5g/L in 180mL. The spiked harvested cell culture was sheared using the CSD and the samples were collected in a conical bottom reservoir with three inlets (article # ACBT-050- C1N, Repligen, MA, US). This reservoir was sparged with nitrogen (N₂) prior to sample collection in order to mimic the low oxygen conditions at large scale and then clarified in a bench-top centrifuge. The clarified material was sterile filtered, subjected to hold of up to 30 days at room temperature, protein A purified and analysed for antibody reduction via capillary electrophoresis (method described in **Section 2.1.3.11**) or immediately purified for HCP levels determination (**Section 2.1.3.10**).

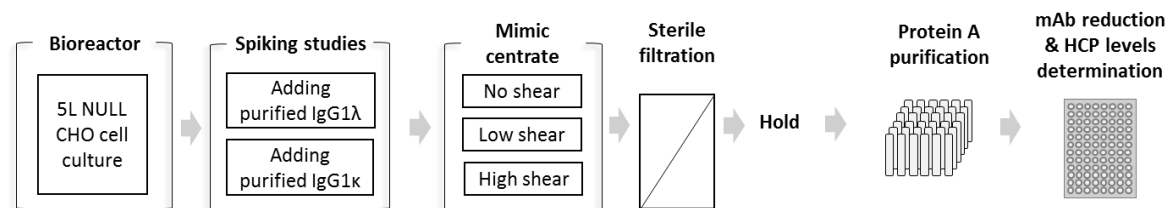


Figure 4.1 Experimental setup used for GS-CHO Null spiking studies, investigating the impact of upstream conditions (cell cultures harvested at different time points) and centrifugation shear (using a CSD centrifugation mimic) on the levels of HCP and mAb reduction

4.2.3 Experimental setup for studying the impact of centrifugation and depth filtration on antibody reduction

The samples from a process development 500L and 5L bioreactor runs were subjected to different levels of shear. The sheared material was clarified in order to generate centrate mimic, approximately 200mL per condition (**Section 2.1.2.2**). The samples were filtered at constant flux of 150LMH and held for up to 2.5 hours, then sterile-filtered and protein A purified (the method is described in **Section 2.1.2.5**). The purified samples were analysed for levels of antibody reduction using the Agilent 2100 Bioanalyzer system (Agilent Technologies, Inc, USA) – as described in **Section 2.1.3.11.2**. A description of the experimental setup can be found in **Figure 4.2**.

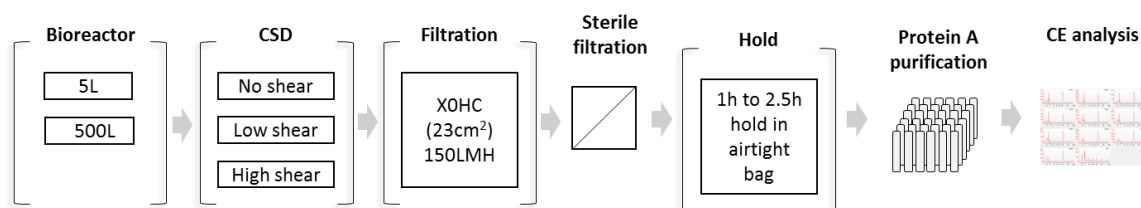


Figure 4.2 Experimental setup for studying the impact of centrifugation shear (using a CSD centrifugation mimic), secondary depth filtration (using a bench-scale setup at constant flow) and filtrate hold on antibody reduction measured via capillary electrophoresis (CE analysis) using a BioAnalyzer.

4.2.4 Ambr3 and ambr4 DoE studies

Two separate DoE studies were investigated in this chapter performed in the ambr15 system – the studies were designated as ambr3 and ambr4. The ambr3 experiment was based on a small Central Composite Design (set up using Design-Expert®) performed in replicates. Each replicate was a CCD consisting of six axial points, four factorial points and two centre points. One replicate was used for reduction studies (using the nitrogen-sparged vessel described in **Section 4.2.2**) and the other replicates were used for generating the mimic centrate and cholesterol analysis. Ambr4 was also based on CCD (using Design-Expert®) with 12 factorial points, six centre points and six axial points, however, the harvest day in the experiment deviated from the setup due to drop in the cell culture viability. For ambr4, all samples were collected in a syringe, which was void of air, part of the sample was spun and sterile filtered as per method described in **Section 4.2.3** and 10mL of the sample were used to generated mimic centrates as per **Section 2.1.2.2**.

Table 4.2 Summary of experimental conditions in ambr 3 and 4

| Ambr3 | | | | Ambr4 | |
|--|---------------------------|----------------------------|-------------------|--------------------------------------|-------------------|
| Goal of the study | <i>Reduction studies</i> | <i>Cholesterol studies</i> | Target set points | <i>Cholesterol/reduction studies</i> | Target set points |
| Culture station (CS) | CS1 | CS2 | | CS1 & 2 | |
| Seeding density (10 ⁶ cells/mL) +/- (std. dev) | 0.5 n=3 +/- (0.04)* | 0.5 n=3 +/- (0.04) | (0.4) | 0.46 +/- (0.06) n=7 | (0.4) |
| | 0.8 n=6 +/- (0.04) | 0.8 n=6 +/- (0.04) | (0.8) | 0.71 +/- (0.07) n=10 | (0.8) |
| | 1.2 n=3 +/- (0.07) | 1.2 n=3 +/- (0.01) | (1.2) | 0.92 +/- (0.08) n=7 | (1.2) |
| Shear level (mL/min) | 0 n=3 | | | 0 n=7 | |
| | 41 n=3 | | | 41 n=8 | |
| | 21 n=6 | | | 21 n=9 | |
| Harvest day | 10.7 n=3 | | (12) | 9.9 n=7 | (12) |
| | 12.8 n=6 | | (14) | 11.9 n=17 | (14&16) |
| | 13.8 n=3 | | (16) | | |

*indicates standard deviation

4.2.5 Antibody size analysis

The LabChip GXII analyzer (Perkin Elmer, Waltham, MA, USA) generates a CSV file for each analysis. A program was built in Matlab® (The MathWorks, Inc., Version 2015 to 2018b, Natick, MA), which compiles the data into a table format as described below.

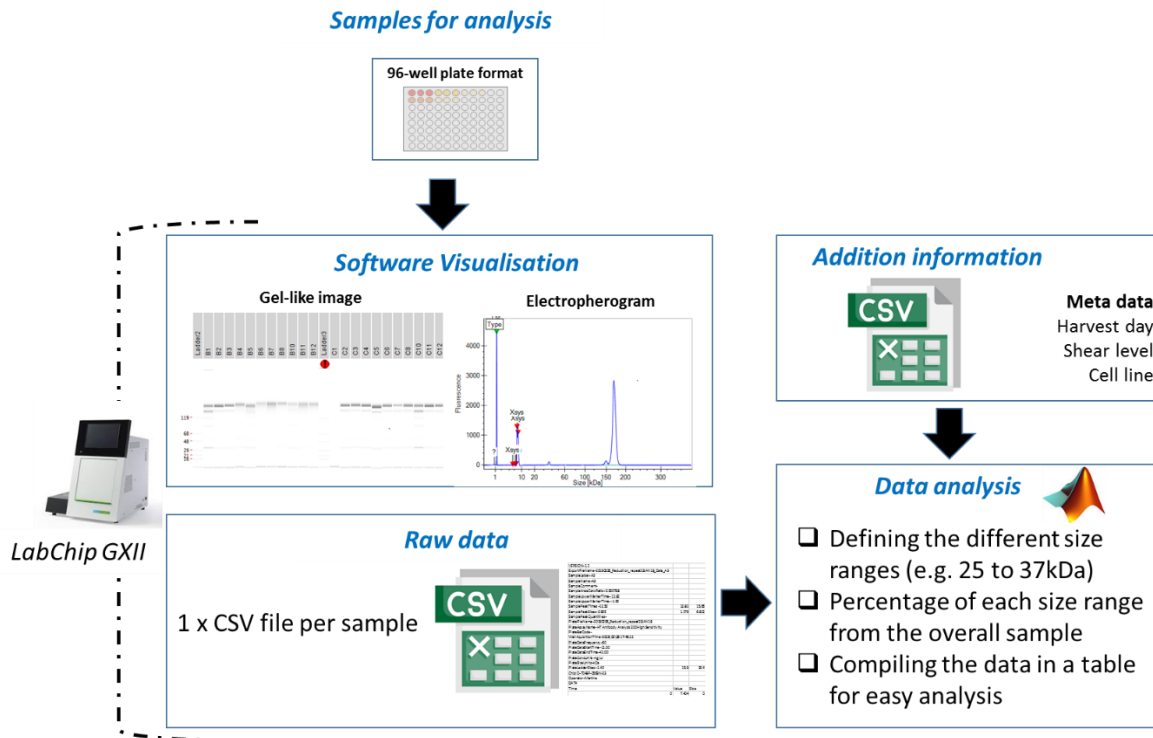


Figure 4.3 Workflow for analysis of the size data from the LabChip GXII. The data is first visualised for quick analysis. The CSV files from the LabChipGXII are imported in Matlab. The data is analysed for the different size antibodies and fragments generated from reduction at the disulfide bridge and is combined with all additional information available for the samples (e.g. harvest day, shear levels etc.).

4.3 Results and discussion

As discussed in **Section 4.1** the standard approach for characterising the centrifugation operation is through the decoupling of the shear and clarification effect. This approach was applied to successfully characterise two pilot scale centrifuges (pilot scale 1 = LAPX404 and pilot scale 2 = MBPX404) and the results from the characterisation can be found in the **Annex for Chapter 4**. The initial study revealed that the cell lysis due to shear in the pilot scale 1 centrifuge setup (at flowrate = 120Lh^{-1} and bowl speed = 7000 RPM) corresponded to 21mL/min in the CSD and for pilot scale centrifuge 2 (flowrate = 120L/h and bowl speed of 7000RPM and 8000RPM) to 31mL/min and 41mL/min in the CSD. The bowl speed applied in the pilot scale centrifuge was often defined by the process development team as the material was generated as part of their routine operations.

Measuring cell disruption due to shear using LDH relies on the increase in LDH post shear or due to chemical lysis (method described in **Section 2.1.3.5**). However, for low viability cell cultures, the harvested cells may have lost membrane integrity and hence shear may not lead to additional release of LDH. To overcome this challenge the current section presents a novel approach using [cholesterol] to characterise the centrifugation shear in **Section 4.3.1**. Furthermore, it links the [cholesterol] to the filterability for various concentrates in **Section 4.3.2**.

The levels of shear that were identified typical for the pilot scale centrifuge were investigated for their impact on the levels of antibody reduction and HCPs and the results are presented in **Sections 4.3.3** and **4.3.4**.

4.3.1 Centrifuge characterisation for low viability cell cultures using [cholesterol]

The current study proposes the use of [cholesterol] measurements instead of LDH for characterising shear for low viability cell cultures. Cholesterol is an integral part of the cell membrane and hence even for low viability cell culture, it was hypothesized that applying shear may lead to additional release of cholesterol in the cell culture medium. To test this hypothesis a low viability (28%) cell culture material (cell culture C in **Table 4.1**) was used in the shearing studies. **Figure 4.4a** shows that there is an increase in the [cholesterol] for the mimic centrates generated at different levels of shear - 20 to 55 mL/min flowrate in the CSD and 9000RPM in the pilot scale centrifuge. The shear did not lead to an increase in LDH levels between fresh, lysed and sheared samples (data not shown). **Figure 4.4b** shows that the mimic (generated at 52.5 mL/min) and the pilot scale centrate have comparable flux declines, which indicates comparable filterability and PSD between the centrates. These results demonstrated the ability of this novel approach to characterise the shear of a pilot scale centrifuge without the need for LDH analysis.

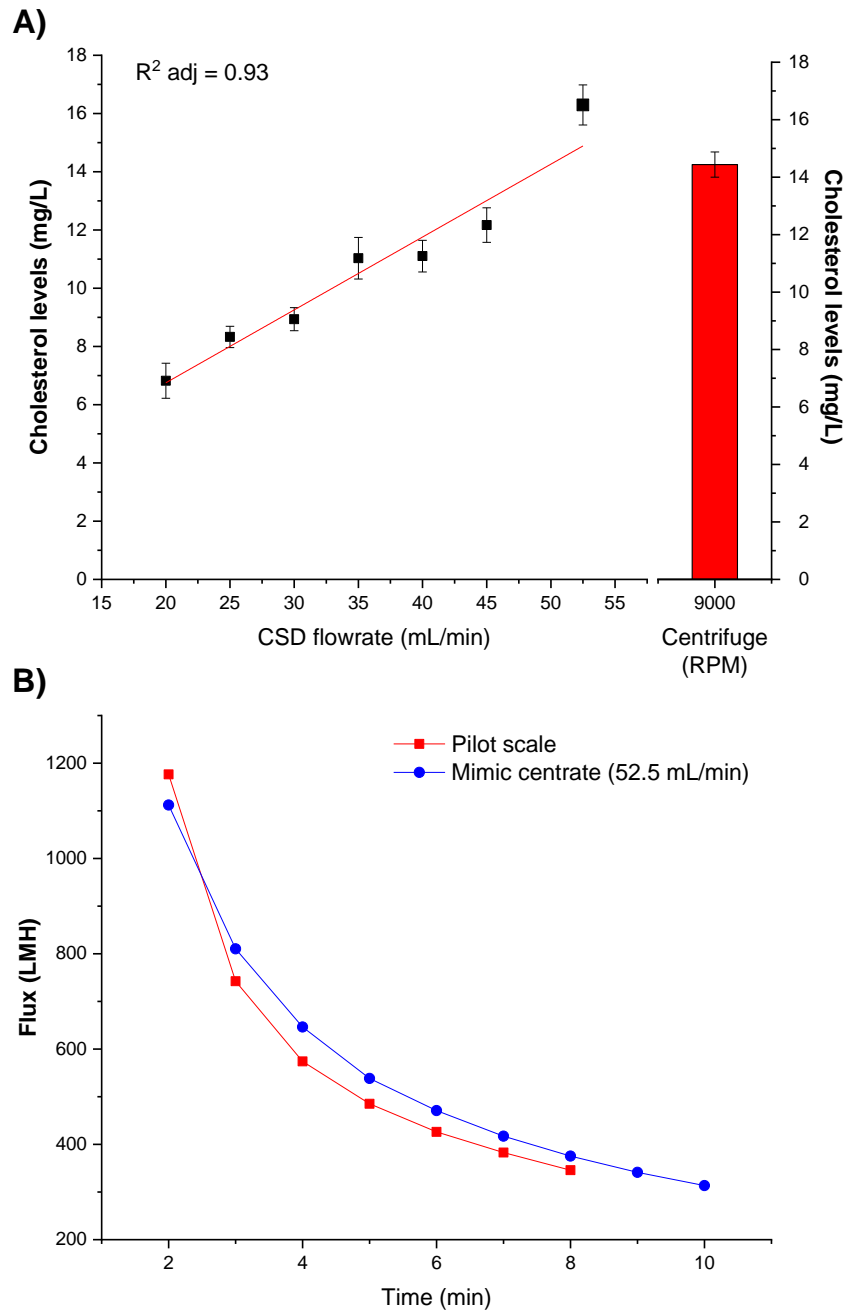


Figure 4.4 Pilot scale centrifuge characterisation studies using A) comparison in the cholesterol levels between the mimic centrate generated using different CSD flowrates (■) and the pilot scale centrifuge MBPX404 ran at 9000RPM and 120L/h (■) and B) comparison in the depth filtration (X0HC 23cm²) flux declines between the mimic centrate generate at 52.5 mL/min flowrate in the CSD and the pilot scale centrate (generated at 9000RPM and 120L/h).

4.3.2 Using [cholesterol] to predict filter capacity (L/m²)

Predicting the depth filtration requirements for a process is challenging due to the limited suitable scale-down models. The goal in this section is to address this issue through the development of [cholesterol]-based method for predicting filter capacity. It was important to demonstrate the suitability of the [cholesterol] – filter capacity correlation for a wide variety of feed material. **Table 4.3** describes the properties of the centrates used in the studies – the cell culture material was from separate bioreactor runs, of different viabilities (28 to 98%), days of harvest (10 to 13) and it was subjected to different levels of shear in the CSD to generate centrate mimic and from the pilot scale centrifuge).

Figure 4.5 reveals a good correlation between the centrate's [cholesterol] and the filter capacity (L/m²) described by a power regression equation ($R^2_{adj.} = 0.93$). These results are in line with previous studies performed by Senczuk et al. (2016), where similar correlations were derived linking the filter capacity (L/m²) to [cholesterol].

Predicting filter capacity using [cholesterol] measurements will enable a more thorough investigation into what plays a key role in the secondary depth filtration. For instance, it will enable investigating the impact of upstream and centrifugation conditions on the depth filtration requirements earlier in the development cycle. It will also facilitate the evaluation of how different methods for conditioning the cell culture material – e.g. flocculation and precipitation – may impact on the filterability. Moreover, having a method to easily anticipate filter capacity will enable comparing different filter media to identify the optimum configurations for the process.

Table 4.3 Summary of results from bench-scale filter sizing experiments using X0HC secondary depth filter (23cm²) at constant pressure. The filter capacity was calculated using V_{max} .

| Cell culture | Viability (%) | VCD (10 ⁶ cells/mL) | CSD flowrate (mL/min) | Centrifuge bowl speed (RPM) | Harvest day | Cholesterol (mg/L) | Filter capacity (L/m ²) |
|--------------|---------------|--------------------------------|-----------------------|-----------------------------|-------------|--------------------|-------------------------------------|
| A | 98 | 31.2 | 41 | | 12 | 28.1 | 115 |
| | 97 | 31.1 | 0 | | 13 | 4.4 | 895 |
| | 97 | 31.1 | 21 | | 13 | 16.8 | 323 |
| B | 28 | 8.5 | | 9000 | 13 | 14.4 | 325 |
| C | 96 | 37.4 | 21 | | 10 | 5.9 | 936 |
| | 88 | 31.1 | 21 | | 12 | 7.7 | 499 |
| | 96 | 37.4 | 41 | | 10 | 18.7 | 152 |
| | 88 | 31.1 | 41 | | 12 | 27.3 | 150 |

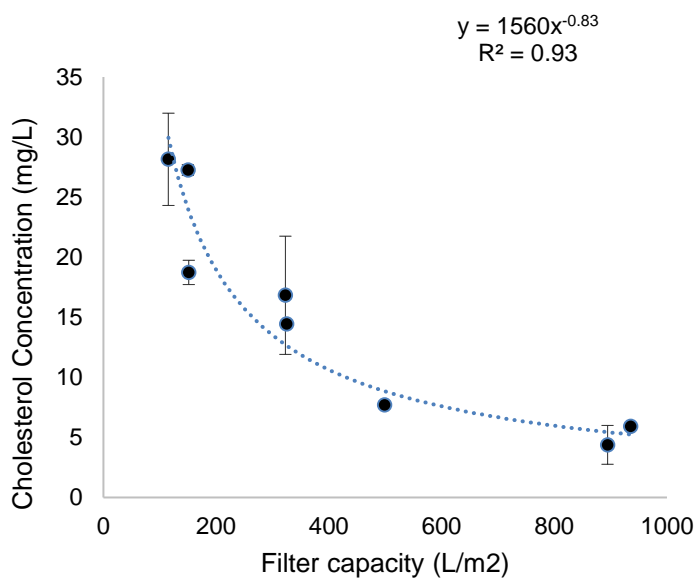


Figure 4.5 Cholesterol concentration (mg/L) versus filter capacity (L/m²) for the cell culture and harvest conditions described in **Table 4.3**

4.3.3 The impact of the recovery operation on monomer content and HCPs

Cell culture material was spiked with purified monoclonal antibodies as described in **Section 4.2.2**. The goal was to decouple the impact of the overall cell culture process from the cell culture properties at harvest (e.g. cell culture viability) on the levels of intact (non-reduced) antibody and HCPs. The following harvest parameters were investigated – harvest day (reflecting differences in cell culture viability at harvest) and different levels of shear.

The intact antibody was considered at around the 150kDa peak (containing two heavy and two light chains). The size of the light chain is typically 25kDa, the heavy chain is 50kDa and there can be combinations of the light and the heavy chain (e.g. 75kDa, 100kDa, etc.) that can lead to different sizes. It is also important to note that glycosylation of the heavy or the light chain can generate species that fall out of the discrete increments of 25kDa (de Haan et al., 2020; Higel et al., 2016; Huang et al., 2016; Valliere-Douglass et al., 2009; Zauner et al., 2013).

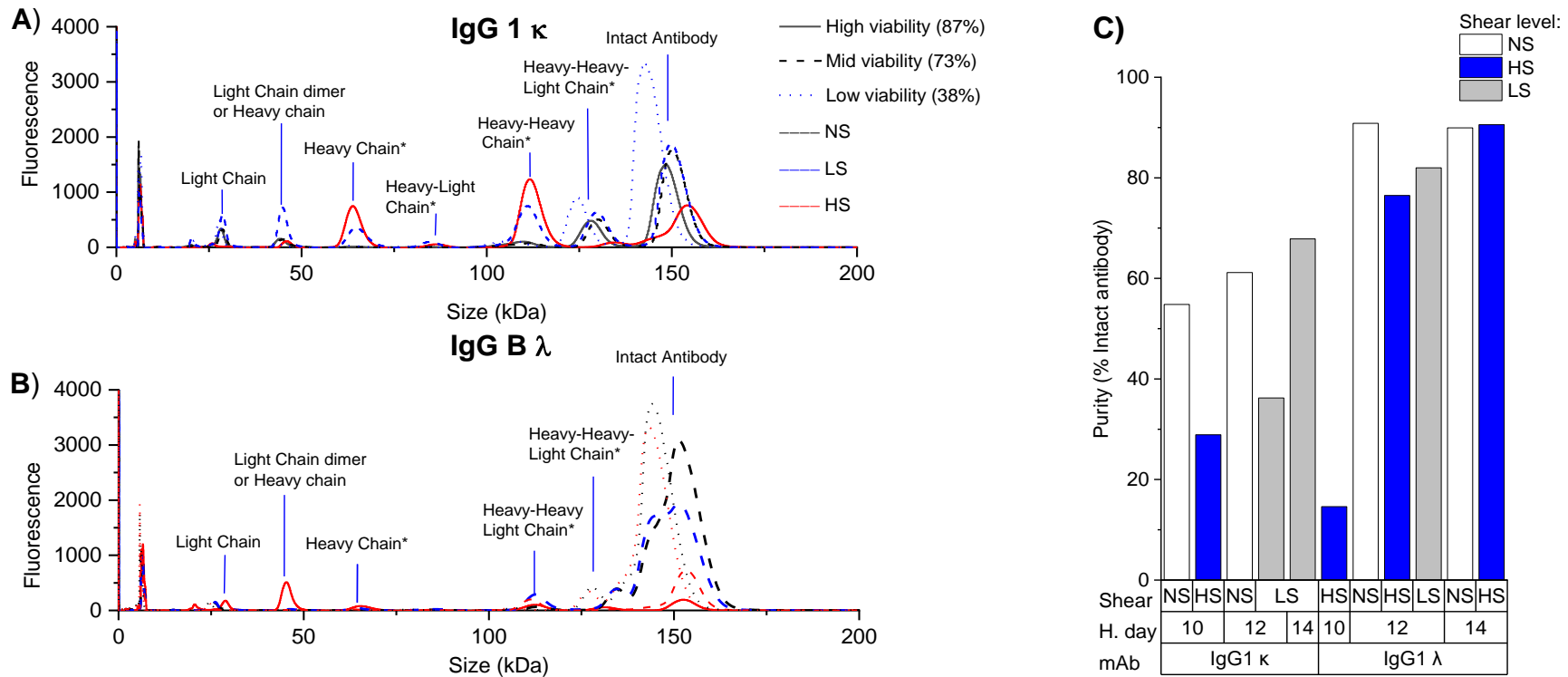


Figure 4.6 Antibody size distribution for IgG1 λ and IgG1 κ after the fully purified mAb was spiked into a non-producer cell line (GS-CHO Null) and subjected to different levels of shear: NS – no shear, LS – low shear (21mL/min in the CSD) and HS- high shear (41mL/min in the CSD). Electropherogram (as outputted from LabChip GXII) for A) IgG 1 κ and B) IgG1 λ showing the different antibody fragments and C) a summary of the total intact antibody calculated as a percentage of the area of intact antibody from the overall area.

Figure 4.6 revealed a decrease in the intact antibody concentration for the early harvest day and high shear conditions. The highest levels of intact antibody were observed for the last harvest day 14 – 83%, regardless of the level of shear compared to 33% for the early harvest day 10. It is important to note that the viability of the cells on day 10 was higher at 87% compared to 38% on day 14. The low viability on day 14 indicates that the cells have lost membrane integrity, hence it can be inferred that cell contents were already released in the cell culture medium. Consequently, for cells that are already lysed, applying shear to the sample may not lead to additional release of intracellular components. Since the antibody reduction is often attributed to the release of intracellular reducing enzymes and proteins, this could explain why shear did not increase reduction for the low viability conditions.

The opposite was observed for the high viability conditions (day 10) where shear led to loss of Intact antibody content. The decrease in the levels of intact antibody content for early cell harvest can be attributed to the potential presence of more active reducing enzymes (vs the late harvest day). It is interesting to note that to force the reduction event the samples were held in the cell culture material for 30 days. The samples without a hold step were also analysed but no antibody reduction was observed.

The HCP analysis for the spiking studies in **Figure 4.7** revealed that for one of the mAbs - IgG1 λ – the average levels of HCPs were much higher than for the other mAb - IgG1 κ – 1,323 ng/mAb g vs 325 ng/mAb g. This may be due to the association of the mAbs with the HCPs (Liu et al., 2019; Nogal et al., 2012; Tarrant et al., 2012). Moreover, for IgG1 λ , the level of shear led to an increase in the HCPs content

post purification, while for the IgG1 κ , there was little increase in the overall HCP levels between the no shear and shear conditions. These findings highlight the importance of understanding how the product-specific characteristics may interact with the centrifugation performance. For instance, high shear may have less of an impact on HCPs content for an antibody that does not tend to co-purify with HCPs, however, for molecules that interact and co-purify with HCPs, shear may lead to increase in the HCP levels. These findings are corroborated by Tait et al. (2012), who also demonstrated that the HCPs levels will depend on the cell viability, the mAbs and the cells' sensitivity to shear. The same study also highlighted that the composition of HCPs changed between different harvest days, which may explain why there was not a clear trend in the overall HCP content between different days of harvest. Wilson et al. (2022) used mass spectroscopy to analyse the population of HCPs post protein A purification from a CHO cell culture between days 8 and 17 and demonstrated that different HCPs were present on days 8, 10, 13 and 17 with an overall increase in the levels of HCPs. Hamaker et al. (2022) also observed changes in the HCP composition when profiling more than 1500 types of HCPs over a 60 day seed train. Similarly, changes in HCP profiles over the cell culture duration were also observed by Park et al. (2017). HCPs that were present on the different days of harvest may have different tendencies for associating with the mAb, therefore, further analysis would be required to understand what leads to increase or decrease in HCP levels post protein A.

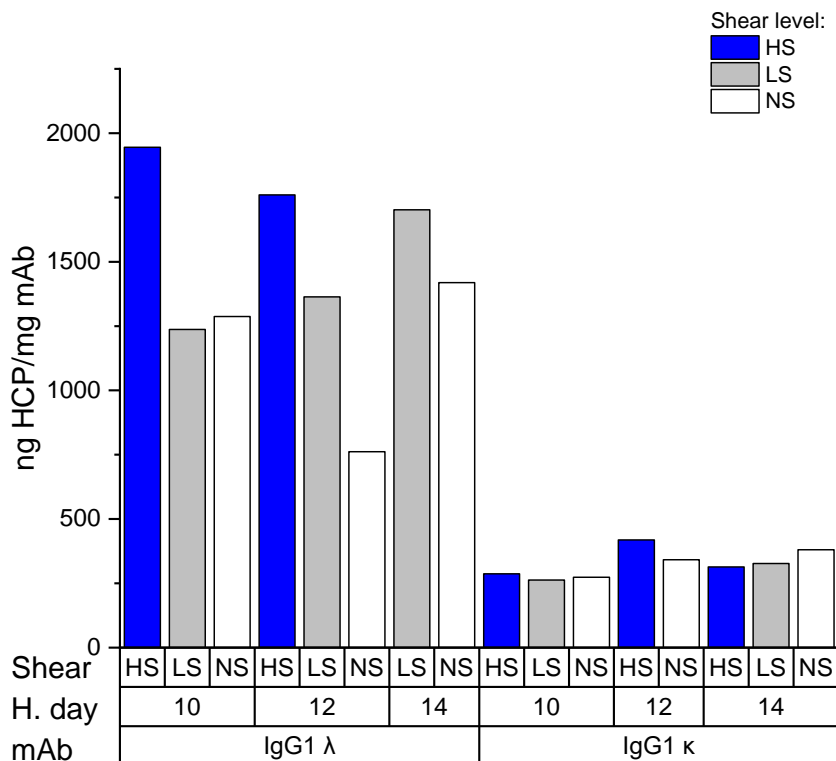


Figure 4.7 HCP concentration (ng HCP/g mAb) for IgG1 λ and IgG1 κ , which were spiked into CS-CHO Null cell culture harvests collected on day 10, 12 or 14 of cell culture. The samples were subjected to different levels of shear (no shear (NS) = 0 mL/min in the CSD (□), low shear (LS) = 21 mL/min in the CSD (■), high shear (HS) = 41 mL/min (■)).

4.3.4 The impact of depth filtration, centrifugation shear and hold on antibody reduction

The analysis so far focused on the impact of centrifugation shear on antibody reduction. In this section it was extended to explore the combined impact of both centrifugation shear and the following secondary depth filtration on reduction. For this study, a different antibody was used that was known to have a higher propensity for reduction and so did not require a 30-day hold. The harvest used for the study

was from 500L process development run on day 14 at viable cell density of 16.14 ($\times 10^6$ cells/mL) and 91% viability.

Figure 4.8 revealed that reduction was only observed for the conditions at high shear (lane 4 and 9, CSD flowrate of 41mL/min). Furthermore, higher levels of reduction were observed for the process where the concentrate was also subjected to depth filtration – 48% intact antibody (high shear and depth filtration) vs 79% intact antibody when only high shear was applied (without depth filtration). Although the depth filtration reinforced the levels of antibody reduction for higher shear conditions, the depth filtration operation did not lead to antibody reduction when coupled with low or no shear conditions. The observed reduction post depth filtration for the high shear conditions may be explained with the low oxygen conditions in the depth filter, which may favour the reduction process (Trexler-Schmidt et al., 2010). Furthermore, this sample had a longer hold time, which further reinforces the notion that it may be the drop in oxygen that led to increase in antibody reduction. However further studies would be needed to confirm this.

A) Gel electrophoresis image

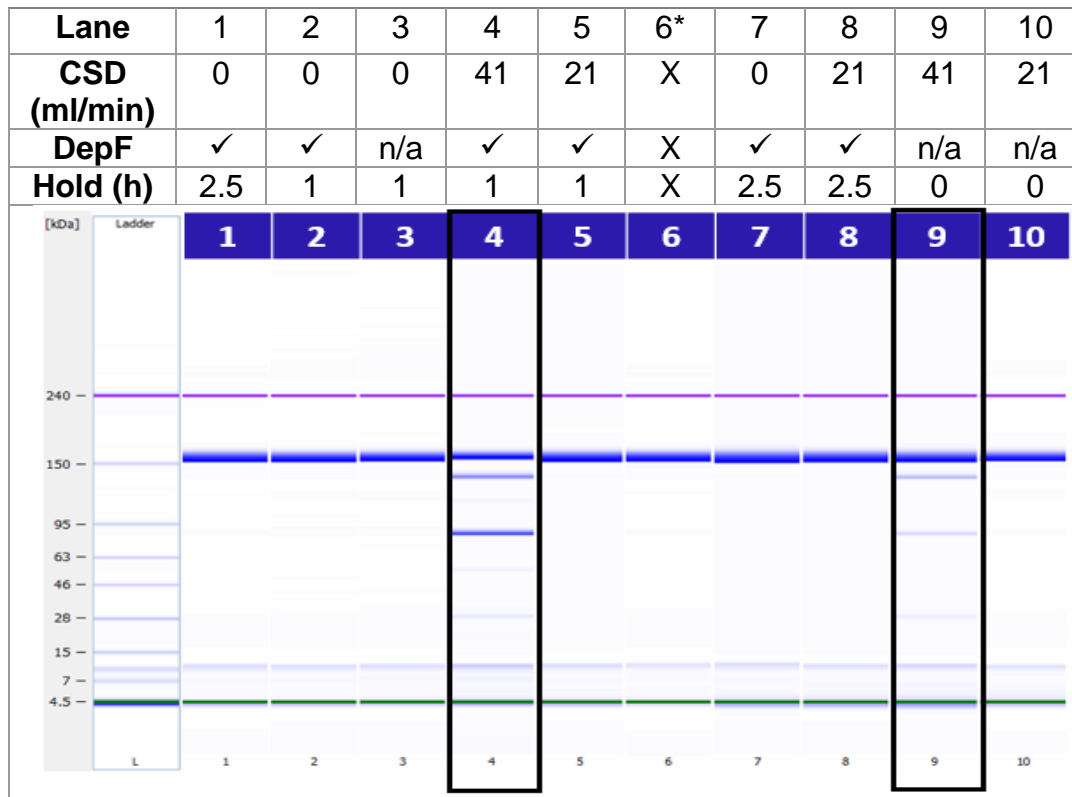
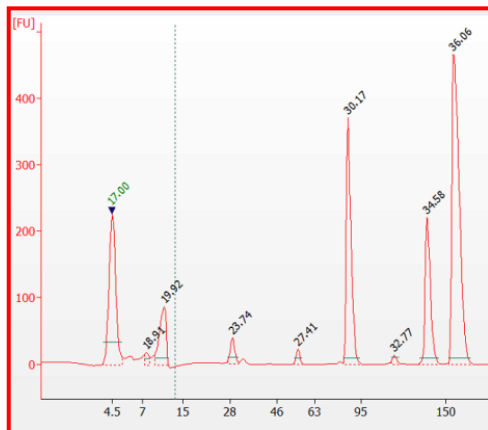
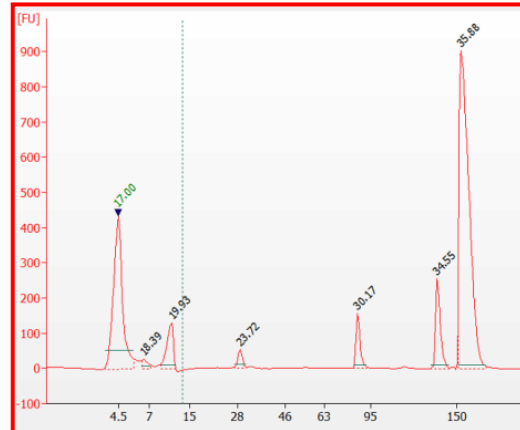
B) Electropherogram - Lane 4
(48% Intact antibody)C) Electropherogram - Lane 9
(79% Intact antibody)

Figure 4.8 Gel electrophoresis image showing the levels of intact antibody – band at > 150 kDa – A) for different shear levels (flowrates mL/min) in the capillary shear device, hold (hold time in the cell culture material) and the use of DepF (Depth filtration); B) showing the electropherogram for lane 4 and 9 where antibody reduction was observed.

4.3.5 Linking the ambr to the centrifugation mimic

The work presented so far in this chapter aimed at establishing tools that will enable linking upstream conditions and centrifugation shear to key performance metrics such as product and process related impurities and depth filter requirements post centrifugation. In this section the ambr was linked to the centrifugation mimic and this integrated scale-down platform was used to investigate how conditions in upstream (harvest day and seeding density) and centrifugation (level of shear) impact on the levels of antibody reduction and [cholesterol] that acted as a correlate for centrate filterability. The goal also was to derive correlations to map the upstream and recovery design space and identify potential process trade-offs.

4.3.5.1 Amb3 and ambr4 growth culture kinetics

Two ambr runs were performed with varying seeding densities and harvest days (conditions described in **Table 4.2**) with the goal of investigating the impact of these upstream conditions on the upstream-recovery sequence performance. In this section, the impact of seeding density and harvest on cell culture viability is going to be considered. The cell culture viability can influence the recovery sequence as it has been shown to be linked to the levels of antibody reduction (**Section 4.2.2**) and [solids] (**Chapter 4**). Therefore, it is important to understand how seeding density and harvest day influence the final cell culture viability.

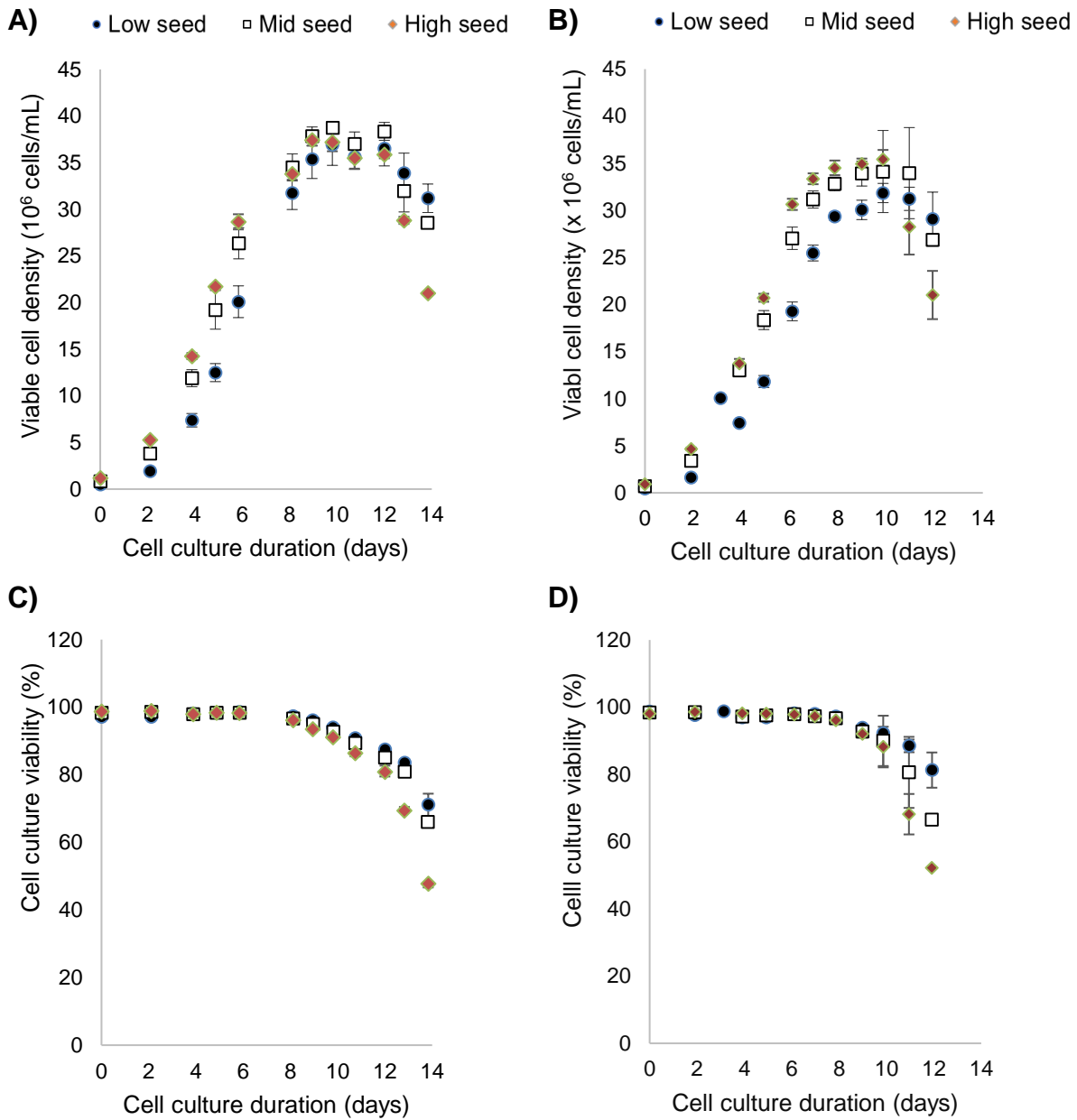


Figure 4.9 Growth culture kinetics for ambr3 and ambr4 showing viable cell density (cells/mL) for A) ambr3 and B) ambr4 and cell culture viability (%) for C) ambr3 and D) ambr4. A description of the low, mid and high seeding density levels can be found in **Table 4.2**.

Figure 4.9 reveals an inverse trend between the seeding density and resulting cell culture viability. More specifically, the average cell culture viability at the end of the process was lower for the high seeding density conditions; for example 48% (harvest day 14, ambr3) compared to 71% (harvest day 14, ambr3). The lower seeding density conditions led to lower maximum viable cell count but the viability was maintained for longer. The ambr4 experienced a drop of viability on day 12, which was a lot lower than usually observed for the process, and the run was discontinued. The reason for the lower viability was not identified; it was hypothesized that it may be due to variations in the seed train, the cell bank or other variations in the media composition. The exponential population doubling times between the ambr3 and 4 were comparable at approximately 31 hours. However, the ambr3 showed higher cell specific productivity (average of 16.4 pg/cell/day) than ambr4 (average of 15.7 pg/cell/day). The average IVC for ambr3 was also higher at 6.8×10^{12} cell hr/L compared to 5.3×10^{12} cell hr/L for ambr4.

4.3.5.2 **Impact of ambr cell culture conditions and recovery operation on monomer content (intact antibody)**

As demonstrated earlier, the cell culture viability may impact on the levels of intact antibody leading to lower levels of intact monomer when viable cells (early harvest day) are subjected to shear (**Section 4.3.3**). For high viability cells, cell membrane is relatively intact and hence there is the potential for shear to more drastically increase the release of intracellular products into the media than it is the case for cell cultures that have already lost membrane integrity. To better understand the increase in cell lysis and the concomitant release of intracellular material, the cell

culture LDH release was measured pre-and post-shear and these levels were linked to the levels of intact antibody.

Figure 4.10 shows that for ambr4 the intact antibody content is highest for the low viability cultures (high LDH), both pre-shear and post-shear. Examining box A in **Figure 4.10** for 10% to 30% LDH release pre-shear i.e. high viability cultures - it can be seen that those not exposed to shear tend to have 80 to 84% intact antibody and for those exposed to shear it is slightly lower at 77% to 80%. In contrast, at 100% LDH release pre-shear (box B **Figure 4.10**) i.e. low viability cultures, the levels of % intact antibody were close to the controls at no shear (90 to 95%).

The higher levels of intact antibody for the low viability cell culture may be attributed to the potentially less reducing environment in terms of DO and the absence of active reducing enzymes e.g. (reductase) compared to higher viability cell culture. It is possible that the viable cells depleted the oxygen quicker during the harvest step leading to lower DO and that they contain more active reducing enzymes – the negative impact of DO and the intracellular reducing species on intact antibody content has been described elsewhere (Chung et al., 2017; Handlogten et al., 2017; Handlogten et al., 2020; Kao et al., 2010; Mun et al., 2015; Trexler-Schmidt et al., 2010).

The antibody size analysis for ambr3 showed no significant loss in monomer content in any of the samples. This may be due to the differences in harvesting approach between the two ambr (described in **Section 4.2.4**)

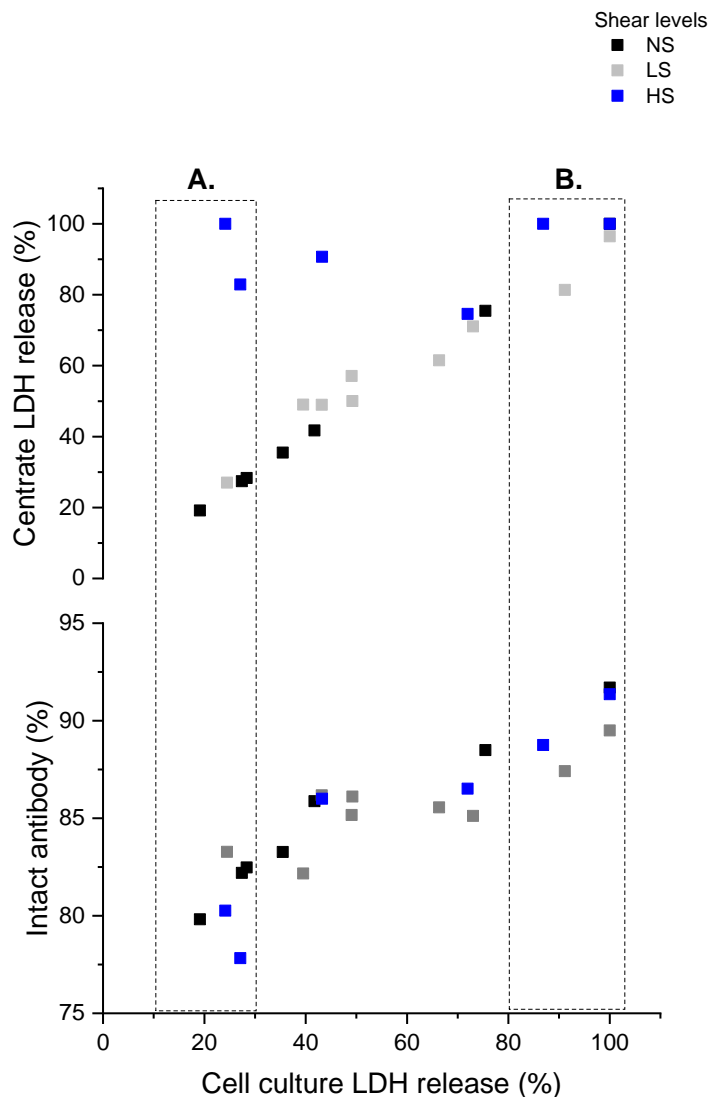


Figure 4.10 Levels of intact antibody (%) vs A) cell culture LDH release (%) and B) Centrate LDH release (%) for different levels of shear ((■ – no shear (NS); ■ – low shear (LS) and ■ – high shear (HS)) for ambr4 harvests.

4.3.5.3 Deriving cause-and-effect correlations for upstream and recovery metrics

In this section the impact of upstream conditions and centrifugation shear on upstream (titre) and recovery metrics ([solids], [cholesterol] and OD_{550}) was investigated and cause-and-effect correlations were generated for the key metrics

that are to be used as input for the bioprocess economics model in the next chapter. The titre was chosen as an important metric that will dictate facility sizing and the ability to meet target throughput. Higher harvest's [solids] leads to more frequent centrifuge's discharges, which decreases the step's yield and may exceed the equipment solids handling capacity. The harvest's turbidity (OD_{550}) is an indication of the harvest's solids content as well as the PSD – the increase in smaller particles tends to increase the turbidity. Therefore, the increase in turbidity is an indicator that the harvest may be getting harder to clarify.

Table 4.4 summarises the OD_{550} , titre and [solids] for the different harvest days and seeding density conditions. The analysis revealed that the increase in cell culture duration led to an increase in OD_{550} and titre and a decrease in [solids] across almost all seeding density conditions. For ambr3 the increase in seeding density led to increase in titre for the earlier days of cell culture (8 and 11) but not for days 12, 13 and 14, which may be explained by the drop in viability for the later days of cell culture for the high seeding density conditions. The increase in seeding density led to increase in OD_{550} across almost all scenarios, which can be attributed to the increase in [solids] with time and also to the drop in viability and appearance of cell debris for the late days of cell culture. For the [solids], day 13 and 14 of harvest and high seeding density led to decrease in [solids], this may be due to the lower viability for these conditions, which may result in smaller particles (cell debris) that would be harder settle and form a pellet during the centrifugation for PCV analysis (**Section 2.1.3.4**) or are better compacted and lead to lower solids volumes. Later in the thesis in **Section 6.3.4** the cell culture PSD was used to predict the [solids] concentration

and LDH release. Using PSD instead of PCV to evaluate the [solids] would facilitate more measurements over the cell culture duration and could provide a more accurate estimation of the [solids]. Furthermore, using PSD can reveal further correlations between the upstream and the recovery performance; for instance the upstream conditions could be directly linked to changes in the PSD.

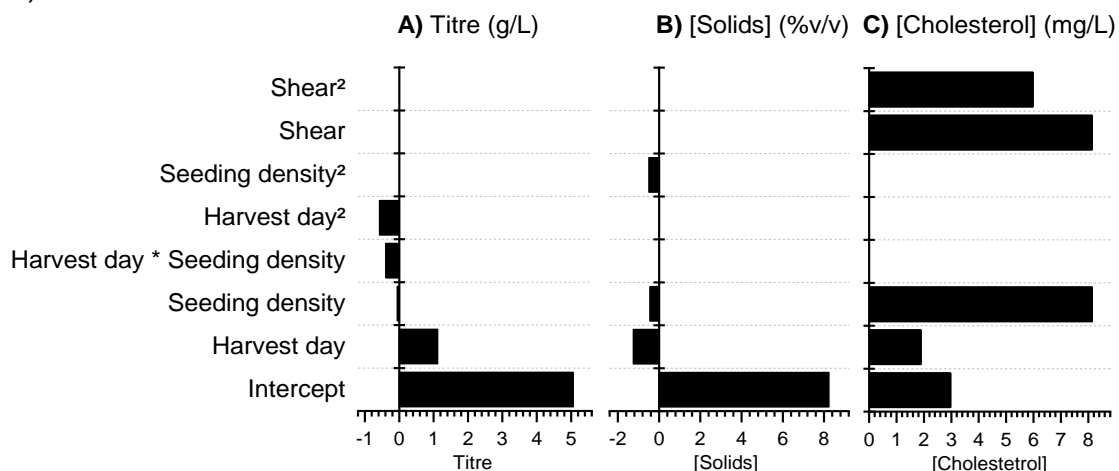
Table 4.4 Summary of key results for titre, [solids] and OD550 for various harvest days and seeding densities for A) ambr3 and B) ambr4

| | | Harvest day | | | | | | | | | | |
|--|------------------------------------|-------------------------------------|-------------------------------------|-------------------------------------|-------------------------------------|---------------------------------|--------------------------|------------------------------------|--------------------------|---------------------------|------------------------------------|---------------------------|
| | | 8 | 11 | 12 | 13 | 14 | 11 | 13 | 14 | 11 | 13 | 14 |
| | | Titre (g/L) | | | | | [Solids] (% v/v) | | | OD _{550nm} (abs) | | |
| Seeding density (x10 ⁶ cells/mL) | 0.5 +/- (0.039) n=6 | 1.4 +/- (0.25)* n=6 | 2.9 +/- (0.23) n=6 | 5.1 +/- (0.35) n=5 | 5.7 +/- (0.29) n=5 | 6.1 +/- (0.22) n=3 | 8.8 n/a n=2 | 8.2 n/a n=2 | 7.1 n/a n=2 | 4.5 n/a n=2 | 6.9 n/a n=2 | 13.9 n/a n=2 |
| | 0.8 +/- (0.04) n = 12 | 1.9 +/- (0.22) n=12 | 3.6 +/- (0.13) n=12 | 5.3 +/- (0.12) n=10 | 5.5 +/- (0.14) n=10 | 5.5 n/a n=2 | 9.3 n/a n=2 | 7.9 +/- (0.74) n=8 | 7.1 n/a n=2 | 4.9 n/a n=2 | 7.1 +/- (0.72) n=8 | 12.7 n/a n=2 |
| | 1.2 +/- (0.053) n=6 | 2.2 +/- (0.09) n=6 | 3.8 +/- (0.06) n=6 | 4.9 +/- (0.13) n=3 | 5.0 +/- (0.14) n=3 | 5.5 n/a n=2 | 8.7 n/a n=2 | 6.8 n/a n=2 | 6.2 n/a n=2 | 5.5 n/a n=2 | 8.1 n/a n=2 | 14.9 n/a n=2 |

| | | Harvest day | | | | | | | | |
|--|-----------------------------------|-----------------------------------|-----------------------------------|-----------------------------------|-----------------------------------|-----------------------------------|---------------------------------|------------------------------------|-----------------------------------|--|
| | | 7 | 8 | 10 | 11 | 12 | 10 | 12 | 12 | |
| | | Titre (g/L) | | | | | [Solids] (% v/v) | | OD ₅₅₀ (abs) | |
| Seeding density (x10 ⁶ cells/mL) | 0.46 +/- (0.06) n=7 | 0.90 +/- (0.24) n=7 | 1.35 +/- (0.2) n=7 | 3.07 +/- (0.1) n=7 | 3.68 +/- (0.07) n=7 | 4.09 +/- (0.48) n=7 | 7.4 +/- (0.54) n=3 | 6.6 +/- (1.08) n= 4 | 5.37 +/- (0.37) n=4 | |
| | 0.71 +/- (0.07) n=10 | 1.38 +/- (0.12) n=10 | 2.15 +/- (0.14) n=10 | 3.71 +/- (0.46) n=10 | 4.24 +/- (0.72) n=10 | 4.32 +/- (0.84) n=10 | n/a | 6.2% +/- (1.22) n= 10 | 5.74 +/- (0.5) n= 10 | |
| | 0.92 +/- (0.08) n=7 | 1.54 +/- (0.14) n=7 | 2.12 +/- (0.21) n=7 | 3.56 +/- (0.62) n=7 | 4.08 +/- (0.92) n=7 | 4.05 +/- (1.12) n=7 | 7.8 +/- (1.11) n=4 | 6.2 +/- (1.04) n= 3 | 6.02 +/- (0.27) n= 3 | |

*Standard deviation

A)



D)

| Metrics | Equation |
|-----------------------------|---|
| Titre (g/L) | $-46.56 + 7.16 * H. \text{ day} + 7.94 * S. \text{ density} - 0.66 * H. \text{ day} * S. \text{ density} - 0.24 * H. \text{ day}^2$ |
| [Solids] (%v/v) | $16.82 - 0.81 * H. \text{ day} + 4.34 * S. \text{ density} - 3.33 * S. \text{ density}^2$ |
| [Cholesterol] (mg/L) | $-20.2 + 1.92 * H. \text{ day} + 4.91 * S. \text{ density} - 0.19 * \text{Shear} + 0.014 * \text{Shear}^2$ |

Figure 4.11 The predictive equations in terms of coded factors for A) titre (g/L); B) [solids] (% v/v) and C) [cholesterol] (mg/mL) and actual coefficients for all three models summarised in D). The statistics for the model are as follows adj. $R^2 = 0.82$ (titre model), pred. $R^2 = 0.76$ (titre model), k-fold $R^2 = 0.75$ (titre model); adj. $R^2 = 0.77$ ([solids] model), pred. $R^2 = 0.71$ [solids] model, k-fold $R^2 = 0.66$ [solids] model, adj. $R^2 = 0.82$ ([cholesterol] model), pred. $R^2 = 0.75$ ([cholesterol] model, k-fold $R^2 = 0.76$ ([cholesterol] model. The predictors for the equations are H.day – harvest day, S.density – seeding density and shear level (mL/min in CSD).

As mentioned earlier titre, [solids] and [cholesterol] can be used to size the bioreactor, centrifugation and subsequent depth filtration operation. Therefore, deriving cause-and-effect correlations for these metrics would be key for building a bioprocess model. Similarly to **Chapter 3** cause-and-effect correlations were derived

for ambr3 to predict the titre, [solids] and [cholesterol]. A summary of the equations in terms of coded and actual factors can be found in **Figure 4.11**. The analysis revealed that the seeding density and harvest day impacted on all three metrics. Furthermore, it showed that there are trade-offs between the outputs. For instance, increasing the seeding density led, on one hand, to the undesirable increase in [cholesterol] but, on the other hand, it also led to an increase in [titre].

4.4 Conclusions

The work presented in this chapter described a novel framework for mapping the design space for the upstream and recovery operation taking into consideration product purity (HCPs and intact monomer content), titre, [solids] and filterability of the centrate. The shear in a pilot plant centrifuge was successfully characterised using a capillary shear device and two shear levels were applied based on this characterisation – low shear (21mL/min in the CSD) and high shear (41mL/min and 52.5mL.min in the CSD). The results from a bench-scale and an ambr DoE study revealed that applying high shear (41mL/min) to high viability cell cultures leads to the highest loss of monomer content. To model the depth filtration operation a [cholesterol] – based correlation was established to predict the centrate filterability. When the [cholesterol] correlation was implemented in a DoE study using the upstream-recovery mimic (ambr + CSD) it revealed important trade-offs for the process where seeding density increased titre but also [cholesterol]. The results from the DoE laid the foundation for the work in the next chapter, which will incorporate the cause-and-effect correlations in an overall bioprocess model.

Chapter 5

5 Building a decisional tool for the recovery operation of mammalian cell processes

5.1 Introduction

In the previous chapters the goal was to build cause-and-effect correlations that link the upstream conditions to the recovery performance. **Chapter 3** was focused on the impact of the upstream conditions (pH, temperature, seeding density and day of harvest) on the input to the recovery operations, while **Chapter 4** linked the seeding density in the bioreactor, the cell culture duration and the level of shear in the centrifugation operation to the upstream and primary and secondary recovery performance. This chapter incorporates these predictive correlations into a bioprocess economics model for an overall evaluation of the process and facility fit.

As discussed in **Section 1.1.2** biopharmaceutical companies have widely adopted platform processes for the manufacture of mAbs, where the unit operations used are largely conserved between different products and scales (Shukla and Thömmes, 2010). However, for primary cell culture clarification the techniques used for separation can vary between scales (Felo et al., 2013). For instance, for the small scale process manufacturers may use a low shear primary depth filtration setup, while the pilot or commercial-scale process may employ a high shear centrifugation

operation. Even when the same clarification approach is used across scales, it is possible that there is a change in the shear levels between systems and it is important to understand how this may impact on the process.

In terms of economics assessment of the recovery operation, Dryden et al. (2021) and Felo et al. (2013) present an economic evaluation of the primary recovery operation comparing the COG of a process using primary depth filtration or a centrifugation operation. The conclusion from both studies was that as the process scale increases it was more cost efficient to use centrifugation instead of depth filtration for primary clarification. Both of these studies assume that the increase in titre is independent from the [solids] in the harvest or the filterability of the centrate. However, the increase in titre is often achieved through reaching higher cell densities or extending the cell culture duration, which may result in lower viabilities on the day of harvest (as seen in **Chapter 3** and **Chapter 4**). The increase in cell density and the lower viability will change the [solids] and the particle size distribution, parameters that we have demonstrated to impact the primary and secondary clarification (**Chapter 3** and **Chapter 4**).

However, no study to date links upstream conditions and centrifugation shear to the economics of the recovery operation. In this chapter we address this gap through the creation of a bioprocess modelling tool, which links bioprocess economics to experimentally derived cause-and-effect correlations. This way the titre, filterability and [solids] are not independent user-defined inputs but defined by the bioprocess conditions.

The economics model developed in this chapter is based on the platform for commercial-scale manufacture in mammalian cell processes – centrifugation followed by depth filtration. The economics model uses common existing technologies to facilitate an accurate representation of the COG of recovery ($\text{COG}_{\text{REC}}/\text{g}$) for the operation. **Section 5.2** describes the methodology applied to build the model. It starts with the creation of a centrifugation and depth filtration databases for equipment and consumables as well as the equations applied for each step. Then it continues with the overall assumptions for the process, costs and COG equations. In **Section 5.3** four different case studies were investigated. In the first case study (**Section 5.3.1**) a deterministic analysis was performed to identify the main cost drivers for the recovery platform. Then in the second case study (**Section 5.3.2**) the COG for the secondary depth filtration operation were compared for a process with stainless steel and single-use housings across different yearly demands and titres scenarios. In the third case study (**Section 5.3.3**) the correlations from **Chapter 3** were applied to investigate how cell culture conditions such as pH, temperature shift and seeding density impact on facility design and COG. Then in **Section 5.3.4** the predictive models from **Chapter 4** were used to investigate the impact of shear, harvest day and seeding density on the process. First, the analysis was focused on the impact of these parameters on facility design. Then these correlations were applied for a fixed facility scenario: on one hand to demonstrate the impact of process variability on risk to facility fit and on the other hand to develop strategies to mitigate against that risk. The overall goal of this chapter was to provide tools to perform an economics evaluation of the recovery step and enable a decision-

making process that accounts for inherent process variability, changes in shear (e.g. upon tech transfer) and risk-reward metrics.

5.2 Methodology

5.2.1 Model description

An existing decisional tool developed at the Biochemical Engineering Department at UCL was extended to enable the work performed in this chapter; this tool is described in more details elsewhere (Farid et al., 2007; Mahal et al., 2021; Stamatis and Farid, 2021) and a summary of the different equations can be found in **Section 5.2.4**. This decisional tool is operated through Jupyter Notebook and linked to an Excel spreadsheet that contains the main inputs – process assumptions, equipment databases and costs. The model was extended to incorporate the following new features: 1) two additional blocks in the model – one for centrifugation and one for depth filtration with equations to link the equipment design and size to the use of reagents, floor space and labour, 2) a detailed database (in Excel) of common equipment and consumables used in the recovery operation, 3) incorporating predictive cause-and-effect correlations for the bioreactor, centrifugation and depth filtration step, 4) default parameters for the centrifugation and depth filtration process and 5) application of stochasticity to key inputs for the process. All these features will be discussed in more details later in this section. Here, the goal is to present a high level overview of the recovery model and how it is linked to the overall decisional tool.

Figure 5.1 gives an overview of the recovery decisional tool – its key inputs, outputs and models. The economics model was operated in two facility sizing modes: rating

and design mode. In the rating mode, the design of the upstream and recovery steps was fixed, while in the design mode the equipment was sized to meet a target throughput at minimum cost. One of the key features of the recovery model are the predictive correlations for [solids], filter capacity and titre. Three process steps can be impacted by their outputs: centrifugation yield and sizing is impacted by the [solids], the titre impacts on the bioreactor size (in sizing mode) or the throughput (in rating mode) and filter capacity will define the required filter area (in sizing mode) or the loss in the filtration operation (in rating mode). Stochasticity can be applied to the bioprocess parameters such as seeding density to investigate the impact of inherent biological variability on the process economics. One of the main outputs are the COG of the recovery operation (COG_{REC}) calculated for the centrifugation and depth filtration steps.

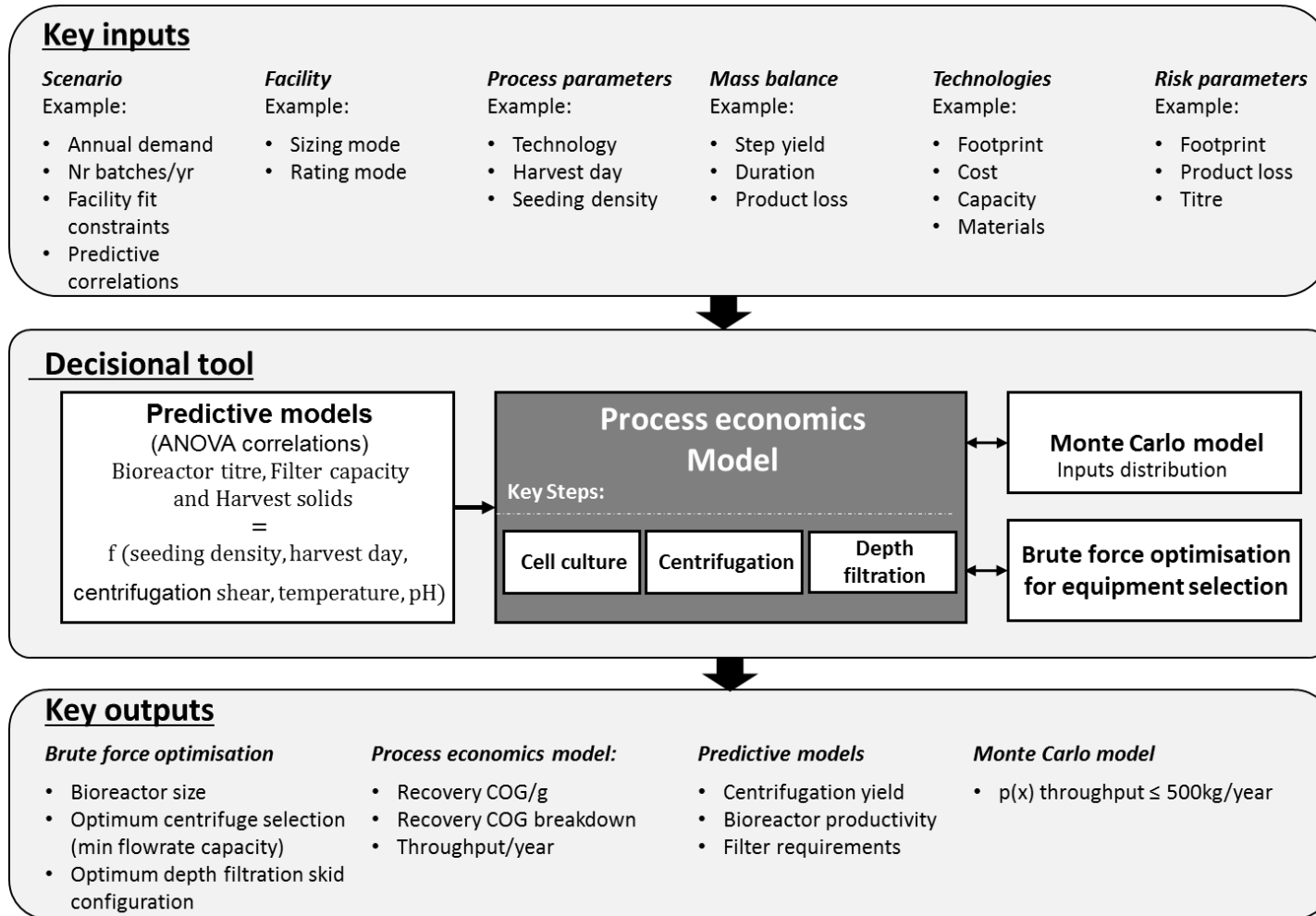


Figure 5.1 Structure of the decisional tool used for the recovery operation assessment

5.2.2 Upstream and recovery unit operations sizing

5.2.2.1 Bioreactor

In sizing mode the bioreactor size ($V_{bioreactor}$) depends on the upstream productivity (T), annual demand (Throughput) and the overall downstream yield (Y_{DSP}) so that:

$$V_{bioreactor} = \frac{\text{Throughput}}{N_{bioreactor} * T * Y_{DSP}} \quad (5.1)$$

The min required bioreactor volume will be calculated as follows:

$$V_{size} = \frac{V_{bioreactor}}{\varepsilon_{space}} \quad (5.2)$$

Where ε_{space} is the space efficiency (%). In design mode the model selects the smallest bioreactor from the available bioreactors' list that is bigger or equal to V_{size} .

5.2.2.2 Centrifugation

A database was built consisting of centrifuges commonly used for the harvest of shear sensitive mammalian cell cultures. The key design characteristics that were needed for the equipment sizing in the economics model were the maximum flowrate, the solids holding space, the bowl volume and the sigma value. The centrifugation flowrate determines the time the centrifugation needs to be run for to clarify a given volume of feed. The operation duration is key since the product is still in the cell culture medium, where HCPs with detrimental impact on product quality may be present. The solids holding space will determine the frequency of solids discharge. Most centrifuges have a maximum solids handling capacity, which can be defined by the maximum frequency of discharge (Richardson and Walker,

2018a). The bowl volume will determine the amount of cleaning reagents needed to clean the centrifuge.

The list of centrifuges in **Table 5.1** shows examples of common centrifuges used in industry. However this list is not exhaustive, and moreover, centrifuges are often custom designed for the manufacturers (Felo et al., 2013). Therefore, it was important to be able to size the centrifugation step without the need to specify the exact model of the centrifuge. For this purpose the database of centrifuges was used to derive correlations to describe the relationship between the centrifuge maximum flowrate and the solids holding space, footprint and reagent usage. These ratios were discussed with Alpha Laval representatives and industry experts and examples are given in **Appendix (Figure 5.1-A)**.

In **Table 5.2** is a summary of the key equations used in the centrifugation model. As it can be seen the bowl volume was correlated to the centrifuge flowrate **Equation (5.3)** and solids holding space was correlated to the bowl volume **Equation (5.4)**. The centrifugation flowrate was also correlated the centrifuge footprint – the higher the centrifuge flowrate the bigger the centrifuge footprint **Equation (5.5)**. The centrifugation operation requires time to accelerate to target bowl speed and decelerate to stop. The bigger the centrifuge, the longer the time required for that.

Table 5.1 Summary of the database of common centrifuges and their key characteristics used in the decisional tool

| Centrifuge model | Max flowrate $Q_{max_{Cent}}$ (l/h) | Solids holding space (L) V_{Sol} | Bowl volume V_{Bowl} (L) | Reference sigma (m^2) | Ref |
|-----------------------|---|--|----------------------------------|---------------------------------|----------|
| Clara 20/LAPX404 | 120 | 1.1 | 2.2 | 5,000 | [2] |
| Alfa Laval MBPX404 | 180 | 1.1 | 2.2 | 5,000 | |
| BTPX205 | 250 | 1.2 | 3.1 | 11,000 | |
| BTPX305 | 251 | 1.1 | 3.1 | 12,000 | [3] |
| Culturefuge 100 | 450 | 1.1 | 3.1 | 12,000 | [4][5] |
| MBPX 810SGV-34CL | 1,600 | 6.7 | 15 | 76,000 | [6] |
| Culturefuge 200 | 2,700 | 6.7 | 15 | 70,000 | [7] |
| MBPX 810HGV-34C | 3,200 | 4.8 | 15 | 83,000 | [8][9] |
| BTAX215 | 4,500 | 14 | 52 | 202,000 | [10][11] |
| Culturefuge 300 | 6,000 | 20 | 30 | 127,000 | [12] |
| Culturefuge 400 (v 1) | 8,000 | 10 | 30 | 180,000 | [13][14] |
| Culturefuge 400 (v 2) | 8,000 | 14.8 | 30 | 130,000 | [13][14] |

| | |
|--|--|
| <p>[1] Personal communication with AlfaLaval [2] AlfaLaval, Clara 20, separator [leaflet], PCHS0001EN 0701 [3] AlfaLaval, BTPX 30, system [leaflet], PPM00107EN 0410 [4] AlfaLaval, Centrifuge 100, separator [leaflet], PPM00037EN 0303 [5] AlfaLaval, Centrifuge 100, separator [leaflet], PPM00036EN 0304 [6] AlfaLaval, MBPX 810, separator [leaflet], PCHS00021EN 0701 [7] AlfaLaval, Centrifuge 200, system [leaflet],</p> | <p>[8] AlfaLaval, MBPX 810 H, system [leaflet], PPI00507EN 1205 [9] AlfaLaval, MBPX 810 H, separator [leaflet], PPI00507EN 1205 [10] AlfaLaval, MBPX 215, separator [leaflet], LS000177EN 0409 [11] Hutchinson, 2007, New Ultra Scale-down Principles for Monoclonal Antibody Recovery and Purifications [12] AlfaLaval, Culturefuge 300 separator [leaflet], PCHS00107EN 1306 [13] AlfaLaval, Culturefuge 400 separator [leaflet], PCHS00004EN 0803 [14] AlfaLaval, Culturefuge 400 system [leaflet], PLS00068EN 0803</p> |
|--|--|

Table 5.2 Key equations for the centrifugation design and operation

| | Equations | # |
|--|---|--------|
| Design characteristics | | |
| Bowl volume (L) | $V_{Bowl} = 2.1 + 0.0039 * Q_{maxCent}$ | (5.3) |
| Solids holding space (L) | $V_{Sol} = V_{Bowl}/2.4$ | (5.4) |
| Centrifuge footprint (m ²) | $F_{footrpint} = 0.53 + 0.0005 * Q_{maxCent}$ | (5.5) |
| Centrifugation operation | | |
| Time to start the centrifuge | $t_{CentStart} = 0.0036 * Q_{Cent}$ | (5.6) |
| Time to stop the centrifuge | $t_{CentStop} = 0.0036 * Q_{Cent}$ | (5.7) |
| Maximum time for clarification | $t_{centprocess\ max} = t_{Cent\ max} - (t_{Cent\ prep} + t_{Cent\ turn} + t_{Cent\ stop} + t_{Cent\ start})$ | (5.8) |
| Centrifuge operational flowrate | $Q_{Cent} = V_{BiorIn}/t_{centprocess\ max}$ | (5.9) |
| Discharge interval | $t_{DischInt} = \frac{V_{Sol}}{C_{BiorSol} * (1 + F_{sol\ safety}) * Q_{Cent}}$ | (5.10) |
| Number of discharges | $N_{Disch} = \frac{V_{BiorIn}/Q_{Cent}}{t_{DischInt}}$ | (5.11) |
| Centrifugation reagents use* | | |
| WFI use discharge | $V_{DisCentWFI} = N_{Disch} * (0.59 + 0.021 * V_{Bowl})$ | (5.12) |
| PW usage cleaning | $V_{clCentPW} = \frac{V_{Bowl}}{t_{rCentPW}} * t_{clCentPW}$ | (5.13) |
| WFI usage cleaning | $V_{clCentWFI} = \frac{V_{Bowl}}{t_{rCentWFI}} * t_{clCentWFI}$ | (5.14) |
| CIP reagents usage | $V_{clCentCIP} = \frac{V_{Bowl}}{t_{rCentCIP}} * t_{clCentCIP}$ | (5.15) |

| | | | |
|-------------------|--|-----------------|--|
| Q_{Cent} | Centrifugation flowrate (L/h) | $t_{rCentPW}$ | PW residence time in the centrifugation |
| $t_{Cent\ prep}$ | Time for preparation of the centrifugation (h) | $t_{rCentWFI}$ | WFI residence time in the centrifugation |
| $t_{Cent\ turn}$ | Turnaround time for the centrifugation (h) | $t_{rCentCPI}$ | CPI residence time in the centrifugation |
| $C_{BiorSol}$ | Solids concentration in the bioreactor (%v/v) | $t_{clCentPW}$ | Time for cleaning with PW |
| $t_{Cent\ max}$ | Maximum allowed time for centrifugation (h) | $t_{clCentWFI}$ | Time for cleaning with WFI |
| $F_{sol\ safety}$ | Safety factor for the solids holding space | $t_{clCentCIP}$ | Time for cleaning with CPI |
| V_{BiorIn} | Feed volume from the bioreactor | | |

*(Allen et al., 2008)

5.2.2.3 Depth filtration

For the depth filtration operation two main approaches were considered: 1) stainless steel housing (usually a dome), which houses a filter cartridge and is in direct product contact and 2) single use filter housing in the form of a single use capsule, which encapsulates the filter media; the encapsulated filters are mounted onto a filter holder, which has no product contact. In both formats the filter media is used once in the process, however, the process with stainless steel housings requires cleaning and it is more labour-intensive due to the need for dismantling of the housing and cleaning of the hardware, including any stainless steel piping (assuming that the flowpath is not single use). The single use format uses single use capsules and flowpath, which eliminates the need for cleaning as there is no product contact with the equipment. In **Table 5.3** can be found a summary of some of the most common equipment and consumables on the market and relevant information about their sizes and configuration. Here, only dual layer filtration media was considered similar to the one used to generate the experimental results in **Chapter 4**.

For the capsules, the holders can consist of multiple racks – the maximum number of racks depends on the filter holder design. Each rack has a maximum number of filter capsules that can be fitted. The maximum area for filtration in each rack was calculated as follows:

$$\text{Maximum Filtration Area}_{rack} = \text{Max number of capsules}_{rack} * \text{Max area}_{capsule} \quad (5.16)$$

However the filtration area per rack will change depending on the number of capsules and the size of the capsules.

$$Filter\ area_{rack} = \sum_{i=1}^n filter\ area\ capsule_1 + filter\ area\ capsule_2 + \dots + filter\ area\ capsule_n \quad (5.17)$$

The final area for filtration in the filter holder will be a sum of the filter area in each rack:

$$Filter\ area_{holder} = \sum_{i=1}^n Filter\ area_{Rack_1} + Filter\ area_{Rack_2} + Filter\ area_{Rack_n} \quad (5.18)$$

Table 5.3 Summary of depth filtration equipment and consumables used in the model.

| | Vendor | Diameter of stainless steel domes | Racks per holder | Filtration area per capsule or cartridge (m ²) | Max number of capsules or cartridges per filter holder or housing | Facility area (m ²) | Sources | |
|--------------------|------------|-----------------------------------|------------------|--|---|---------------------------------|-----------------|-----------|
| Consumables | Capsules | | 3M | 1.60 | | | [1][2][3][4][5] | |
| | | | MM* | 0.11 | | | [18][19] | |
| | | | | 0.55 | | | [20][21] | |
| | | | | 1.10 | | | | |
| | | | | 0.25 | | | [14][15] | |
| | Cartridges | Pall | | | 0.50 | | | |
| | | | | | 1.00 | | | |
| | | | | | 0.26 | | | [6][8][9] |
| | | | | 3M | 1.50 | | | |
| | | | | | 3.20 | | | |
| | MM | | 1.80 | | | [16][20] | | |
| Equipment | Capsules | | 1 | | 1 | 0.49 | [1][2][3] | |
| | | | 1 | | 7 | 2.20 | [4][5] | |
| | | | 3M | 3 | 21 | 7.25 | [12][13] | |
| | | | | 5 | 35 | 7.25 | | |
| | | | MM | 1 | 10 | 2.50 | [17][19] | |
| | | | | 2 | 20 | 2.50 | [20] | |
| | | | | 3 | 30 | 2.50 | | |
| | | | Pall | 1 | 2 | 0.27 | [14] | |
| | | | | 1 | 5 | 0.92 | [15] | |
| | | | | 1 | 10 | 0.92 | | |
| | Cartridges | 3M | 8" | | 4 | 0.09 | [7][8][9] | |
| | | | 12" | | 4 | 0.16 | [10][11] | |
| | | | 16" | | 4 | 0.30 | | |
| MM | | | 16" | 8 | 0.30 | [16][20] | | |

* MM- Merck Millipore

[1] 3M (2013), 3M Innovative Biopharma Solutions [leaflet]

[2] 3M (2012) Zeta Plus™ Single-Use Depth Filtration [brochure]

[3] 3M (2019) Zeta Plus™ Single-Use Depth Filtration Portfolio (brochure)

[4] 3M (2016) Zeta Plus™ ZB Series Filters [brochure]

[5] VWR (2020) 3M™ Zeta Plus™ ZA Series Filter Capsule

with ZB Series Media, 3M [personalised PDF catalogue]

[6] 3M, (2014) Zeta Plus™ EXT Series Products [brochure]

[7] 3M, (2012) ZetaPlus 12ZP Housing Range [brochure]

[8] 3M (2008), Zeta Plus™ H Series Depth Filter Cartridges & Capsules

[brochure]

[9] 3M (2016) 3M™ Zeta Plus™ SP Series Filter [brochure]

[10] O'Brien et al. (2012) Large-Scale, Single-Use Depth Filtration Systems for Mammalian Cell Culture Clarification, Bioprocess International

[11] 3M (2011) Zeta Plus Model ZPB Sanitary Filter Housing [brochure]

[12] 3M (2007) Zeta Plus® CP&SP Series [brochure]

[13] 3M Zeta Plus™ Single-Use Depth Filtration [brochure]

[14] Pall (2015) Stax™ Disposable Depth Filter Systems

[15] Pall (2007) SUPRAdisc™ HP Depth Filter Modules For High Performance Cell Clarification [brochure]

[16] Millipore (2016) Millistak+® Depth Filters Lenticular Depth filter media to optimize your process [data sheet]

[17] Millipore (2014) Hardware for Pod disposable depth filter systems [data sheet]

[18] Millipore (2017) Millistak+® HC Pro [data sheet]

[19] Millipore (2019) Millistak+® Pod disposable

depth filter system [data sheet]

[20] Millipore (2016) Clarification Portfolio Guide [brochure]

[21] Millipore (2017) Clarification of mammalian cell cultures by depth filtration [brochure]

In **Figure 5.2** can be seen a schematic representation of the filter holder with one rack and with two racks. The model is designed to select the configuration with the minimum number of racks required to meet filter area requirements.

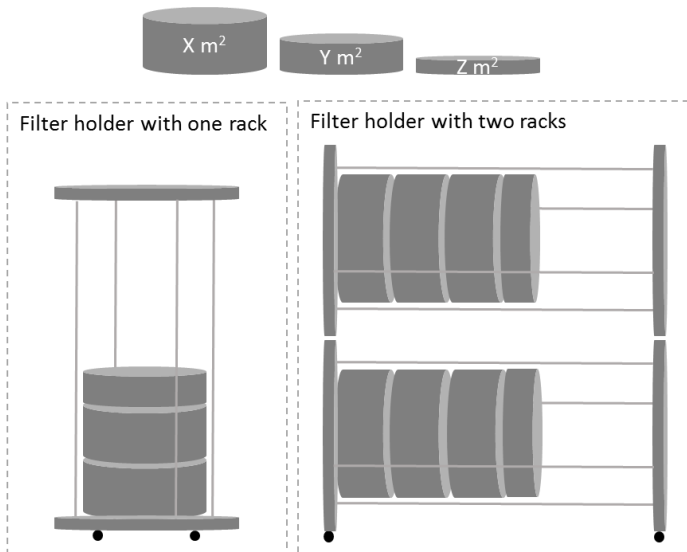


Figure 5.2 A schematic representation of a filter holder that can fit different filters of size X, Y and Z and can accommodate multiple racks (right-hand side)

For the stainless steel configuration the housing are of pre-defined diameter and cartridges are designed to fit this diameter (**Figure 5.3**).

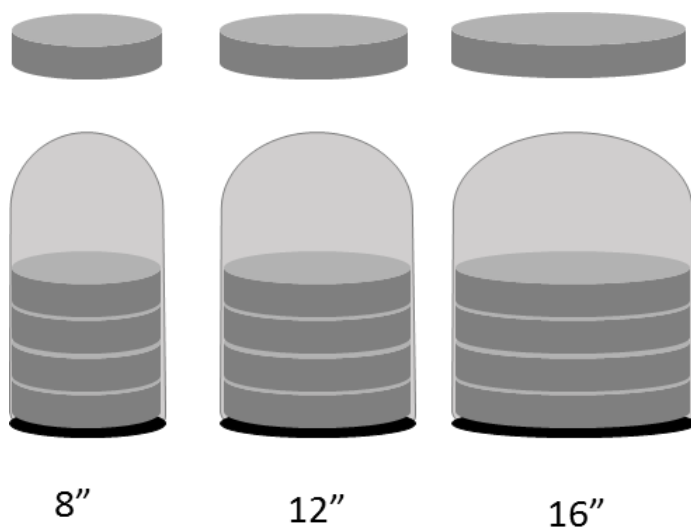


Figure 5.3 A schematic representation of stainless steel domes of different diameters.

The key equations for the depth filtration process are summarized in **Table 5.4** . The required filter area is defined by two parameters the volume fed into the step, which depends on the number and size of bioreactors and the filter capacity, which depends on the centrate quality. The total operators' time is used to calculate the number of operators on annual basis and based on that the annual labour COG.

Table 5.4 Key equations for the depth filtration operation

| Equations | # |
|---|--|
| Design characteristics | |
| Filter area required (m ²) | $A_{\text{filter}} = \frac{V_{\text{in}}}{FC} \quad (5.19)$ |
| Facility footprint (m ²) | $F_{\text{footprint}} = Eq_ft_{\text{filtr}} * F_{\text{ut footprint}} * F_{\text{p footprint}} \quad (5.20)$ |
| Depth filtration operation | |
| Processing time | $t_{\text{DepF process}} = \frac{V_{\text{in}}}{A_{\text{filter}}} * \text{Flux}_{\text{DepF}} \quad (5.21)$ |
| Recovery time | $t_{\text{DepF recovery}} = \frac{V_{\text{DFilt holdup}}}{\text{Flux}_{\text{DepF}}} * F_{\text{recovery}} \quad (5.22)$ |
| Operation time | $t_{\text{DepF operation}} = t_{\text{DepF process}} + t_{\text{DepF recovery}} \quad (5.23)$ |
| Prep & turnaround time | $t_{\text{DepF prep\&turn}} = t_{\text{DFilt prep}} + t_{\text{DFilt Skid turn}} + t_{\text{DFilt turn}} \quad (5.24)$ |
| Total operators time | $t_{\text{DepF operators}} = t_{\text{DepF operation}} + t_{\text{DepF prep\&turn}} \quad (5.25)$ |
| Depth filtration reagents cleaning* | |
| CIP usage/dome | $V_{\text{cl DepF CIP}} = t_{\text{cl DepF CIP}} * Q_{\text{DFilt CIP Rinse}} * N_{\text{DFilt CIP Rinse}} \quad (5.26)$ |
| WFI usage/dome | $V_{\text{cl DepF WFI}} = t_{\text{cl DepF WFI}} * Q_{\text{DFilt WFI Rinse}} * N_{\text{DFilt WFI Rinse}} \quad (5.27)$ |
| PW usage/dome | $V_{\text{cl DepF PW}} = t_{\text{cl DepF PW}} * Q_{\text{DFilt PW Rinse}} * N_{\text{DFilt PW Rinse}} \quad (5.28)$ |
| Other reagents use WFI flush and recovery | $V_{\text{flush\&recovery DepF WFI}} = A_{\text{filter}} * V_{\text{flush}} + V_{\text{hold-up}} * F_{\text{recovery}} \quad (5.29)$ |

*(MerckMillipore, 2007)

| | | | |
|------------------------------|---|------------------------------|--|
| V_{in} | volume in depth filtration (L) | $t_{\text{cl DepF WFI}}$ | Time for clean using WFI (h) |
| FC | filter capacity (L/m ²) | $Q_{\text{DFilt WFI Rinse}}$ | WFI flowrate (L/h) |
| Eq_ft_{filtr} | Equipment footprint (m ²) | $N_{\text{DFilt WFI Rinse}}$ | Number of cleaning cycles with WFI (bursts) |
| $F_{\text{utFootprint}}$ | Factor facility footprint utilities (m ²) | $t_{\text{cl DepF PW}}$ | Time for clean using PW (h) |
| $F_{\text{pFootprint}}$ | Factor facility footprint personnel (m ²) | $Q_{\text{DFilt PW Rinse}}$ | PW flowrate (L/h) |
| F_{recovery} | Recovery factor | $N_{\text{DFilt PW Rinse}}$ | Number of cleaning cycles with PW |
| $V_{\text{holdup DepF}}$ | Filter holdup volume (L/m ²) | $t_{\text{DFilt Skid turn}}$ | Preparation Time |
| $t_{\text{cl DepF CIP}}$ | Time for cleaning with CIP (h) | $t_{\text{DFilt turn}}$ | Turnaround time per skid |
| $Q_{\text{DFilt CIP Rinse}}$ | CIP flowrate (L/h) | $t_{\text{DFilt prep}}$ | Preparation/turnaround time per filter cartridge/capsule |
| $N_{\text{DFilt CIP Rinse}}$ | Number of cleaning cycles with CIP (bursts) | | |

5.2.3 Recovery model assumptions

5.2.3.1 Process assumptions

The model used a number of process assumptions, which are summarized in **Table 5.4**. These were selected based on literature and discussions with experts. One of the main differences between the stainless steel and the single use depth filtration housing is the need for cleaning and the associated volumes of CIP, PW and WFI reagents. The second key differences is in the equipment footprint, the stainless steel equipment has a higher footprint utilities factor ($F_{ut\text{footprint}}$) to account for the space needed for the fixed piping and control skids. For the single use approach, the footprint of the skid is reduced since there is no requirement for CIP and the flowpath is single use rather than fixed-in-place stainless steel piping.

Table 5.4 Model assumptions for the recovery operation

| | <i>Parameter</i> | <i>Value</i> | | |
|-------------------------|-----------------------------|--|-------------------------|-------------------|
| Centrifugation | $t_{Cent_{prep}}$ | Centrifuge prep time | 1 hr | |
| | $t_{Cent_{turn}}$ | Centrifuge turnaround time | 1 hr | |
| | Y_{Cent} | Centrifuge step yield | 95% | |
| | $t_{Cent_{max}}$ | Centrifugation duration limit | 12 hr | |
| | Op_{Cent} | No. of Operators per unit | 2 | |
| | $t_{rCent_{PW}}$ | PW residence time in the centrifugation (cleaning) | 8 min | |
| | $t_{rCent_{WFI}}$ | WFI residence time in the centrifugation | 8 min | |
| | $t_{rCent_{CPI}}$ | CPI residence time in the centrifugation | 8 min | |
| | $t_{cl_{Cent_{PW}}}$ | Time for cleaning with PW (min) | 60 min | |
| | $t_{cl_{Cent_{WFI}}}$ | Time for cleaning with WFI (min) | 67.5 min | |
| | $t_{cl_{Cent_{CPI}}}$ | Time for cleaning with CPI (min) | 37.5 min | |
| Depth filtration | $t_{DFilt_{dur}}$ | Depth filtration duration limit | 5 hr | |
| | $V_{DFilt_{Flush}}$ | Depth filtration flush volume | 100 L/m ² | |
| | $T_{DFilt_{Flush}}$ | Depth filtration filter flush duration | 1 hr | |
| | $t_{DFilt_{Flush_{Recov}}}$ | Depth filtration flush recovery | 30 min | |
| | $V_{DFilt_{holdup}}$ | Depth filtration hold-up volume | 10 L/m ² | |
| | $Flux_{DFilt}$ | Flux | 200 L/m ² /h | |
| | Y_{DFilt} | Depth filtration step yield | 95% | |
| | $F_{recovery}$ | Flush recovery factor | 0.5 | |
| | | | Stainless steel | Single use |
| | $F_{p_{Footprint}}$ | Factor facility footprint personnel (m ²) | 2 | 2 |
| | $F_{u_{Footprint}}$ | Factor facility footprint utilities (m ²) | 7 | 1 |
| | $t_{DFilt_{prep}}$ | Preparation Time | 20 min | 15 min |
| | $t_{DFilt_{Skid_{turn}}}$ | Turnaround time per skid | 45 min | 30 min |
| | $t_{DFilt_{unit_{prep}}}$ | Preparation/turnaround time per filter cartridge/capsule | 3 min | 0.5 min |
| | $t_{DFilt_{turn}}$ | Turnaround Time | 0.5 hr | 0.5 hr |
| | $t_{cl_{Dep_{FPW}}}$ | PW Rinse | 5 min | 0 |
| | $t_{cl_{Dep_{FWFI}}}$ | WFI Rinse | 2 min | 0 |
| | $t_{cl_{Dep_{FCIP}}}$ | CIP Rinse | 1 min | 0 |
| | $N_{DFilt_{PWRinse}}$ | PW bursts per housing | 3 | |
| | $N_{DFilt_{WFIrinse}}$ | WFI bursts per housing | 3 | 0 |
| | $N_{DFilt_{CIPrinse}}$ | CIP bursts per housing | 3 | 0 |
| | $Q_{DFilt_{PWRinse}}$ | PW flowrate | 83 L/min | 0 |
| | $Q_{DFilt_{WFIrinse}}$ | WFI flowrate | 83 L/min | 0 |
| | $Q_{DFilt_{CIPrinse}}$ | CIP flowrate | 83 L/min | 0 |
| | Op_{Cent} | Min no. of Operators per unit | 2 | 2 |

5.2.3.2 Costs

In this section is a summary of some of the main cost inputs for the model. As it can be seen in **Table 5.5** the cost of the single use capsules is higher than the cost of the cartridges (average price for filter capsules between with 1 and 2m² area for filtration is 642\$/m² for the capsules compared to 314\$/m² for the cartridges). This is expected since the capsules have a more complicated design - for instance, they need to withstand higher pressure than the cartridges.

Table 5.5 Filtration capsules and filtration cartridges costs

| | Vendor | Area for filtration (m ²) | Cost (\$) | |
|----------------------|-----------------|---------------------------------------|---------------------------------------|-----------|
| Filtration capsule | 3M | 1.60 | 809 | |
| | Merck Millipore | 0.11 | 211 | |
| | | 0.55 | 359 | |
| | | 1.10 | 556 | |
| | Pall | 0.25 | 300 | |
| | | 0.50 | 350 | |
| 1.00 | | 560 | | |
| | Vendor | Cartridge diameter | Area for filtration (m ²) | Cost (\$) |
| Filtration cartridge | 3M | 8" | 0.26 | 200 |
| | | 12" | 1.50 | 600 |
| | | 16" | 3.20 | 1,200 |
| | Merck Millipore | 16" | 1.80 | 412 |

Apart from the single use capsules, the fully single use process also uses manifolds, various tubings and connectors and single use pump heads (**Table 5.6**). In the model it is assumed that these costs increase with the number of housings or racks.

Table 5.6 Other consumables used with filter holders and capsules

| Other consumables | Price (\$) |
|---------------------------------|------------|
| Manifold (unit/housing) | 400 |
| Tubing & connectors (unit/rack) | 400 |
| Pump (unit/housing or rack) | 1,024 |

In **Table 5.7** is presented a summary of the costs for the filter holders and domes that were used in the model. To operate the process, in addition to the filter holders and domes, the commercial-scale process would require a control skid. For the single-use configuration there are off-the-shelf control systems such as the Mobius® FlexReady Solution (Millipore Sigma, MA, US) or Allegro® MVP (Pall Corporation, NY, US), which allow for automated control and GMP operation (e.g. availability of audit trails). Additionally, there is also the need for pumps for the process. All these costs are lumped in skid costs for the single and stainless steel process (**Table 5.8**).

Table 5.7 Summary of the costs for the filter holders and domes

| | Vendor | # of racks | Price (\$) |
|---|-----------------|-----------------|------------|
| Filter holder (for capsules) | 3M | 1 | 15,868 |
| | | 1 | 51,000 |
| | | 3 | 98,592 |
| | | 5 | 133,953 |
| | Merck Millipore | 1 | 31,000 |
| | | 2 | 56,000 |
| | | 3 | 79,000 |
| | Pall | 1* ¹ | 8,000 |
| | | 1* ² | 15,000 |
| 1* ³ | | 25,000 | |
| | Vendor | Dome diameter | Price (\$) |
| Stainless steel domes (for cartridges) | 3M | 8 | 9,830 |
| | | 12 | 13,652 |
| | | 16 | 20,000 |
| | Merck Millipore | 16 | 29,938 |

*¹ One holder with 2 capsules capacity; *² One holder with 5 capsules capacity; *³ One holder with 10 capsules capacity

Table 5.8 Costs of depth filtration and centrifugation kids

| | Base size | Cost (\$) |
|---------------------------------------|------------------------------|-----------|
| Skid for filter holders | 1 rack | 311,000 |
| Skid for stainless steel domes | 50m ² filter area | 506,000 |
| Centrifugation skid | 20,000 L/h | 1,359,000 |

Below is a summary of some of the additional costs for the model such as the costs of WFI, CIP and PW used for the cleaning and operation of the centrifuge and for the stainless steel domes in the depth filtration operation (**Table 5.9**).

Table 5.9 Other key costs for the process (Reagents and Labour cost assumptions)

| Cost parameter | Value (\$) |
|----------------------------|------------|
| WFI (\$/L) | 1.50 |
| CIP (\$/L) | 2.50 |
| PW (\$/L) | 0.07 |
| Operator salary (\$/year)* | 100,000 |

* Including the overheads costs

5.2.4 COG calculations

The fixed capital investment costs for the process were calculated as follows:

$$FCI = TEPC * L_f \quad (5.30)$$

where the TEPC is the total equipment purchase cost and L_f is the Lang factor. In this case TEPC accounted for main equipment for the recovery operations, namely the disc-stack centrifuge skid and the depth filtration housing and skid:

$$TEPC = \sum Cost_{Equipment} \quad (5.31)$$

The cost of the filtration skids and centrifugation equipment were calculated as follows:

$$Eq Cost_2 = Eq Cost_1 \cdot \left(\frac{Eq Size_2}{Eq Size_1} \right)^{F_{scale}} \quad (5.32)$$

where F_{scale} is a scaling factor, $Cost_1$ is a known cost for equipment of size $Eq size_1$.

The Lang factor L_f was estimated using the following equation:

$$L_f = c \cdot \sum f_i \quad (5.33)$$

where c is the contingency factor and f are the rest of the factors shown in **Table 5.10**.

Table 5.10 Parameters used for estimating the Lang factor for the recovery process (adapted from Novais et al. (2001) and Pollock, (2014))

| Factors | Domes | Filter Holders |
|----------------------------------|-------------|----------------|
| Equipment | 1 | 1 |
| Pipework and installation | 0.9 | 0.3 |
| Process control | 0.37 | 0.37 |
| Instrumentation | 0.6 | 0.4 |
| Electrical power | 0.24 | 0.24 |
| Building works | 1.66 | 1.33 |
| Detail Engineering | 0.77 | 0.39 |
| Construction and site management | 0.4 | 0.30 |
| Commissioning | 0.07 | 0.07 |
| Validation | 1.06 | 0.53 |
| Contingency Factor | 1.15 | 1.15 |
| Lang factor | 8.13 | 4.73 |

A summary of the remaining equations used to calculate the COG of the recovery operation (COG_{REC}) in the model can be found in **Table 5.12**. As it can be seen in the table the costs were split into direct and indirect costs. The direct costs include reagents and material costs, while the indirect costs refer to the facility overhead costs such as maintenance and insurance (Farid et al., 2020). The labour was calculated as indirect cost with fixed-annual wage based on the number of operators required (rather than using hourly rate).

Table 5.11 Process economics main equations*

| COG calculations (\$) | Equation | |
|----------------------------|---|--------|
| Depreciation per year | $Cost_{Depr} = \frac{FCI}{Y_{Depreciation}}$ | (5.34) |
| Maintenance per year | $Cost_{Maint} = FCI \cdot F_{Maint}$ | (5.35) |
| Insurance per year | $Cost_{Ins} = FCI \cdot F_{Ins}$ | (5.36) |
| Local taxes per year | $Cost_{Tax} = FCI \cdot F_{Tax}$ | (5.37) |
| Operating labour per year | $Cost_{lab_oper} = N_{operators} \cdot Wage_{annual}$ | (5.38) |
| Supervisor labour per year | $Cost_{lab_sup} = Cost_{lab_oper} \cdot F_{lab_supervisor}^a$ | (5.39) |
| Management labour per year | $Cost_{lab_manage} = Cost_{lab_oper} \cdot F_{lab_management}^b$ | (5.40) |
| QC labour per year | $Cost_{lab_QC} = Cost_{lab_oper} \cdot F_{lab_QC}^c$ | (5.41) |
| Total labour costs | $Cost_{lab} = Cost_{lab_oper} + Cost_{lab_sup} + Cost_{lab_manage} + Cost_{lab_QC}$ | (5.42) |
| Utilities per year | $Cost_{Ut} = Unit\ Cost_{Ut} \cdot F_{footprint}$ | (5.43) |
| Chemicals per batch | $Cost_{Chem} = Vol_{Chem} \cdot Unit\ Cost_{Chem}$ | (5.44) |
| Consumables per batch | $Cost_{cons} = N_{cons} \cdot Unit\ Cost_{cons}$ | (5.45) |
| QC materials per batch | $Cost_{QC}^d$ | |
| Miscellaneous per batch | $Cost_{misc} = Misc_{f^e} \cdot (Cost_{chem} + Cost_{cons})$ | (5.46) |
| Indirect COG | | |
| per batch | $Cost_{Ind_batch} = \frac{(Cost_{Depr} + Cost_{Maint} + Cost_{Ins} + Cost_{Tax} + Cost_{Lab} + Cost_{Ut})}{N_{batch}}$ | (5.47) |
| per gram | $Cost_{Ind_gram} = \frac{(Cost_{Depr} + Cost_{Maint} + Cost_{Ins} + Cost_{Tax} + Cost_{Lab} + Cost_{Ut})}{D_{Prod}}$ | (5.48) |
| Direct COG | | |
| per batch | $Cost_{Dir_batch} = Cost_{Chem} + Cost_{cons} + Cost_{Misc} + Cost_{QC}$ | (5.49) |
| per gram | $Cost_{Dir_gram} = \frac{N_{batch} \cdot (Cost_{Chem} + Cost_{cons} + Cost_{Misc} + Cost_{QC})}{D_{Prod}}$ | (5.50) |

* Some equations were adapted from Mahal et al. (2021)

Equations' notation

| | | | |
|--------------------|--|---------------------|---|
| $Cost_{Equipment}$ | cost of equipment directly involved* in recovery operation (\$/unit) | $F_{footprint}$ | footprint of equipment (m^2) |
| L_f | Lang factor | Vol_{Chem} | volume of chemicals (L/batch) |
| Y_{Depr} | years of depreciation | $Unit\ Cost_{Chem}$ | cost of chemicals (\$/L) |
| F_{Maint} | maintenance factor | N_{cons} | number of consumables used (unit/batch) |
| F_{Ins} | insurance factor | $N_{batches}$ | Number of batches per year |
| F_{Tax} | local taxes factor | $Unit\ Cost_{cons}$ | cost per unit (\$/unit) |
| $N_{operators}$ | number of operators (op/y) | F^{Misc} | Miscellaneous factor |
| $Wage_{annual}$ | operators wage per year (\$/y) | $D_{product}$ | Demand of product per year (kg) |
| $F_{personnel}$ | factor accounting for other personnel involved in the operation. It corresponds to the sum of the factors for management, supervisor QA/QC plus 1. | $Cost_{QC}$ | Cost of QC materials per batch |
| $Unit\ Cost_{Ut}$ | Annual cost of utilities per square meter of facility | | |

^a $F_{lab_supervisor} = 0.2$; ^b $F_{lab_management} = 1$

^c F_{lab_QC} ; ^c $F_{lab_QC} = 1$

^d $Cost_{QC} = 35,000\$/batch$

^e $Misc_f = 0.1$

5.2.5 Case studies assumptions

The goal of the first case study (**Section 5.3.1**) was to identify key cost drivers for different manufacturing scenarios. For this purpose, a deterministic analysis was performed for a ranges of titres and demand scenarios. **Table 5.12** shows the main process assumptions made for the economics appraisal. For the deterministic analysis titres in the range of 3 to 9 g/L were modelled, which is in line with the titres obtained through the experimental work as well as titres reported in literature. The demands investigated were in the range of 100 to 900 kg/year, which reflects current trends in the mAbs industry. Furthermore, this is the range, in which the highest variation in COG was observed in the preliminary analysis.

The model was run either using design or rating mode. In design mode, the annual demand was fixed and the equipment sizes required were determined. If multiple bioreactors were required they were assumed to run in parallel and be pooled prior to primary recovery operations. An alternative setup to minimise idle time for the recovery operations would have been to consider staggering the bioreactors. In rating mode, the equipment sizes were fixed and the annual output was determined based on fluctuations in the process parameters; this mode was used in the uncertainty analysis.

Table 5.12 Overall process assumptions used for assessing the COG of the recovery operation for different titre and demand scenarios in **Section 5.3.1**

| <i>Process step</i> | <i>Parameter</i> | <i>Value</i> |
|------------------------------|-----------------------------|-----------------------------------|
| Scenarios | Titre | 3, 6 and 9 g/L |
| | Demand | 100, 500 and 900 kg/year |
| Overall process | Number of batches/year | 21 |
| | DSP yield | 68 % |
| | Facility sizing | Design mode |
| Upstream | Bioreactor space efficiency | 75 % |
| Disc-stack centrifuge | Number of parallel units | 1 |
| | Duration limit | 12 h/batch |
| | Yield | 95 % |
| Depth filtration | Filtration media | Dual layer X0HC (Merck Millipore) |
| | Equipment type | Filter holder or Domes |
| | Yield | 95% |

In the second case study in **Section 5.3.2** the yearly demand was fixed at 500 kg/year. The experimental data from ambr3 was used to investigate the impact of the upstream conditions on the recovery operation and COG of the recovery (**Table 5.13**).

Table 5.13 Key assumptions used to investigate the impact of pH, seeding density and temperature shift on the recovery process economics in **Section 5.3.2**

| | <i>Parameter</i> | <i>Value</i> |
|------------------------------|-------------------------|--|
| Scenarios | pH | 6.8, 7.0, 7.2 |
| | Seeding density | 0.5 to 0.9 x 10 ⁶ cells/mL |
| | Temperature | 35.5°C or shift to 33.5° on day 4 from 35.5°C |
| Overall process | Demand | 500 kg/year |
| | Facility sizing | Design mode |
| Upstream | Titre | f (SD*, T** and pH) |
| | [Solids] | f (SD, T and pH) |
| Disc-stack centrifuge | Yield | f ([Solids]) |
| Depth filtration | Equipment type | Filter holder (Merck Millipore) |
| | Consumable | Dual layer capsule (X0HC) |
| | Maximum filtration area | 55m ² in one filter holder |

*SD: seeding density, **T: temperature

The third case study (**Section 5.3.2.2**) investigated the impact of harvest days, bioreactor seeding density and shear on the process performance (**Table 5.14**).

Table 5.14 Key assumptions used in **Section 5.3.2.2** to investigate the impact of bioreactor seeding density, harvest day and centrifugation on recovery process economics

| | <i>Parameter</i> | <i>Value</i> |
|------------------------------|-------------------------|---|
| Scenarios | Shear level | Low and high |
| | Seeding density | 0.5 to 1.3 x 10 ⁶ cells/mL |
| | Harvest day | 10 to 14 |
| Overall process | Demand kg/year | 500 |
| | Facility sizing | Design mode |
| Upstream | Titre | f (*SD and **HD) |
| | [Solids] | f (SD and HD) |
| Disc-stack centrifuge | Yield | f ([Solids]) |
| Depth filtration | Maximum filtration area | 33m ² in one filter holder (Millipore) |
| | Consumable | Dual layer capsule (X0HC) |
| | Filter capacity | f (SD, Shear and pH) |

*SD: seeding density, **: harvest day

Table 5.15 Case studies 4 and 5 on facility fit assessment. A) Overall setup for the cases studies; B) Scenarios used for building a window of operation in case study 4 (**Section 5.3.3.1**) C) Monte Carlos simulation in case study 5 (**Section 5.3.3.2**)

A)

| | <i>Parameter</i> | <i>Value</i> |
|------------------------------|-------------------------|--|
| Overall process | Demand kg/year | 500 |
| | Facility sizing | Rating mode |
| Upstream | <i>Titre</i> | $f(SD \text{ and } HD)$ |
| | Bioreactor size | 10,000L |
| | [Solids] | $F(SD \text{ and } HD)$ |
| Disc-stack centrifuge | <i>Yield</i> | $f([Solids])$ |
| | Centrifugation skid | Culturefuge 200 (Table 5.1) Culturefuge 300 (Table 5.1) |
| Depth filtration | <i>Filter capacity</i> | $f(SD^*, \text{ Shear and } HD^{**})$ or fixed at 300L/m ² |
| | # of filter holders | 1 |
| | Maximum filtration area | 33m ² in one filter holder (Millipore) |
| | Consumable | Dual layer capsule (X0HC) |

B)

| | | |
|----------------------------|--------------------|---------------------------------------|
| Window of operation | <i>Shear level</i> | <i>Low and high</i> |
| | Seeding density | 0.5 to 1.3 x 10 ⁶ cells/mL |
| Scenarios | Harvest day | 10 to 14 |

C)

| Monte Carlos simulations scenarios | Scenarios | 1 | 2 | 3 | 4 |
|---|---|----------------------|---------------------|-------------------|---------------------|
| | Harvest day | Tr*** (11, 11.5, 12) | Tr (11.5, 12, 12.5) | Tr (12, 12.5, 13) | Tr (12.5, 13, 13.5) |
| Seeding density | Tr (0.5, 0.8, 1.1) x10 ⁶ cells/ mL | | | | |
| Shear | Low or high | | | | |
| Number of simulations | 500 | | | | |

*SD: seeding density, **HD: harvest day, ***Tr: triangular distribution

In the remaining case studies 4 and 5 (**Section 5.3.3**), a fixed-facility scenarios was investigated. In **Table 5.15a** is given the overall setup that applies to both cases studies. **Table 5.15b** describes case study 4 where a window of operation was built for varying seeding densities and harvest days, and **Table 5.15c** describes case

study 5 where stochasticity was applied to the process inputs (seeding density and harvest day) to assess the robustness of the process.

5.3 Results and Discussion

5.3.1 COG_{REC} comparison for different scenarios

The economics model was initially used to evaluate how the COG_{REC} and cost drivers for the recovery operation change across different titre and demand scenarios. Then it was applied to understand the cost-effectiveness of the single-use approach for the secondary depth filtration operation across the different demand and titres. This analysis is important to validate the economics model and to understand the key levers for reducing the COG_{REC}/g.

5.3.1.1 COG comparison across different titres and demands

Figure 5.4 shows the COG_{REC}/g for a recovery operation consisting of disc-stack centrifugation followed by a depth filtration step using stainless steel domes for varying titre (3 to 9g/L) and demand (100 to 900kg/yr) scenarios. The analysis reveals that the centrifugation has a greater cost contribution to the recovery operation irrespective of the demand or titre - an average ratio of approximately 60:40 (centrifugation: depth filtration) for the 100-900 kg/year scenarios. This is due to the higher direct costs for the centrifugation across all scenarios (average 67% higher than depth filtration) and higher indirect costs (average increase of 25% compared to depth filtration) in all scenarios apart from the low titre and high demand scenario. The overall COG_{REC}/g is highest for the low titre and high demand scenario (22\$/g) and decreases with increasing demand due to economies of scale, down to 3.5\$/g for the high titre and high demand scenario.

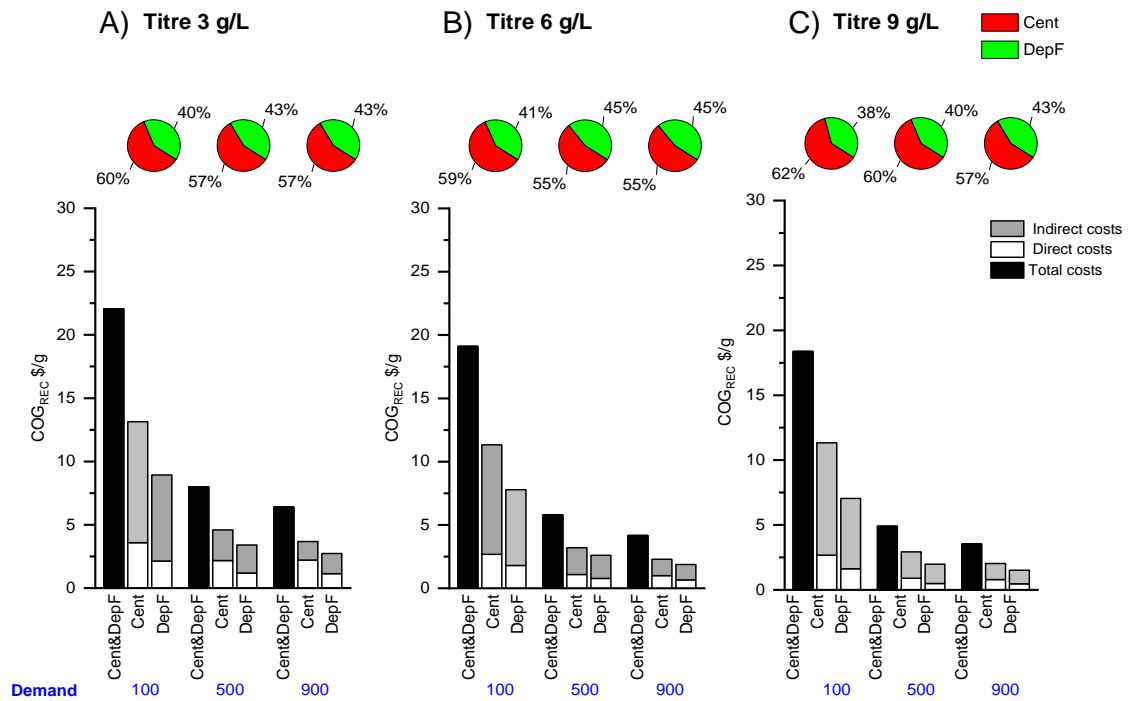


Figure 5.4 Comparison of the contribution to the overall $\text{COG}_{\text{REC}}/\text{g}$ between centrifugation and the depth filtration operation for different manufacturing scenarios: yearly demand of 100kg, 500kg and 900kg and titre of A) 3 g/L, B) 6g/L and C) 9 g/L. The black bars describe the overall costs of the recovery operation consisting of the primary recovery (centrifugation) and secondary recovery (depth filtration). The white colour describes the direct costs for the centrifugation (Cent) or depth filtration step (DepF) and the dark grey describes the indirect costs for the steps. The pie charts for each titre and demand scenario show the distribution in costs between the centrifugation and depth filtration step.

As can be seen in **Figure 5.4**, the indirect costs dominate over the direct costs in all scenarios apart from the low titre and high demand scenario. The change in yearly demand from 100kg/yr to 900kg/yr has a more dramatic impact on the $\text{COG}_{\text{REC}}/\text{g}$ than the change due to increase in titre. For the high titre scenario, there is a decrease of 81% in $\text{COG}_{\text{REC}}/\text{g}$ as the demand goes from low (100kg/yr) to high (900kg/yr), while for the low titre this decrease is 71%. The increase in titre from 3g/L to 9g/L leads to the highest decrease in $\text{COG}_{\text{REC}}/\text{g}$ of 45% for the high demand

scenario compared to 39% for the mid demand (500kg/yr) and 20% decrease for the low demand respectively. The increase in titre from 6 g/L to 9g/L has the most significant impact for the mid and high demand scenarios, leading to decrease in COG_{REC}/g of 15%. From the analysis, it is clear that the impact of titre would be important for the annual demands above 500kg/yr.

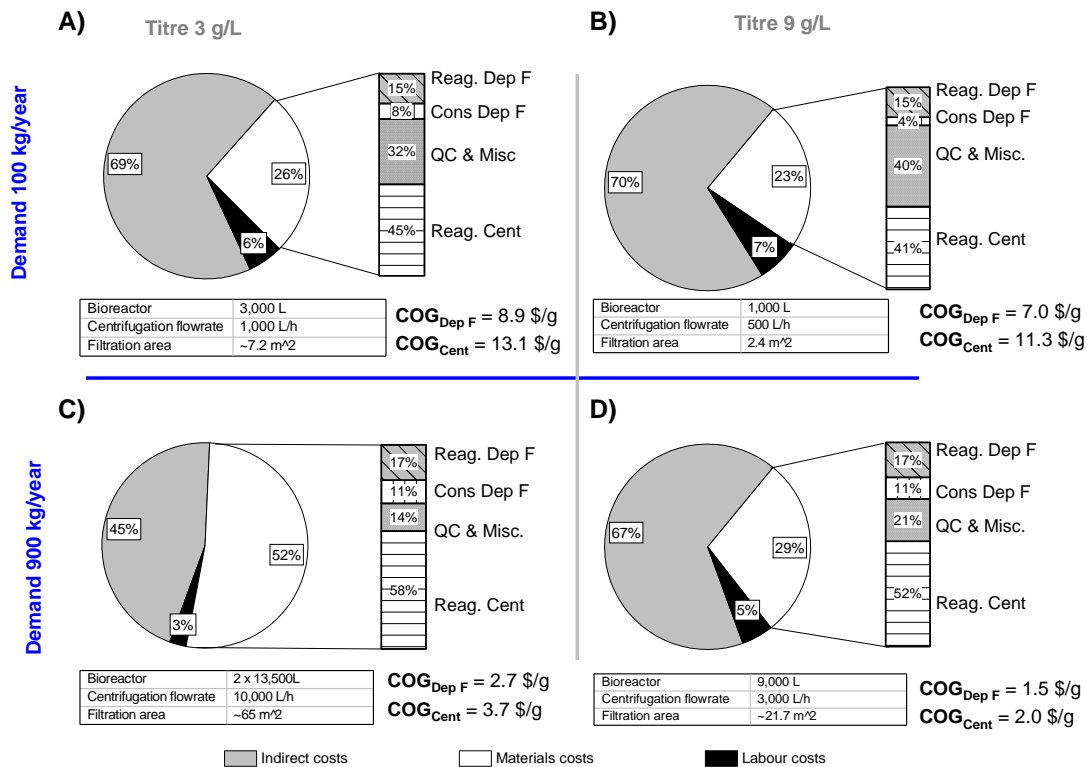


Figure 5.5 Overall breakdown for the COG_{REC}/g for different scenarios for A) low titre of 3g/L and low demand of 100kg/year; B) high titre of 9g/L and low demand of 100 kg/year; C) low titre of 3 g/L and high demand of 900 kg/year and D) high titre 9g/L and high demand of 900 kg/year. For the pie charts the white colour describes the material costs (including consumables and reagents), the black represents the labour costs and grey colour corresponds to the indirect costs. The process economics model was run in design mode using, stainless steel bioreactors, disc-stack centrifuge (Cent) and stainless steel domes for filtration (Dep F).

A closer examination of the extreme points – high and low demand and high and low titre – reveals a change in the cost breakdown for the different scenarios **Figure 5.5**.

The indirect facility-related costs dominate (67% to 70%) for the scenarios that result in lower scales of production (e.g. 3000L at low titre, low demand (**Figure 5.5a**) or 9000L at high titre, high demand (**Figure 5.5d**)), whereas the direct costs dominate (e.g. >50%) for those translating into larger scales of production (e.g. 2x 13,500L at low titre, high demand (**Figure 5.5c**)). Hence this reinforces the impact of economies of scale where the relative proportion of indirect costs goes down as the production scale increases.

When looking at the breakdown of the direct recovery costs, the reagents costs always form the biggest proportion – from 56% for the high titre and low demand scenario to 75% for the low titre and high demand scenario. The reagents costs are mainly attributed to the centrifugation cleaning and operation as well as to the cleaning of the depth filtration stainless steel domes and the depth filters flush. The next cost contributor for the material costs is the QC and Miscellaneous costs. Since the QC costs are fixed per batch, their importance decreases with increasing scale.

Labour costs represent the lowest COG contributor in this case. Since they are calculated as indirect costs, the costs also go down with increasing scale – from 7% for the 1,000L bioreactor (high titre and low demand) to 3% for the two 13,000 bioreactor (low titre and high demand).

5.3.1.2 **COG comparison between single use and stainless steel filter housings**

In the biopharmaceutical industry there has been a strong drive for moving towards using single use technologies. This reduces the costs of cleaning as well as the cleaning validation effort. Furthermore, it may reduce the time and effort for

changeover between products for multi-product facilities. The economics model presented here enables COG comparison for the secondary depth filtration operation using either single-use capsules with single-use flowpath vs single-use cartridges within a stainless steel housing, which requires cleaning. The costs of changeover and validation were not included in the model. **Figure 5.6** reveals that the process using depth filtration holders is 15 to 25% cheaper than the process using domes. This is largely driven by the lower indirect costs with average decrease of 37% for the filter holders compared to the stainless steel domes operation. **Figure 5.6** also reveals that the direct costs for the process also have a different distribution. For the process with domes the largest proportion of direct costs are for reagents (39% to 51% across the different scenarios), while for the filter holders process the consumables are the main proportion of the direct costs (40% to 67% across the different scenarios). When switching from stainless steel domes to filter holders with a single-use flowpath, it is also important to consider the environmental and sustainability impact. Since depth filters are not re-used, they would be discarded after each use in both cases. The solid waste is expected to be slightly higher for the filter holder option since it would include the filter capsules with their heavier casing and the single-use flowpath; in contrast for the stainless steel domes this would mainly be the filter cartridges. The key difference expected would be related to the liquid waste where the stainless steel domes and piping require extensive cleaning which consumes cleaning solutions, water for injection and electricity. Hence, future work could examine the process mass intensity and carbon footprint of the options to weigh up the trade-offs between liquid and solid waste. Studies have suggested

that single-use can have an overall lower environmental impact than stainless steel despite the extra solid waste as summarized by Ottinger et al. (2022).

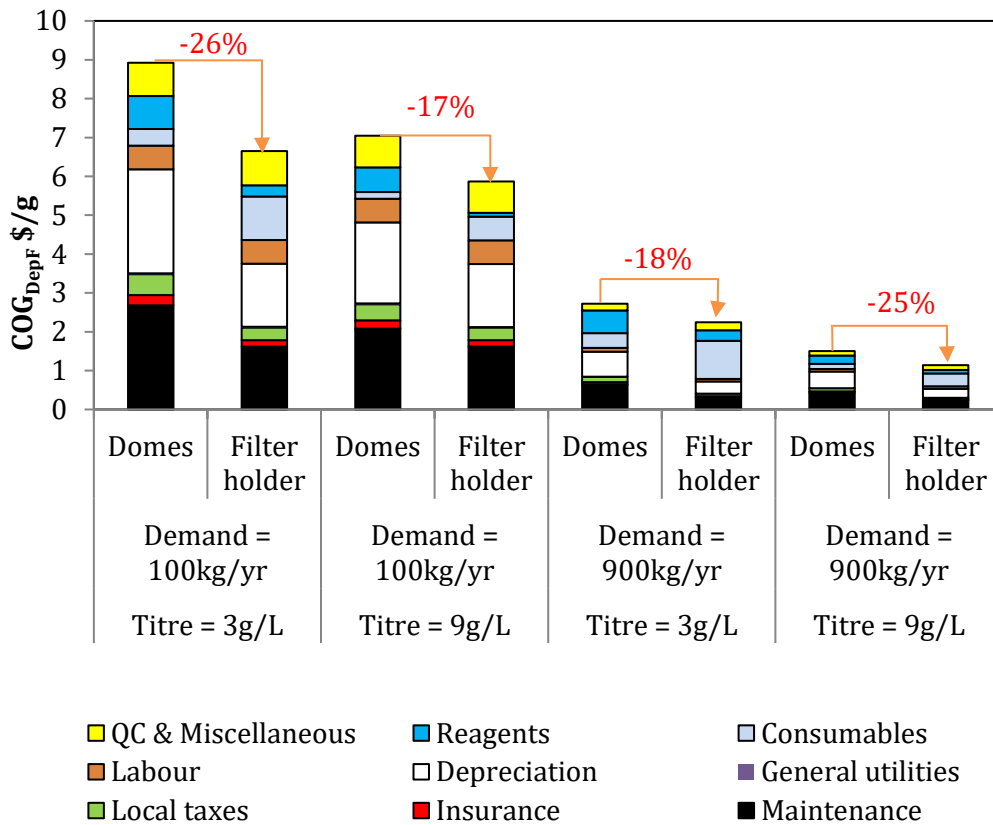


Figure 5.6 Comparison of the COG \$/g between a depth filtration operation using stainless steel domes vs. filter holders for different manufacturing scenarios (left to right): low titre of 3 g/L and low demand of 100kg/year; high titre of 9g/L and low demand of 100kg/year; low titre of 3g/L and high demand of 900kg/year and D) high titre of 9g/L and high demand of 900kg/year.

5.3.2 The impact of upstream conditions on COG_{REC}

In the previous section, the economics model was applied to different demand and titre scenarios in order to understand how these impact on the COG_{REC}. However, titre as well as other key recovery performance metrics – filter capacity and [solids] – were manually set. Therefore, it was not clear how the different performance

metrics correlate, for instance, how the process conditions that resulted in high titre may impact centrate filterability and harvest [solids]. In this section, the goal was to address this through the use of predictive correlations for the key upstream and recovery performance metrics derived in **Chapters 3** and **4**. Furthermore this allowed the impact of upstream variability to be captured on the recovery performance and economics.

5.3.2.1 **The impact of temperature, pH and seeding density on COG_{REC}**

The recovery platform investigated here is based on a disc-stack centrifuge followed by filter holders and the facility was sized using the correlations for titre and [solids] described in **Chapter 3**. Consequently, the COG_{REC} was linked to the titre and [solids], which were a function of the upstream conditions, namely temperature, pH and seeding density. The target demand was set to 500kg/yr, which was the mid-scale investigated earlier; this was also one of the scenarios for which titre had a significant impact on the recovery process economics. Modelling the titre is important for understanding the recovery economics, since titre will determine the bioreactor size (**Equation (5.3)**), which will be the feed volume for the recovery process – the required centrifugation flowrate (**Equation (5.8)**) and depth filtration area (**Equation (5.41)**) for a facility design scenario, while the [solids] will impact the centrifugation yield and the discharge interval, which can in turn impact on the required bioreactor size.

To better understand how the [solids] impact on the COG_{REC}/g, two scenarios were investigated – sizing the centrifugation operation disregarding constraints due to [solids] (conventional approach) and sizing accounting for the [solids]. In the first case, the feed volume determines the required centrifugation flowrate to process the

harvest within a certain time (**Equation (5.8)**), while in the second case the centrifugation also needs to satisfy a minimum discharge interval, which depends on the [solids] (**Equation (5.11)**). .

Figure 5.7 shows the first scenario when the [solids] is not considered for sizing. In this case, the lowest COG_{REC}/g was achieved for the conditions with highest titre (medium pH, high seeding density) and lower upstream and recovery scales, for both the conditions with and without a temperature shift (**Figure 5.7a** and **d**). This was expected since the increase in titre drives down the bioreactor volume – 5,000L at the highest titre (10.5g/L) versus 13,000L at the lowest titre (3.6 g/L) for the conditions without a temperature shift, while for the conditions with a temperature shift the bioreactor volume was 7,000L for the highest titre (6.9g/L) and 20,500 for the lowest titre (2.3g/L) (**Figure 5.7b** and **e**). The smaller feed volumes from upstream, would require centrifuges with lower flowrate -1,500L/h for the 5,000L bioreactor versus 5,000L/h for the 13,000L bioreactor (no temperature shift) and 2,000L/h for the 7,000L bioreactor versus 6,000L/h for the 20,500L bioreactor (temperature shift).

In contrast, the highest increase in COG_{REC}/g was seen for conditions with lowest titre (high pH, low seeding density). For the case with a temperature shift, this resulted not only in larger bioreactor and centrifuge scales but also multiple filter holders to process the higher volumes (**Figure 5.7b** and **e**) and COG differences of up to 113% compared to 65% without a temperature shift (**Figure 5.7a** and **d**).

Figure 5.7c and **f** show the impact of the upstream conditions on the predicted [solids] and the required frequency of solids discharge for the centrifugation operation. Centrifuges are often designed with a maximum discharge interval of >~

120s, which is violated for the cases highlighted in yellow (**Figure 5.7d** and **f**). This is due to the elevated [solids] for these conditions – up to 8% for the conditions without a temperature shift and 10% for the conditions with a temperature shift. This analysis demonstrates that when the [solids] is not considered for sizing, it can lead to a centrifugation process that violates the discharge interval limitation. Consequently, lowering the seeding density can be used as a strategy to decrease the [solids] and increase the discharge interval. However, the lower seeding density would also lead to lower titre and hence impact on the ability to meet demand for this process.

Figure 5.8 shows the improved approach to centrifugation sizing where the centrifugation's holding capacity is taken into consideration indicating the need for bigger centrifuges as highlighted in yellow in **Figure 5.8b** and **e**.

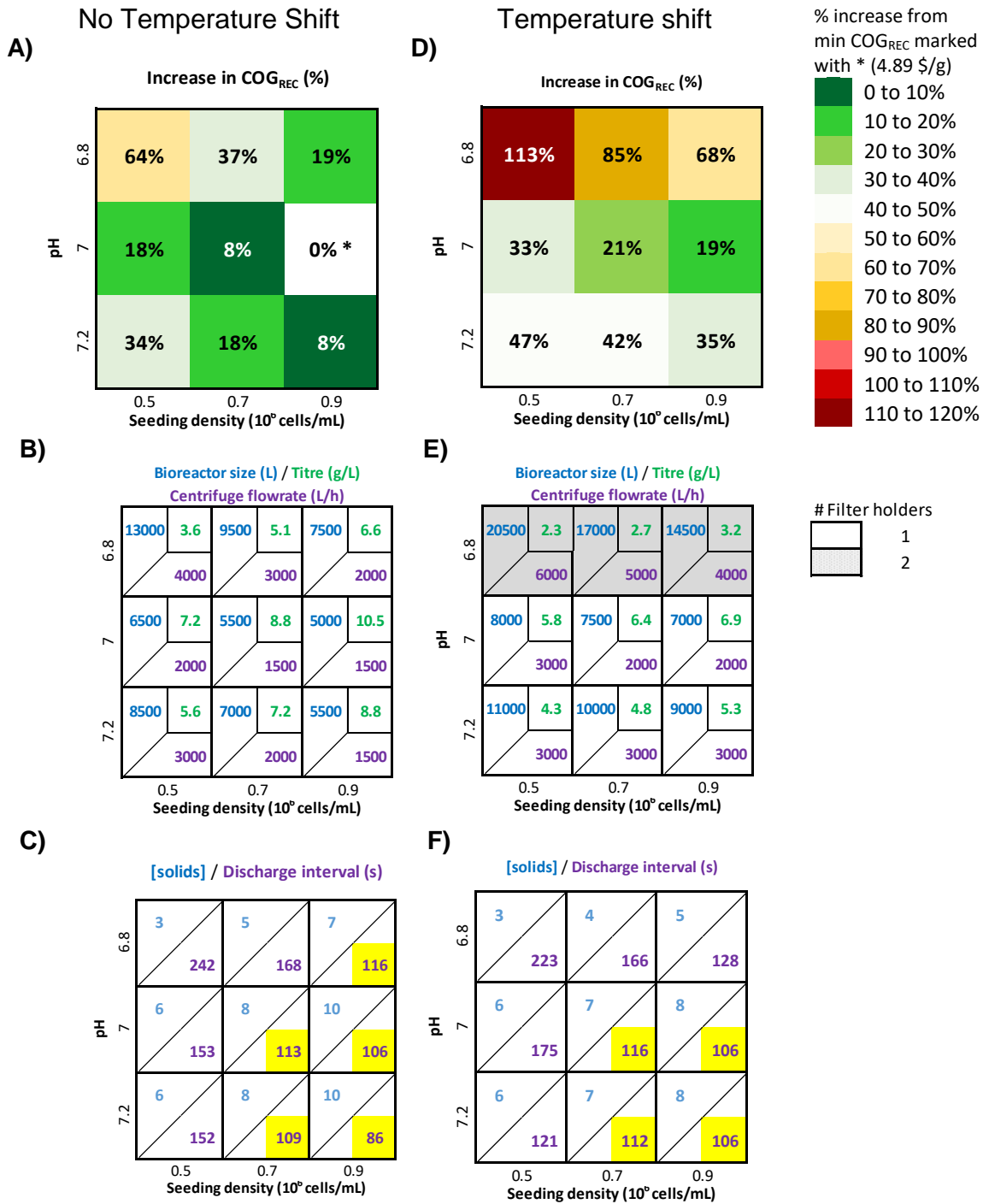


Figure 5.7 Impact of pH and seeding density on A) and D) percentage change in COG from the optimum COG_{REC} (g/\$) = 4.89 marked with a star; B) and E) Bioreactor volume (L) in blue, titre in green and centrifuge size (L/h) in purple; C) and F) the [solids] (% v/v) in blue and discharge interval (s) in purple - the yellow box shows the conditions, where the solids discharge interval violates the 120s limit. The harvest day is set to 14, demand is set to 500 kg/yr, the centrifuge was sized based on flowrate, the filtration area is max 55m² per filter holder and the filter capacity is 300L/m².

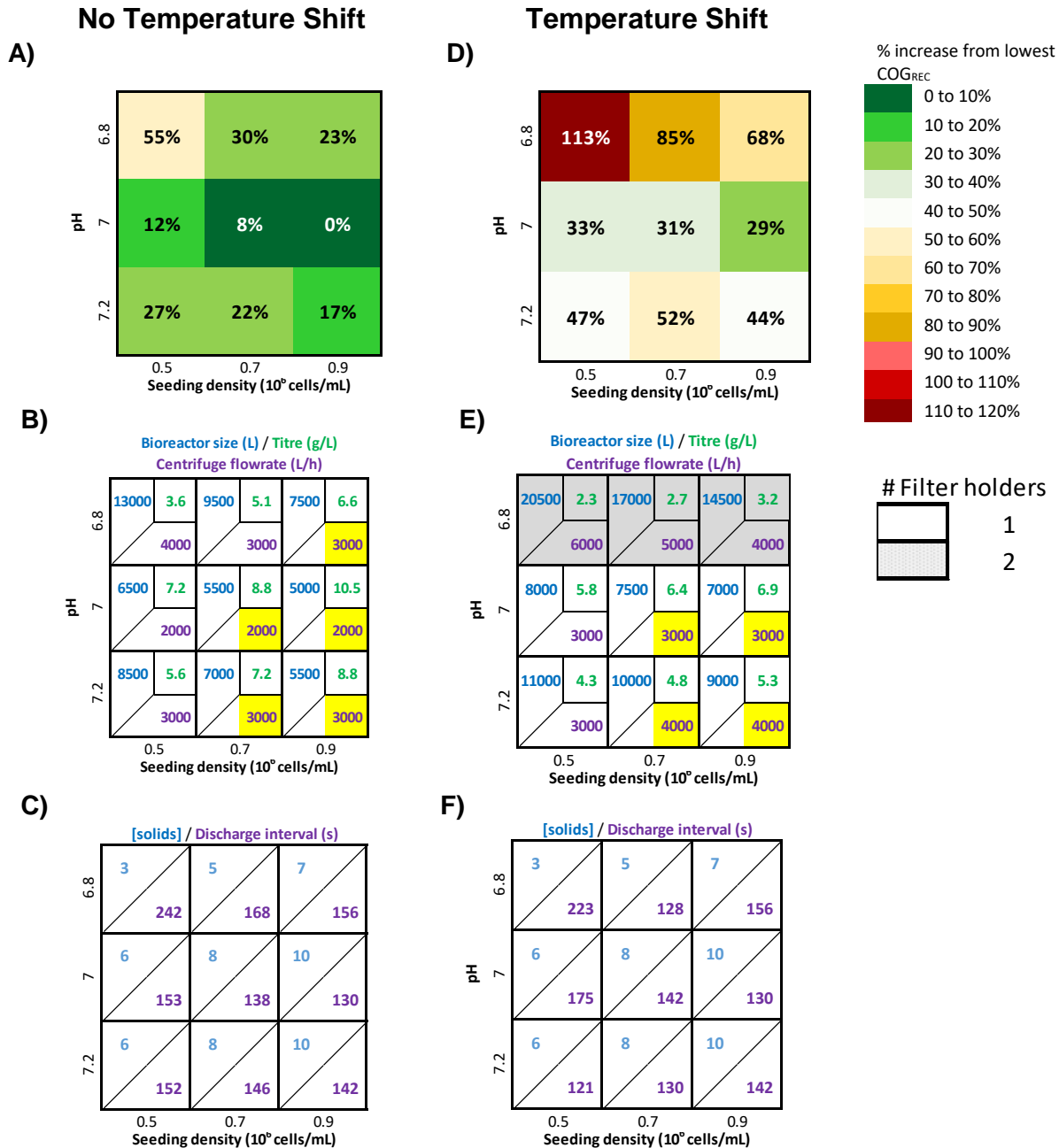


Figure 5.8 Applying an improved approach to centrifugation sizing accounting for the impact of [solids] to investigate the impact of pH and seeding density on A) and D) percentage change in COG from the optimum COG_{REC} (5.2 \$/g); B) and E) Bioreactor volume (L) in blue, titre (g/L) in green and centrifuge size (L/h) in purple; C) and F) the [solids] (% v/v) in blue and discharge interval (s) in purple - the yellow box shows the conditions, where the centrifuge has increased in size to meet the max discharge interval of 120s. A); B) and C) conditions without a temperature shift and D); E) and F) conditions with a temperature shift. The harvest day is set to 14, demand is set to 500 kg/yr, the centrifuged was sized based on flowrate, the filtration area is max 55m² per filter holder and the filter capacity is 300L/m².

5.3.2.2 The impact of shear, seeding density and harvest day

In the previous section the focus was on the upstream conditions that are typically investigated during early process development, namely pH and temperature. In this section the focus is on parameters that are hard to control during scale-up (levels of shear and seeding density) or easier to change during late process development – e.g. time of harvest. For this purpose the correlations for ambr3 (**Chapter 4**) were implemented in the economics model to size the upstream and recovery operation across varying seeding densities, harvest days and levels of shear. The goal was to identify the optimum COG_{REC} and understand what drives the change in COG_{REC} for the different conditions leveraging the predictive correlations for the process performance metrics of titre, [solids] and filterability.

Figure 5.9 reveals that the minimum COG_{REC} was achieved at low seeding density and harvest day 13 or 14 for both low and high shear. The highest COG_{REC} values were reached for harvest day 10, which was driven by the higher [solids] – 9% to 10% compared 5% to 7% for the late harvest day – and higher feed volumes due to lower titre (1.9g/L to 3g/L) resulting in higher filtration area (up to 36m² for low shear and 114m² for high shear) and higher centrifuge flowrates (UP TO45,000 L/h) (**Figure 5.9 b**). The increase in shear leads to higher COG_{REC} due to the lower filterability and consequently the increase in filter area and filter holder requirements compared to the low shear process (**Figure 5.9c** and **f**). Since the volume also impacts on the filter area requirements, the highest COG_{REC} values are for the early harvest day, despite the better centrate filterability at that stage (531L/m² for harvest day 10, low shear and low seeding density versus 161L/m² for harvest day 14 and high seeding density).

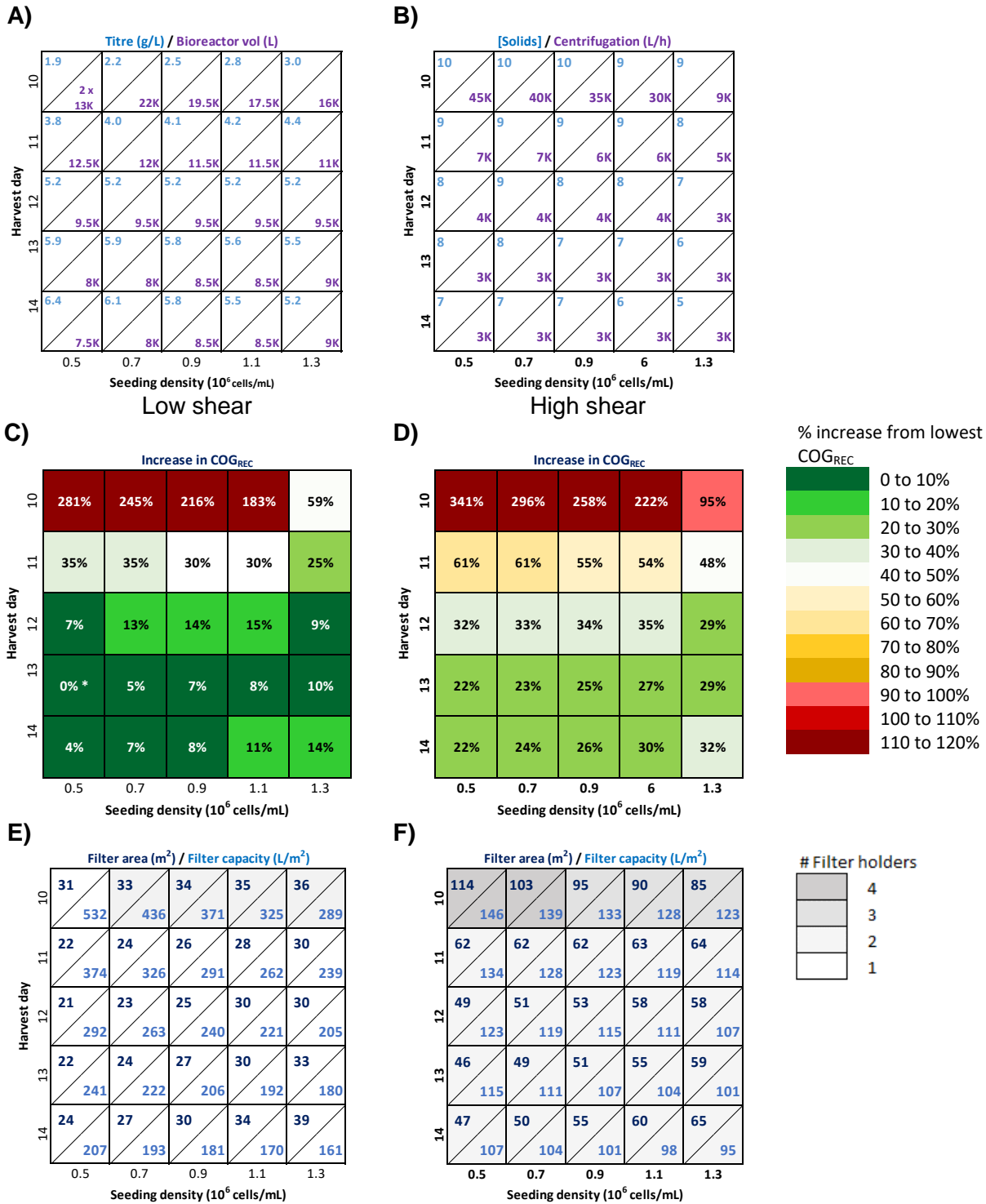


Figure 5.9 The impact of harvest day and seeding density on A) Bioreactor volume (in purple) and titre (in blue); B) [solids] (in blue) and centrifuge flowrate (in purple); the increase in COG_{REC}(%) compared to an optimum (marked with an asterisk(*)) for C) low shear and D) high shear conditions; and filter area (m², in dark blue) and filter capacity (L/m² in blue) for E) low shear and F) high shear. The max filter holder capacity is 33m².

5.3.3 The impact of process variability on facility fit

5.3.3.1 Windows of operation for low and high shear

The use of a platform approach for mAb manufacture means that a new process often needs to fit into a pre-existing facility. Therefore, it is important to understand how different process parameters such as day of harvest, seeding density and level of shear may impact on facility fit, identify the key trade-offs for the process and find strategies to mitigate against risk to facility fit. For this purpose the facility design was fixed as described in **Table 5.15**. The hypothetical process needed to satisfy a number of performance metrics: 1) a minimum target throughput of 550kg/year in order to meet yearly demand; 2) a minimum upstream productivity of 5.5g/L; 3) a maximum percentage product loss in the secondary depth filtration step due to capacity limitations of 10%; 4) a maximum [solids] of 9% v/v and 5) a maximum COG_{REC} of 7\$/g.

To better understand the impact of the filterability correlations on the window of operation, two different scenarios were compared – one where the filter capacity was fixed at 300L/m² and a second one that uses the predictive correlations from **Chapter 4** to determine filter capacity as a function of day of harvest day, seeding density and level of shear; in both cases the predictive correlations for titre were still applied.

Figure 5.10 reveals that the use of the predictive correlations reduces the size of the window of operation – without the predictive correlations for filter capacity and [solids] the window is only constrained by titre (**Figure 5.10a**), and implementing the predictive correlations shows that the high seeding density and late harvest day conditions lead to product loss and increased COG_{REC}, which adds additional

constraints to the window (**Figure 5.10g**). For the scenario with fixed filterability, the throughput and COG_{REC} are determined by the titre and the contours follow the same shape as the titre (**Figure 5.10b, c and d**); furthermore, there is no product loss as the filter area requirement is $\sim 22m^2$ across all scenarios (max filter area available is $33m^2$). The predictive correlation for filter capacity reveals a reduction in throughput for the high seeding density and late harvest day conditions (**Figure 5.10k**), which is due to highest filter area requirements (**Figure 5.10l**), which exceed the constraint of $33m^2$ and consequently lead to product loss. The reduced filter capacity for the late day of harvest can be explained by the increase in cellular debris due to cell culture decline, while the higher seeding density leads to overall increase in solids. The correlation reveals that the increase in titre for the late harvest day and high seeding density conditions is not sufficient to counter the negative of product loss on the process and reduce the COG_{REC} to the target value (**Figure 5.10j**).

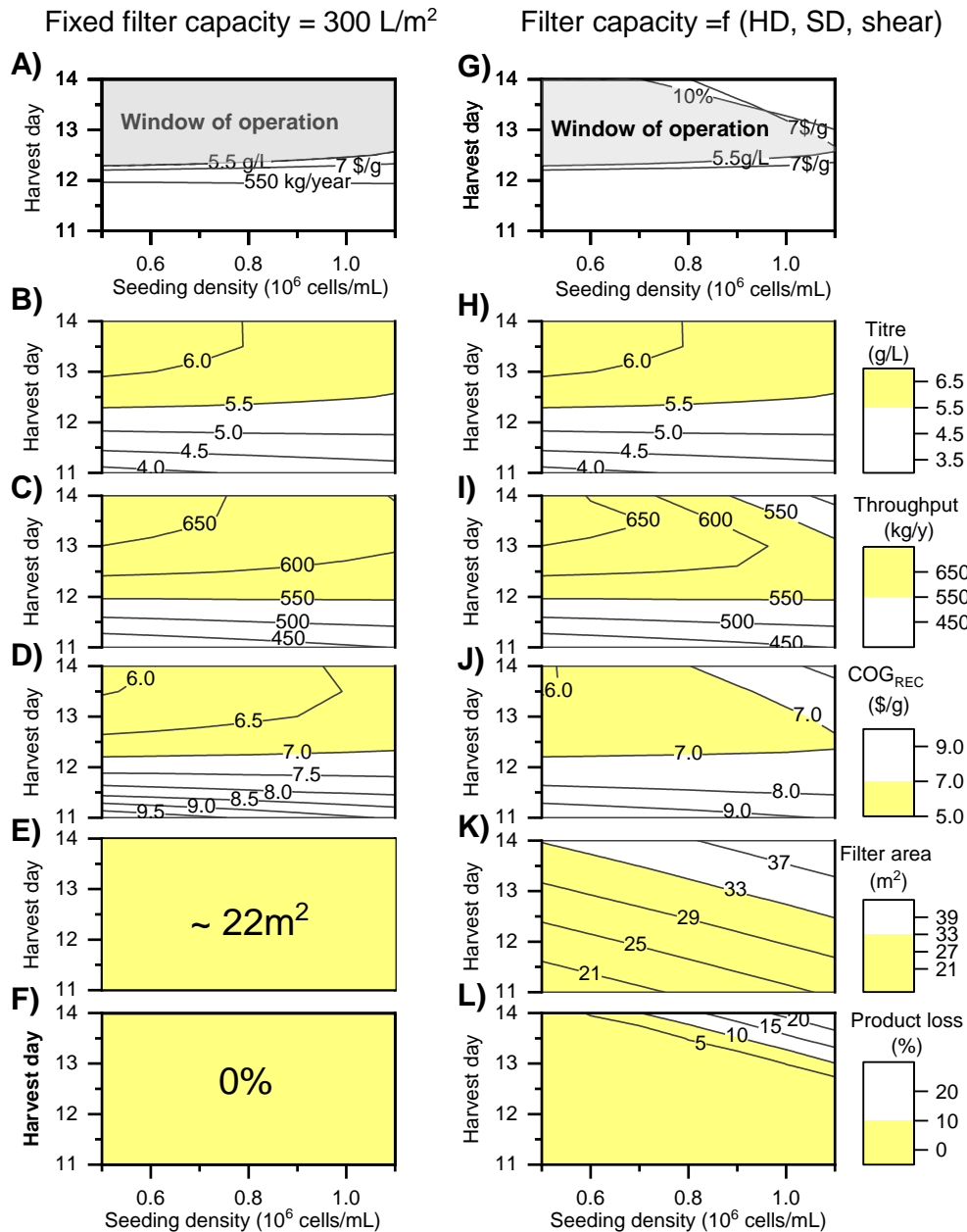


Figure 5.10 Window of operation in grey for varying seeding densities and harvest days for a scenario A) without the use of predictive correlations for filter capacity, and [solids] using a fixed depth filtration filterability = 300L/m² and [solids] = 5%; G) with predictive correlations. The windows are constrained by B) and H) titre (g/L); C) and I) Throughput (kg/yr); D) and J) COG_{REC} (\$/g), E) and K) depth filtration area (m²); F) and L) product loss due to depth filtration capacity. The window in A) is constrained by B); C); D); E) and F) and the window in G) is constrained by H); I); J); K) and L). The process is based on Merck Millipore filter holder with max holder capacity of 33m², Culturefuge 300 with max flowrate of 6,000L/h and solids holding space of 20L and a bioreactor size of 10,000L. The yellow area indicates process constraints. HD is harvest day and SD is seeding density.

Often during tech transfer and scale up, the impact of shear on facility fit is overlooked. It could be that the shear level during the clarification operation is lower for the early process development due to the use of a different technology, such as primary depth filtration, the use of a pilot scale centrifuge with lower levels of shear or setups that generates different shear levels between scales (as described in **Section 1.2.2**). In all cases the impact of high shear on the overall process can be overlooked when scaling up. It is important to note that the levels of shear also depend on the centrifuge bowl speed required for clarification. This can be explained by the approach used for scaling up the centrifugation operation, based on constant clarification efficiency Q/Σ , where Q is the centrifugation flowrate and Σ is the equivalent settling area, which is a function of the bowl rotational speed. This means that to maintain the same Q/Σ for a higher flowrate the centrifugation bowl speed needs to go up (**Appendix, Figure 5.2-A**), which in turn increases the level of shear.

Figure 5.11 reveals that no window of operation was formed for the high shear conditions investigated in **Chapter 4**. The lowest COG_{REC} (**Figure 5.11a**) and highest throughput (**Figure 5.11b**) were achieved for harvest day 13-13.5 and low seeding density conditions, and hence these could be considered the optimum conditions. The largest filtration area and biggest product loss were reached for the high seeding density and late harvest day conditions (**Figure 5.11c and d**).

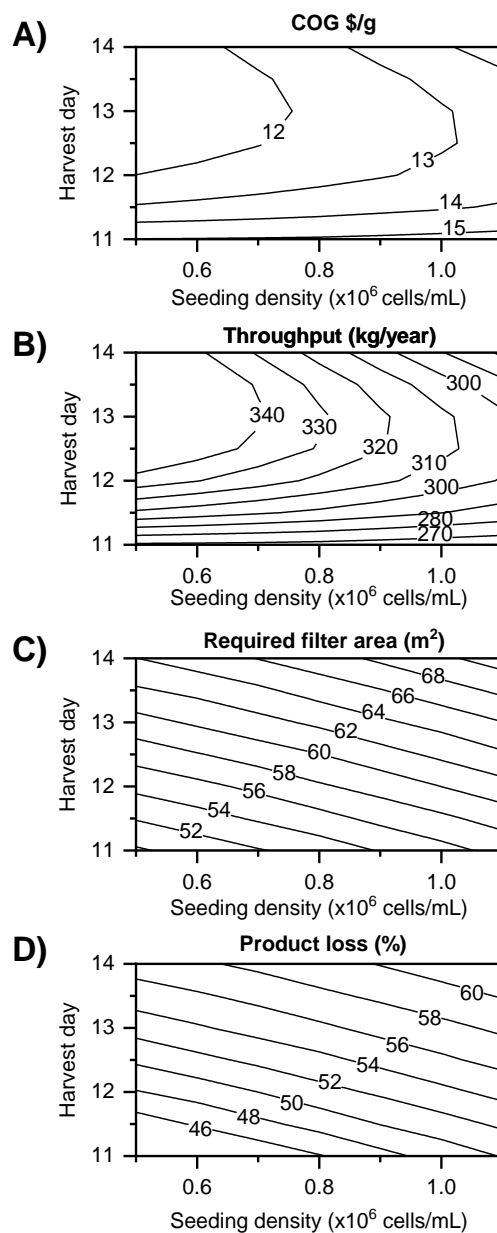


Figure 5.11 Contour plots for the recovery operation for a process with a high shear, showing the impact of seeding density and harvest day on A) COG_{REC} \$/g; B) Filter requirements (m²); C) Product loss (%) and D) Throughput (kg/year). The process is based on Merck Millipore filter holder with max holder capacity of 33m², Culturefuge 300 with flowrate of 6,000L/h and solids holding space of 20L and a bioreactor size of 10,000L.

5.3.3.2 Uncertainty analysis for the depth filtration operation

The goal of this section is to develop a risk-based approach to bioprocess decision making under manufacturing uncertainty linked to the variability in the process inputs – target seeding density and time of harvest. For this purpose, the seeding density and the harvest timing were set as stochastic inputs and the outputs from the model were presented as probability distributions.

As seen in the previous section, variability in the [solids] and centrate filterability can impact on facility fit. To better understand the impact of each performance metric on the process, two scenarios were investigated - one with no facility fit limitations due to the centrifugation step (using larger centrifuge, e.g. Culturefuge 300, **Table 5.1**) and one where the centrifugation step was limiting (using smaller centrifuge, e.g. Culturefuge 200, **Table 5.1**).

Four metrics were investigated: 1) target throughput of min 550 kg/yr; 2) COG_{REC} of max 7 \$/g; 3) max product loss due to centrifugation of 10% and 2) max product loss due to depth filtration of 10%. **Figure 5.12** depicts the two scenarios – using the smaller centrifuge size (harvest day 13.5 as a base case) and using a larger one with a bigger solids holding capacity. The throughput and COG_{REC}/g were set as a hard targets (solid line) and the rest of the metrics were set as soft metrics (dashed lines). The maximum allowable risk in both scenarios for all metrics was set at 10% (horizontal red dashed line in **Figure 5.12**).

As it can be seen in **Figure 5.12a** when harvested on day 13.5, the risk of not reaching the target throughput exceeds 10%. This is due to the increased loss in the depth filtration operation. One way to debottleneck the process would be to harvest earlier (day 13) where the throughput is maximized. Bringing the harvest earlier than day 13 leads to lower throughput due to lower titre and higher [solids]. **Figure 5.12b** shows that a larger centrifuge may enable a later harvest (day 13.5). However, this solution violates the risk of exceeding the target $\text{COG}_{\text{REC}}/\text{g}$. Therefore, for this scenario harvesting a half a day earlier seems to better satisfy the two target metrics – min throughput and max $\text{COG}_{\text{REC}}/\text{g}$.

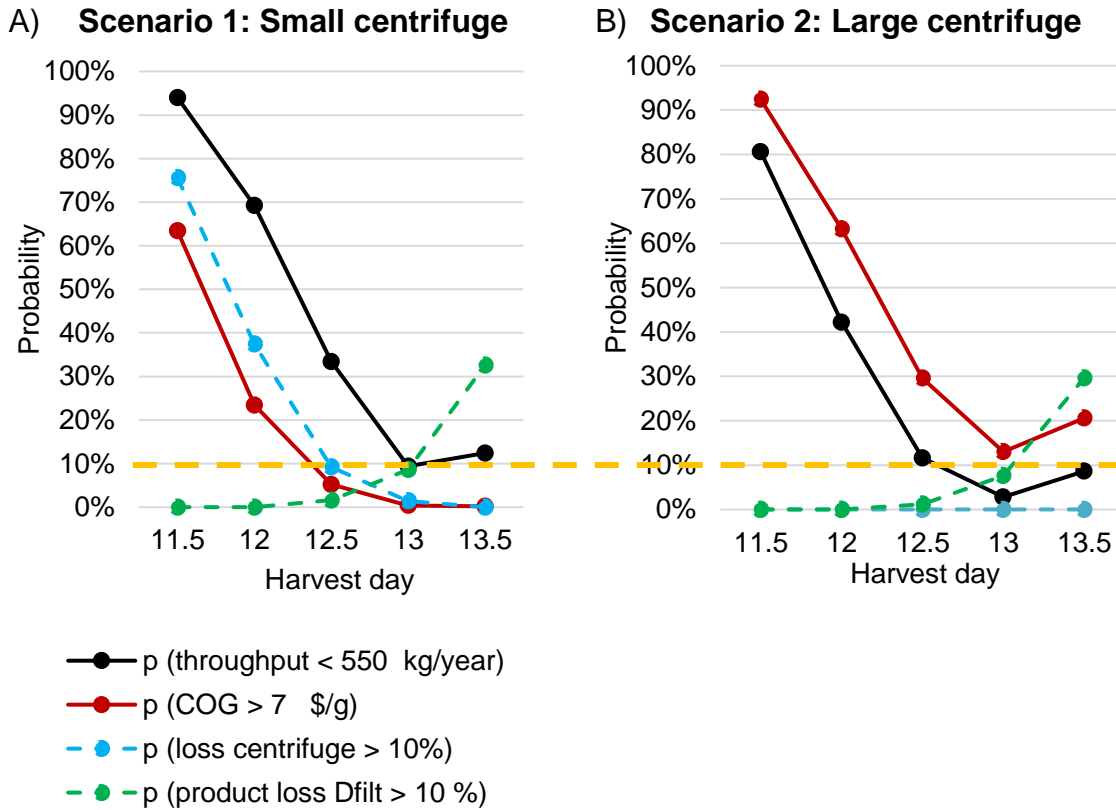


Figure 5.12 Risk analysis showing the impact of seeding density and harvest day variation for different target harvest days on the probability of failing to meet target metrics - minimum throughput of 550 kg/year (black line —), maximum COG_{REC} of 7 \$/g (red line —), maximum loss due to the centrifugation step of more than 10% (blue dashed line - -), maximum product loss due to the secondary depth filtration of 10% (green dashed line - -) for a process using A) a small centrifuge with 6.7 L solids holding space and B) a large centrifuge with 20 L solids holding space. The orange dashed line (- -) shows the maximum acceptable level of risk for the target throughput and COG_{REC} .

5.4 Conclusions

The recovery economics model presented in this chapter allowed the identification of key cost drivers for the recovery operations across different manufacturing scenarios. As the scale increased from a 1000L bioreactor (100kg/year demand and 9g/L titre) to 2 x13,500L bioreactor (900kg/year demand and 3g/L titre) the main cost driver switched from the indirect costs (75% of the recovery COG/g) to the direct costs (52% of the recovery COG/g). The predictive correlations derived in **Chapter 3** and incorporated in the bioprocess model shed light onto how the process conditions impacted on facility design. This understanding will aid the decision making in early process development work, when pH and temperature conditions are often set. The predictive correlations from **Chapter 4** enabled better understanding about the impact of shear and variability of the seeding density on process design and facility fit. The predictive correlations were applied to define a window of operation for a fixed process that needed to meet min COG_{REC} and facility fit constraints. The stochastic aspect of the model enabled the identification of optimum conditions for the process using a risk-based approach.

Chapter 6

6 Enhanced harvest performance predictability through advanced multivariate data analysis of mammalian cell culture particle size distribution

6.1 Introduction

Chapters 4 and **5** demonstrated the importance of [solids] and cell culture viability (levels of cell lysis) on process performance. **Chapter 4** showed that high cell culture viability and lysis due to centrifugation shear for high viability cell cultures can increase the propensity for antibody reduction, while **Chapter 5** revealed the impact of [solids] and shear on process economics and facility fit. The aim of this chapter is to leverage routinely used cell counting data to develop reliable and rapid tools for evaluating cell lysis and [solids]. The speed and reliability of the tools developed here enables their application for high throughput small scale experimentation platforms such as the ambr, which are typically deployed for early process development.

Cell culture viability can be defined as the ratio of dead-to-live cells, where dead cells are considered cells that have lost plasma membrane integrity or have broken into

discrete fragments (Galluzzi et al., 2015). Typically, cell culture viability can be measured directly – through counting live and dead cells, for instance, using a live/dead dye – or indirectly through other correlates indicating membrane disintegration (cell lysis) such as the release of intracellular enzymes – for instance, the LDH (dead-to-live cells' intracellular components release ratio).

The trypan blue staining method is a gold standard for routine viability measurements; it uses the permeability of the dead cells to the dye in order to differentiate between viable and non-viable cells. Nowadays cell counts using this method are often automated, performed with automated cell counters (Cedex, Innovatis, Bielefeld, Germany and Vi-Cell™ XR - described in **Section 2.1.3.1**), which provide cell counts, viability and particle size distribution data (Li et al., 2010). This method relies on the ability of the instrument to accurately count the number of dead and live cells based on the images. However, dead cells may have completely disintegrated or shrunk and not be accounted for.

As mentioned earlier cell culture viability can also be measured through the level of cell lysis and the concomitant release of LDH. LDH is an ubiquitous intracellular enzyme found in nearly all mammalian cells. Its release in the cell culture media indicates that the integrity of the cell membrane has been compromised (Riss et al., 2004). Although absolute LDH can be measured with high throughput methods, it suffers from being sensitive to media composition and culture operating conditions (Hiebl et al., 2017; Méry et al., 2017). Therefore, it is common to measure LDH release based on the ratio of the sample's LDH relative to the total LDH released upon chemical lysis (Cummings and Schnellmann, 2004). The need for triplicates,

additional cell lysing step and time to read the samples increases the experimental workload for the measurement (**Section 2.1.3.5**).

There are other indirect indicators of cell culture viability that are not routinely used. For instance, information about cell culture viability can be deduced from the appearance of cell debris. Lebeau *et al.* (2019) proposed a method for measuring cell viability through staining the cell debris with trypan blue and measuring the turbidity of the sample. However, this method is laborious and hence not suitable for high throughput operations. It is important to note that while this method uses the overall amount of cell debris to measure cell viability, to date there are no studies that leverage the entire cell culture particle size distribution (PSD) for this purpose.

[Solids] measurements are usually performed using packed cell volume (PCV) tubes (TTP®, Trasadingen, Switzerland). As described in **Section 2.1.3.4** the measurement is carried out in triplicates and each sample is 40 μ L. Other sources suggest even higher volumes of 100 μ L (Stettler *et al.*, 2006). The sample volume, the manual nature of the measurement and the need for triplicates makes it cumbersome for high throughput experimentation such as the ambr platform.

The challenges with the current [solids] and LDH-based cell lysis measurement techniques can explain why these are often omitted during early process development. For instance, for the ambr platform, the analysis is usually limited to cell counts via automated cell counters and high throughput metabolites analytics, while other in process samples (for product quality) are frozen for later analysis.

The work presented in this chapter aims to address these challenges through developing a rapid and simplified method for measuring [solids] and LDH suitable

for the high number of experiments at the development stage. For this purpose, a novel approach was developed to predict the [solids] and LDH release in the cell culture harvest. The methodology used the routinely collected PSD data from the automated cell counter Vi-Cell XR and MVDA techniques to build the predictive models. **Section 6.3.1** investigated the relationship between LDH release and viability and the impact of shear on the cell counts as outputted from the Vi-Cell XR. The PSD analysis in **Section 6.3.1** revealed that there was a change in PSD as cell culture viability dropped towards the end of the run. In **Section 6.3.3** a novel method was applied that successfully leveraged the PSD using PLS models to predict the LDH in the cell culture, while in **Section 6.3.4** a similar approach was applied to predict the [solids]. The rapid and resource-efficient nature of the novel tools developed in this chapter makes them perfectly suited to be used with the scale-down upstream-recovery framework described earlier. These tools will facilitate process knowledge at early development stages whilst reducing the labour, sample and material requirements.

6.2 Methodology

6.2.1 Case study set up

The data used in the study was generated from five different ambr runs, four 5L bench scale bioreactor runs and two 500L pilot scale runs described in **Table 6.1**.

Table 6.1 Summary of experimental data used to build the PLS models for LDH release and [solids]

| Dataset | Experiment # | Project ID | Vessel ID | Shear | Harvest Day | Seeding density**** | Source |
|--------------------------------------|---------------|--------------|----------------|---------------|---------------|---------------------|----------------|
| LDH release with PSD analysis | | | | | | | |
| Calibration | L1 to L12 | Project Null | Bench BR 1 | No, Low, High | 8,9,10,12 | Mid point | Chapter 4 |
| | L13 to L24 | | Bench BR 2 | No, Low, High | 8,9,10,12 | Mid point | Chapter 4 |
| | L25 to L45 | Project A | AMBR 3 | No | 11, 13, 14 | Low, Mid, High | Chapter 4 |
| | L46 to L63 | | AMBR 4 | No | 10 and 12 | Low, Mid, High | Chapter 4 |
| Validation | L64 | Project B | Bench BR 3 | No | 13 | Mid point | PD* |
| | L65 to L67 | | Pilot BR 1 | No | 12 and 13 | Mid point | PD |
| | L68 to L72 | Project C | Bench BR 4 | No, Low, High | 12 | Mid point | PD |
| | L73 to L78 | | Pilot BR 2 | No, Low, High | 11 and 12 | Mid point | PD |
| Solids concentration | | | | | | | |
| Calibration | S1 to S19 | Project A | AMBR 3 | N/A | 11, 13, 14 | Low, Mid, High | Chapter 4 |
| | S20 to S68 | | AMBR 2 | N/A | 8, 13 and 15 | Low, Mid, High | Chapter 3 |
| | S69 to S87 | Project D | AMBR 5** | N/A | 12, 13 and 14 | Low, Mid, High | Historic |
| | S88 to S107 | | AMBR 6**** | N/A | 13, 14 and 15 | Low, Mid, High | Historic |
| Validation | S108 to S1114 | Project A | Bench BR 2 & 3 | N/A | 11, 12 and 13 | Mid point | Chapter 4 & PD |
| | S115 to S128 | Project D | AMBR 2 | N/A | 8, 13 and 15 | Low, Mid, High | Chapter 3 |

*PD – process development run; ** DoE centre composite design (face centred): target T^oC of 35.5^oC, shift on day 6 from 35.5^oC to 34.5 or to 33.5^oC; target pH of 7.0, pH shift on day 5 from 7.0 to 6.8 or 7.2; harvest day 13, 14 and 15; target seeding density of 0.5, 0.75 and 1 x 10⁶ cells/mL; *** screening DoE: target T^oC of 35.5^oC and shift on day 4 from 35.5^oC to 33.5^oC; target pH of pH 6.8, 7 and 7.2; harvest day 13, 14 and 15; target seeding density of 0.5, 0.75 and 1 x 10⁶ cells/mL; **** Mid point refers to processes where there was no specific target seeding density.

6.2.2 Particle size analysis

Each cell count measurement on the Vi-Cell XR generates a CSV file, containing the number of particles sized ~6 μ m to 50 μ m split into 140 discrete particle size bins. A program was built in Matlab® (The MathWorks, Inc., Natick, MA) to import and pre-treat the raw PSD data as described in **Figure 6.1** - normalized and/or binned at different intervals. The PSD and metadata were used to build predictions for [solids] and LDH release using PLS models. The approach for building and selecting the optimum PLS was described in **Section 2.3.4**.

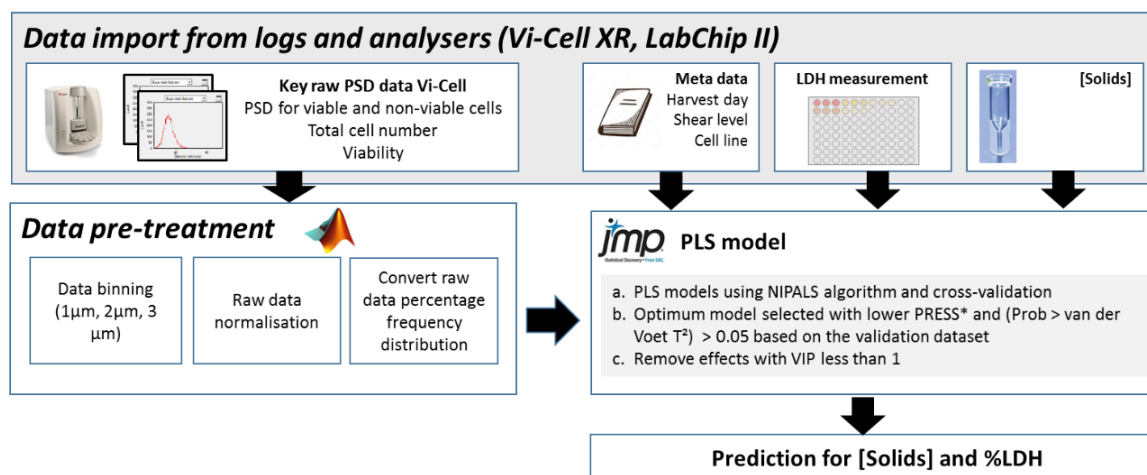


Figure 6.1 Workflow for analysing the PSD data outputted from Vi-Cell XR. The raw data is extracted from the Vi-Cell XR in the form of CSV files and an algorithm in Matlab was used to pre-treat and structure the data for further analysis. PLS models were built for the pre-treated data using Jmp.

As part of the data pre-treatment the PSD data was normalised to a frequency distribution as follows:

$$P_s^{particle} = \frac{N_s^{particle}}{\sum_{s=1}^n N_s^{particle}} \quad (6.1)$$

where $P_s^{particle}$ is percentage P of particles of channel s (a channel or bin is defined by upper and lower bound for a particle size range) and $N_s^{particle}$ is the number of particles N in channel s and n is the total number of channels.

6.3 Results and discussion

As mentioned in **Section 6.1** there are limitations with the current techniques for measuring cell death. This section first explores these limitations for measuring cell lysis occurring either as a result of natural decline in cell health towards the end of cell culture or due to centrifugation shear. Then the PSD for the cells as outputted from the Vi-Cell XR is investigated for different days of cell culture and linked to cell health. PLS models were built leveraging the PSD data to predict the levels of LDH release and the cell culture [solids].

6.3.1 Relationship between LDH release and cell culture viability

The relationship between LDH release and cell culture viability as outputted from the Vi-Cell XR was investigated for fresh cell culture harvests using historical data from different bioreactor runs (**Table 6.1**). This dataset featured a wide distribution of cell culture viabilities ($\mu_{viability} = 79\%$ and $\sigma_{viability} = 17\%$) and LDH release measurements ($\mu_{R^{LDH}} = 44\%$ and $\sigma_{R^{LDH}} = 26\%$). The LDH release was plotted against the Vi-Cell cell culture viability (**Figure 6.2**). Below 60% viability, the LDH release was close to 100%, which indicated that cells had lost membrane integrity. As a result, there was no significant difference in the intracellular and extracellular

LDH concentration. Therefore, linear regression analysis was performed only for the samples above 60% viability (as outputted from the Vi-Cell), and a weak correlation ($R^2_{adj.} = 0.66$) was observed between the LDH release and the Vi-Cell viability measurements. The weak correlation indicated that it may not be possible to use the Vi-Cell viability measurements to gauge the levels of LDH release. This may be due to the fact that the cell membrane was sufficiently compromised to release the intracellular contents despite cells not being stained by the trypan blue. It is also possible that an overestimation of cell culture viability using the trypan blue method (Vi-Cell) was observed attributed to the fact that some dead cells had fully disintegrated and were not counted (Weisenthal et al., 1983) or as a result of trypan blue dye toxicity leading to the formation of diffuse objects, which would not be detected and counted as cells (Chan et al., 2020). It is important to note that the LDH can be degraded over time and also lead to overestimation of the cell culture viability (Riss et al., 2004), however, here the viability using the LDH method was lower than for the Vi-cell measurements.

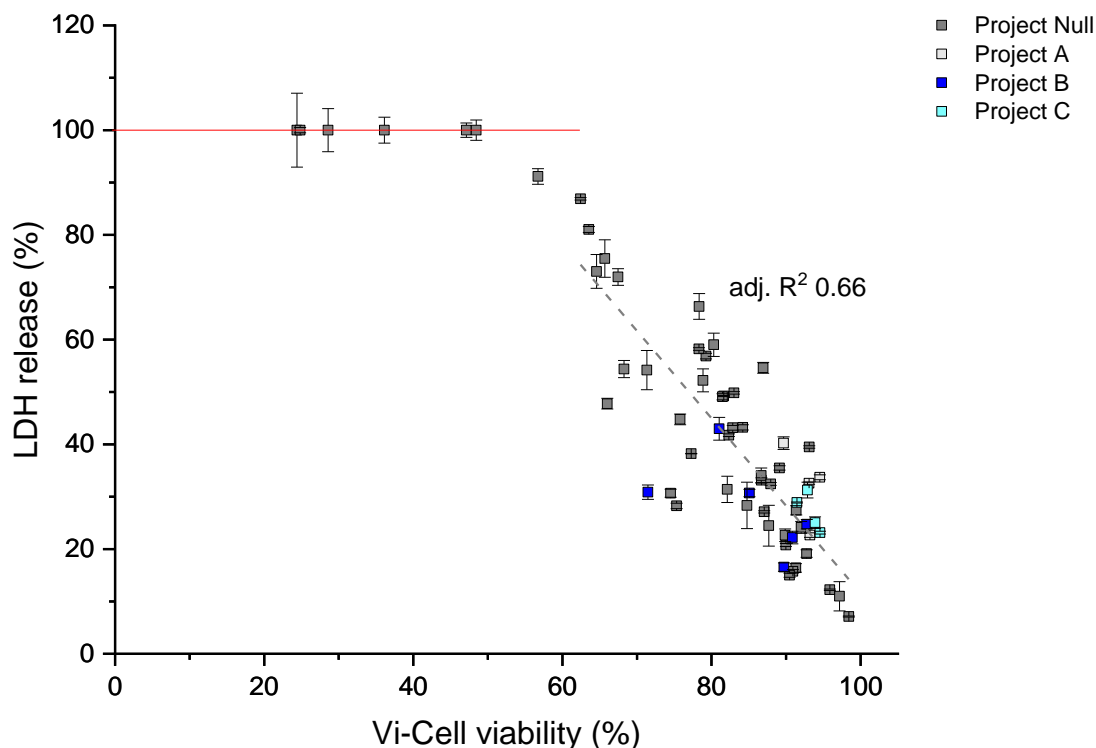


Figure 6.2 Percentage LDH release vs Vi-Cell XR viability measurements for the fresh harvest (no shear) described in **Table 6.1** for four different projects: Project null (GS-CHO Null) in dark grey (■), Project A in light grey (◻), Project B in dark blue (■) and Project C in light blue (◻). The red line (—) indicates 100% LDH release. All samples above 95% have been adjusted to 100%. The points below 100% LDH and 60% viability (as outputted from the Vi-Cell) release were used to plot the grey line of best fit (---).

As mentioned earlier both LDH and trypan blue exclusion methods are used to measure cell lysis or viability and as such can be applied to evaluate the level of cell damage due to the centrifugation operation (Joseph *et al.*, 2016; Tait *et al.*, 2013; Westoby *et al.*, 2011). However, to date there has been no detailed investigation of the impact of shear on the viability measurement as outputted from the Vi-Cell XR or a comparison between the LDH and trypan blue as methods for evaluating cell damage due to shear.

The CSD described in **Chapter 4** was used to apply shear to various cell culture samples. In **Figure 6.3** the cell culture viability (Vi-Cell) was measured for samples at no shear, low shear (21mL/min) and high shear (41mL/min). For all starting cell culture material the viability was relatively high (above 80%) and the total cell count was in the range of 25 to 40 million cells/mL (**Figure 6.3a**).

The analysis revealed that the shear impacted on the ability of the trypan blue method to accurately detect the total amount of cells (**Figure 6.3a**). When shear was applied, it led to apparent increase or decrease of the total number of cells. The apparent increase in total cell number is likely due to the increase in cellular debris while the decrease in particles can be attributed to the formation of cell clumps or aggregates (**Figure 6.3b**). The change in apparent total cell number questions the reliability of the viability measurements obtained for sheared samples using the trypan blue exclusion method since the viability is calculated as a ratio of viable to total number of cells.

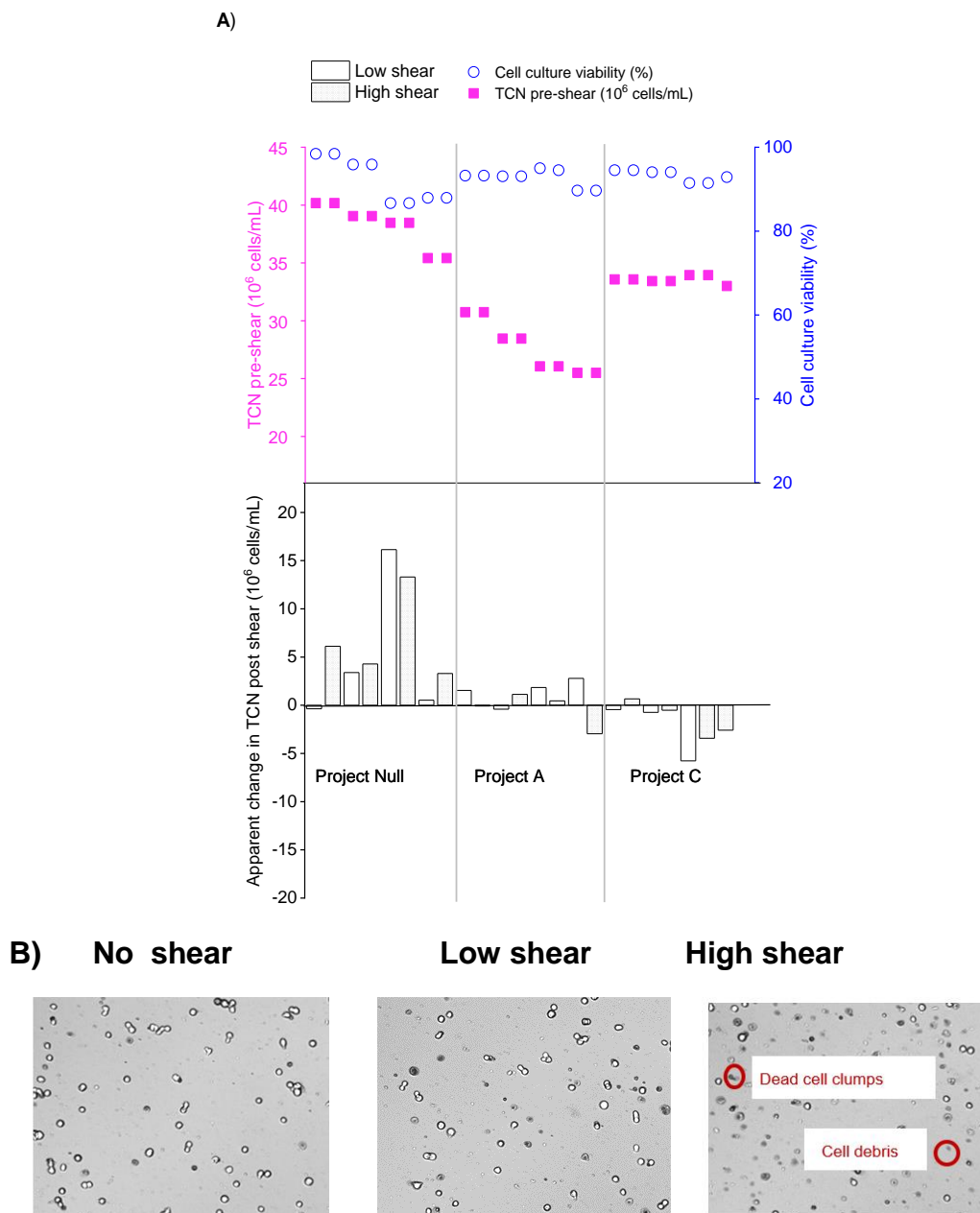


Figure 6.3 Impact of shear on (A) apparent change in total cell number (TCN) as outputted from the Vi-Cell XR for various mammalian cell culture harvests for three projects and (B) the appearance of cell debris and dead cells clumps for high shear samples compared to no and low shear. Harvests from four different bench scale runs were collected on different days of cell culture: day 8, 10, 12 and 14 and subsequently subjected to low and high shear in the capillary shear device. The apparent total cell number change was calculated as a difference between the total cell number before and after shear.

It is important to note that the automated cell counter was optimised for routine use in the lab and the parameters were not adapted for each individual run, e.g. tuning the instrument's settings for decluttering of live cells or altering the criteria for counting a particle as cell such as size and circularity. Adjusting these parameters would have introduced additional variability in the measurements and would have not suited the high throughput experimentation approach sought here...

6.3.2 Investigating the relationship between Vi-Cell XR PSD data and cells viability

As discussed in the previous section, LDH is suitable for measuring damage to cells' membrane post shear. However, it is cumbersome to determine percentage LDH release on a daily basis for high throughput experimentation. For instance, for each measurement, a sample needs to be chemically lysed, which requires a 30 min incubation period. Therefore, it was important to find more efficient methods for estimating the level of LDH release such as the change in PSD.

For the cell culture experiments performed in the previous chapters a change in particle size distribution was observed as cell culture viability declined. To better understand how the PSD changes with the drop in viability, the PSD data from ambr4 **Chapter 4** was analysed and compared between different harvest days.

In **Figure 6.4** the averaged PSD across all bioreactor experiments can be found for different harvest days, described by the solid line with the upper and lower dotted lines indicating the standard deviation for the measurements. It was revealed that, the PSD remains narrow during the first few days of cell culture, with one single peak observed around 15 μm . However, during the later days of cell culture, and

especially during the stationary and death phases (day 12), a peak split was observed and there was significant increase in the standard deviation (**Figure 6.4d**). Further investigation into the last harvest day, with the biggest standard deviation, reveals that the particle size distribution changed with cell culture viability. To simplify the analysis, the samples from day 12 were grouped by cell culture viability (**Figure 6.4e**). For instance, for viability above 85%, the PSD was shifted to the right with a pronounced peak observed at about 20 μ m. For viability between 72% and 82%, there was one broad peak between 10 and 20 μ m. For the lower range between 62% and 67%, there was a peak to the left at around 10 μ m, which became even more pronounced as the viability dropped down to 24% to 36%. This analysis suggests that the PSD changes with viability. The following sections investigate whether this change in PSD can be further leveraged to gain insights into the harvest properties, and in particular the level of % LDH release and [solids].

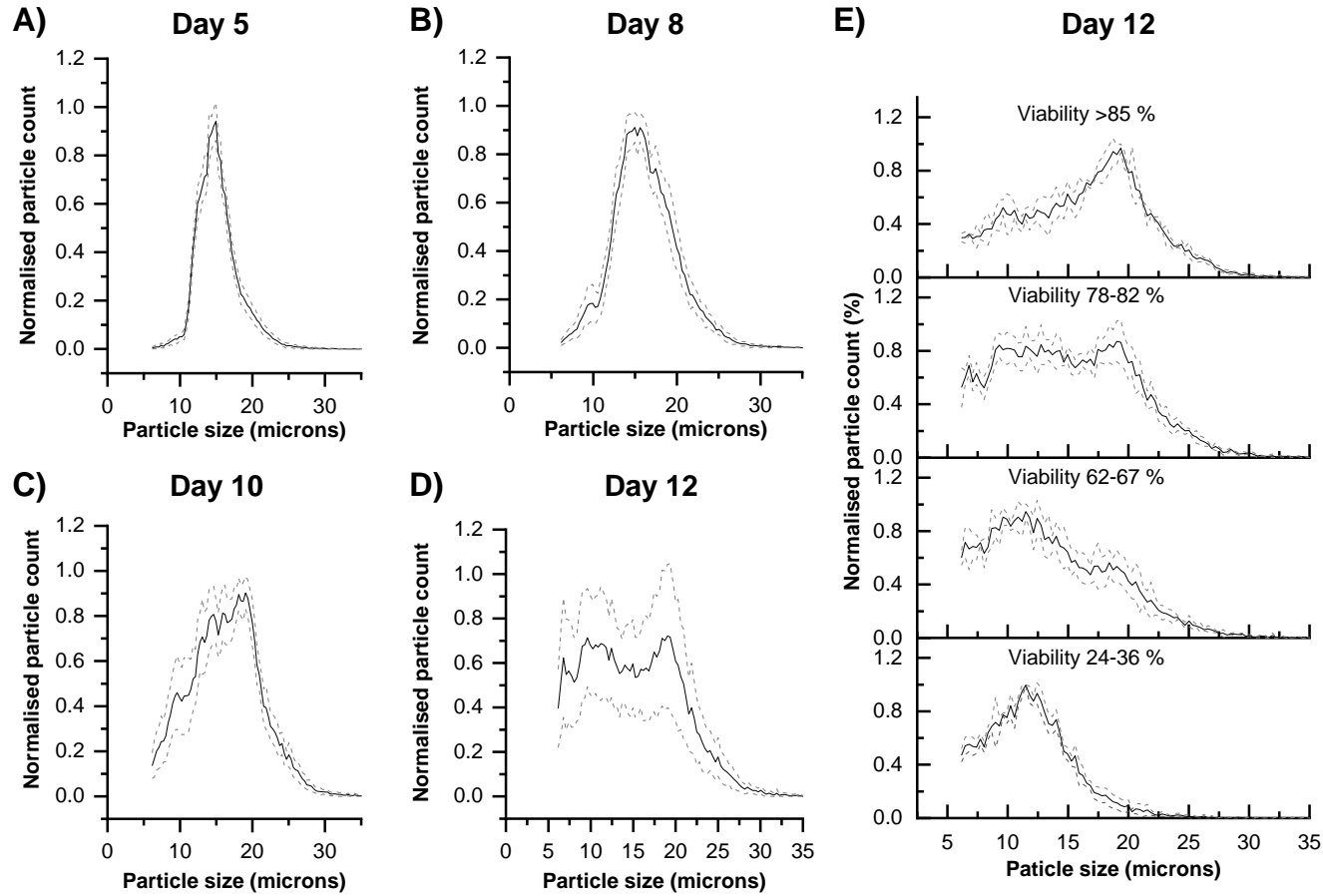


Figure 6.4 Particle size data distribution for ambr4 experiments as outputted from the Vi-Cell for 24 bioreactor runs with different target seeding densities and harvest days. The solid line depicts the mean of the PSD, the dotted lines depict the standard deviation for A) Day 5 (n=24), B) Day 8 (n=24), C) Day 10 (n=24). D) Day 12 (n=17) and E) Day 12 for various viability ranges (>85% viability and n=3; 72% to 82% and n=6; 62% to 67% and n=4; 24% to 36% and n=3)

6.3.3 Leveraging PSD data to predict LDH release using PLS techniques

The previous section demonstrated that the particle size distribution changes with cell culture viability. The goal of this section was to build PLS models using the PSD data to predict the levels of LDH release for various cell cultures from different projects and conditions. For the analysis the data was smoothed and then different inputs for the model were tested – for instance, PSD of the total number of cells and of the viable cells. Based on this preliminary analysis, it was decided to bin the data at 1 μ m and use the frequency PSD for the viable cells.

Figure 6.5a revealed that the PLS model could accurately predict the % LDH release for an unknown test sample ($R^2_{adj.} = 0.90$ for a parity plot, which can be found in **Appendix, Figure 6.1-A**). The PLS model was built using the NIPALS algorithm and internal cross validation (k-fold = 7). The R^2Y for the model was 82% showing the percentage variance of Y (predicted variable) that could be explained by the model and the R^2X was 96% showing the percentage of variance in X (the predictor) that can be explained by the model.

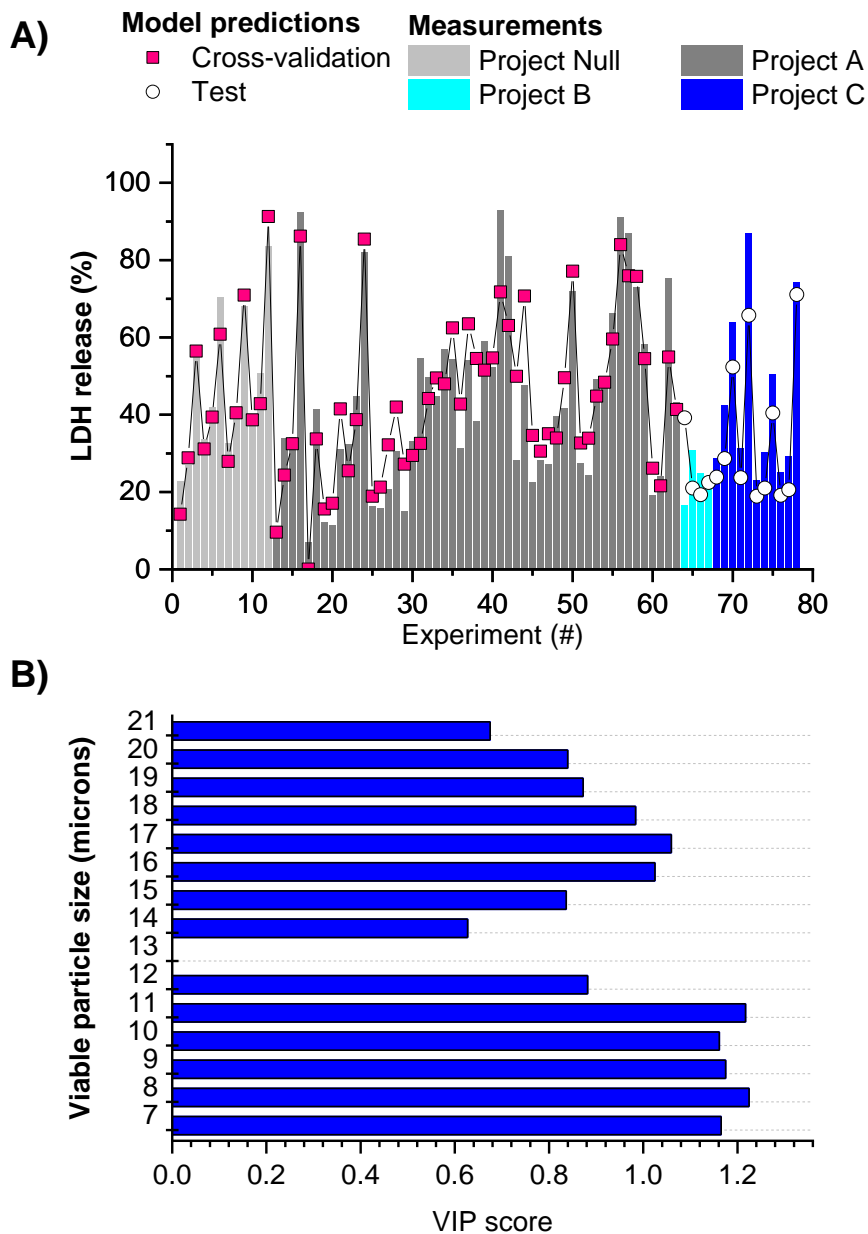


Figure 6.5 PLS model predicting LDH release using PSD data for the viable cells as outputted from the Vi-Cell. In A) the actual LDH release is shown by the bars, the filled squares depict the predicted LDH release for the dataset used to calibrate the model, while the empty circles show the predicted percentage solids concentration for the external validation (test) dataset. The different colour bars refer to different projects - project null (■); project A (■); project B (■) and project C (■), $R^2Y = 83\%$ and $R^2X = 96\%$ and the R^2 for the test (external validation dataset) is 90%.

The VIP plot in **Figure 6.5b** shows the predictors that were used in the PLS model – mainly particle sizes below 21 μm . The remaining PSD data above 21 μm was removed to improve the model – the VIP score was used as a criteria for the model “pruning” (details can be found in **Appendix, Table 6.1** and **Table 6.2**). The range of predictor variables (PSD size data) used in the PLS model is in line with the expected cell size - up to 21 μm . The highest VIP is for the lower end of the PSD, which could be explained by increase in smaller particles for the lower viability cell cultures that was observed earlier.

6.3.4 Levering PSD data to predict [solids] using PLS techniques

As demonstrated in **Chapter 4** and **5** the levels of [solids] in the cell culture harvest is a key parameter for the harvest operation as it impacts the centrifugation yield. The approach that was developed to leverage the PSD data to predict the levels of LDH release was also applied to predict the levels of [solids]. A total of 117 measurements for cell culture [solids] and Vi-Cell cell count data (including PSD, total and viable cell number and cell culture viability) were used for the study; the data was generated from ambr and bench scale bioreactor runs (as described in **Table 6.1**). The conditions varied largely between the different projects and that led to cell cultures with a wide range of viabilities ($\mu_{viability} = 85\%$ and $\sigma_{viability} = 14\%$) and densities ($\mu_{TCN} = 30$ million cells/mL and $\sigma_{TCN} = 10$ million cells/mL). The particle size distribution measurements were analysed using the same Matlab program as described for the LDH analysis. The viability, the total and viable cell number together with the frequency PSD data (binned at 1 μm) for the viable number of cells were used to build a PLS model that predicts the [solids] in the harvest. The

calibration data set used to build the model consists of 4 independent ambr runs, while the validation dataset consists of a bench scale run and a separate culture station from one of the ambr runs. A total of 6 factors (latent variables) were used to build the model.

Figure 6.6a revealed that the model provided a good prediction for the [solids] with $R^2Y = 84\%$ and $R^2=0.86$ for actual vs predicted (parity plot). The VIP plot in **Figure 6.6b** revealed that the most important predictors in the model are the total and viable cell counts and the particle size around $13 \mu\text{m}$, which is very close the actual average CHO cells' size.

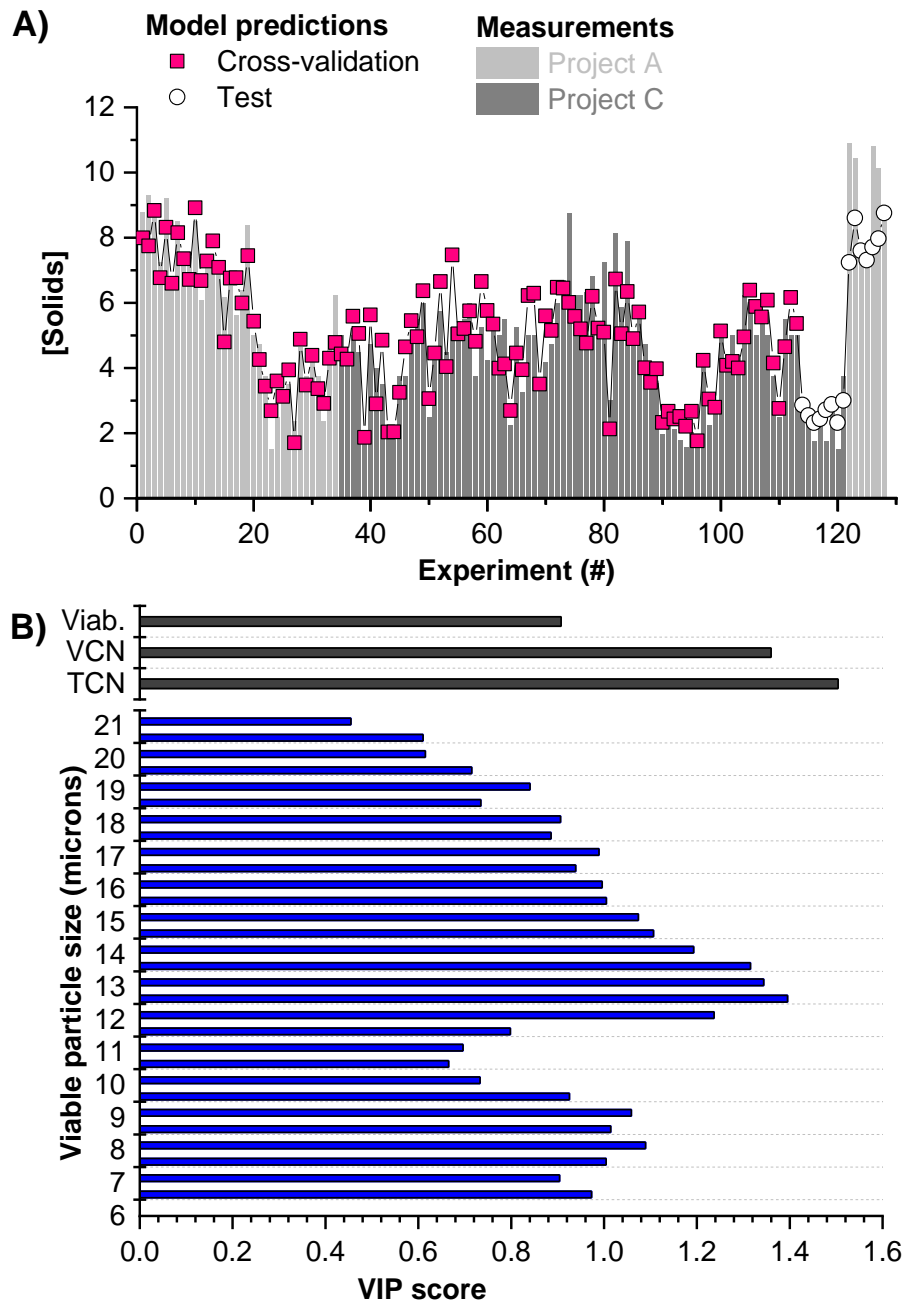


Figure 6.6 PLS model for [solids] with A) actual versus predicted [solids] and B) VIP plot with the predictors used in the model. In A) the actual [solids] are shown by bars, the filled squares depict the predicted solids concentration for the dataset used to calibrate the model, while the empty circles show the predicted percentage solids concentration for the validation dataset. The different colour bars refer to different projects (A – light grey and C – dark grey), $R^2Y = 81\%$ and $R^2X = 86\%$. TCN-total cell number (million cells/mL), VCN – Viable cell number (million cells/mL), viab. – Viability.

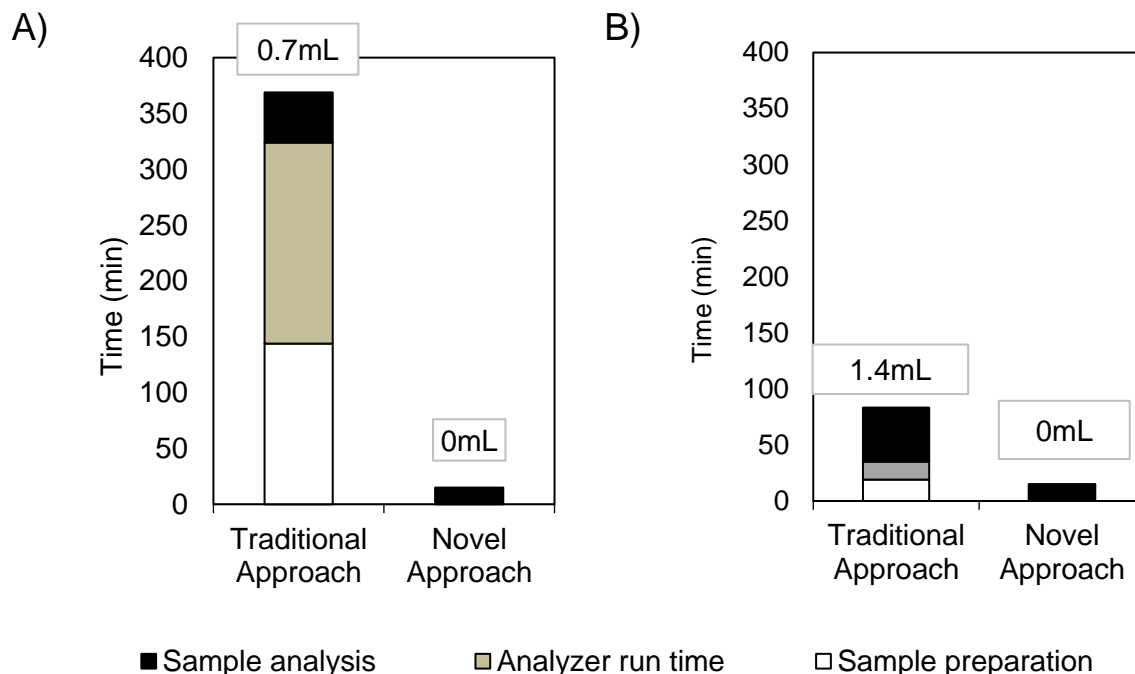


Figure 6.7 Comparison in time and volume daily requirement for ambr15 with 48 vessels for A) LDH release measurements using manual sampling and a colorimetric assay vs the novel PLS –based estimation and B) [Solids] measurements using manual sampling vs the novel PLS –based estimation. The assumptions for the calculations can be found in **Appendix (Table 6.3 A)**

6.3.5 Volume and time savings

Figure 6.7 summarises the savings for the daily analysis of the 48 vessels of ambr15 in terms of time applying the novel workflow vs traditional sampling and analytics techniques. The figure highlights that savings of over 6 hours for the LDH release measurement and over an hour for the [solids] analysis can be achieved when leveraging the PSD data instead of the traditional offline analytics. In addition, the volume savings per vessel per run were determined to be over 2 ml (1.4 ml for the [solids] and 0.7 ml for the LDH measurement), which is significant considering the working volume of each ambr vessel (15ml). Hence, the proposed approach using

the PSD data to predict these metrics can be particularly valuable during high throughput experiments.

6.4 Conclusions

The current chapter described a novel approach that leveraged routinely collected PSD data from an automated cell counter and PLS models to accurately predict cell culture solids concentration and cell lysis (% LDH release) for the harvest operation. This avoids the need for offline analytics for such measurements. Applying the novel approach it was possible to predict the % LDH release and [solids] for a test dataset with R^2 adj. of 0.90 and 0.86 respectively (based on actual vs predicted parity plots). This novel workflow used a Matlab program to import, pre-treat and restructure the data before importing it into Jmp to generate the predictions, thus reducing significantly the analytics burden for measuring the % LDH and [solids]. The chapter highlights the volume and time savings by leveraging the PSD data rather than using offline analytics, with the analytics time reducing from more than 6 hours using the conventional approach to a few minutes with the proposed workflow. The speed and resource-efficiency of this tool makes it best suited for early high throughput experimentation. This will enable gaining understanding about cell lysis and [solids] in the cell culture earlier in the development cycle. Adopting such an approach will facilitate earlier identification of challenging harvests that can exceed the centrifuge capacity and hence inform process modifications that lead to more robust processes and improved facility fit.

Chapter 7

7 Conclusions and future work

7.1 Introduction

The work presented in this thesis provided an integrated framework for mapping the upstream – recovery sequence. A number of novel tools were developed to support the framework creation: 1) an experimental platform linking the ambr15 to a CSD – based centrifugation mimic; 2) a [cholesterol]-based correlation for predicting a centrate’s filterability; 3) MVDA correlations for the upstream and recovery process; 4) a bioprocess economics model for the recovery operations using stochastic inputs and predictive correlations based on experimental data; 5) Matlab programs for big data import and pre-treatment to facilitate PLS models development; 6) a novel approach for leveraging underutilised PSD data for rapid prediction of [solids] and cell lysis. A summary of the key results from the thesis are presented below. The thesis chapters reflect core work established using the scale-down mimics for cell culture and recovery, initially separately and then integrating them to form the upstream-recovery framework.

7.2 Key conclusions

In **Chapter 3**, scale-down experiments using the ambr system were carried out to establish the link between upstream conditions and the input to recovery operations. DoE studies were performed in the ambr1 and ambr2 showing that seeding density, temperature, pH and harvest day impact on upstream productivity as well as on key

recovery inputs such as [solids] and turbidity. Moreover, the analysis revealed important trade-offs whereby parameters that maximised titre (target pH of 7 and high seeding density and no temperature shift) also led to undesirable high [solids] and turbidity. The results from the study showed that increasing the seeding density can be used to lower the negative impact of suboptimal pH (lower or higher than 7) or suboptimal temperature (lower than 35.5°C) on the upstream productivity.

In **Chapter 4**, the utility of the scale-down centrifugation mimic and centrate filterability mimic were initially established before integrating the operations to form the integrated framework. Regarding the utility of the scale-down centrifugation mimic, it was successfully applied to study the impact of centrifugation shear on monomer content and HCP levels for different cell culture viabilities and mAbs. The results revealed that applying high shear in the CSD for high viability cell cultures (harvest day 10 and 83% viability) led to the lowest levels of monomer content for both mAbs (29% for IgG1 k and 15% for IgG1 λ). For the HCP content, the mAb type had a higher impact on HCP levels than the shear and cell culture viability. To further extend the scope of the upstream-recovery framework, a correlate for filterability post centrifugation was developed based on [cholesterol]. This novel approach enabled linking the ambr and the centrifugation mimic to the depth filtration performance without the need for scaling down the depth filtration operation. A DoE study using the novel integrated experimental platform consisting of the ambr coupled with the centrifugation mimic was used to derive predictive correlations linking the seeding density, harvest day and levels of centrifugation shear to the levels of monomer content and [cholesterol] as a predictor of filterability. The predictive correlations laid

the foundation for the work in the next chapter, which integrated the cause-and-effect correlations within an overall bioprocess model.

In **Chapter 5**, a novel economics model for the recovery operation was successfully built identifying the main cost drivers for the varying titre and demand scenarios. The economics model incorporated the predictive correlations for titre, [solids] and [cholesterol] and determined the mass throughput and the cost of goods. The model was used to define a window of operation for the process to meet targets for titre, product loss, throughput, filtration area, [solids] and COG_{REC} . These insights were then used to devise mitigation strategies against failing to meet target throughput and COG_{REC} through the reduction in the cell culture duration.

Chapter 6 addressed the challenges of measuring [solids] and LDH release for high throughput small scale experiments, where the required volume and manual operation can make it impossible to perform the measurements using traditional offline analytics. The workflow developed for predicting the [solids] and LDH release applied MVDA techniques to routinely collected PSD data to derive these. This led to significant savings in time and resources for measuring these metrics – from more than 6 hours/day for ambr15 with 48 vessels to under an hour with the novel approach. This approach required devising programs to handle big data and transform and pre-treat it prior to using it for correlation generation. This can help to identify challenging harvests early on in development and improve facility fit as a result.

The holistic approach to upstream-recovery optimization described in this thesis has the potential to accelerate process development workflow and generate an optimized process at small scale.

7.3 Limitations of the work

The thesis presented a novel approach to mapping the upstream-recovery sequence and linking it to process economics. The work was limited by the equipment that was available to use, and therefore it did not explore some novel industry relevant approaches such as continuous discharge centrifuges, which can cope with higher solids concentration or centrifuges with hydrohermetic design that would exert lower levels of shear (Richardson and Walker, 2018; Roush and Lu, 2008). The ambr4 cell culture experiment in Chapter 4 yielded unexpected lower cell growth, while there was limited information in Chapter 3 for ambr2 due to a faulty instrument. As a consequence there was a limited number of upstream experiments to develop the correlations. The correlations were needed to build the bioprocess economics model but further experiments are required to make them more widely applicable.

7.4 Future work

The work presented in this thesis can be extended in the future to explore a few different avenues. The upstream-recovery mimic can be linked to scale-down downstream platforms for a holistic view of the entire bioprocessing flowsheet. Such an end-to-end mimic can be applied to investigate the impact of upstream and recovery operations on the chromatography steps (e.g. protein A, CEX and AEX).

This would enable entire flowsheets to be future-proofed with high throughput small scale experimentation.

A mimic for the whole bioprocess flowsheet will enable developing cause-and-effect correlations that link the upstream and centrifugation to the DSP. The model can also be applied to investigate the impact of process uncertainty (e.g. seeding density) or centrifugation operation (e.g. level of shear) on the whole manufacturing flowsheet. For instance, it would be important to consider the impact of shear and the concomitant increase in cellular debris on the capture step –usually protein A chromatography – or how the change and HCP and DNA profiles due to upstream conditions or centrifugation shear impact on the overall downstream operation. This will help identify further competing metrics with respect to maximising for efficient downstream process – reducing the levels of impurities– and upstream and recovery process – aiming for high titre, centrifugation and filtration yield.

The bioprocess economics analysis can also be extended to consider the entire process flowsheet and incorporate the experimentally-derived correlations for the end-to-end process. Such an extended bioprocess economics model with predictive process models for each step will enable the selection of optimum conditions in the upstream, recovery and downstream depending on the manufacturer's constraints and priorities.

The current and extended integrated platform can also be applied to the earlier stages of process development such as clones screening. In this way the lead candidate can be selected considering the whole bioprocess flowsheet rather than a limited number of quality metrics as it is done today.

In this thesis there were two quality metrics that were investigated - HCP levels and monomer content. However, there was no in-depth analysis of the type of HCPs that were present in the cell culture medium. It would be important to understand how the type of HCPs changes with varying upstream and recovery conditions (e.g. centrifugations shear) and how efficient the downstream process is in removing the different HCPs. Future work could focus on what upstream and recovery conditions lead to the increase in the levels of “problematic” HCPs and in particular those that co-purify with the product (Jones et al., 2021). Furthermore, the cell culture conditions and the mixture of HCPs present in the medium can impact on a number of quality attributes – glycosylation patterns, charge variants, fragmentation and aggregation.

The recent developments in process analytical technologies (PAT) may enable the investigation of additional metrics that are currently too expensive or cumbersome to perform for high throughput experimentation such as protein aggregation, titre, cell metabolism (Maruthamuthu et al., 2020), charge and product size variants (Camperi et al., 2020 and Liu et al., 2022). The application of PAT to the whole bioprocess flowsheet may shed light onto further process trade-offs and synergies between unit operation metrics (aggregation, titre, mAb charge and size variants). The program developed in this thesis for pre-treatment and structuring of big data sets can be extended to these additional metrics. The data generated from the whole bioprocess flowsheet is likely to contain high-dimensional data sets and machine learning algorithms can be applied to further analyze the data and derive meaningful conclusions (Walsh et al., 2022).

The PSD can be further correlated to other PAT for biomass estimation such as capacitance and dielectric spectroscopy (Bergin et al., 2022; Downey et al., 2014; Lemke et al., 2023; Opel et al., 2010). Both approaches enable on-line monitoring but the measurements are dependent on the cell size and viability (Metze et al., 2020 and Cannizzaro et al., 2003). Therefore, linking PSD to these PAT tools can further improve biomass and cell viability estimation.

The drive for innovation in the biopharmaceutical industry has led to the development of novel antibody designs e.g. bi-specific antibodies (Zhong and D'Antona, 2021) and antibody drug-conjugates (Leung et al., 2020). These novel molecular designs are posing new challenges for the existing purification platforms (Chen and Zhang, 2021; Matsuda, 2022) The integrated framework can be applied to these new modalities linking the upstream and centrifugation conditions to product-specific quality metrics in order to identify bottlenecks and trade-offs for the process.

References

- Affandy, A., Keshavarz-Moore, E. and Versteeg, H.K. 2013. Application of filtration blocking models to describe fouling and transmission of large plasmids DNA in sterile filtration. *Journal of Membrane Science*. **437**, pp.150–159.
- Agbogbo, F.K., Ecker, D.M., Farrand, A., Han, K., Khoury, A., Martin, A., McCool, J., Rasche, U., Rau, T.D., Schmidt, D., Sha, M. and Treuheit, N. 2019. Current perspectives on biosimilars. *Journal of industrial microbiology & biotechnology*. **46**(9–10), pp.1297–1311.
- Agilent Technologies 2006. Agilent 2100 Bioanalyzer 2100 Expert User's Guide Technology Licenses.
- Allen, A., James, L., Trotter, M. and Rohr, M. 2008. Introduction to Centrifugation For The Biotechnology Industry. [Accessed 3 January 2020]. Available from: <https://studylib.net/doc/11893432/introduction-to-centrifugation-for-the-biotechnology-indu...>
- Allmendinger, R., Simaria, A.S., Turner, R. and Farid, S.S. 2014. Closed-loop optimization of chromatography column sizing strategies in biopharmaceutical manufacture. *Journal of Chemical Technology and Biotechnology*. **89**(10), pp.1481–1490.
- Ambler, C. 1959. The theory of scaling up laboratory data for the sedimentation type centrifuge. *J Biochem Microbiol Technol Eng*. **1**(2), pp.185–205.
- Antemie, A.M. 2016. *Linking high throughput cell culture, multivariate analysis and*

economics for more effective process integration. Thesis (PhD) University College London.

Aucamp, J.P., Davies, R., Hallet, D., Weiss, A. and Titchener-Hooker, N.J. 2014. Integration of host strain bioengineering and bioprocess development using ultra-scale down studies to select the optimum combination: An antibody fragment primary recovery case study. *Biotechnology and Bioengineering*. **111**(10), pp.1971–1981.

Bacchin, P., Meireles, M. and Aimar, P. 2002. Modelling of filtration: From the polarised layer to deposit formation and compaction. *Desalination*. **145**(1–3), pp.139–146.

Banerjee, S., Afzal, M.A., Chokshi, P. and Rathore, A.S. 2021. Mechanistic modelling of Chinese hamster ovary cell clarification using acoustic wave separator. *Chemical Engineering Science*. **246**, p.116894.

van den Berg, G.B. and Smolders, C. a. 1990. Flux decline in ultrafiltration processes. *Desalination*. **77**, pp.101–133.

Bergin, A., Carvell, J. and Butler, M. 2022. Applications of bio-capacitance to cell culture manufacturing. *Biotechnology Advances*. **61**, p.108048.

Boi, C., Malavasi, A., Carbonell, R.G. and Gilleskie, G. 2020. A direct comparison between membrane adsorber and packed column chromatography performance. *Journal of Chromatography A*. **1612**, p.460629.

Bollati-Fogolín, M., Forno, G., Nimitz, M., Conradt, H.S., Etcheverrigaray, M. and Kratje, R. 2005. Temperature reduction in cultures of hGM-CSF-expressing

- CHO cells: Effect on productivity and product quality. *Biotechnology Progress*. **21**(1), pp.17–21.
- Bolton, G., LaCasse, D. and Kuriyel, R. 2006. Combined models of membrane fouling: Development and application to microfiltration and ultrafiltration of biological fluids. *Journal of Membrane Science*. **277**(1–2), pp.75–84.
- Boychyn, M., Yim, S.S.S., Ayazi Shamlou, P., Bulmer, M., More, J. and Hoare, M. 2001. Characterization of flow intensity in continuous centrifuges for the development of laboratory mimics. *Chemical Engineering Science*. **56**(16), pp.4759–4770.
- Boychyn, M., Yim, S.S.S., Bulmer, M., More, J., Bracewell, D.G. and Hoare, M. 2004. Performance prediction of industrial centrifuges using scale-down models. *Bioprocess and biosystems engineering*. **26**(6), pp.385–391.
- Broly, H., Mitchell-Logean, C., Costioli, M.D. and Guillemot-Potelle, C. 2010. Cost of Goods Modeling and Quality by Design for Developing Cost-Effective Processes. *Biopharm Internationala*. **23**(6).
- Brunner, M., Fricke, J., Kroll, P. and Herwig, C. 2017. Investigation of the interactions of critical scale-up parameters (pH, pO₂ and pCO₂) on CHO batch performance and critical quality attributes. *Bioprocess and Biosystems Engineering*. **40**(2), p.251.
- Büchs, J., Maier, U., Milbradt, C. and Zoels, B. 2000. Power consumption in shaking flasks on rotary shaking machines: II. Nondimensional description of specific power consumption and flow regimes in unbaffled flasks at elevated liquid

viscosity. *Biotechnology and bioengineering*. **68**(6), pp.594–601.

Camperi, J., Dai, L., Guillarme, D. and Stella, C. 2020. Fast and Automated Characterization of Monoclonal Antibody Minor Variants from Cell Cultures by Combined Protein-A and Multidimensional LC/MS Methodologies. *Analytical Chemistry*. **92**(12), pp.8506–8513.

Cannizzaro, C., Gügerli, R., Marison, I. and Von Stockar, U. 2003. On-line biomass monitoring of CHO perfusion culture with scanning dielectric spectroscopy. *Biotechnology and Bioengineering*. **84**(5), pp.597–610.

Caputo, F., Vogel, R., Savage, J., Vella, G., Law, A., Della Camera, G., Hannon, G., Peacock, B., Mehn, D., Ponti, J., Geiss, O., Aubert, D., Prina-Mello, A. and Calzolari, L. 2021. Measuring particle size distribution and mass concentration of nanoplastics and microplastics: addressing some analytical challenges in the sub-micron size range. *Journal of Colloid and Interface Science*. **588**, pp.401–417.

Chan, G., Booth, A.J., Mannweiler, K. and Hoare, M. 2006. Ultra scale-down studies of the effect of flow and impact conditions during E. coli cell processing. *Biotechnology and bioengineering*. **95**(4), pp.671–83.

Chan, L.L.-Y., Rice, W.L. and Qiu, J. 2020. Observation and quantification of the morphological effect of trypan blue rupturing dead or dying cells J. Chalmers, ed. *PLOS ONE*. **15**(1), p.e0227950.

Chandler, M. and Zydney, A. 2004. High throughput screening for membrane process development. *Journal of Membrane Science*. **237**(1–2), pp.181–188.

- Chatel, A., Kumpalume, P. and Hoare, M. 2014. Ultra scale-down characterization of the impact of conditioning methods for harvested cell broths on clarification by continuous centrifugation-Recovery of domain antibodies from rec E. coli. *Biotechnology and bioengineering*. **111**(5), pp.913–24.
- Chen, C., Wong, H.E. and Goudar, C.T. 2018. Upstream process intensification and continuous manufacturing. *Current Opinion in Chemical Engineering*. **22**, pp.191–198.
- Chen, S.W. and Zhang, W. 2021. Current trends and challenges in the downstream purification of bispecific antibodies. *Antibody therapeutics*. **4**(2), pp.73–88.
- Chon, J.H. and Zarbis-Papastoitsis, G. 2011. Advances in the production and downstream processing of antibodies. *New Biotechnology*. **28**(5), pp.458–463.
- Chung, S., Tian, J., Tan, Z., Chen, J., Lee, J., Borys, M. and Li, Z.J. 2018. Industrial bioprocessing perspectives on managing therapeutic protein charge variant profiles. *Biotechnology and Bioengineering*. **115**(7), pp.1646–1665.
- Chung, W.K., Russell, B., Yang, Y., Handlogten, M., Hudak, S., Cao, M., Wang, J., Robbins, D., Ahuja, S. and Zhu, M. 2017. Effects of antibody disulfide bond reduction on purification process performance and final drug substance stability. *Biotechnology and Bioengineering*.
- Clarkson, A.I., Lefevre, P. and Titchener-Hooker, N.J. 1993. A study of process interactions between cell disruption and debris clarification stages in the recovery of yeast intracellular products. *Biotechnology progress*. **9**(5), pp.462–7.

- Clincke, M.-F., Mölleryd, C., Zhang, Y., Lindskog, E., Walsh, K. and Chotteau, V. 2013. Very high density of CHO cells in perfusion by ATF or TFF in WAVE bioreactor™. Part I. Effect of the cell density on the process. *Biotechnology progress*. **29**(3), pp.754–67.
- Collins, M., Lari, H., Anderson, S., Leibnitz, R., Kumar, A. and Kuriyel, R. 2009. Investigating flow distribution and its effects on scale-up. *BioProcess International*. **7**(9), pp.46–52.
- Comisel, R.M., Kara, B., Fiesser, F.H. and Farid, S.S. 2021. Lentiviral vector bioprocess economics for cell and gene therapy commercialization. *Biochemical Engineering Journal*. **167**, p.107868.
- Cummings, B.S. and Schnellmann, R.G. 2004. Measurement of Cell Death in Mammalian Cells. *Current Protocols in Pharmacology*. **25**(1).
- Curling, J. 2009. The Development of Antibody Technologies. *Process scale purification of antibodies*. **17**, pp.25–51.
- Darja, O., Stanislav, M., Saša, S., Andrej, F., Lea, B. and Branka, J. 2016. Responses of CHO cell lines to increased pCO₂ at normal (37°C) and reduced (33°C) culture temperatures. *Journal of Biotechnology*. **219**, pp.98–109.
- Delahaye, M., Lawrence, K., Ward, S.J. and Hoare, M. 2015. An ultra scale-down analysis of the recovery by dead-end centrifugation of human cells for therapy. *Biotechnology and Bioengineering*. **112**(5), pp.997–1011.
- deZengotita, V.M., Schmelzer, A.E. and Miller, W.M. 2002. Characterization of hybridoma cell responses to elevated pCO₂ and osmolality: Intracellular pH, cell

- size, apoptosis, and metabolism. *Biotechnology and Bioengineering*. **77**(4), pp.369–380.
- Doig, S.D., Pickering, S.C.R., Lye, G.J. and Baganz, F. 2005. Modelling surface aeration rates in shaken microtitre plates using dimensionless groups. *Chemical Engineering Science*. **60**(10), pp.2741–2750.
- Doran, P.M. 2013. Unit Operations. *Bioprocess Engineering Principles.*, pp.445–595.
- Downey, B.J., Graham, L.J., Breit, J.F. and Glutting, N.K. 2014. A Novel Approach for Using Dielectric Spectroscopy to Predict Viable Cell Volume (VCV) in Early Process Development. *Biotechnology Progress*. **30**(2), p.479.
- Dryden, W.A., Larsen, L.M., Britt, D.W. and Smith, M.T. 2021. Technical and economic considerations of cell culture harvest and clarification technologies. *Biochemical Engineering Journal*. **167**, p.107892.
- Ecker, D.M., Jones, S.D. and Levine, H.L. 2015. The therapeutic monoclonal antibody market. *mAbs*. **7**(1), pp.9–14.
- Eriksson, L., Johansson, E., Kettaneh-Wold, N., Trygg, C., Wikström, C. and Wold, S. 2006. PCA. *Multi- and Megavariate Data Analysis Part 1, Basic Principles and Applications.*, pp.39–62.
- Farid, S.S. 2012. Evaluating and Visualizing the Cost-Effectiveness and Robustness of Biopharmaceutical Manufacturing Strategies. *Biopharmaceutical Production Technology, Volume 1 & Volume 2*. **2**, pp.717–741.
- Farid, S.S., Baron, M., Stamatis, C., Nie, W. and Coffman, J. 2020. Benchmarking

biopharmaceutical process development and manufacturing cost contributions to R&D. *mAbs*. **12**(1).

Farid, S.S., Washbrook, J. and Titchener-Hooker, N.J. 2008. Decision-Support Tool for Assessing Biomanufacturing Strategies under Uncertainty: Stainless Steel versus Disposable Equipment for Clinical Trial Material Preparation. *Biotechnology Progress*. **21**(2), pp.486–497.

Farid, S.S., Washbrook, J. and Titchener-Hooker, N.J. 2007. Modelling biopharmaceutical manufacture: Design and implementation of SimBiopharma. *Computers and Chemical Engineering*. **31**(9), pp.1141–1158.

Felo, M., Christensen, B. and Higgins, J. 2013. Process cost and facility considerations in the selection of primary cell culture clarification technology. *Biotechnology Progress*. **29**(5), pp.1239–1245.

Fox, S.R., Tan, H.K., Tan, M.C., Wong, S.C.N.C., Yap, M.G.S. and Wang, D.I.C. 2005. A detailed understanding of the enhanced hypothermic productivity of interferon-gamma by Chinese-hamster ovary cells. *Biotechnology and applied biochemistry*. **41**(Pt 3), pp.255–64.

Furukawa, K. and Ohsuye, K. 1998. Effect of culture temperature on a recombinant CHO cell line producing a C-terminal ??-amidating enzyme. *Cytotechnology*. **26**(2), pp.153–164.

Gagnon, P. 2012. Technology trends in antibody purification. *Journal of Chromatography A*. **1221**, pp.57–70.

Galluzzi, L., Bravo-San Pedro, J.M., Vitale, I., Aaronson, S.A., Abrams, J.M., Adam,

D., Alnemri, E.S., Altucci, L., Andrews, D., Annicchiarico-Petruzzelli, M., Baehrecke, E.H., Bazan, N.G., Bertrand, M.J., Bianchi, K., Blagosklonny, M. V, Blomgren, K., Borner, C., Bredesen, D.E., Brenner, C., Campanella, M., Candi, E., Cecconi, F., Chan, F.K., Chandel, N.S., Cheng, E.H., Chipuk, J.E., Cidlowski, J.A., Ciechanover, A., Dawson, T.M., Dawson, V.L., De Laurenzi, V., De Maria, R., Debatin, K.-M., Di Daniele, N., Dixit, V.M., Dynlacht, B.D., El-Deiry, W.S., Fimia, G.M., Flavell, R.A., Fulda, S., Garrido, C., Gougeon, M.-L., Green, D.R., Gronemeyer, H., Hajnoczky, G., Hardwick, J.M., Hengartner, M.O., Ichijo, H., Joseph, B., Jost, P.J., Kaufmann, T., Kepp, O., Klionsky, D.J., Knight, R.A., Kumar, S., Lemasters, J.J., Levine, B., Linkermann, A., Lipton, S.A., Lockshin, R.A., López-Otín, C., Lugli, E., Madeo, F., Malorni, W., Marine, J.-C., Martin, S.J., Martinou, J.-C., Medema, J.P., Meier, P., Melino, S., Mizushima, N., Moll, U., Muñoz-Pinedo, C., Nuñez, G., Oberst, A., Panaretakis, T., Penninger, J.M., Peter, M.E., Piacentini, M., Pinton, P., Prehn, J.H., Puthalakath, H., Rabinovich, G.A., Ravichandran, K.S., Rizzuto, R., Rodrigues, C.M., Rubinsztein, D.C., Rudel, T., Shi, Y., Simon, H.-U., Stockwell, B.R., Szabadkai, G., Tait, S.W., Tang, H.L., Tavernarakis, N., Tsujimoto, Y., Vanden Berghe, T., Vandenabeele, P., Villunger, A., Wagner, E.F., Walczak, H., White, E., Wood, W.G., Yuan, J., Zakeri, Z., Zhivotovsky, B., Melino, G. and Kroemer, G. 2015. Essential versus accessory aspects of cell death: recommendations of the NCCD 2015. *Cell death and differentiation*. **22**(1), pp.58–73.

Gherghescu, I. and Delgado-Charro, M.B. 2021. The Biosimilar Landscape: An Overview of Regulatory Approvals by the EMA and FDA. *Pharmaceutics*. **13**(1),

pp.1–16.

Gilbert, A., Huang, Y. and Ryll, T. 2014. Identifying and eliminating cell culture process variability Pharmaceutical. . **2**(6), pp.519–534.

Gimenez, L., Kawkabani, E.E., Jacobs, P. and Malphettes, L. 2015. Overcoming the clarification challenges of high cell density culture. *BMC Proceedings 2015 9:9*. **9**(9), pp.1–2.

Goldrick, S., Holmes, W., Bond, N.J., Lewis, G., Kuiper, M., Turner, R. and Farid, S.S. 2017. Advanced multivariate data analysis to determine the root cause of trisulfide bond formation in a novel antibody-peptide fusion. *Biotechnology and Bioengineering*. **114**(10), pp.2222–2234.

Goldrick, S., Joseph, A. and Gruber, D. 2016. Predicting Performance of Constant Flux Depth Filtration using Constant Pressure Filtration Data. , pp.1–26.

Goldrick, S., Joseph, A., Mollet, M., Turner, R., Gruber, D., Farid, S.S. and Titchener-Hooker, N.J. 2017. Predicting performance of constant flow depth filtration using constant pressure filtration data. *Journal of Membrane Science*. **531**, pp.138–147.

Goldrick, S., Lovett, D., Montague, G. and Lennox, B. 2018. Influence of Incident Wavelength and Detector Material Selection on Fluorescence in the Application of Raman Spectroscopy to a Fungal Fermentation Process. *Bioengineering 2018, Vol. 5, Page 79*. **5**(4), p.79.

Goldrick, S., Umprecht, A., Tang, A., Zakrzewski, R., Cheeks, M., Turner, R., Charles, A., Les, K., Hulley, M., Spencer, C. and Farid, S.S. 2020. High-

- Throughput Raman Spectroscopy Combined with Innovate Data Analysis Workflow to Enhance Biopharmaceutical Process Development. *Processes* 2020, Vol. 8, Page 1179. **8**(9), p.1179.
- Gronemeyer, P., Ditz, R. and Strube, J. 2014. Trends in Upstream and Downstream Process Development for Antibody Manufacturing. *Bioengineering (Basel, Switzerland)*. **1**(4), pp.188–212.
- Gupta, A., Amara, J.P., Gousseinov, E. and Cacace, B. 2020. Recent advances in harvest clarification for antibodies and related products. *Approaches to the Purification, Analysis and Characterization of Antibody-Based Therapeutics.*, pp.117–136.
- de Haan, N., Falck, D. and Wuhrer, M. 2020. Monitoring of immunoglobulin N- and O-glycosylation in health and disease. *Glycobiology*. **30**(4), pp.226–240.
- Hadpe, S.R., Mohite, V., Alva, S. and Rathore, A.S. 2020. Pretreatments for enhancing clarification efficiency of depth filtration during production of monoclonal antibody therapeutics. *Biotechnology Progress*. **36**(5), p.e2996.
- Häggmark, C. and Königsson, S. 2018. Rheological Characterization of Solids Phase in Biomass Processes of Disc-Stack Centrifuges. *Chemical Engineering & Technology*. **41**(12), pp.2289–2297.
- Hamaker, N.K., Min, L. and Lee, K.H. 2022. Comprehensive assessment of host cell protein expression after extended culture and bioreactor production of CHO cell lines. *Biotechnology and Bioengineering*. **119**(8), pp.2221–2238.
- Han, Y.K., Koo, T.Y. and Lee, G.M. 2009. Enhanced interferon- β production by CHO

cells through elevated osmolality and reduced culture temperature. *Biotechnology Progress*. **25**(5), pp.1440–1447.

Handlogten, M.W., Lee-O'Brien, A., Roy, G., Levitskaya, S. V., Venkat, R., Singh, S. and Ahuja, S. 2018. Intracellular response to process optimization and impact on productivity and product aggregates for a high-titer CHO cell process. *Biotechnology and Bioengineering*. **115**(1), pp.126–138.

Handlogten, M.W., Wang, J., Ahuja, S., Sciences, A., Bio, V. and Way, M. 2020. Online control of cell culture redox potential prevents antibody interchain disulfide bond reduction. *Biotechnology and Bioengineering*. **117**(5), pp.1329–1336.

Handlogten, M.W., Zhu, M. and Ahuja, S. 2017. Glutathione and thioredoxin systems contribute to recombinant monoclonal antibody interchain disulfide bond reduction during bioprocessing. *Biotechnology and Bioengineering*. **114**(7), pp.1469–1477.

He, Q., Rehmann, M.S., Tian, J., Xu, J., Sabino, L., Vandermark, E., Basson, Z., Po, I., Bierilo, K., Tremml, G., Rizzi, G., Langsdorf, E.F., Qian, N.X., Borys, M.C., Khetan, A. and Li, Z.J. 2022. Improved Titer in Late-Stage Mammalian Cell Culture Manufacturing by Re-Cloning. *Bioengineering*. **9**(4).

Hennicke, J., Reinhart, D., Altmann, F. and Kunert, R. 2019. Impact of temperature and pH on recombinant human IgM quality attributes and productivity. *New Biotechnology*. **50**, pp.20–26.

Hermann, R., Lehmann, M. and Büchs, J. 2003. Characterization of gas-liquid mass

- transfer phenomena in microtiter plates. *Biotechnology and bioengineering*. **81**(2), pp.178–86.
- Herzer, S., Bhangale, A., Barker, G., Chowdhary, I., Conover, M., O'Mara, B.W., Tsang, L., Wang, S.-Y., Krystek, S.R., Yao, Y. and Rieble, S. 2015. Development and scale-up of the recovery and purification of a domain antibody Fc fusion protein-comparison of a two and three-step approach. *Biotechnology and bioengineering*. **112**(7), pp.1417–28.
- Hiebl, B., Peters, S., Gemeinhardt, O., Niehues, S.M. and Jung, F. 2017. Impact of serum in cell culture media on in vitro lactate dehydrogenase (LDH) release determination. *Journal of Cellular Biotechnology*. **3**(1), pp.9–13.
- Higel, F., Seidl, A., Sörgel, F. and Friess, W. 2016. N-glycosylation heterogeneity and the influence on structure, function and pharmacokinetics of monoclonal antibodies and Fc fusion proteins. *European Journal of Pharmaceutics and Biopharmaceutics*. **100**, pp.94–100.
- Hong, J.S., Azer, N., Agarabi, C. and Fratz-Berilla, E.J. 2020. Primary Clarification of CHO Harvested Cell Culture Fluid using an Acoustic Separator. *JoVE (Journal of Visualized Experiments)*. **2020**(159), p.e61161.
- Hsu, W.T., Aulakh, R.P.S., Traul, D.L. and Yuk, I.H. 2012. Advanced microscale bioreactor system: A representative scale-down model for bench-top bioreactors. *Cytotechnology*. **64**(6), pp.667–678.
- Huang, T., Chen, X., Gu, H., Zhao, C., Liu, X., Yan, M., Deng, X., Zhang, Z. and Gu, J. 2016. Fractionation of Fab glycosylated immunoglobulin G with concanavalin

A chromatography unveils new structural properties of the molecule. *Oncotarget*. **7**(21), p.31166.

Hundley, R. and Königsson, S. 2020. Development of a Single-Use, Hermetic Centrifuge System For Mammalian Harvests with Moderate to High Cell Content. *BioProcess International*. **18**(10).

Hutchinson, N., Bingham, N., Murrell, N., Farid, S. and Hoare, M. 2006. Shear stress analysis of mammalian cell suspensions for prediction of industrial centrifugation and its verification. *Biotechnology and bioengineering*. **95**(3), pp.483–91.

Hwang, S.J., Yoon, S.K., Koh, G.Y. and Lee, G.M. 2011. Effects of culture temperature and pH on flag-tagged COMP angiopoietin-1 (FCA1) production from recombinant CHO cells: FCA1 aggregation. *Applied Microbiology and Biotechnology*. **91**(2), pp.305–315.

Iammarino, M., Nti-gyabaah, J., Chandler, M., Roush, D. and Göklen, K. 2007. Impact of Cell Density and Viability. *Bioprocess International*. (November), pp.38–50.

Iordan, A., Duperray, A. and Verdier, C. 2008. Fractal approach to the rheology of concentrated cell suspensions. *Physical Review E - Statistical, Nonlinear, and Soft Matter Physics*. **77**(1), p.011911.

Ivarsson, M., Noh, H., Morbidelli, M. and Soos, M. 2015. Insights into pH-induced metabolic switch by flux balance analysis. *Biotechnology Progress*. **31**(2), pp.347–357.

- Ivarsson, M., Villiger, T.K., Morbidelli, M. and Soos, M. 2014. Evaluating the impact of cell culture process parameters on monoclonal antibody N-glycosylation. *Journal of biotechnology*. **188**, pp.88–96.
- Jackson, N.B., Liddell, J.M. and Lye, G.J. 2006. An automated microscale technique for the quantitative and parallel analysis of microfiltration operations. *Journal of Membrane Science*. **276**(1), pp.31–41.
- Janakiraman, V., Kwiatkowski, C., Kshirsagar, R., Ryll, T. and Huang, Y.-M. 2015. Application of high-throughput mini-bioreactor system for systematic scale-down modeling, process characterization, and control strategy development. *Biotechnology Progress*. **31**(6), pp.1623–1632.
- De Jesus, M. and Wurm, F.M. 2011. Manufacturing recombinant proteins in kg-ton quantities using animal cells in bioreactors. *European Journal of Pharmaceutics and Biopharmaceutics*. **78**(2), pp.184–188.
- Jin, L., Wang, Z.S., Cao, Y., Sun, R.Q., Zhou, H. and Cao, R.Y. 2021. Establishment and optimization of a high-throughput mimic perfusion model in ambr ® 15. *Biotechnology letters*. **43**(2), pp.423–433.
- Jones, M., Palackal, N., Wang, F., Gaza-Bulseco, G., Hurkmans, K., Zhao, Y., Chitikila, C., Clavier, S., Liu, S., Menesale, E., Schonenbach, N.S., Sharma, S., Valax, P., Waerner, T., Zhang, L. and Connolly, T. 2021. “High-risk” host cell proteins (HCPs): A multi-company collaborative view. *Biotechnology and Bioengineering*. **118**(8), pp.2870–2885.
- Joseph, A., Goldrick, S., Mollet, M., Turner, R., Bender, J., Gruber, D., Farid, S.S.

- and Titchener-Hooker, N. 2017. An automated laboratory-scale methodology for the generation of sheared mammalian cell culture samples. *Biotechnology Journal*. **12**(5), p.1600730.
- Joseph, A., Kenty, B., Mollet, M., Hwang, K., Rose, S., Goldrick, S., Bender, J., Farid, S.S. and Titchener-Hooker, N. 2016. A scale-down mimic for mapping the process performance of centrifugation, depth and sterile filtration. *Biotechnology and Bioengineering*. **113**(9), pp.1934–1941.
- Joseph, J.R., Sinclair, A., Titchener-Hooker, N.J. and Zhou, Y. 2006. A framework for assessing the solutions in chromatographic process design and operation for large-scale manufacture. *Journal of Chemical Technology & Biotechnology*. **81**(6), pp.1009–1020.
- Kamachi, Y. and Omasa, T. 2018. Development of hyper osmotic resistant CHO host cells for enhanced antibody production. *Journal of bioscience and bioengineering*. **125**(4), pp.470–478.
- Kang, Y.K., Hamzik, J., Felo, M., Qi, B., Lee, J., Ng, S., Liebisch, G., Shanehsaz, B., Singh, N., Persaud, K., Ludwig, D.L. and Balderes, P. 2013. Development of a novel and efficient cell culture flocculation process using a stimulus responsive polymer to streamline antibody purification processes. *Biotechnology and Bioengineering*. **110**(11), pp.2928–2937.
- Kao, Y.H., Hewitt, D.P., Trexler-Schmidt, M. and Laird, M.W. 2010. Mechanism of antibody reduction in cell culture production processes. *Biotechnology and Bioengineering*. **107**(4), pp.622–632.

- Karst, D.J., Serra, E., Villiger, T.K., Soos, M. and Morbidelli, M. 2016. Characterization and comparison of ATF and TFF in stirred bioreactors for continuous mammalian cell culture processes. *Biochemical Engineering Journal*. **110**, pp.17–26.
- Kaufmann, H., Mazur, X., Fussenegger, M. and Bailey, J.E. 1999. Influence of low temperature on productivity, proteome and protein phosphorylation of CHO cells. *Biotechnology and Bioengineering*. **63**(5), pp.573–582.
- Kelley, B., Blank, G. and Lee, a 2009. Downstream processing of monoclonal antibodies: current practices and future opportunities. ... *Scale Purification of Antibodies.*, pp.1–24.
- Kelley, B., Kiss, R. and Laird, M. 2018. A different perspective: How much innovation is really needed for monoclonal antibody production using mammalian cell technology? *Advances in Biochemical Engineering/Biotechnology*. **165**, pp.443–462.
- Kelly, W., Scully, J., Zhang, D., Feng, G., Lavengood, M., Condon, J., Knighton, J. and Bhatia, R. 2014. Understanding and modeling alternating tangential flow filtration for perfusion cell culture. *Biotechnology progress*. **30**(6), pp.1291–1300.
- Khan, K.H. 2013. Gene expression in Mammalian cells and its applications. *Advanced pharmaceutical bulletin*. **3**(2), pp.257–63.
- Kimura, R. and Miller, W.M. 1996. Effects of elevated pCO₂ and/or osmolality on the growth and recombinant tPA production of CHO cells. *Biotechnology and*

Bioengineering. **52**(1), pp.152–160.

King, J.M.P., Titchener-Hooker, N.J. and Zhou, Y. 2007. Ranking bioprocess variables using global sensitivity analysis: A case study in centrifugation.

Bioprocess and Biosystems Engineering. **30**(2), pp.123–134.

Kishishita, S., Katayama, S., Kodaira, K., Takagi, Y., Matsuda, H., Okamoto, H., Takuma, S., Hirashima, C. and Aoyagi, H. 2015. Optimization of chemically defined feed media for monoclonal antibody production in Chinese hamster ovary cells. *Journal of bioscience and bioengineering*. **120**(1), pp.78–84.

Kong, S., Aucamp, J. and Titchener-Hooker, N.J. 2010. Studies on membrane sterile filtration of plasmid DNA using an automated multiwell technique. *Journal of Membrane Science*. **353**(1–2), pp.144–150.

Lau, E.C., Kong, S., McNulty, S., Entwisle, C., McIlgorm, A., Dalton, K. a and Hoare, M. 2013. An ultra scale-down characterization of low shear stress primary recovery stages to enhance selectivity of fusion protein recovery from its molecular variants. *Biotechnology and bioengineering*. **110**(7), pp.1973–83.

Lebeau, P.F., Chen, J., Byun, J.H., Platko, K. and Austin, R.C. 2019. The trypan blue cellular debris assay: a novel low-cost method for the rapid quantification of cell death. *MethodsX*. **6**, pp.1174–1180.

Lemke, J., Söldner, R. and Austerjost, J. 2023. Online deployment of an O-PLS model for dielectric spectroscopy-based inline monitoring of viable cell concentrations in Chinese hamster ovary cell perfusion cultivations. *Engineering in Life Sciences*. **23**(6).

- Leung, D., Wurst, J., Liu, T., Martinez, R., Datta-Mannan, A. and Feng, Y. 2020. Antibody Conjugates-Recent Advances and Future Innovations. *Antibodies (Basel, Switzerland)*. **9**(1), p.2.
- Levy, M.S., Collins, I.J., Yim, S.S., Ward, J.M., Titchener-Hooker, N., Ayazi Shamlou, P. and Dunnill, P. 1999. Effect of shear on plasmid DNA in solution. *Bioprocess Engineering*. **20**(1), pp.7–13.
- Li, F., Vijayasankaran, N., Shen, A. (Yijuan), Kiss, R. and Amanullah, A. 2010. Cell culture processes for monoclonal antibody production. *mAbs*. **2**(5), pp.466–477.
- Li, R. and Lin, D.K.J. 2003. Analysis Methods for Supersaturated Design: Some Comparisons. *Journal of Data Science*. **1**, pp.249–260.
- Liu, H.F., Ma, J., Winter, C. and Bayer, R. 2010. Recovery and purification process development for monoclonal antibody production. *mAbs*. **2**(5), pp.480–499.
- Liu, S., Simaria, A.S., Farid, S.S. and Papageorgiou, L.G. 2013. Mixed integer optimisation of antibody purification processes. *Computer Aided Chemical Engineering*. **32**, pp.157–162.
- Liu, Y., Zhang, C., Chen, J., Fernandez, J., Vellala, P., Kulkarni, T.A., Aguilar, I., Ritz, D., Lan, K., Patel, P. and Liu, A. 2022. A Fully Integrated Online Platform For Real Time Monitoring Of Multiple Product Quality Attributes In Biopharmaceutical Processes For Monoclonal Antibody Therapeutics. *Journal of Pharmaceutical Sciences*. **111**(2), pp.358–367.
- Liu, Z., Wickramasinghe, S.R. and Qian, X. 2016. Membrane chromatography for protein purifications from ligand design to functionalization.

<https://doi.org/10.1080/01496395.2016.1223133>. **52**(2), pp.299–319.

Looby, M., Ibarra, N., Pierce, J.J., Buckley, K., O'Donovan, E., Heenan, M., Moran, E., Farid, S.S. and Baganz, F. 2011. Application of quality by design principles to the development and technology transfer of a major process improvement for the manufacture of a recombinant protein. *Biotechnology Progress*. **27**(6), pp.1718–1729.

Los, D.A. and Murata, N. 2004. Membrane fluidity and its roles in the perception of environmental signals. *Biochimica et biophysica acta*. **1666**(1–2), pp.142–57.

Lu, R.M., Hwang, Y.C., Liu, I.J., Lee, C.C., Tsai, H.Z., Li, H.J. and Wu, H.C. 2020. Development of therapeutic antibodies for the treatment of diseases. *Journal of Biomedical Science*. **27**(1), pp.1–30.

Mahal, H., Branton, H. and Farid, S.S. 2021. End-to-end continuous bioprocessing: Impact on facility design, cost of goods, and cost of development for monoclonal antibodies. *Biotechnology and Bioengineering*. **118**(9), pp.3468–3485.

Mannweiler, K. and Hoare, M. 1992a. The scale-down of an industrial disc stack centrifuge. *Bioprocess Engineering*. **8**(1–2), pp.19–25.

Mannweiler, K. and Hoare, M. 1992b. The scale-down of an industrial disc stack centrifuge. *Bioprocess Engineering*. **8**(1–2), pp.19–25.

Maruthamuthu, M.K., Rudge, S.R., Ardekani, A.M., Ladisch, M.R. and Verma, M.S. 2020. Process Analytical Technologies and Data Analytics for the Manufacture of Monoclonal Antibodies. *Trends in Biotechnology*. **38**(10), p.1169.

Mason, R.L., Gunst, R.F. and Hess, J.L. 2003. Statistical Principles in Experimental

- Design *In: Statistical Design and Analysis of Experiments* [Online]. Hoboken, NJ, USA: John Wiley & Sons, Inc., pp.107–139. [Accessed 8 June 2016]. Available from: <http://doi.wiley.com/10.1002/0471458503.ch4>.
- Matsuda, Y. 2022. Current approaches for the purification of antibody–drug conjugates. *Journal of Separation Science*. **45**(1), pp.27–37.
- Maybury, J.P., Hoare, M. and Dunnill, P. 2000. The use of laboratory centrifugation studies to predict performance of industrial machines: studies of shear-insensitive and shear-sensitive materials. *Biotechnology and bioengineering*. **67**(3), pp.265–73.
- McNerney, T., Thomas, A., Senczuk, A., Petty, K., Zhao, X., Piper, R., Carvalho, J., Hammond, M., Sawant, S. and Bussiere, J. 2015. PDADMAC flocculation of Chinese hamster ovary cells: enabling a centrifuge-less harvest process for monoclonal antibodies. *mAbs*. **7**(2), pp.413–427.
- Meleady, P., Doolan, P., Henry, M., Barron, N., Keenan, J., O’Sullivan, F., Clarke, C., Gammell, P., Melville, M.W., Leonard, M. and Clynes, M. 2011. Sustained productivity in recombinant Chinese Hamster Ovary (CHO) cell lines: Proteome analysis of the molecular basis for a process-related phenotype. *BMC Biotechnology*. **11**(1), pp.1–11.
- Mercier, Sarah M, Diepenbroek, B., Dalm, M.C.F., Wijffels, R.H. and Streefland, M. 2013. Multivariate data analysis as a PAT tool for early bioprocess development data. *Journal of biotechnology*. **167**(3), pp.262–70.
- Mercier, Sarah M., Diepenbroek, B., Dalm, M.C.F., Wijffels, R.H. and Streefland, M.

2013. Multivariate data analysis as a PAT tool for early bioprocess development data. *Journal of Biotechnology*. **167**(3), pp.262–270.
- Méry, B., Guy, J.-B., Vallard, A., Espenel, S., Ardail, D., Rodriguez-Lafrasse, C., Rancoule, C. and Magné, N. 2017. In Vitro Cell Death Determination for Drug Discovery: A Landscape Review of Real Issues. *Journal of cell death*. **10**, p.1179670717691251.
- Metze, S., Ruhl, S., Greller, G., Grimm, C. and Scholz, J. 2020. Monitoring online biomass with a capacitance sensor during scale-up of industrially relevant CHO cell culture fed-batch processes in single-use bioreactors. *Bioprocess and Biosystems Engineering*. **43**(2), p.193.
- Micheletti, M., Barrett, T., Doig, S.D., Baganz, F., Levy, M.S., Woodley, J.M. and Lye, G.J. 2006. Fluid mixing in shaken bioreactors: Implications for scale-up predictions from microlitre-scale microbial and mammalian cell cultures. *Chemical Engineering Science*. **61**(9), pp.2939–2949.
- Moore, A., Mercer, J., Dutina, G., Donahue, C.J., Bauer, K.D., Mather, J.P., Etcheverry, T. and Ryll, T. 1997. Effects of temperature shift on cell cycle, apoptosis and nucleotide pools in CHO cell batch cultures. *Cytotechnology*. **23**(1–3), pp.47–54.
- Moses, S. and Manahan, M. 2012. Assessment of AMBRTM as a model for high-throughput cell culture process development strategy. *Advances in Bioscience* **2012**(November), pp.918–927.
- Mullard, A. 2021. FDA approves 100th monoclonal antibody product. *Nature*

- reviews. *Drug discovery*. **20**(7), pp.491–495.
- Mun, M., Khoo, S., Do Minh, A., Dvornicky, J., Trexler-Schmidt, M., Kao, Y.H. and Laird, M.W. 2015. Air sparging for prevention of antibody disulfide bond reduction in harvested CHO cell culture fluid. *Biotechnology and Bioengineering*. **112**(4).
- N. Politis, S., Colombo, P., Colombo, G. and M. Rekkas, D. 2017. Design of experiments (DoE) in pharmaceutical development. *Drug Development and Industrial Pharmacy*. **43**(6), pp.889–901.
- Nguyen, H.C., Languard, A.L., Amara, J.P., Dullen, M., Kahn, D.S. and Costanzo, J.A. 2019. Improved HCP Reduction Using a New, All-Synthetic Depth Filtration Media Within an Antibody Purification Process. *Biotechnology Journal*. **14**(1), p.1700771.
- Nienow, A.W., Rielly, C.D., Brosnan, K., Bargh, N., Lee, K., Coopman, K. and Hewitt, C.J. 2013. The physical characterisation of a microscale parallel bioreactor platform with an industrial CHO cell line expressing an IgG4. *Biochemical Engineering Journal*. **76**, pp.25–36.
- Nogal, B., Chhiba, K. and Emery, J.C. 2012. Select host cell proteins coelute with monoclonal antibodies in protein A chromatography. *Biotechnology progress*. **28**(2), pp.454–458.
- Novais, J.L., Titchener-Hooker, N.J. and Hoare, M. 2001. Economic comparison between conventional and disposables-based technology for the production of biopharmaceuticals. *Biotechnology and bioengineering*. **75**(2), pp.143–153.

- Noyes, A., Basha, J., Frostad, J., Cook, S., Millard, D., Mullin, J., LaCasse, D., Wright, R.S., Huffman, B., Fahrner, R., Godavarti, R., Titchener-Hooker, N., Sunasara, K. and Mukhopadhyay, T. 2015. A modular approach for the ultra-scale-down of depth filtration. *Journal of Membrane Science*. **496**, pp.199–210.
- O'Brien, T.P., Brown, L.A., Battersby, D.G., Rudolph, A.S. and Raman, L.P. 2012. Large-scale, single-use depth filtration systems. *BioProcess International*. **10**(SUPPL. 5), pp.50–57.
- Oguchi, S., Saito, H., Tsukahara, M. and Tsumura, H. 2006. pH Condition in temperature shift cultivation enhances cell longevity and specific hMab productivity in CHO culture. *Cytotechnology*. **52**(3), pp.199–207.
- Opel, C.F., Li, J. and Amanullah, A. 2010. Quantitative modeling of viable cell density, cell size, intracellular conductivity, and membrane capacitance in batch and fed-batch CHO processes using dielectric spectroscopy. *Biotechnology progress*. **26**(4), pp.1187–1199.
- Ottinger, M., Wenk, I., Carvalho Pereira, J., John, G. and Junne, S. 2022. Single-Use Technology in the Biopharmaceutical Industry and Sustainability: A Contradiction? *Chemie-Ingenieur-Technik*. **94**(12), pp.1883–1891.
- Park, J.H., Jin, J.H., Lim, M.S., An, H.J., Kim, J.W. and Lee, G.M. 2017. Proteomic Analysis of Host Cell Protein Dynamics in the Culture Supernatants of Antibody-Producing CHO Cells. *Scientific Reports 2017 7:1*. **7**(1), pp.1–13.
- Pegel, A., Reiser, S., Steurethaler, M. and Klein, S. 2011. Evaluating disposable depth filtration platforms for MAb harvest clarification. *BioProcess International*.

9(9), pp.52–56.

- Pereira Chilima, T.D., Moncaubeig, F. and Farid, S.S. 2020. Estimating capital investment and facility footprint in cell therapy facilities. *Biochemical Engineering Journal*. **155**, p.107439.
- Pollock, J. 2014. Evaluating the Potential of Continuous Processes for Monoclonal Antibodies: Economic, Environmental and Operational Feasibility. *Doctoral thesis, UCL (University College London)*.
- Pollock, J., Ho, S. V. and Farid, S.S. 2013. Fed-batch and perfusion culture processes: Economic, environmental, and operational feasibility under uncertainty. *Biotechnology and Bioengineering*. **110**(1), pp.206–219.
- Popova, D., Stonier, A., Pain, D., Titchener-Hooker, N.J. and Farid, S.S. 2016. Integrated economic and experimental framework for screening of primary recovery technologies for high cell density CHO cultures. *Biotechnology journal*. **11**(7), pp.899–909.
- Qin, J., Wu, X., Xia, Z., Huang, Z., Zhang, Y., Wang, Y., Fu, Q. and Zheng, C. 2019. The effect of hyperosmolality application time on production, quality, and biopotency of monoclonal antibodies produced in CHO cell fed-batch and perfusion cultures. *Applied Microbiology and Biotechnology*. **103**(3), pp.1217–1229.
- Quemada, D. 1998. Rheological modelling of complex fluids. I. The concept of effective volume fraction revisited. *The European Physical Journal Applied Physics*. **1**(1), pp.119–127.

- Rajalahti, T. and Kvalheim, O.M. 2011. Multivariate data analysis in pharmaceuticals : A tutorial review. *International Journal of Pharmaceutics*. **417**(1–2), pp.280–290.
- Rameez, S., Mostafa, S.S., Miller, C. and Shukla, A.A. 2014. High-throughput miniaturized bioreactors for cell culture process development: Reproducibility, scalability, and control. *Biotechnology Progress*. **30**(3), pp.718–727.
- Rathore, A.S., Johnson, R., Yu, O., Ahuja, S., Kirdar, O.A., Annamalai, A. and Ram, K. 2007. Applications of Multivariate Data Analysis in Biotech Processing. *BioPharm International*. **20**(10).
- van Reis, R., Leonard, L.C., Hsu, C.C. and Builder, S.E. 1991. Industrial scale harvest of proteins from mammalian cell culture by tangential flow filtration. *Biotechnology and bioengineering*. **38**(4), pp.413–422.
- van Reis, R. and Zydney, A. 2007. Bioprocess membrane technology. *Journal of Membrane Science*. **297**(1–2), pp.16–50.
- Reynolds, T, Boychyn, M., Sanderson, T., Bulmer, M., More, J. and Hoare, M. 2003. Scale-down of continuous filtration for rapid bioprocess design: Recovery and dewatering of protein precipitate suspensions. *Biotechnology and bioengineering*. **83**(4), pp.454–64.
- Reynolds, Tom, Boychyn, M., Sanderson, T., Bulmer, M., More, J. and Hoare, M. 2003. Scale-down of continuous filtration for rapid bioprocess design: Recovery and dewatering of protein precipitate suspensions. *Biotechnology and Bioengineering*. **83**(4), pp.454–464.

- Rezaei, M., Zarkesh-Esfahani, S.H. and Gharagozloo, M. 2013. The effect of different media composition and temperatures on the production of recombinant human growth hormone by CHO cells. *Research in pharmaceutical sciences*. **8**(3), pp.211–7.
- Richardson, A. and Walker, J. 2018a. Continuous Solids Discharging centrifugation to Solve Clarifying High-Cell-Density Mammalian Cell CulturesBioProcess International. *BioProcess Technical*. **16**(4), pp.38–47.
- Richardson, A. and Walker, J. 2018b. Continuous Solids Discharging centrifugation to Solve Clarifying High-Cell-Density Mammalian Cell CulturesBioProcess International. *BioProcess International*. **16**(4), pp.38–47.
- Riske, F., Schroeder, J., Belliveau, J., Kang, X., Kutzko, J. and Menon, M.K. 2007. The use of chitosan as a flocculant in mammalian cell culture dramatically improves clarification throughput without adversely impacting monoclonal antibody recovery. *Journal of Biotechnology*. **128**(4), pp.813–823.
- Riss, T., Niles, A., Moravec, R., Karassina, N. and Vidugiriene, J. 2004. *Cytotoxicity Assays: In Vitro Methods to Measure Dead Cells* [Online]. Eli Lilly & Company and the National Center for Advancing Translational Sciences. [Accessed 29 September 2020]. Available from: <http://www.ncbi.nlm.nih.gov/pubmed/31070879>.
- Roque, a. C. a, Lowe, C.R. and Taipa, M.Â. 2004. Antibodies and genetically engineered related molecules: Production and purification. *Biotechnology Progress*. **20**(3), pp.639–654.

- Roush, D.J. and Lu, Y. 2008a. Advances in primary recovery: Centrifugation and membrane technology. *Biotechnology Progress*. **24**(3), pp.488–495.
- Roush, D.J. and Lu, Y. 2008b. Advances in Primary Recovery: Centrifugation and Membrane Technology. *Biotechnology Progress*. **24**(3), pp.488–495.
- Royzman, I. and Shah, K. 2019. 10 years of biosimilars: lessons and trends. *Nature Reviews Drug Discovery*.
- Russel, E., Wang, a and Rathore, a 2007. *Process Scale Bioseparations for the Biopharmaceutical Industry*.
- Salte, H., King, J.M., Baganz, F., Hoare, M. and Titchener-Hooker, N.J. 2007. A Methodology for Centrifuge Selection for the Separation of High Solids Density Cell Broths by Visualisation of Performance Using Windows of Operation. *Biotechnology and Bioengineering*. **96**(6), pp.1199–1210.
- Sampath, M., Shukla, A. and Rathore, A. 2014. Modeling of Filtration Processes—Microfiltration and Depth Filtration for Harvest of a Therapeutic Protein Expressed in *Pichia pastoris* at Constant Pressure. *Bioengineering*. **1**(4), pp.260–277.
- Sandner, V., Pybus, L.P., McCreath, G. and Glassey, J. 2018. Scale-Down Model Development in ambr systems: An Industrial Perspective. *Biotechnology Journal*. **14**(4)
- Sarkadi, B., Attisano, L., Grinstein, S., Buchwald, M. and Rothstein, A. 1984. Volume regulation of Chinese hamster ovary cells in anisoosmotic media. *Biochimica et biophysica acta*. **774**(2), pp.159–168.

- SAS Institute Inc. 2009. *JMP® 8 Design of Experiment Guide* [Online]. Available from: http://link.springer.com/content/pdf/10.1007/978-1-84628-473-1_6.pdf.
- Schellenberg, J., Nagraik, T., Wohlenberg, O.J., Ruhl, S., Bahnemann, J., Scheper, T. and Solle, D. 2022. Stress-induced increase of monoclonal antibody production in CHO cells. *Engineering in Life Sciences*. **22**(5), pp.427–436.
- Schmitt, M.G., Rajendra, Y., Hougland, M.D., Boyles, J.S. and Barnard, G.C. 2017. Polymer-mediated flocculation of transient CHO cultures as a simple, high throughput method to facilitate antibody discovery. *Biotechnology Progress*. **33**(5), pp.1393–1400.
- Senczuk, A., Petty, K., Thomas, A., McNerney, T., Moscariello, J. and Yigzaw, Y. 2016. Evaluation of predictive tools for cell culture clarification performance. *Biotechnology and Bioengineering*. **113**(3), pp.568–575.
- Sewell, D.J., Turner, R., Field, R., Holmes, W., Pradhan, R., Spencer, C., Oliver, S.G., Slater, N.K.H. and Dikicioglu, D. 2019. Enhancing the functionality of a microscale bioreactor system as an industrial process development tool for mammalian perfusion culture. *Biotechnology and bioengineering*. **116**(6), pp.1315–1325.
- Shang, M., Kwon, T., Hamel, J.F.P., Lim, C.T., Khoo, B.L. and Han, J. 2021. Investigating the influence of physiologically relevant hydrostatic pressure on CHO cell batch culture. *Scientific Reports 2021 11:1*. **11**(1), pp.1–9.
- Shanklin, T., Roper, K., Yegneswaran, P.K. and Marten, M.R. 2001. Selection of bioprocess simulation software for industrial applications. *Biotechnology and*

bioengineering. **72**(4), pp.483–9.

Shukla, A. a and Kandula, J.R. 2009. Harvest and recovery of monoclonal antibodies: cell removal and clarification. *Process Scale Purification of Antibodies*. (May), pp.53–78.

Shukla, A.A., Hubbard, B., Tressel, T., Guhan, S. and Low, D. 2007. Downstream processing of monoclonal antibodies--application of platform approaches. *Journal of chromatography. B, Analytical technologies in the biomedical and life sciences*. **848**(1), pp.28–39.

Shukla, A.A. and Thömmes, J. 2010. Recent advances in large-scale production of monoclonal antibodies and related proteins. *Trends in Biotechnology*. **28**(5), pp.253–261.

Shukla, A.A., Wolfe, L.S., Mostafa, S.S. and Norman, C. 2017. Evolving trends in mAb production processes. *Bioengineering & Translational Medicine*. **2**(1), pp.58–69.

Singh, N., Arunkumar, A., Chollangi, S., Tan, Z.G., Borys, M. and Li, Z.J. 2016. Clarification technologies for monoclonal antibody manufacturing processes: Current state and future perspectives. *Biotechnology and Bioengineering*. **113**(4), pp.698–716.

Singh, N., Pizzelli, K., Romero, J.K., Chrostowski, J., Evangelist, G., Hamzik, J., Soice, N. and Cheng, K.S. 2013. Clarification of recombinant proteins from high cell density mammalian cell culture systems using new improved depth filters. *Biotechnology and Bioengineering*. **110**(7), pp.1964–1972.

- Sisodiya, V.N., Lequieu, J., Rodriguez, M., McDonald, P. and Lazzareschi, K.P. 2012. Studying host cell protein interactions with monoclonal antibodies using high throughput protein A chromatography. *Biotechnology journal*. **7**(10), pp.1233–41.
- Sissolak, B., Lingg, N., Sommeregger, W., Striedner, G. and Vorauer-Uhl, K. 2019. Impact of mammalian cell culture conditions on monoclonal antibody charge heterogeneity: an accessory monitoring tool for process development. *Journal of Industrial Microbiology & Biotechnology*. **46**(8), p.1167.
- Somasundaram, B., Pleitt, K., Shave, E., Baker, K. and Lua, L. 2018. Progression of continuous downstream processing of monoclonal antibodies: Current trends and challenges. *Biotechnology and bioengineering*. **115**(12).
- Sou, S.N., Sellick, C., Lee, K., Mason, A., Kyriakopoulos, S., Polizzi, K.M. and Kontoravdi, C. 2015. How does mild hypothermia affect monoclonal antibody glycosylation? *Biotechnology and Bioengineering*. **112**(6), pp.1165–1176.
- Stamatis, C. and Farid, S.S. 2021. Process economics evaluation of cell-free synthesis for the commercial manufacture of antibody drug conjugates. *Biotechnology Journal*. **16**(4), p.2000238.
- Stettler, M., Jaccard, N., Hacker, D., De Jesus, M., Wurm, F.M. and Jordan, M. 2006. New Disposable Tubes for Rapid and Precise Biomass Assessment for Suspension Cultures of Mammalian Cells. *Biotechnology and bioengineering*. **95**(6), pp. 1228-1233
- Stonier, A., Simaria, A.S., Smith, M. and Farid, S.S. 2012. Decisional tool to assess

current and future process robustness in an antibody purification facility. *Biotechnology Progress*. **28**(4), pp.1019–1028.

Su, Y., Wei, Z., Miao, Y., Sun, L., Shen, Y., Tang, Z., Li, L., Quan, Y., Yu, H., Wang, W.C., Zhou, W. and Tian, J. 2021. Optimized process operations reduce product retention and column clogging in ATF-based perfusion cell cultures. *Applied Microbiology and Biotechnology*. **105**(24), pp.9125–9136.

Suarez-Zuluaga, D.A., Borchert, D., Driessen, N.N., Bakker, W.A.M. and Thomassen, Y.E. 2019. Accelerating bioprocess development by analysis of all available data: A USP case study. *Vaccine*. **37**(47), pp.7081–7089.

Tae Kyung Kim, Joon Soo Ryu, Joo Young Chung, Min Soo Kim and Gyun, M.L. 2000. Osmoprotective effect of glycine betaine on thrombopoietin production in hyperosmotic Chinese hamster ovary cell culture: Clonal variations. *Biotechnology Progress*. **16**(5), pp.775–781.

Tait, a. S., Aucamp, J.P., Bugeon, a. and Hoare, M. 2009. Ultra scale-down prediction using microwell technology of the industrial scale clarification characteristics by centrifugation of mammalian cell broths. *Biotechnology and Bioengineering*. **104**(2), pp.321–331.

Tait, A.S., Hogwood, C.E.M., Smales, C.M. and Bracewell, D.G. 2012. Host cell protein dynamics in the supernatant of a mAb producing CHO cell line. *Biotechnology and bioengineering*. **109**(4), pp.971–982.

Tait, A.S., Tarrant, R.D.R., Velez-Suberbie, M.L., Spencer, D.I.R. and Bracewell, D.G. 2013. Differential response in downstream processing of CHO cells grown

- under mild hypothermic conditions. *Biotechnology progress*. **29**(3), pp.688–96.
- Tarrant, R.D.R., Velez-Suberbie, M.L., Tait, A.S., Smales, C.M. and Bracewell, D.G. 2012. Host cell protein adsorption characteristics during protein a chromatography. *Biotechnology Progress*. **28**(4), pp.1037–1044.
- Tebbe, H., Lutkemeyer, D., Gudermann, F., Heidemann, R. and Lehmann, J. 1996. Lysis-free separation of hybridoma cells by continuous disc stack centrifugation. *Cytotechnology*. **22**(1–3), pp.119–127.
- Torres-Acosta, M.A., Aguilar-Ya??ez, J.M., Rito-Palomares, M. and Titchener-Hooker, N.J. 2015. Economic analysis of royalactin production under uncertainty: Evaluating the effect of parameter optimization. *Biotechnology Progress*., pp.744–749.
- Toussaint, C., Henry, O. and Durocher, Y. 2016. Metabolic engineering of CHO cells to alter lactate metabolism during fed-batch cultures. *Journal of Biotechnology*. **217**, pp.122–131.
- Trexler-Schmidt, M., Sargis, S., Chiu, J., Sze-Khoo, S., Mun, M., Kao, Y.H. and Laird, M.W. 2010. Identification and prevention of antibody disulfide bond reduction during cell culture manufacturing. *Biotechnology and Bioengineering*.
- Trummer, E., Fauland, K., Seidinger, S., Schriebl, K., Lattenmayer, C., Kunert, R., Vorauer-Uhl, K., Weik, R., Borth, N., Katinger, H. and Müller, D. 2006. Process parameter shifting: Part I. Effect of DOT, pH, and temperature on the performance of Epo-Fc expressing CHO cells cultivated in controlled batch bioreactors. *Biotechnology and Bioengineering*. **94**(6), pp.1033–1044.

- Tsanaktsidou, E., Karavasili, C., Zacharis, C.K., Fatouros, D.G. and Markopoulou, C.K. 2020. Partial Least Square Model (PLS) as a Tool to Predict the Diffusion of Steroids Across Artificial Membranes. *Molecules (Basel, Switzerland)*. **25**(6).
- Tustian, A.D., Salte, H., Willoughby, N.A., Hassan, I., Rose, M.H., Baganz, F., Hoare, M. and Titchener-Hooker, N.J. 2007. Adapted Ultra Scale-Down Approach for Predicting the Centrifugal Separation Behavior of High Cell Density Cultures. *Biotechnology Progress*. **23**(6), pp.1404–1410.
- del Val, I.J., Kontoravdi, C. and Nagy, J.M. 2010. Towards the implementation of quality by design to the production of therapeutic monoclonal antibodies with desired glycosylation patterns. *Biotechnology progress*. **26**(6), pp.1505–27.
- Valliere-Douglass, J.F., Brady, L.J., Farnsworth, C., Pace, D., Balland, A., Wallace, A., Wang, W., Treuheit, M.J. and Yan, B. 2009. O-Fucosylation of an antibody light chain: Characterization of a modification occurring on an IgG1 molecule. *Glycobiology*. **19**(2), pp.144–152.
- Walsh, I., Myint, M., Nguyen-Khuong, T., Ho, Y.S., Ng, S.K. and Lakshmanan, M. 2022. Harnessing the potential of machine learning for advancing “Quality by Design” in biomanufacturing. *mAbs*. **14**(1).
- Wang, A., Lewus, R. and Rathore, A.S. 2006. Comparison of different options for harvest of a therapeutic protein product from high cell density yeast fermentation broth. *Biotechnology and Bioengineering*. **94**(1), pp.91–104.
- Wang, B., Albanetti, T., Miro-Quesada, G., Flack, L., Li, L., Klover, J., Burson, K., Evans, K., Ivory, W., Bowen, M., Schoner, R. and Hawley-Nelson, P. 2018.

- High-throughput screening of antibody-expressing CHO clones using an automated shaken deep-well system. *Biotechnology progress*. **34**(6), pp.1460–1471.
- Wang, S., Godfrey, S., Ravikrishnan, J., Lin, H., Vogel, J. and Coffman, J. 2017. Shear contributions to cell culture performance and product recovery in ATF and TFF perfusion systems. *Journal of Biotechnology*. **246**, pp.52–60.
- Weisenthal, L.M., Dill, P.L., Kurnick, N.B. and Lippman, M.E. 1983. Comparison of Dye Exclusion Assays with a Clonogenic Assay in the Determination of Drug-induced Cytotoxicity. *Cancer Research*. **43**(1).
- Westoby, M., Rogers, J.K., Haverstock, R., Romero, J. and Pieracci, J. 2011. Modeling industrial centrifugation of mammalian cell culture using a capillary based scale-down system. *Biotechnology and Bioengineering*. **108**(5), pp.989–998.
- Wilson, L.J., Lewis, W., Kucia-Tran, R. and Bracewell, D.G. 2022. Identification and classification of host cell proteins during biopharmaceutical process development. *Biotechnology Progress*. **38**(1), p.e3224.
- Wold, S., Geladi, P., Esbensen, K. and Öhman, J. 1987. Multi-way principal components-and PLS-analysis. *Journal of Chemometrics*. **1**(1), pp.41–56.
- Wold, S., Sjöström, M. and Eriksson, L. 2002. Partial Least Squares Projections to Latent Structures (PLS) in Chemistry *In: Encyclopedia of Computational Chemistry* [Online]. Chichester, UK: John Wiley & Sons, Ltd. [Accessed 29 April 2020]. Available from: <http://doi.wiley.com/10.1002/0470845015.cpa012>.

- Wu, M., Ozcelik, A., Rufo, J., Wang, Z., Fang, R. and Jun Huang, T. 2019. Acoustofluidic separation of cells and particles. *Microsystems & Nanoengineering* 2019 5:1. **5**(1), pp.1–18.
- Xu, J., Rehmann, M.S., Xu, M., Zheng, S., Hill, C., He, Q., Borys, M.C. and Li, Z.J. 2020. Development of an intensified fed-batch production platform with doubled titers using N-1 perfusion seed for cell culture manufacturing. *Bioresources and Bioprocessing*. **7**(1), pp.1–16.
- Xu, J., Rehmann, M.S., Xu, X., Huang, C., Tian, J., Qian, N.X. and Li, Z.J. 2018. Improving titer while maintaining quality of final formulated drug substance via optimization of CHO cell culture conditions in low-iron chemically defined media. *mAbs*. **10**(3), p.488.
- Yao, G., Aron, K., Borys, M., Li, Z., Pendse, G. and Lee, K. 2021. A Metabolomics Approach to Increasing Chinese Hamster Ovary (CHO) Cell Productivity. *Metabolites*. **11**(12).
- Yavorsky, D., Blanck, R., Lambalot, C. and Brunkow, R. 2003. The Clarification of Bioreactor Cell Cultures for Biopharmaceuticals. *Pharmaceutical Technology*. (March), pp.62–76.
- Yigzaw, Y., Piper, R., Tran, M. and Shukla, A.A. 2006. Exploitation of the adsorptive properties of depth filters for host cell protein removal during monoclonal antibody purification. *Biotechnology Progress*. **22**(1), pp.288–296.
- Yoon, S.K., Choi, S.L., Song, J.Y. and Lee, G.M. 2005. Effect of culture pH on erythropoietin production by Chinese hamster ovary cells grown in suspension

- at 32.5 and 37.0C. *Biotechnology and Bioengineering*. **89**(3), pp.345–356.
- Yu, L.X., Amidon, G., Khan, M.A., Hoag, S.W., Polli, J., Raju, G.K. and Woodcock, J. 2014. Understanding pharmaceutical quality by design. *The AAPS journal*. **16**(4), pp.771–83.
- Yuk, I.H., Zhang, B., Yang, Y., Dutina, G., Leach, K.D., Vijayasankaran, N., Shen, A.Y., Andersen, D.C., Snedecor, B.R. and Joly, J.C. 2011. Controlling glycation of recombinant antibody in fed-batch cell cultures. *Biotechnology and Bioengineering*. **108**(11), pp.2600–2610.
- Zanghi, J.A., Schmelzer, A.E., Mendoza, T.P., Knop, R.H. and Miller, W.M. 1999. Bicarbonate concentration and osmolality are key determinants in the inhibition of CHO cell polysialylation under elevated pCO₂ or pH. *Biotechnology and Bioengineering*. **65**(2), pp.182–191.
- Zhang, Y. 2009. Approaches to optimizing animal cell culture process: substrate metabolism regulation and protein expression improvement. *Advances in biochemical engineering/biotechnology*. **113**, pp.177–215.
- Zhang, Y., Stobbe, P., Silvander, C.O. and Chotteau, V. 2015. Very high cell density perfusion of CHO cells anchored in a non-woven matrix-based bioreactor. *Journal of biotechnology*. **213**, pp.28–41.
- Zheng, Y., Sun, M., Sun, X., Sun, C. and Fang, Y. 2023. The role of protein concentration in heat-induced particulation of soy proteins at different pHs: Structure and functional properties. *Food Frontiers*. **4**(2), pp.955–965.
- Zhong, X. and D'Antona, A.M. 2021. Recent Advances in the Molecular Design and

Applications of Multispecific Biotherapeutics. *Antibodies (Basel, Switzerland)*.
10(2).

Zhu, M.M., Goyal, A., Rank, D.L., Gupta, S.K., Vanden Boom, T. and Lee, S.S. 2005.
Effects of elevated pCO₂ and osmolality on growth of CHO cells and production
of antibody-fusion protein B1: A case study. *Biotechnology Progress*. **21**(1),
pp.70–77.

Appendix

Chapter 3 Appendix

Table 3.1A Example of prediction models for titre (ambr1) generated using stepwise regression. The selection rule is based on maximising R^2 k-fold. The stepwise regression was performed in Jmp. The models in terms of actual factors as well as the R^2 predicted for the models were generated in Design-Expert, all other statistics were computed in Jmp.

| Equation in terms of actual factors | Eqn. # | # of terms | RMSE | AIC | BIC | R^2 adj. | R^2 pred. | R^2 k-fold |
|---|--------|------------|------|-----|-----|------------|-------------|--------------|
| 724+4246 * Seed | 1 | 1 | 1743 | 431 | 434 | 0.17 | 0.05 | 0.02 |
| At temperature = 33.5°C Titre = 2499 | 2 | 1 | 1762 | 432 | 434 | 0.15 | 0.03 | -0.08 |
| At temperature = 35.5°C Titre = 2499 | | | | | | | | |
| -26814+4302 * pH | 3 | 1 | 1770 | 432 | 435 | 0.20 | 0.02 | -0.02 |
| -33348+4828 * pH+ 4706 * Seed | 4 | 2 | 1518 | 427 | 429 | 0.37 | 0.26 | 0.26 |
| At temperature = 33.5°C -267+4479* Seed | 5 | 2 | 1536 | 427 | 430 | 0.35 | 0.24 | 0.17 |
| At temperature = 35.5°C 1431.7+4478.8 * Seed | | | | | | | | |
| At temperature = 33.5°C -276153+4302*pH | 6 | 2 | 1596 | 429 | 432 | 0.30 | 0.17 | 0.08 |
| At temperature = 35.5°C -26013+4302* pH | | | | | | | | |
| At temperature = 33.5°C -34531+4854 * pH+4943 * Seed | 7 | 3 | 1243 | 419 | 422 | 0.58 | 0.50 | 0.47 |
| At temperature = 35.5°C -32823+4854 * pH+4943 * Seed | | | | | | | | |
| -2046265 + 4801 * Seed + 580311*pH - 41105 * pH^2 | 8 | 3 | 1403 | 425 | 427 | 0.46 | 0.29 | 0.31 |
| -39736 +4900*pH+25133*Seed -15989* Seed^2 | 9 | 3 | 1445 | 426 | 429 | 0.42 | 0.32 | 0.34 |
| At temperature = 33.5°C -2052149+581681 * pH+5039 * Seed -41201 * pH^2 | 10 | 4 | 1072 | 414 | 416 | 0.68 | 0.59 | 0.54 |
| At temperature = 35.5°C -2050438+581681 * pH+5039 * Seed-41201 * pH^2 | | | | | | | | |
| At temperature = 33.5°C -32123+4678 * pH + 3043 * Seed | 11 | 4 | 1176 | 419 | 421 | 0.62 | 0.57 | 0.54 |
| At temperature = 35.5°C -33153+4678* pH +7568 * Seed | | | | | | | | |
| At temperature = 33.5°C -39047.4+4903.9 * pH+19666 * Seed-11538 * Seed^2 | 12 | 4 | 1207 | 420 | 422 | 0.60 | 0.50 | 0.48 |
| At temperature = 35.5°C -37474 + 4904 * pH + 19666 * Seed - 11538 * Seed^2 | | | | | | | | |
| At temperature = 33.5°C -2327337+660994 * pH+2685 * Seed-46882 * pH^2 | 13 | 5 | 908 | 409 | 410 | 0.77 | 0.70 | 0.69 |
| At temperature = 35.5°C -2329037+660994 * pH+8323 * Seed-46882 * pH^2 | | | | | | | | |

| | | | | | | | | |
|--|----|---|------|-----|-----|------|------|------|
| At temperature = 33.5°C -2015483+201 * Harvest day + 570347 * pH + 5129 * Seed -40391 * pH^2 At temperature = 35.5°C -2013706+201 * Harvest day +570347 * pH + 5129 * Seed -40391 * pH^2 | 14 | 5 | 1073 | 417 | 418 | 0.68 | 0.55 | 0.58 |
| At temperature = 33.5°C -1893241+535887 * pH+9337 * Seed-37929 * pH^2-3375 * Seed^2 At temperature = 35.5°C -1891570+535887 * pH+9337 * Seed-37929 * pH^2 - 3375 * Seed^2 | 15 | 5 | 1096 | 418 | 419 | 0.67 | 0.54 | 0.57 |
| At temperature = 33.5°C -2775393-18424 * Harvest day+825646 * pH+3975 * Seed+654 * Harvest day^2-58636* pH^2 At temperature = 35.5°C -2773623-18424 * Harvest day+825646 * pH+3975 * Seed+654 * Harvest day^2-58636 * pH^2 | 16 | 6 | 918 | 413 | 413 | 0.77 | 0.66 | 0.69 |
| At temperature = 33.5°C -2292768+134 * Harvest day+650520 * pH+2832 * Seed-46133 * pH^2 At temperature = 35.5°C -2294298+134 * Harvest day+650520 * pH+8262 * Seed-46132 * pH^2 | 17 | 6 | 919 | 413 | 413 | 0.77 | 0.68 | 0.68 |
| At temperature = 33.5°C -2305720+656314 * pH-14442 * Seed+2444 * pH * Seed-46654 * pH^2 At temperature = 35.5°C -2307463+656314 * pH-8760 * Seed+2444 * pH * Seed-46654 * pH^2 | 18 | 6 | 927 | 413 | 413 | 0.76 | 0.69 | 0.68 |
| Temperature 33 -2884864-15471* Harvest day+851548 * pH+2237 * Seed+548 * Harvest day^2-60497 * pH^2 Temperature 35.5 -2885863-15471* Harvest day+851548 * pH+6786 * Seed+548* Harvest day^2-60497 * pH^2 | 19 | 7 | 791 | 410 | 407 | 0.83 | 0.74 | 0.76 |
| At temperature = 33.5°C -2414124-110 * Harvest day+686295 * pH + 2555 * Seed-48690 * pH^2 At temperature = 35.5°C -2422740+380 * Harvest day+686295 * pH + 8212* Seed -48690 * pH^2 | 20 | 7 | 892 | 415 | 413 | 0.78 | 0.70 | 0.70 |
| At temperature = 33.5°C -2227118-511 * Harvest day+634333 * pH-10669 * Seed+971 * Harvest day * Seed -44977 At temperature = 35.5°C -2228711-511 * Harvest day + 634333 * pH -5250 * Seed 971 * Harvest day * Seed-44977 * pH^2 | 21 | 7 | 914 | 417 | 414 | 0.77 | 0.69 | 0.69 |
| At temperature = 33.5°C -2966935-15040 * Harvest day+874648 * pH+2019 * Seed+526 * Harvest day^2-62149 * pH^2 At temperature = 35.5°C -2974177-14610 * Harvest day+874648 * pH+6803 * Seed+526 * Harvest day^2-62149 * pH^2 | 22 | 8 | 765 | 412 | 407 | 0.84 | 0.77 | 0.78 |
| At temperature = 33.5°C -3185465-16246 * Harvest day+939599 * pH-5024 * Seed+577 * Harvest day^2-66789* pH^2+5595 * Seed^2 At temperature = 35.5°C -3186534-16246 * Harvest day+939599 * pH-226 * | 23 | 8 | 796 | 414 | 409 | 0.83 | 0.71 | 0.72 |

| | | | | | | | | |
|--|----|---|-----|-----|-----|------|------|------|
| Seed+577 * Harvest day²-66789 * pH²+5595 * Seed² | | | | | | | | |
| At temperature = 33.5°C -2843966-14963 * Harvest day+839127 * pH+ -978* Seed+233 * Harvest day * Seed+525 * Harvest day²-59610 * pH² At temperature = 35.5°C -2845003-14963 * Harvest day+839127 * pH+3605 * Seed+233 * Harvest day * Seed+525* Harvest day²-59610* pH² | 24 | 8 | 815 | 416 | 410 | 0.82 | 0.72 | 0.74 |

Chapter 4 Appendix

Characterising the pilot-scale centrifuge using established approaches

Two pilot scale centrifugation characterisation studies were performed – the first set of results were focused on characterising a pilot-scale centrifuge (LAPX-404) using an established method based on LDH release, PSD and filter capacity and the second set of results is focused on characterising a pilot- scale centrifuge (MBPX404) Both studies were also used to inform the ranges of shear that were used in this work. The LDH release was used as a measurement of cell disruption due to shear forces. The material from cell culture A (**Table 4.1**) was processed in the pilot scale centrifuge (flowrate = 120L/h and bowl speed = 7040 RPM) and also exposed to different flowrates in the capillary shear device. **Figure 4.1-A** reveals the levels of LDH release for the different flowrates in the CSD and the pilot scale centrifuge. The results show that the shear in the pilot scale centrifuge corresponds to approximately 21 mL/min in the CSD. These results were largely in line with the studies performed by Joseph et al. (2016).

This experiment was also used to determine the impact of holding the harvested cell culture sample at room temperature for prolonged periods prior to LDH analysis on the results from the LDH assay. This was important as high throughput experimentation (with multiple runs in the ambr) may lead to prolonged sample hold time, which may introduce variation in the results. **Figure 4.1-A** shows that the samples that were processed 121 min after collection had lower standard deviation between the replicate measurements compared to the samples processed after 313

min. However, there was no trend observed for over or underestimation of the LDH release.

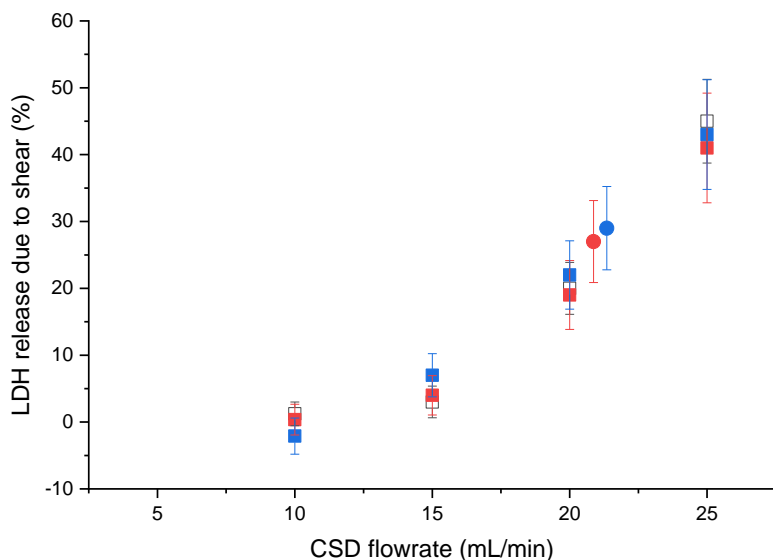


Figure 4.1-A Pilot scale centrifuge shear characterisation through LDH measurements in the pilot scale centrifuge at 120L/H and 7000 rpm and the capillary shear device at various flowrates for cell culture A (**Table 4.1**). The squares (■) indicate that the measurement was for the CSD device and the circle (●) is the LDH measurement for the pilot scale centrifuge – flowrate for that measurement is calculated using linear regression for LDH vs flowrate for the CSD. The colour indicates different hold times before measurement – white (hold=121 min), red (hold = 260 min) and blue (hold = 313 min). The total cell number was 17.63×10^6 cells/mL and the viability was 88.7%.

Comparison of the filterability of the mimic and pilot scale centrates

In the previous section the extent of cell lysis during the pilot scale centrifuge was found to be comparable to ~ 21 mL/min in the CSD. Therefore, the same conditions in the CSD were used for these studies. The mimic centrates were generated using the Sigma theory to scale down from the pilot scale centrifuge ($cQ/\Sigma = 4.31 \times 10^{-8}$ m/s). The correction factor was assumed to be 0.27 (Joseph et al., 2016) and to

reach the target clarification efficiency the samples were spun using 20mL volume in a 50mL Flakon centrifuge tube (Corning™) at 4000RPM for 330s in a Soval™ Legend™ XTR. Multiple mimic centrate samples (20 mL each) were pooled together to generate enough feed material for the depth filtration studies (approx. 200 to 300mL per run). The cell culture material was sourced from two bioprocess development runs (culture X and Y). The CSD centrate had comparable turbidity to the pilot scale centrate – 537 NTUs for the pilot scale centrate compared to 512 NTUs for the CSD centrate (Cell culture X) and 494 NTUs for the PS centrate compared to 478 NTUS for the CSD centrate for Cell culture Y. **Table 4.1-A** shows the results from filter capacity studies for cell culture X and Y using constant pressure and constant flow at two different pressures – 10 and 15PSI. In **Figure 4.2-A** the CSD vs PS filter capacities are plotted on a parity plots showing good correlation between the two fluxes, while **Figure 4.3-A** shows good overlap between the filtration flux decline and pressure increase between the mimic and pilot scale centrates.

Table 4.1-A Filter capacity studies to support pilot scale centrifuge 1 characterisation

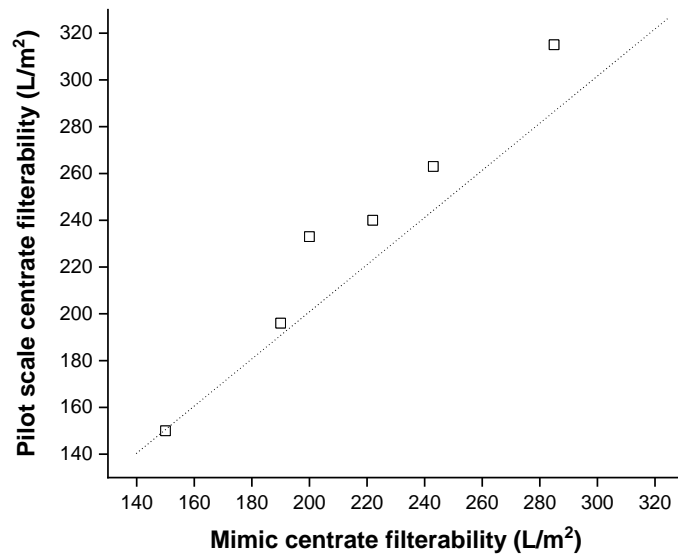
| Cell culture | Total cell number (x10 ⁶) | Viability (%) | Filter sizing approach* | Pressure** (PSI) | Centrifugation scale*** (PS or CSD) | Filter capacity**** (L/m ²) |
|----------------|--|---------------|-------------------------|------------------|-------------------------------------|---|
| Cell culture X | 30 | 39 | constant flow | 10 | PS | 222 |
| | | | constant flow | | CSD | 240 |
| | | | constant flow | 15 | PS | 315 |
| | | | constant flow | | CSD | 285 |
| | | | constant pressure | 10 | PS | 190 |
| | | | constant pressure | | CSD | 196 |
| | | | constant pressure | 15 | PS | 243 |
| | | | constant pressure | | CSD | 263 |
| Cell culture Y | 34 | 57 | constant flow | 10 | PS | 150 |
| | | | constant flow | | CSD | 150 |
| | | | constant flow | 15 | PS | 200 |
| | | | constant flow | | CSD | 233 |

*Filter sizing approach constant flow is based on max P_{max} and sizing approach constant pressure is based at V_{max} (at constant pressure)

**Pressure is the maximum pressure for the P_{max} approach or the constant pressure for the V_{max} sizing approach.

*** Centrifugations scale: CSD – capillary shear device, PS – Pilot scale centrifuge.

**** Filter capacity at P_{max} or using the V_{max} calculation



Figurer 4.2-A Pilot scale versus mimic centrates' filterability for the experiments described in **Table 4.1-A**

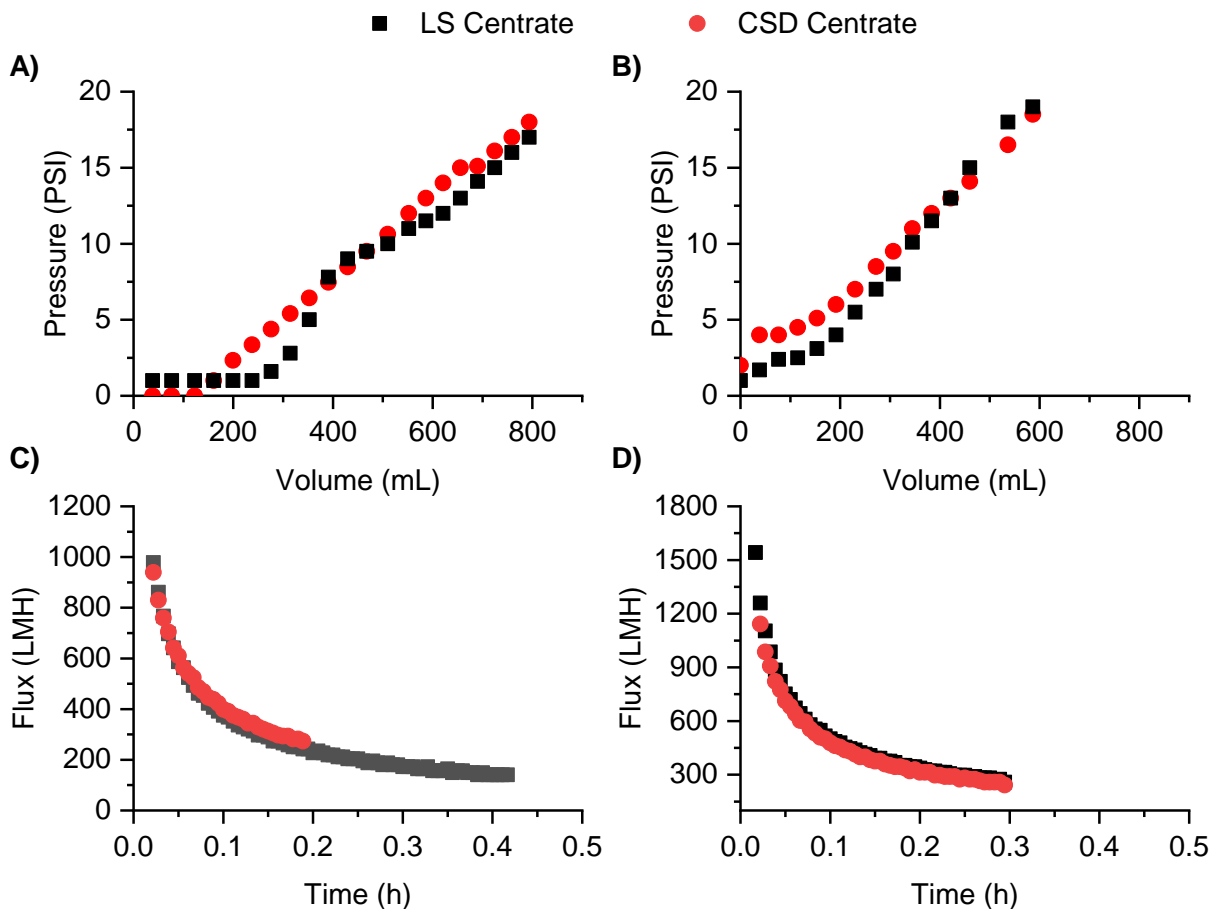


Figure 4.3-A Comparison of pressure increase in A) and B) and the flux decline in C) and D) between large scale (■ LS) and mimic generated using the capillary shear device (● CSD) at the mimic conditions described before. The constant flux is at 100LMH for cell culture A, B), the constant pressure is at 10PSI for C) and 15PSI for D).

Mimic low (7000RPM) and high shear (8000 RPM)

Cell culture B (**Table 4.1**) was used to generate the mimic centrates and pilot scale centrates investigated in this section. For the pilot scale centrifugation process each bowl speed in the centrifuge was run for at least 30 min and the turbidity was

measured for the bulk centrate. Preliminary investigation indicated that the shear for this process was higher than for the pilot scale centrifuge described in earlier in this section, therefore, a higher range of flowrates in the CSD was investigated – 30 to 45 mL/min. The new centrifuge had the same setting area but a different correction factor ($c=0.55$, derived experimentally but not shown here). **Figure 4.4-A(a)** shows two levels of LDH release for different flowrates in the CSD and two conditions in the pilot scale centrifuge– bowl speed of 7,000 RPM and 8,000 RPM, both at the same flowrate of 120 L/h. The results reveal that the condition at 7,000 RPM correspond to approximately 31mL/min and the condition at 8,000 RPM correspond to 41 mL/min. **Figure 4.4-A(b)** shows a comparison in the flux declines between the centrate generated using the pilot scale centrifuge (8,000 RPM and 120L/h) and the mimic centrate at 41mL/min. The two flux declines overlap, which demonstrates comparable filterability between the centrates and suggests comparable particle size distributions between the two centrates.

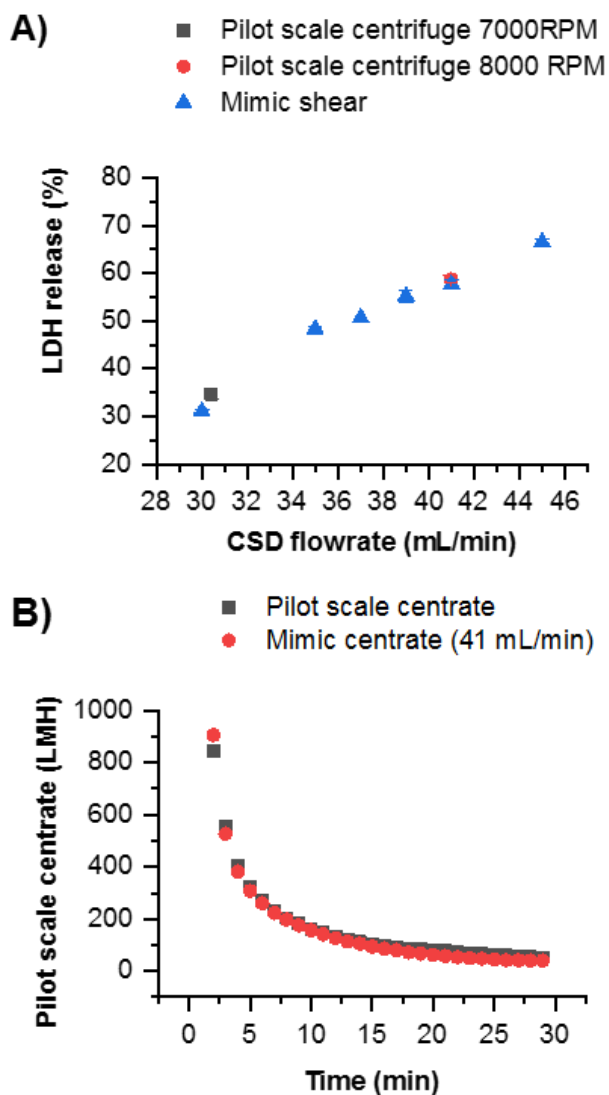
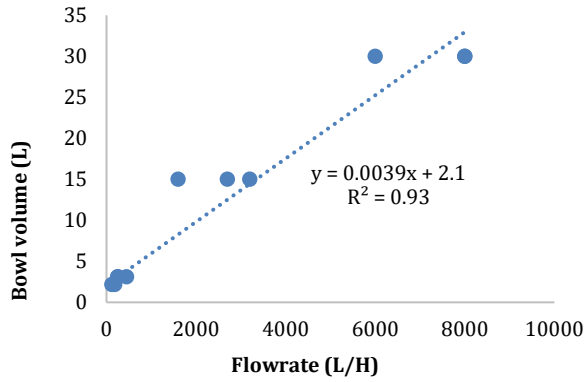


Figure 4.4-A Pilot scale centrifuge (MPBX404, Alfa Laval, Lund, Sweden) characterisation based on A) LDH release upon shear in the pilot scale centrifuge at 7000RPM (■) and 8000RPM (●) and for the CSD at flowrate between 30 and 45mL/min flowrate B) Comparison in the flux decline between the pilot scale at 8000RPM and mimic centrate at 41mL/min. The cell culture material was from a pilot scale run, harvested at day 15 (**Table 4.1**).

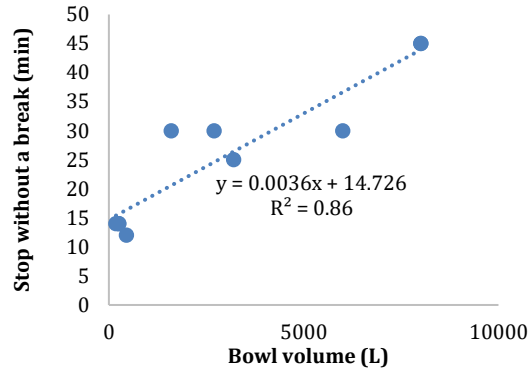
Chapter 5 Appendix

A)



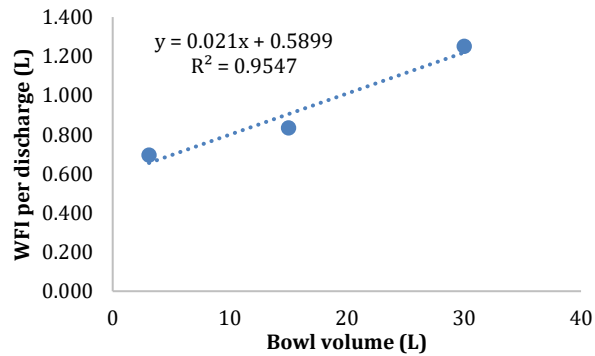
| Vendor | Max flowrate (L/h) | Bowl volume (L) |
|-----------------------|--------------------|-----------------|
| Clara 20/LAPX404 | 120 | 2.2 |
| Alfa Laval MBPX404 | 180 | 2.2 |
| BTPX205 | 250 | 3.1 |
| BTPX305 | 251 | 3.1 |
| Culturefuge 100 | 450 | 3.1 |
| MBPX810SGV-34CL | 1600 | 15 |
| Culturefuge 200 | 2700 | 15 |
| MBPX 810HGV-34C | 3200 | 15 |
| Culturefuge 300 | 6000 | 30 |
| Culturefuge 400 (v 1) | 8000 | 30 |
| Culturefuge 400 (v 2) | 8001 | 30 |

B)



| Vendor | Bowl volume (L) | Stop time without a break (min) |
|-----------------------|-----------------|---------------------------------|
| Alfa Laval MBPX404 | 2.2 | 14 |
| BTPX205 | 3.1 | 14 |
| BTPX305 | 3.1 | 14 |
| Culturefuge 100 | 3.1 | 12 |
| MBPX810SGV-34CL | 15 | 30 |
| Culturefuge 200 | 15 | 30 |
| MBPX 810HGV-34C | 15 | 25 |
| Culturefuge 300 | 30 | 30 |
| Culturefuge 400 (v 1) | 30 | 45 |
| Culturefuge 400 (v 2) | 30.01 | 45 |

C)



| Bowl volume | WFI consumption per discharge (L) | |
|-----------------|-----------------------------------|------|
| Culturefuge 100 | 3.1 | 0.69 |
| Culturefuge 200 | 15 | 0.83 |
| Culturefuge 300 | 30 | 1.25 |

Figure 5.1-A Ratios between various disc-stack centrifuges design parameters A) bowl volume (L) vs flowrate (L/h); B) stopping time vs bowl volume (L) and C) WFI per discharge vs bowl volume (L)

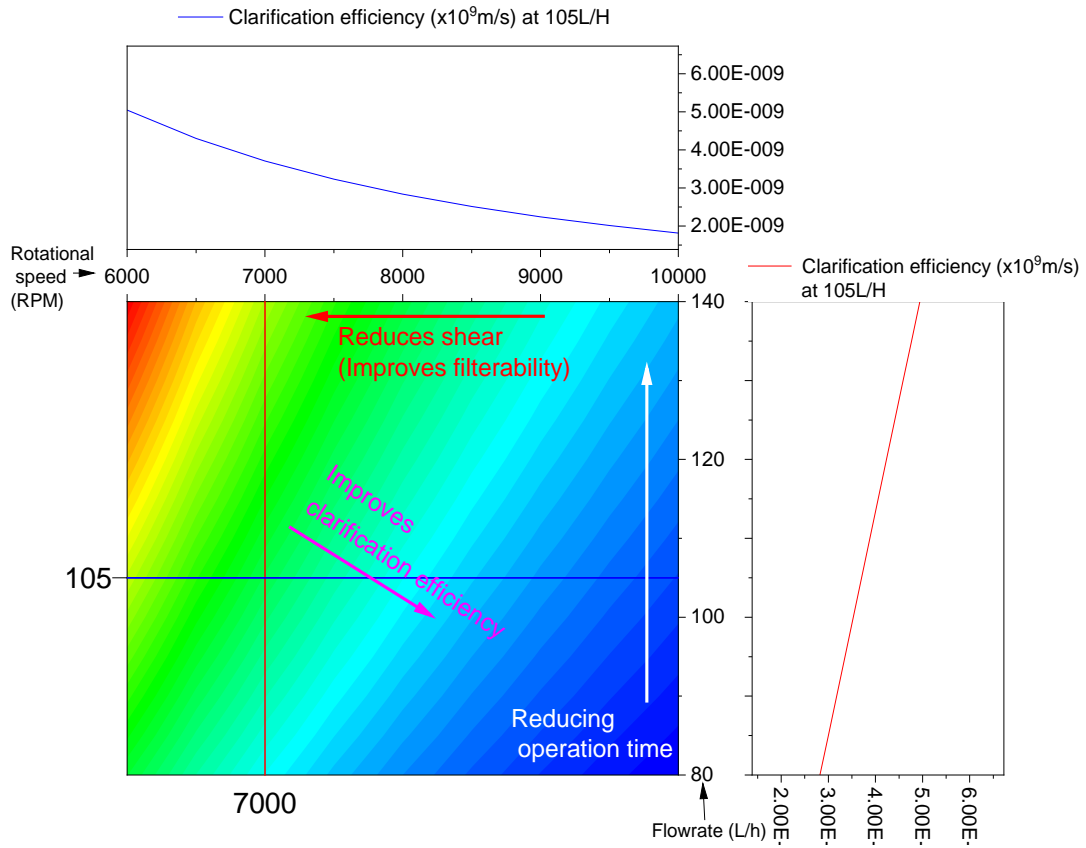


Figure 5.2-A The impact of centrifugation flowrate and bowl rotation speed on the levels of shear, operation time and clarification efficiency. Centrifuge LAPX404 used for the calculation.

Table 5.1-A Examples of process duration (hours) for different filter capacities and fluxes

| | | Filter capacity (L/m²) | | | | | | | |
|-------------------|------------|--|------------|------------|------------|------------|------------|------------|------------|
| | | 100 | 200 | 300 | 400 | 500 | 600 | 700 | 800 |
| Flux (LMH) | 100 | 1.0 | 2.0 | 3.0 | 4.0 | 5.0 | 6.0 | 7.0 | 8.0 |
| | 150 | 0.7 | 1.3 | 2.0 | 2.7 | 3.3 | 4.0 | 4.7 | 5.3 |
| | 200 | 0.5 | 1.0 | 1.5 | 2.0 | 2.5 | 3.0 | 3.5 | 4.0 |
| | 250 | 0.4 | 0.8 | 1.2 | 1.6 | 2.0 | 2.4 | 2.8 | 3.2 |
| | 300 | 0.3 | 0.7 | 1.0 | 1.3 | 1.7 | 2.0 | 2.3 | 2.7 |
| | 350 | 0.3 | 0.6 | 0.9 | 1.1 | 1.4 | 1.7 | 2.0 | 2.3 |
| | 400 | 0.3 | 0.5 | 0.8 | 1.0 | 1.3 | 1.5 | 1.8 | 2.0 |

Chapter 6 Appendix

Table 6.1-A Jmp report on PLS models generation with different number of factors (latent variables) using the NIPALS algorithm and k-fold cross validation with k-fold = 7. The models are generated using all PSD data for the viable cells.

| Number of factors | Root Mean PRESS | van der Voet T ² | Prob > van der Voet T ² | Q ² | Cumulative Q ² | R ² X | Cumulative R ² X | R ² Y | Cumulative R ² Y |
|-------------------|-----------------|-----------------------------|------------------------------------|----------------|---------------------------|------------------|-----------------------------|------------------|-----------------------------|
| 0 | 1.084 | 18.35 | <.0001* | -0.10 | -0.10 | 0.000 | 0.000 | 0.000 | 0.000 |
| 1 | 0.643 | 5.323 | 0.0160* | 0.614 | 0.614 | 0.485 | 0.485 | 0.664 | 0.664 |
| 2 | 0.548 | 0.000 | 1.0000 | 0.719 | 0.892 | 0.208 | 0.692 | 0.104 | 0.768 |
| 3 | 0.551 | 0.040 | 0.8670 | 0.717 | 0.969 | 0.128 | 0.821 | 0.017 | 0.786 |
| 4 | 0.550 | 0.005 | 0.9480 | 0.718 | 0.991 | 0.154 | 0.975 | 0.012 | 0.798 |
| 5 | 0.565 | 0.289 | 0.6150 | 0.702 | 0.997 | 0.017 | 0.992 | 0.010 | 0.808 |
| 6 | 0.627 | 2.968 | 0.1000 | 0.633 | 0.999 | 0.003 | 0.995 | 0.045 | 0.852 |
| 7 | 0.611 | 2.153 | 0.1440 | 0.651 | 1.000 | 0.001 | 0.996 | 0.012 | 0.865 |
| 8 | 0.631 | 3.102 | 0.0700 | 0.628 | 1.000 | 0.001 | 0.996 | 0.010 | 0.874 |
| 9 | 0.673 | 5.065 | 0.0140* | 0.577 | 1.000 | 0.001 | 0.997 | 0.006 | 0.881 |
| 10 | 0.722 | 8.033 | 0.0030* | 0.513 | 1.000 | 0.001 | 0.998 | 0.007 | 0.888 |
| 11 | 0.756 | 9.150 | 0.0020* | 0.466 | 1.000 | 0.001 | 0.998 | 0.007 | 0.895 |
| 12 | 0.757 | 8.471 | 0.0010* | 0.464 | 1.000 | 0.000 | 0.999 | 0.005 | 0.900 |
| 13 | 0.753 | 8.582 | 0.0030* | 0.470 | 1.000 | 0.000 | 0.999 | 0.004 | 0.903 |
| 14 | 0.738 | 8.130 | 0.0020* | 0.491 | 1.000 | 0.000 | 0.999 | 0.003 | 0.906 |
| 15 | 0.757 | 8.621 | 0.0020* | 0.466 | 1.000 | 0.000 | 0.999 | 0.003 | 0.909 |

Table 6.2-A Jmp report on PLS models generation with different number of factors (latent variables) using the NIPALS algorithm and k-fold cross validation with k-fold = 7. This is a pruned model using only PSD data (predictors) with VIP score higher than 0.8. The box highlighted in purple shows the final PLS model that was chosen based on min Pres and max Prob>van der Voet T².

| Number of factors | Root Mean PRESS | van der Voet T ² | Prob > van der Voet T ² | Q ² | Cumulative Q ² | R ² X | Cumulative R ² X | R ² Y | Cumulative R ² Y |
|-------------------|-----------------|-----------------------------|------------------------------------|----------------|---------------------------|------------------|-----------------------------|------------------|-----------------------------|
| 0 | 1.097 | 18.67 | <.0001* | -0.21 | -0.21 | 0.000 | 0.000 | 0.000 | 0.000 |
| 1 | 0.541 | 2.049 | 0.1630 | 0.705 | 0.705 | 0.608 | 0.608 | 0.767 | 0.767 |
| 2 | 0.519 | 0.309 | 0.5930 | 0.729 | 0.920 | 0.260 | 0.869 | 0.026 | 0.793 |
| 3 | 0.517 | 0.165 | 0.7390 | 0.731 | 0.979 | 0.056 | 0.924 | 0.022 | 0.815 |
| 4 | 0.510 | 0.000 | 1.0000 | 0.739 | 0.994 | 0.032 | 0.956 | 0.014 | 0.830 |
| 5 | 0.563 | 6.674 | 0.0100* | 0.681 | 0.998 | 0.008 | 0.964 | 0.016 | 0.846 |
| 6 | 0.568 | 5.918 | 0.0120* | 0.675 | 0.999 | 0.007 | 0.971 | 0.004 | 0.849 |
| 7 | 0.575 | 6.168 | 0.0110* | 0.668 | 1.000 | 0.005 | 0.976 | 0.001 | 0.850 |
| 8 | 0.579 | 6.630 | 0.0090* | 0.663 | 1.000 | 0.006 | 0.982 | 0.000 | 0.851 |
| 9 | 0.580 | 6.420 | 0.0060* | 0.662 | 1.000 | 0.005 | 0.987 | 0.000 | 0.851 |
| 10 | 0.581 | 6.420 | 0.0130* | 0.660 | 1.000 | 0.004 | 0.991 | 0.000 | 0.851 |
| 11 | 0.581 | 6.370 | 0.0060* | 0.661 | 1.000 | 0.003 | 0.994 | 0.000 | 0.851 |
| 12 | 0.581 | 6.400 | 0.0140* | 0.661 | 1.000 | 0.003 | 0.997 | 0.000 | 0.851 |
| 13 | 0.581 | 6.398 | 0.0180* | 0.661 | 1.000 | 0.002 | 0.998 | 0.000 | 0.851 |
| 14 | 0.581 | 6.398 | 0.0100* | 0.661 | 1.000 | 0.002 | 1.000 | 0.000 | 0.851 |

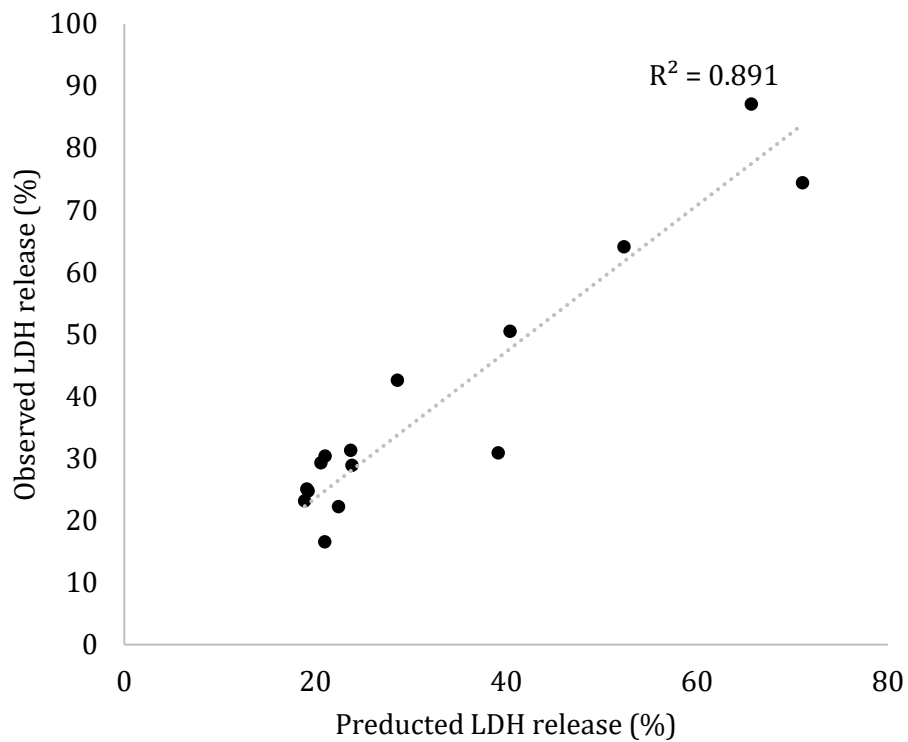


Figure 6.1-A Actual vs predicted parity plot for the LDH release vs the PLS model selected in **Table 6.2-A**.

Table 6.3-A Assumptions used in the calculation of volumes and time required for LDH and PCV ([solids]) measurements using the traditional wet-lab approach and the novel PLS-based method

| Activity | Process and Analytics Details |
|--|--|
| Cell culture | Ambr15 with 48 bioreactors |
| | 14 days process |
| | Cell counts every 2 days |
| LDH release measurement based on a 96-well plate format and a and Optima plate reader | 100 μ L per sample |
| | 6 measurements per sample* |
| | 30 sec preparation time per sample |
| | 60 min instrument running time per 96-well plate |
| | 15 min analysis per 96-well plate |
| PCV measurements using PCV tubes | 50 μ L per sample** |
| | Two min per centrifuge spin |
| | 24 samples per centrifuge spin |
| | Four measurements per sample |
| | 6 min analysis per 24 samples |
| | 6 sec prep per sample |

* Triplicates for lysed and measured sample

** 40 μ L required per sample plus 10 μ L overage